JAERI-M
91-141

PROCEEDINGS OF THE TOKYO INTERNATIONAL SYMPOSIUM '90 ON FREE ELECTRON LASERS, 29-30, JANUARY 1990, TOKYO

September 1991

Promotion Committee on Nuclear Cross-Over Research
Specialist Committee on Laser Technology
Science and Technology Agency

日本原子力研究所
Japan Atomic Energy Research Institute

JAERI-Mレポートは，日本原子力研究所が不定期に公刊している研究報告書です。
入手の問合わせは，日本原子力研究所技術情報部情報資料課（〒319-11茨城県那珂郡東海村）あて，お申しこしください。なお，このほかに財団法人原子力弘済会資料センター（〒319-11 茨城県那珂郡東海村日本原子力研究所内）で複写による実費頒布をおこなっております。

JAERI-M reports are issued irregularly.
Inquiries about availability of the reports should be addressed to Information Division Department of Technical Information, Japan Atomic Energy Research Institute, Tokai-mura, Naka-gun, Ibaraki-ken 319-11, Japan.

編集兼発行　日本原子力研究所
印　　刷　いばらき印刷㈱

JAERI-M 91-141

Proceedings of the Tokyo International Symposium '90 on Free Electron Lasers, 29-30, January 1990, Tokyo

Promotion Committee on Nuclear Cross-Over Research
Specialist Committee on Laser Technology
Science and Technology Agency

Tokai Research Establishment
Japan Atomic Energy Research Institute
Tokai-mura, Naka-gun, Ibaraki-ken

(Received August 7, 1991)

Four important and strategic areas are emphasized as the Underlying Technology of Nuclear Research: the research and development of nuclear materials, the application of Artificial Intelligence (AI), the application of laser for nuclear energy, and the assessment and reduction of radiation risks. To promote effectively the research and development on these areas, the research potential of industrial, academic and governmental organizations must be employed and the collaboration among these organizations should be enhanced. To attain this objective, the system of Cross-Over Research on Underlying Technology of Nuclear Energy was organized in September 1989 under the collaboration agreement among the Japan Atomic Energy Research Institute, the Power Reactor and Nuclear Fuel Development Corporation, and the Institute of Physical and Chemical Research.

The organization system consists of four Specialist Committees which correspond to the four technological areas under the Promotion Committee on Nuclear Cross-Over Research.

Concerning about the research and development of new lasers for nuclear energy applications (free electron laser), the Specialist Committee on Laser Technology was organized under the system.

The Specialist Committee on Laser Technology has decided to promote positively the R&D of FEL and to hold the Tokyo International Symposium

'90 on Free Electron Lasers to report and discuss the activities and successful results on the research and development of FEL.

The symposium was held from January 29 through 30, at Hotel Pastoral, Tokyo, organized and programmed by "Promotion Committee on Nuclear Cross-Over Research" and "Specialist Committee on Laser Technology" and sponsored by Science and Technology Agency.

Nine persons were invited from foreign countries (7 from U.S.A., 2 from Europe) including Professor John M.J. Madey, and 8 invited talks were performed. From domestic participants were over 170 and 19 papers were reported.

These proceedings consist of the newly revised papers by lectures of the Symposium which were administrated by Department of Physics, Japan Atomic Energy Research Institute.

Keywords: Proceedings, Free Electron Lasers

Symposium Program Committee

Specialist Committee on Laser Technology
Chairman, Hiroto Kuroda (Univ. of Tokyo)
Yuuki Kawarasaki (JAERI)
Isamu Sato (KEK)
Tetsuo Yamazaki (ETL)
Yoshiyuki Kawamura (RIKEN)
Kazumi Ouchi (PNC)

Secretariat of the Symposium
Yoichi Sudo (JAERI)
Masaru Sawamura (JAERI)

JAERI－M 91－141

自由電子レーザー東京国際シンポジウム報文集，1990年１月29日－30日，東京

原子力基盤技術総合的研究推進委員会
原子力レーザー研究交流委員会
科学技術庁

（1991年８月７日受理）

原子力基盤技術として，原子力用材料，原子力用人工知能，原子力用レーザー及び放射線リスク評価・低減化の４つが重点戦略課題として取り上げられている。

この研究開発を，より効果的に推進するために，研究ポテンシャルを有する研究機関間の共同研究等による連携を中心として，産・学・官の研究ポテンシャルを活用し同じ研究課題を効率的・効果的に進める原子力基盤クロスオーバー研究交流システムが1989年９月に発足した。（1989年９月１日付で幹事機関の原研・理研・動燃間の研究協力協定締結）

このシステムは，「推進委員会」及びその下に設けられる４つの技術領域それぞれに対応した４つの「研究交流委員会」から構成されている。

原子力用新レーザーの研究開発（自由電子レーザー）に関しては“原子力用レーザー交流委員会”が設置された。

この交流委員会で検討・審議の結果，参加諸機関における自由電子レーザーの研究・開発のこれまでの成果・現状をシンポジウム形式で発表する研究会を開催することとなった。

このシンポジウムは，原子力基盤技術総合的研究推進委員会・原子力レーザー研究交流委員会主催，科学技術庁後援で1990年１月29，30日の２日間開催された。

外国からは，自由電子レーザーの発明者であるJohn M. J. Madey教授を初めとして計９名（内訳米国７名，ヨーロッパ２名）の参加があり，８件の講演が行われた。一方，国内からは，170 名以上の参加があり，19件の講演が行われた。

この報文集はシンポジウム後に，大半の講演者が新たに執筆した論文をまとめたものである。

なお，日本原子力研究所物理部が本シンポジウムの事務局を担当した。

東海研究所：　〒319-11　茨城県那珂郡東海村白方白根2-4

シンポジウム実行委員会

原子力用レーザー交流委員会	主　査	黒田　寛人（東京大学）
原子力用レーザー交流委員会	委　員	河原崎雄紀（日本原子力研究所）
〃		山崎　鉄夫（電子技術総合研究所）
〃		佐藤　　勇（高エネルギー物理学研究所）
〃		河村　良行（理化学研究所）
〃		大内　和美（動力炉・核燃料開発事業団）

原子力用レーザー研究交流委員会事務局		須藤　洋一（日本原子力研究所）
		沢村　　勝（日本原子力研究所）

Contents

目　　次

JAERI−M 91−141

PROCEEDINGS

Tokyo International Symposium '90 on Free Electron Lasers

January 29-30, 1990
at
Tokyo Toranomon-Pastoral
Tokyo, Japan

Organized and Programmed
by
Specialist Committee on Laser Technology
and
Japan Atomic Energy Research Institute

Sponsored
by
Science and Technology Agency

PREFACE

The Tokyo International Symposium '90 on Free Electron Lasers was timely held from January 29 through 30, at Hotel Pastoral, Toranomon, sponsored by "Promotion Committee on Nuclear Cross-Over Research" and "Specialist Committee on Laser Technology" and supported by Science and Technology Agency of the Japanese Government.

Totally around two hundred persons, nine persons from outside (7 from U.S.A., 2 from Europe), including Professor John M. J. Madey, the inventor of free-electron laser (FEL) and worldwide well known experts in FEL's, accelerator's and laser's research communities, participated and discussed in somewhat exciting atmosphere on the very new technologies together with historical and perspective views.

After the new Japanese guideline for nuclear energy research has been issued in 1987, following The Maekawa Report, the four innovative R&D subjects; new materials, artificial intelligence, new lasers and method for risk assessment in the nuclear energy research field, have first been settled.

The promotion committee on Nuclear Cross-Over Research administrates the whole four subjects, while the four Specialist Committees manage the specific ones. The Specialist Committee on Laser Technology of Nuclear Cross-Over Research has decided to positively promote the R&D of FEL as a new laser in a more close and effective cooperation among industrial, academic and governmental organizations.

The FEL's technology, at the first step in particular, depends strongly on that of accelerator's. Radio-Frequency (RF) accelerators convert the RF-power to kinetic energy of a charged particle beam, while in FEL's the beam power is inversely again transformed to electromagnetic waves but with much shorter wavelengths. Accelerators are further expected to play an important role in the nuclear energy field; as high intensity neutron sources for material testing, high-energy proton-beam sources for incineration of long-lived radioactive wastes and γ-ray sources. Only electromagnetic force in our usual world can be applied to compete with strong force in nuclei.

The symposiums thus been programmed by the acting members, the same as the editors, from the Specialist committee.

Finally, I would like sincerely to express my gratitude to all participants and also to hope and expect the further progress of FEL R&Ds, including the applications to the nuclear energy research field.

Professor Yoichi Fujiie
(Tokyo Institute of Technology)
Chairman, Promotion Committee on
Nuclear Cross-Over Research

PREFACE

The Tokyo International Symposium on Free Electron Lasers was held in success with having over two hundreds active participants.

As mentioned in the preface given by Prof. Fujiie, the promotion committee on Nuclear Cross-Over Research decided to promote the research of superior laser for an atomic energy application.

Along this line, Special Committee on Laser Technology was organized to promote and support the related program.

As a results, in Japan, studies of FEL based on superconducting LINAC, relativistic electron beam and synchrotron radiations are started and it seems that rapid growth is shown in their activities.

Therefore it was quite timely that we had a special international meeting to look around the present status and look for future prospect of FEL and to see what kinds of effort are being devoted in Japan and also other countries.

In this sense, this meeting was successful by gathering the results due to various kinds of effort such as well known LINAC, synchrotron and also new system designing.

One of the strong impression given by some contributors of this meeting is that FEL is growing rapidly to be an exact laser as are solid state lasers and does no more stay in just a demonstrative level.

This meeting was started by the talk given by J.Madey titled as "The birth and future of the FEL", where he summarized his well known pioneer work. Together with historical overview, near future FEL technology as an ideal laser was proposed including the undulator technology in XUV regions.

A more precise talk was given by S.Benson and gave strong impressions to the audience that FEL is under changing to the new generation.

In his talk emphasis was paid to a new theory, a new system and an advanced technology. Harmonic generated light, single mode operation. MOPA System (oscillator plus amplifier), cavity dumping and loss modulation are one of these examples.

A new technology based on a photocathode injector was presented by S.Schriber. This will be soon proved as the key technology to support a compact advanced LINAC equipped with high current and high brightness.

Future application of the advanced FEL was cleaning summarized by C.Brau. Together with possible near future application presented by C.Brau, actually going on program in medical and biomedical application of FEL using 2-8μm was reported by R.Straight.

Beautiful results of FEL work given by Y.Petroff using synchrotron ring was very impressive. Wide variety of effort being devoted in Europe was also summarized by Y.Petroff.

Activities of many organizations in Japan was reported by K.Mima including a new conceptual designing of the advanced FEL. Among them, advanced X-ray undulators presented by H.Kitamura was very attractive. As understood from the titles of the program, various kinds of approach are taken to extend the field of FEL. Superconducting LINAC promoted in JAERI is worth watching.

Anyhow, through the meeting, the advantage of FEL as an electron-photon energy converter and its potential capability become very clear.

Finally as a chairman of the Specialist Committee, I would like to express my sincere thanks to all participants and am looking forward to seeing them again in the next meeting which are now on planning.

Professor Hiroto Kuroda (Univ. of Tokyo)
Chairman, Specialist Committee
on Laser Technology

1. THE BIRTH AND FUTURE OF THE FEL

John M. J. Madey
Duke FEL Laboratory
Duke University
Durham NC 27706 USA

It is a great pleasure to give a talk here on the FEL in general. I am going to talk about the principle of the FEL, its main features, its history, its applications, and problems to be solved to make FEL perfect.

When a relativistic electron beam, proceeding along with a photon beam, makes an oscillatory transverse motion in a "wiggler magnet", the electrons interact with the photons and can give part of their energy to the photons. Because of the bunching process during the course of the interaction, the photon beam becomes coherent, which is called the "free electron laser" or the FEL. A conceptual arrangement of the FEL is illustrated in Fig.1 The main ingredients of a FEL is a wiggler magnet, electron-beam source (accelerator), and optical-cavity mirrors. Also needed are electron "optics" to keep the good beam quality, structural support, and radiation shielding.

The periodic magnetic field of the wiggler is seen from the relativistic electron as a radiation, and then the electron is scattered by the radiation. Both the emission and absorption of photons are possible as shown in the level scheme in Fig.2. Note that the difference in level spacings for absorption and emission.

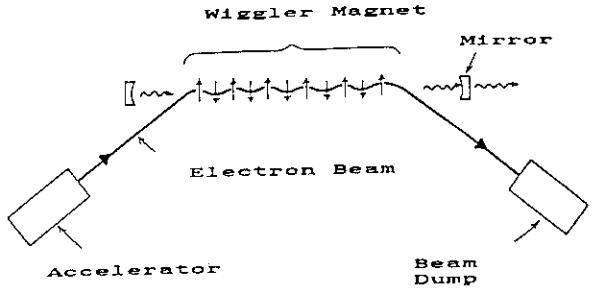

Figure 1 Conceptual arrangement of the FEL

The most salient feature of the FEL is its tunability. FEL operation is possible at all wavelengths longer than about 10nm, and individual FEL can oscillate within a wavelength range usually of factor 2 to 4. The mechanism of tunability is schematically illustrated in Fig.3. Electrons always travel at slightly less velocity than the light velocity because of the wiggling motion. The optical wavelength is equal to the spacing of the wave-fronts. Then, the wavelengths can be changed by altering either the wiggler period or longitudinal electron velocity.

The FEL can convert the electron kinetic energy directly into light. This means that there is no waste heat, in contrast to conventional lasers. Moreover, high peak and average power can be generated. No laser action occurs if no electrons are present, and so

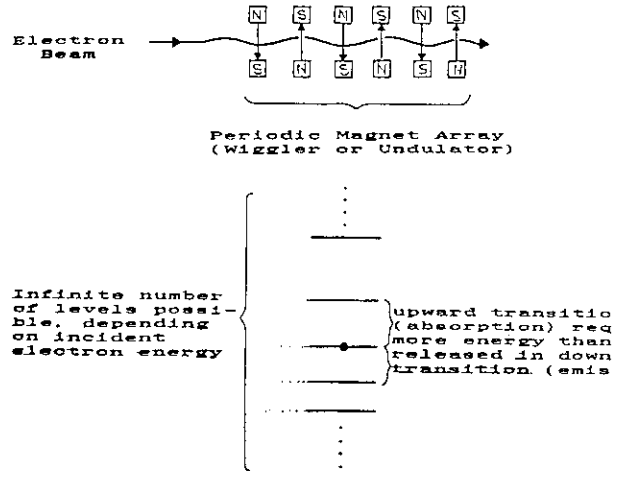

Figure 2 Energy levels of an electron in a periodic magnetic field

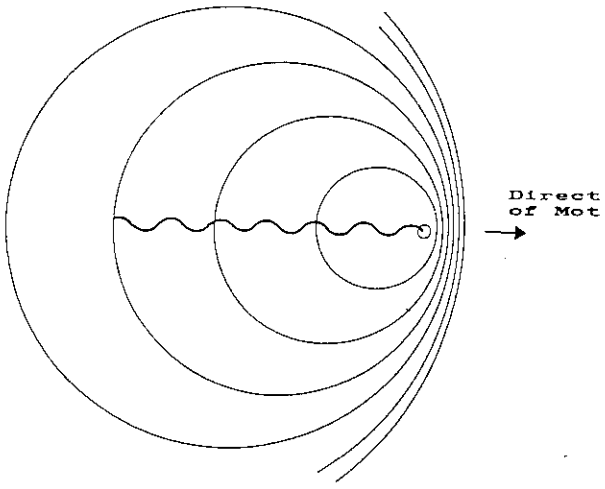

Figure 3 Mechanism of tunability

the pulse structure of the laser output resembles the electron beam structure. In the case of RF accelerators, the electron beam is bunched typically in 1∼10mm, and the bunch spacing is 0.1∼1m, as shown in Fig.4, and thus short-pulse laser can be obtained. High efficiency is achieved in the FEL because the deterioration of the laser medium, which is usual in conventional lasers, does not occur. Finally, the mode quality of the FEL is very good because the off-axis light is not amplified, as shown in Fig.5.

Tab.I shows typical examples of FEL characteristics in three wavelength regions. The FEL is a highly effective means to convert electrical energy into light, with the unique capability to operate at high power and high efficiency and with flexible, precise control of wavelength and pulse structure.

Tab.II shows the historical sequence of the conceptual and technological development before the "Birth of the FEL". The efforts to develop and extend the electron-beam technology ceased around 1960. At

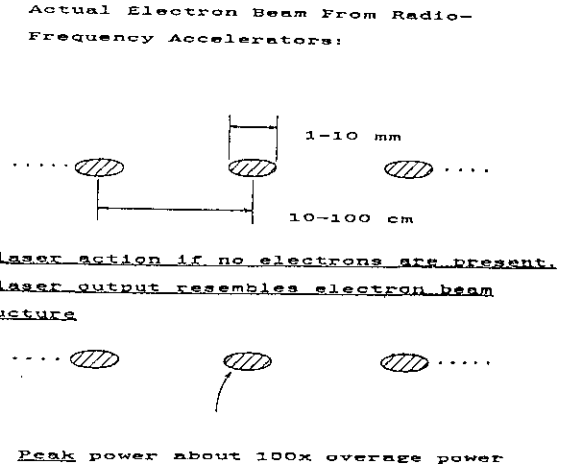

Figure 4 Pulse structure

At mm Wavelengths: ELF (LLL)

λ ~ 8 mm

P ~ 10^9 watts

Efficiency ~ 40%

At IR Wavelengths: MKIII FEL (Duke)

λ ~ 8 microns

P ~ 10^7 watts

Pulse length ~ 2 picoseconds

At UV Wavelengths: Novosibirsk

λ ~ 2500 Å

P ~ 10^4 watts

Pulse length ~ 200 picoseconds

Tabel I Typical examples of FEL characteristics in three wavelength regions

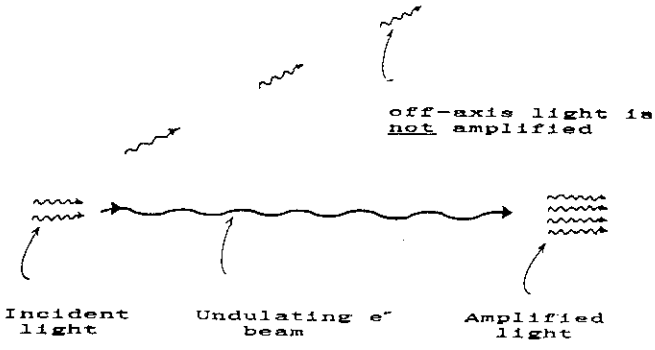

Figure 5 Optical mode formation

the time, there were many conceptual and technological limitations. There were limitations of slow-wave model. Especially there were no general guidance for selection of candidate radiations. As to the models for propagating electromagnetic fields, Fabry- Perot modes were not appreciated as means to couple electromagnetic energy to amplifying medium. The mirror reflectivity was low, and there were problems of optical damage. The iron-free permanent-magnet systems were not fully appreciated. There were no high-remanence magnetic materials, and the current den-

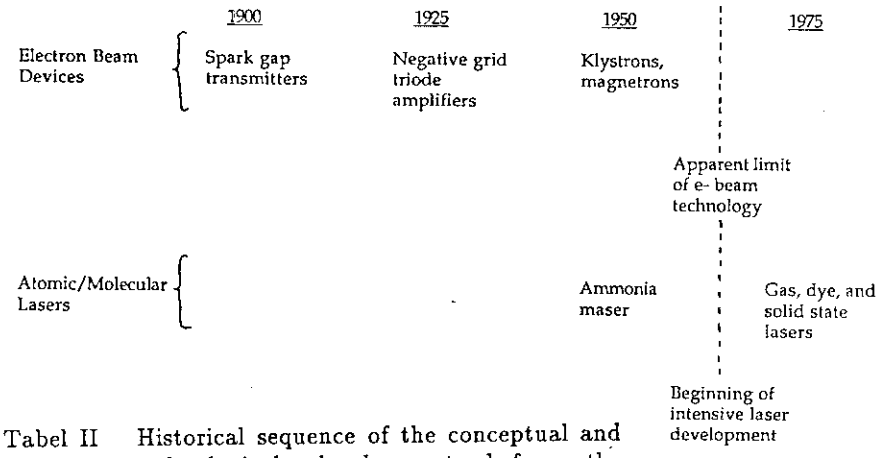

Tabel II Historical sequence of the conceptual and technological development before the "Birth of the FEL"

sity of superconductors was low. The low-gain amplifiers were not appreciated useful for high-power amplifiers. The relativistic electron-beam devices were not appreciated as useful, because the energy spread and emittance were large and the peak current was low.

The "Birth" of the FEL was made possible after many key developments. The conceptual development came from the development of atomic and molecular lasers. The concept of stimulated emission provided general guidance for selection of amplifying media. The "free-space" Fabry-Perot modes were successfully used for coupling, and useful oscillators based on "low-gain" amplifiers were realized. The technical developments came from availability of stable high-current relativistic electron accelerators, high-field superconductors, high-remanence magnetic materials, and laser-grade mirrors. The first measurement of FEL gain was performed at Stanford University superconducting linac by the use of a CO_2 laser, and a superconducting helical wiggler, and the oscillation was successfully achieved at 3.47μm.

The FEL is one of the energy-conversion technologies which have broad impact on many fields such as research, management, production, transportation, and health care. Current (or proposed) applications of FELs are listed in Tab.III. Further conceptual developments may be required in the fields of potential use.

Although the FEL technology has been demonstrated, further incremental engineering developments may be required to produce commercially functional high-power and short- wavelength sources. The FEL interaction must be optimized for higher gain, effective extraction, smaller linewidth, and so on. The supporting technologies should be refined and extended, such as electron gun and accelerators, magnetic undulators, and optics. As to the accelerator technology, the brightness, peak current, and diagnostics and control should be improved. The size and cost should be minimized. The undulator geometry should be optimized to match the laser operating requirements and accelerator specifications. The thermal and UV damage of the optical cavity is another serious problem to be solved. The thermal distortion of the mirrors should be minimized. In the shorter-wavelength region (UV and XUV), the reflectivity of the mirrors should be improved. The intracavity optical elements should be developed for output coupling, narrower bandwidth, and so on.

Electron-beam characteristics affect remarkably the FEL performance. The spatial distributions of the light produced by high-gain FELs is determined by the current, emittance, and energy spread of the electron beam rather than the configuration of the input optical mode. The radii of the propagating eigenmodes remain constant during the interaction (optical guiding). The small-signal growth rates of the propagating eigenmodes are monotonically increasing functions of electron-beam brightness. The radii of the propagating eigenmodes are monotonically decreasing function of the electron-beam brightness. Thus, the high- brightness electron beam is quite important for FELs. The microwave gun was developed to improve the brightness. As an example, Fig.6 shows the effect on the FEL gain of the energy spread and the emittance of electron beam for the proposed XUV FEL at Duke University.

Short-pulse FELs are quite useful for some kinds of applications. A pulse compression is possible using the energy chirping and a grating pair or a prism. A mode- control technique with a Michelson interferometer cavity is being developed.

Initial applications of low-power FELs as research instruments in chemistry, biology, and material science have already begun. The possibility

of exploiting the high peak power and short-pulse capabilities of existing FELs have been proven. The upgraded high-power and short-wavelength FELs are expected to be useful for specialized industrial applications such as isotope separation, XUV lithography, and machining of refractory materials. Refinement of conceptual models for materials processing will lead to more extensive photochemical and processing applications. Finally, the refinement of conceptual models for fusion will lead to proof-of-principle applications in energy production.

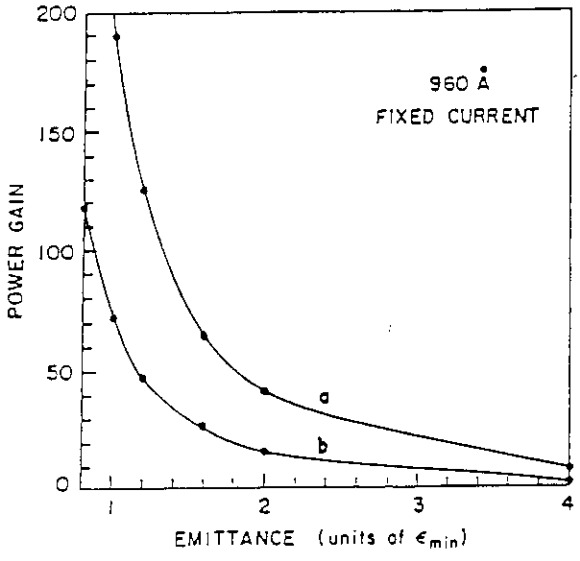

Figure 6 Effect on the FEL gain of the energy spread and the emittance of electron beam for the proposed XUV FEL at Duke University

Research:

Chemistry:
- Study of electronic structure and correlations in isolated atoms and ions
- Analysis of electronic, vibrational, and rotational energy absorption, transfer and dissipation
- Analysis of the conformation of complex and disordered molecules
- Synthesis of novel compounds

Materials:
- Properties of electronic and optical materials
- Properties of surfaces and interfaces
- Nonlinear effects
- Synthesis of new materials

Devices:
- Evaluation of high speed electronic and optical devices

Medicine and Biology:
- Genetics
- Immunology
- Cellular Metabolism

Energy:
- Diagnostics for magnetic confinement fusion

Management:
- Data collection (remote atmospheric sensing)

Production and Services:
- Isotope separation
- Laser machining of refractory materials
- XUV/Soft X-ray lithography

Transportation:

(None to date)

Medical Care:
- Orthopedic Surgery
- Neurosurgery
- Neoplastic Surgery
- Photodynamic Therapy/Blood Purification

Tabel III Current (or proposed) applications of FELs

2. Present Status of Free Electron Laser Research in Japan

K. Mima

Institute of Laser Engineering Osaka University
2-6, Yamada-oka, Suita, Osaka, Japan
(06)877-5111

§1. Introduction

FEL researches are going on at several universities and national laboratories in Japan. They are listed in Table 1.[1)~6)] So far, oscillation and amplification experiments in the optical regime have not been successful, although at ETL and Institute of Molecular Science, an optical klystron, a conventional wiggler and a resonator cavity have been installed to the storage rings.

In the millimeter and submillimeter regimes, the amplification and oscillation of FEL have been demonstrated at ILE / ILT Osaka University and the Institute for Physical and Chemical Research.

Institute	Accelerators	Parameters	Results
Tokyo University	RF linac	∿ 10 Mev	--
	Pulsed power Acc	∿ 1 MeV ∿ 100 A Cylindrical	--
Nippon University	Microtron	∿ 30 Mev 5 turn	--
Kanazawa University	Pulsed Power Acc	∿ 0.5 MeV	--
Osaka University (ILE-ILT & IIS)	Pulsed Power Acc	0.5 MeV ∿ 2 MeV 3 kA 100 ns	MW, Spectrum Narrowing, ASE output DFB FEL CO_2 laser interaction, visible light emission
	Induction Linac	3 ∿ 9 MeV 1 ∿ 10 kA	∿100 kW Oscillation Amplification 0.5 ∿ 2 mm wavelength
	RF Linac	6 MeV 30 MeV 120 MeV	Photo cathode + RF Gun Exp. }　--
Electrotechnical Lab	SR	230 MeV ∿ 10 mA	Gain Measurement Optical Klystron
National High Energy Lab	Induction Linac	∿ 1 MeV	--
JAERI	RF Linac	20 MeV	
	Induction Linac	1 MeV ∿ 2 MeV 3 kA	--
Institute of Molecular Science	SR	280 MeV 10 mA	Gain Measurement
The Institute for Physical & Chemical Research	Pulsed Power Acc	0.6 MeV 1 kA	Mode lock FEL 100 kW output

Table 1. FEL Facilities in Japan.

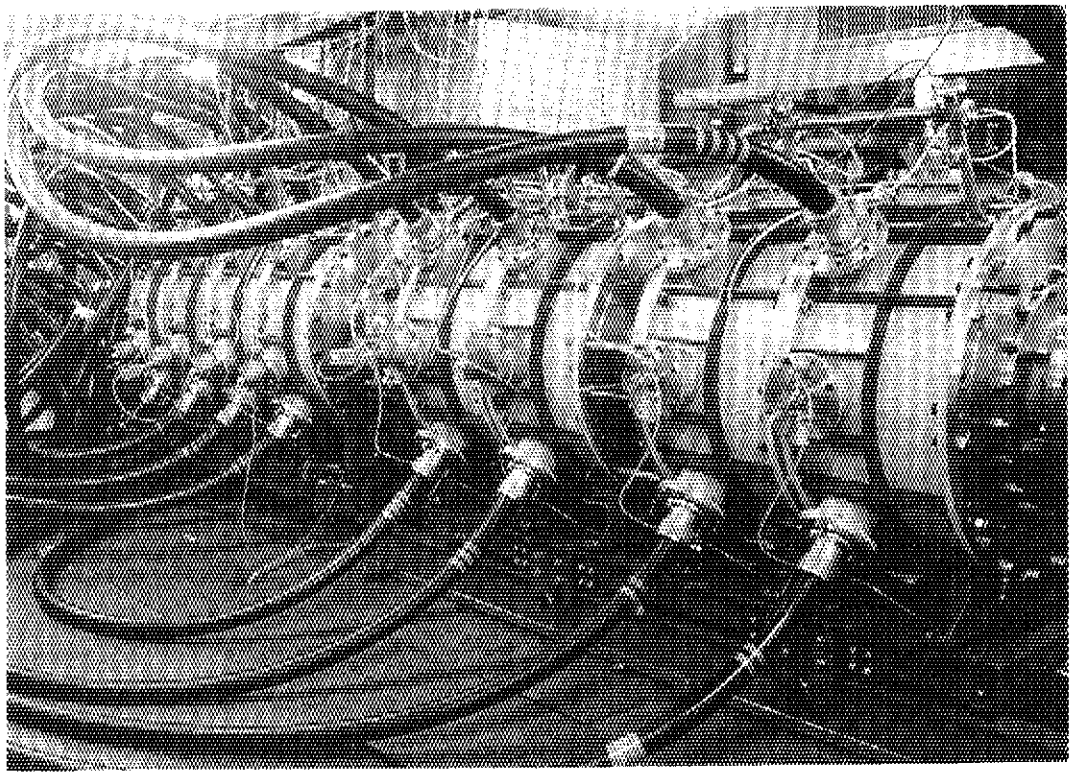

Fig.1 Induction linac at Institute of Laser Engineering

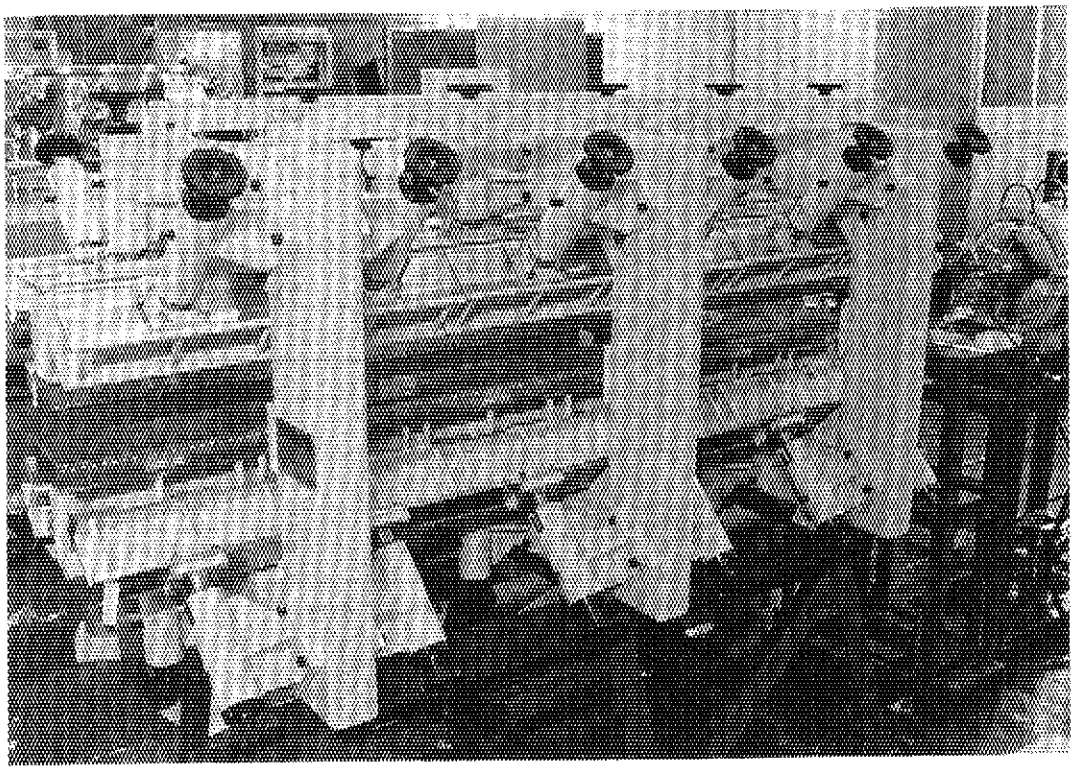

Fig.2 Permanent magnet wiggler at ILE, Osaka University

§2. Long Wavelength FEL Experiments.

At ILE / ILT Osaka University, an induction linac has been constructed (see Fig. 1).[1),2)] The beam energy increases up to 6 MeV. So far, amplified spontaneous emission and distributed feed back oscillation experiments have been done by the electron beam with 1.5~3.0 MeV. When an electron beam of 200A and 3MeV is injected into a 6cm period planer wiggler shown in Fig.2, the spontaneous emission intensity increases with wiggler length as shown in Fig. 3. This result indicates that the one path gain is 30 dB. The mean wavelength of the spontaneous emission is approximately 1 mm. Recently, a new wiggler with a period 2 cm was installed. As shown in Fig. 4, this wiggler has a horizontal focusing force. An example of the particle orbit is shown in Fig. 5.

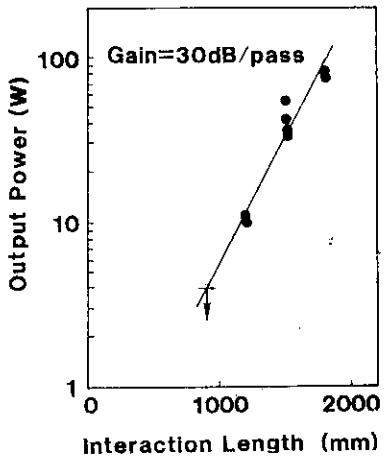

Fig.3 Small signal gain of the induction linac FEL at ILE, Osaka University

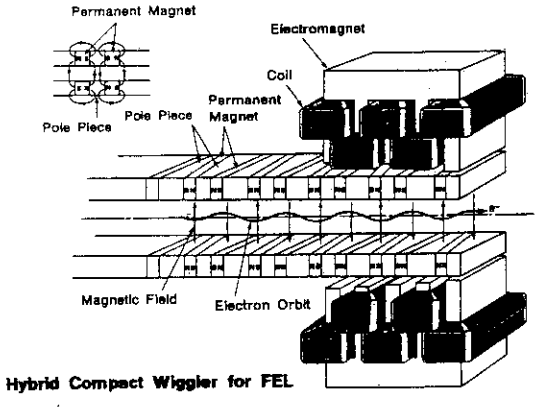

Fig.4

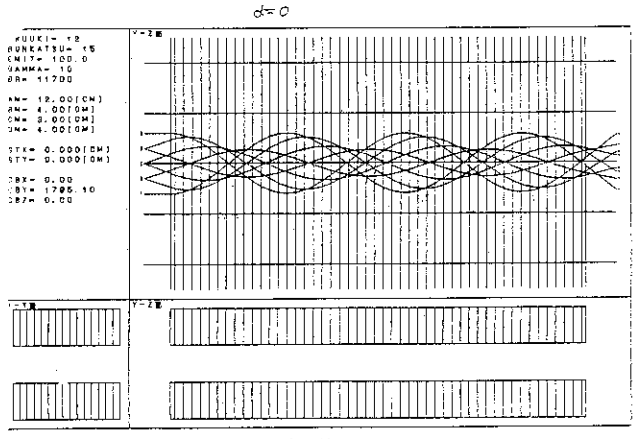

Fig.5

In the distributed feed back FEL experiment[7)], we used a corrugated waveguide shown in Fig. 6. When the Brag's reflection condition,

$$p\,k_d = k_f + k_b \quad o = 1, 2, 3, \cdots\cdots \qquad (1)$$

is satisfied, the radiations emitted by the electron beam are confined in the wave-guide to buid up. Here, $k_d = 2\pi / \lambda_d$, λ_d is the corrugation period, k_f and k_d are the forward and backward wave wavenumbers. In the present experiment, λ_d = 1mm and the FEL resonance occurs approximately at λ = 1mm. The Broag's condition is satisfied for p = 2 in this case. A typical radiation spectrum is shown in Fig. 7. As usual for the DFB laser, the observed spectrum has two peaks (See Fig.7-(b)). In order to clarity the effect of DFB, we compare the spectrum without DFB (Fig.7-(a)) with that with DFB (Fig.7-(b)). The spectral peaks at λ = 1.1 mm and 1.35 mm are significantly higher in Fig.7-(b) than in Fig.7-(a).[7)]

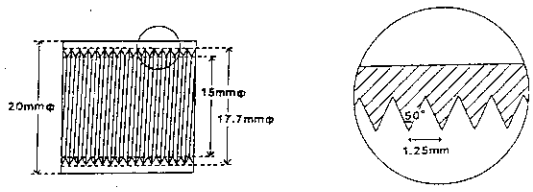

Fig.6 Configuration of DFB inside the waveguide

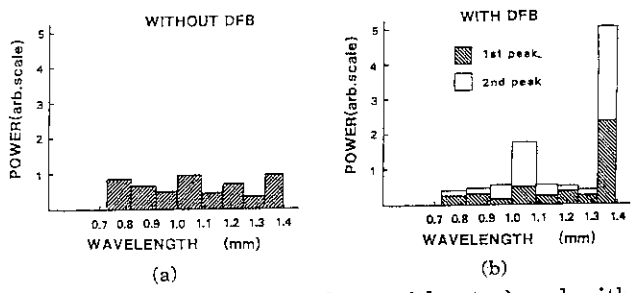

Fig.7 Output pulse waveform without a) and with DFB b).

At the Institute of Physical and Chemical Research, an electrostatic accelerator is used to produce 1 kA, 0.6 MeV beam. As shown in Fig. 8, a cold electron beam generated with a photo-cathode is injected into a wiggler with a period 4 cm.[5] The radiation is confined in a cavity which has tapered waveguide reflectors. The electron pulse length is about 200 ns. The optical pulse consists of a periodical short pulse train (see Fig.9). The period of the pulse train is 23 ns which coincides with the round trip time of a radiation in the cavity. Similar phenomena have been observed at MIT and University of California, Santa Babara.[9] This may be related to the bistability of a laser oscillator.[10] Such out-put power intensity fluctuation will be a serious problem in the FEL applications.

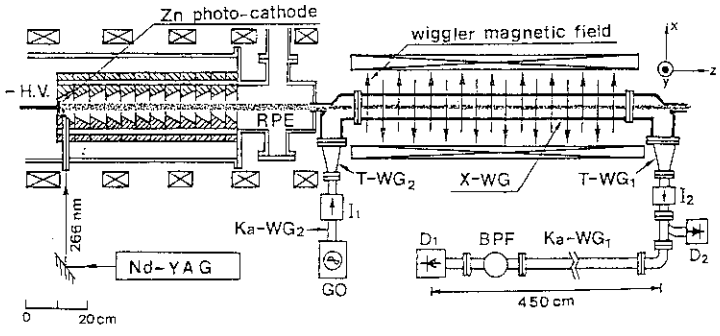

Fig.8 Experimental Facility at I.P.C.R.
(by Kawamura, Toyoda)

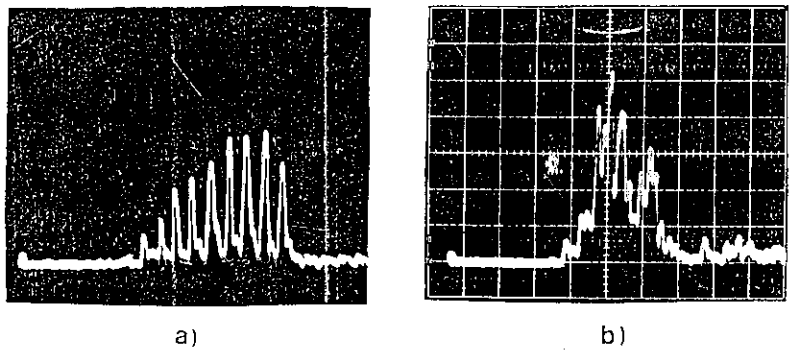

Fig. 9 Oscillation output pulse for Bw=0.54 kG and Bg=2.6 kG a) periodical short pulse train. T=24 ns , τ=4.8 ± 0.3 ns b) random pulse ,50 ns/div

Mode locking ↔ Mode Calculation

§3. Short wavelength FEL

At Electrotechnical Laboratory (ETL),[4] Institute of Molecular Science (IMS), Institute of High Energy Physics (KEK), Japan Atomic Energy Research Institute (JAERT)[5], [6] and Osaka project planned by Foundation of Osaka Science and Technology Center, the plannings, constructions and experiments of FEL driven by high energy electron accelerators are going.

At ETL, a 200MeV~500MeV storage ring (TERAS) is used to achieve FEL oscillation at the wavelength 570nm. In this FEL, a 1.47m optical klystron(O.K.) is installed in the 1.8m straight section of TERAS. The total FEL system was completed on August 1989. The total circumstance of the ring is 30m and the optical cavity length is approximately 5m. Three bunch operation at 240MeV is the operation mode for the FEL experiment. The minimum round trip cavity loss is less than 1×10^{-4} and the achieved one path gain is also 1×10^{-4} for 2 mA stored current. Since 1989, they try to increase the gain up to 1×10^{-3} by improving beam quality. In the same experimental group, a new storage ring (NIJI-IV) is under construction. One of the main objectives of this ring is the ultra violet FEL oscillation. Therefore, the shape of the ring is race track whose straight section is 7 m as shown in the schematic layout of Fig.10. In this straight section, a 6.2 m long optical klystron will be installed within a few years. The designed O.K. has a 43 period modulator (301cm), 21cm dispersive section and a 43 period emission section (301cm). One path gain is expected to be higher than 2.35% at 350 nm for 20 mA, 500MeV electron beam.

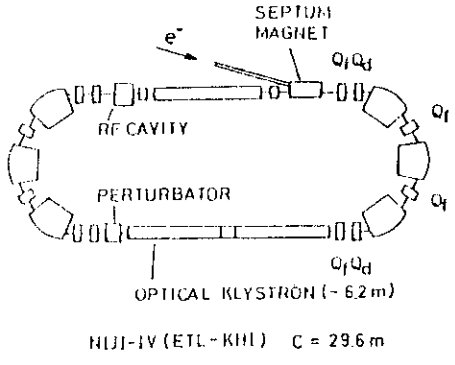

Fig.10Schematic layout of NIJI IV.

At JAERI, a super conducting RF-linac is under construction. The whole period of the project is divided into three phases. The phase-I is basically devoted to the fundamental R&D for 10.6μm wavelength lasing. In the second phase, by adding one more sc-linac and recirculating the electron beam, the beam energy will increase to be 100 MeV to achieve lasing of a visible light. Finally, a beam energy recovery system will be installed in phase-III. The main purpose of this project is the application of FEL to the laser isotope separation.

In the Osaka project planned by FOSTEC, 250 MeV RF linac will be buit for a UV FEL. This project is supported by various industries as well as Japanese government. The term period of the project will be seven years. The high power FEL will be completed within 5 years. After the completion of FEL, the various applications will be investigated.

FEL System for Fundamental Research

Accelerator Energy	250 MeV RF Linac (± 100MeV: Energy Dispersion Cavity)
Wiggler Magnet Field Pitch Length	 0.3 ~ 0.5T 2cm ~ 6cm 5m~8m
Laser out put Wavelength Peak power Average power	 1000 ~5000Å(3Wavelength Out put) 10^7W kW

(c. Table 2. Parameters of FEL Project proposed by Committee of FEL studies at Osaka Science and Technology Center.)

§4. Summary

In Japan, it is a very urgent target to achieve lasing in the optical regime FEL, although Raman regime FELs have been operated successfully. At present, many projects are going on to construct visible FELs at national laboratories and universities. Within a few years, those FELs will achieve lasing and are used for application researches.

References

1) K. Mima et al., Nucl. Instrum. and Methods, A 272 (1988) 106.
2) K. Imasaki et al., nucl. Instrum, and Methods, A 296 (1990) to be published.
3) Y. Kawamura et al., Appl. Phys. Lett. 51 (1987) 795.
4) T. Tomimasu et al., Nucl. Instrum, and Methods (1991) to be published.
5) Y. Kawarazaki et al., Nucl. Instrum and Methods (1991) to be published.
6) S. Takeuchi et al., JAERI-M 87-115 (1987) 16.
7) T. Akiba et al., Appl. Phys. Lett., 56 (1990) 503.
8) E. Jerby et al., MIT Plasma Fusion Center Tech. Report, JA-90-12.
9) L. R. Elias et al., Phys. Rev. Lett. 75 (1986) 424.
10) T. M. Antonsen and B. Levush, Phys. Fluids B1 (1989) 1097 and Phys. Rev. Lett. 62 (1989)1488.

3. Recent Developments in FEL Physics in the USA

Stephen Benson
Physics Department
Duke University
Durham NC 27706 USA

Developments in free-electron laser theory and technology fall into four basic categories—Basic FEL theory, systems demonstration, new accelerator technologies, and new laser technologies. This paper covers developments in these areas, concentrating on research carried out in the U.S.

1. FEL Theory

Three topics in the theory of FELs have been of great interest lately—FEL harmonic output, single mode operation, and laser chaos. New developments have been generated in each of these fields.

Harmonic lasing was achieved at both Stanford and Los Alamos, fulfilling a prediction of theory made by Madey in 1979. The Mark III lased at 4.8μm at the fundamental and 1.6μm at the third harmonic.

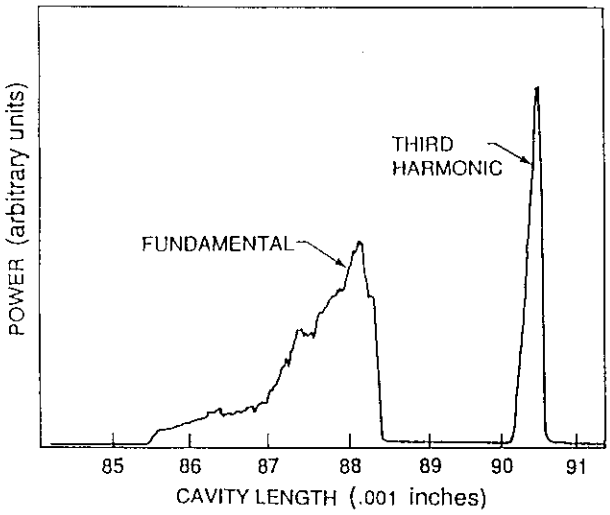

Figure 1 FEL power as a function of the laser cavity length

Figure 1 shows the FEL power as a function of the laser cavity length. The fundamental and third harmonic power are separated due to the dispersion introduced by an intracavity Brewster plate. This allows the laser to operate with either the fundamental or the harmonic with no interference of the two. The ratio of the third harmonic gain to the fundamental gain is seen to be 0.55 from figure 2. This is in quite good agreement with the theoretical prediction of 0.60. The theoretical prediction is actually more uncertain than the experimental number due to the lack of precision in the measurement of the energy spread of the beam. Figure 3 shows the power spectrum of the fundamental and third harmonic. Note that the third harmonic output is not quite at the third harmonic of the fundamental. The discrepancy is partially explained by detuning effects and saturation effects but about a third of the discrepancy is unexplained by one-dimensional theory and may be explained by guiding effects.

The characteristics of the generated harmonics have been studied both theoretically at Los Alamos as well as experimentally at Los Alamos and Stanford (by Deacon Research). In figure 4 we show the power of the generated coherent harmonics measured on the Mark III accelerator and the Los Alamos theory. The agreement is rather good. In figure 5 we show the spectral linewidth as a function of the harmonic number. A simple theory predicts that the linewidth should vary as I/h where h is the harmonic number. This is clearly not the case in the data. The discrepancy is believed to be in the model. The harmonic power is probably not generated uniformly in the microbunch, so it has a much larger spectral bandwidth than expected.

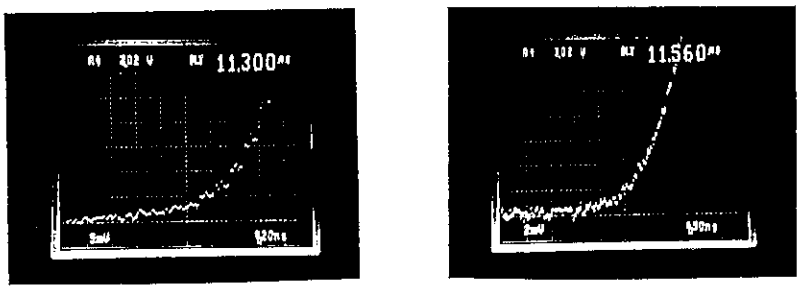

Figure 2 The ratio of the third harmonic gain to the fundamental gain

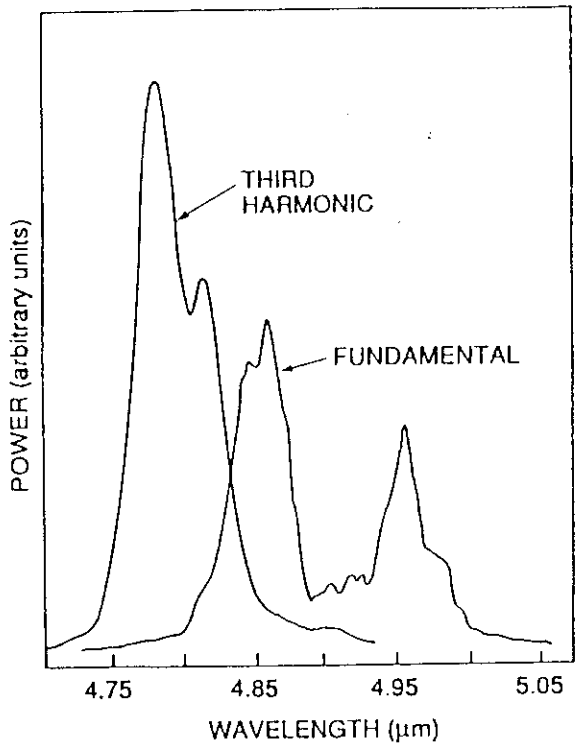

Figure 3 Power spectrum of the fundamental and third harmonic

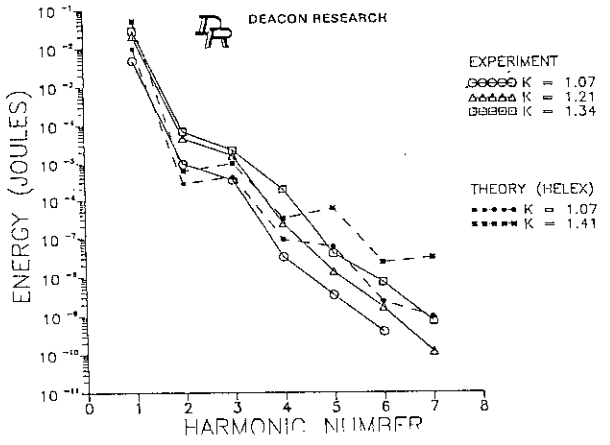

Figure 4 Power of the generated coherent harmonics measured on the Mark III accelerator and the Los Alamos theory

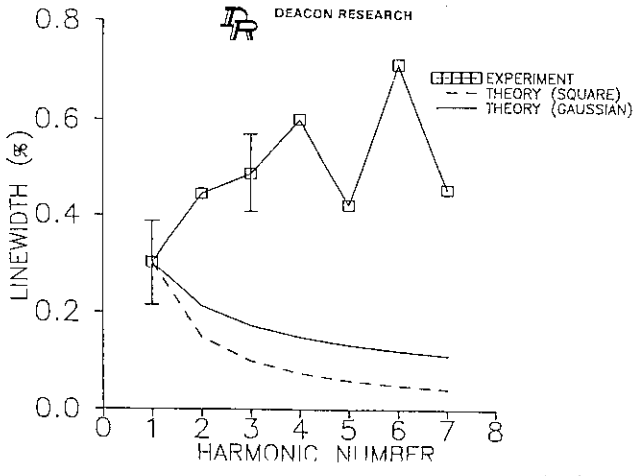

Figure 5 Spectral linewidth as a function of the harmonic number

There has been some speculation that single mode operation in a free-electron laser is possible with no external mode selection. Recently single longitudinal operation of an FEL was demonstrated at UCSB. This is still not completely understood on the theory side. It dose not occur on every laser shot and the discrepancy is not that it occurs at all but that it occurs so often. Only about a third of the pulses are single mode. To be useful, external mode selection is needed.

Finally, a Stanford/TRW collaboration observed chaotic operation at zero cavity length detuning as predicted in FEL simulations. This is shown in figure 6. In figure 6a the power vs. time during a macropulse is shown. For more cavity lengths the power is quite stable. At the synchronous power the power becomes quite unstable and the power is maximized. The spectrum also becomes unstable and the wavelength varies randomly. This behavior is quite similar to prediction of one dimensional simulations with noise added. It is not certain if this is the same behavior however since experimental causes such as frequency jitter have not been ruled out.

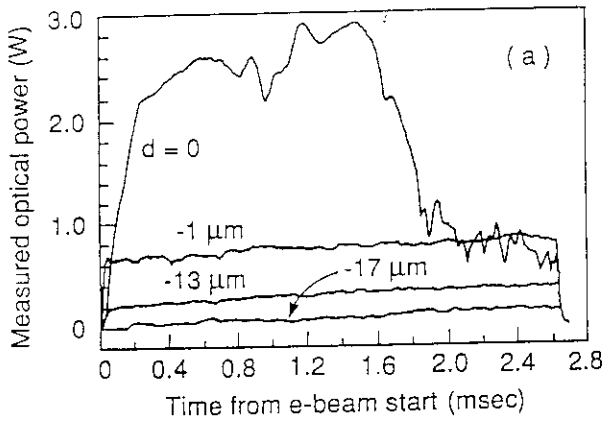

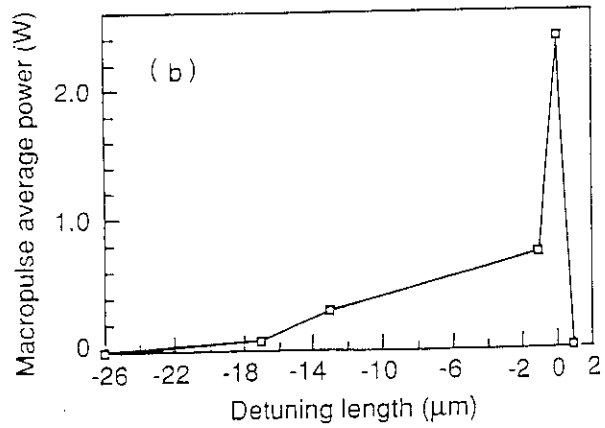

Figure 6 Chaotic operation at zero cavity length detuning

6a Power vs. time during a macropulse

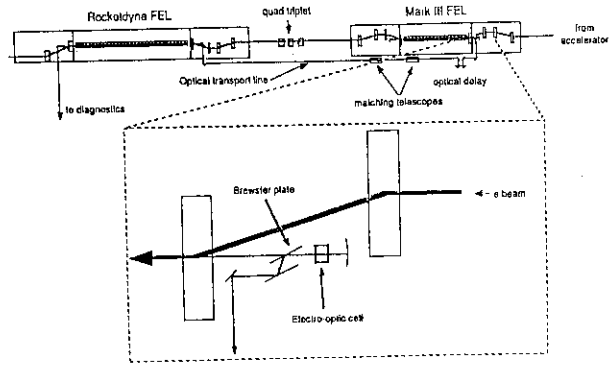

Figure 7 Schematic view of an all FEL MOPA demonstrated at Stanford using the Mark III laser as the master oscillator and the Rockwell laser as the power amplifier.

2. New System

Several new systems have seen operation or are under development. An all FEL MOPA has been demonstrated at Stanford using the Mark III laser as the master oscillator and the Rockwell laser as the power amplifier. This is shown schematically in figure 7. The purpose of this experiment was to study the physics of such a system and to develop related technologies. The design has the advantage of using a single electron beam and if the amplifier is a high gain high extraction device, offers the possibility of high extraction without optical damage problems. The MOPA system has proven to be a very powerful diagnostic. Figure 8 shows the gain vs. delay with theoretical fits assuming a Gaussian and a top hat electron pulse. Obviously the top hat pulse is almost

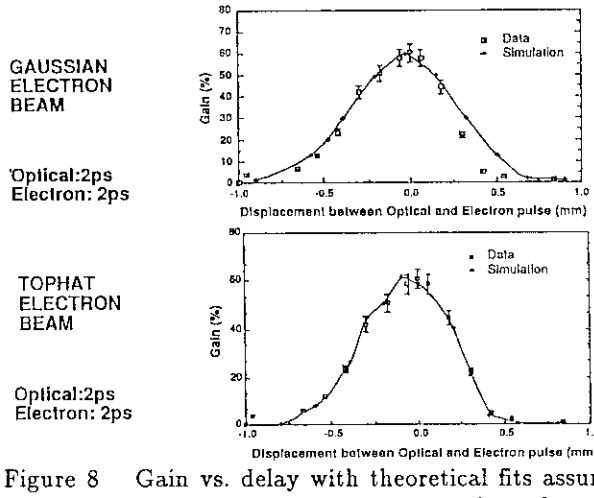

Figure 8 Gain vs. delay with theoretical fits assuming a Gaussian and a top hat electron pulse

perfect. Note that this is the best measurement to date of the electron pulse length in the accelerator. This experiment also demonstrated a very asymmetric gain curve vs. wavelength tuning. This has been shown by simulation to be due to might gain three dimensional effects. It is a clear violation of the Madey gain-spread theorem, which assumes a one-dimensional system. The system has also demonstrated some new technologies with the first demonstration of a intracavity loss-modulator and cavity dumper on a free-electron laser. This is discussed in section 3.

A FEL driven by electrons from a laser-irradiated photocathode was demonstrated for the first time at Stanford in a collaboration between Stanford and Rockwell. The timing sequence for the system is shown in figure 9. A mode locked Nd:YAG laser operating at 95.2MHz is amplified and frequency tripled. The light is then directed onto the LaB_6 cathode surface producing a very bright electron beam. The FEL lased easily with such a high quality beam. The optical microstructure in the laser beam was now evident . The parameters of the system with thermionic and photocathode operation are shown in table 1. Although the beam is of very high quality, further development is needed in the realm of laser stability. Fluctuations in the drive laser caused very large fluctuations in the FEL power as shown in figure 10.

FEL studies are continuing at UCSB with the introduction of a new short period undulator with a tuning range of 130μm to 500μm. Two new systems are soon to come on line elsewhere. Los Alamos has most components of their HIBAF (High Brightness Accelerator Facility) system installed. This system will use a photocathode gun with high conversion efficiency to produce a 45MeV beam with a brightness 100 times better than their previous accelerator.

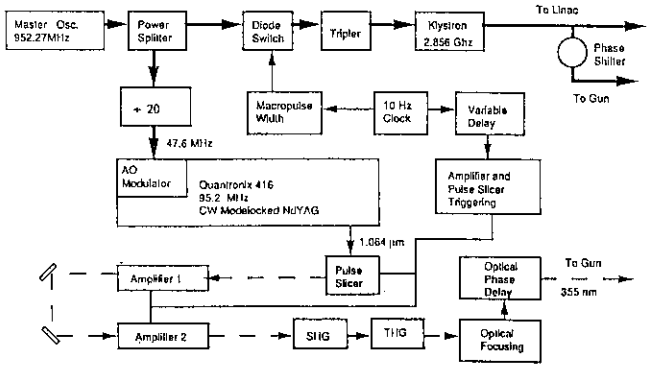

Figure 9 Timing sequence for the system driven by electrons from a laser-irradiated photocathode at Stanford

Parameter	Thermionic Operation	Photocathode Operation	
	typical	typical	Maximum
Small signal gain (per pass)	60%	100%	150%
Micropulse charge (pCoul)	70	170	250
Micropulse current (A)	35	60	85
Normalized emittance (mm-mrad)			
$\gamma\beta\varepsilon_x$	10π	8π	
$\gamma\beta\varepsilon_y$	4π	4π	
Peak brightness (A/m^2)	1.8×10^{11}	3.8×10^{11}	5.4×10^{11}

Tabel I Parameters of the system with thermionic and photocathode operation

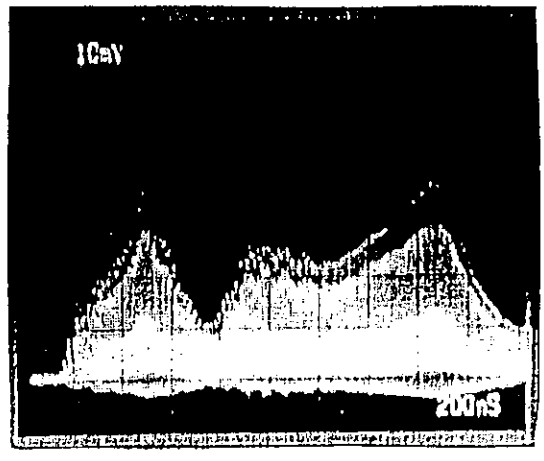

Au - Ge detector

Figure 10 Fluctuations in the FEL power caused by fluctuations in the drive laser

Vanderbilt University is installing an infrared FEL system. This laser will be a user facility and is nearing completion. It is the first commercial FEL system to be built to date.

The other interesting development was the operation of a Van de Graaf accelerator with a continuous 100mA beam at Argonne National lab. This opens the possibility of a CW FEL if the current can be raised by a factor of 20.

3. FEL technology

Most interesting developments in FEL technology relate to the optical cavity. At Los Alamos researchers have successfully suppressed the sideband instability using an intracavity Littrow grating. Used in conjunction with a high extraction efficiency laser this can increase the extraction efficiency by a factor of two to three by preventing detrapping of electrons.

Cavity dumping and loss modulation was tested with a CdTe electro-optical cell in a configuration illustrated in figure 11. The loss-modulated and cavity dumped power output vs. time is shown in figure 12. Only 5 or 6 bunches out of a possible 60 lased and the cavity was dumped in 5 round trips. Insertion losses were quite acceptable initially but gradually increased to over 50% per round trip. This is believed to be be due to some contaminant which migrated from the electrodes or surrounding ceramic to the cell. Though technical problems must be overcome to make this approach work, it dose look promising.

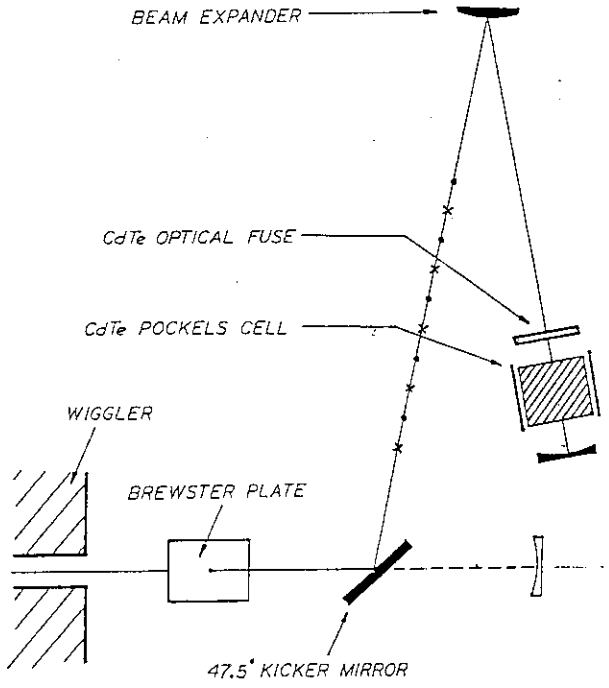

Figure 11 Configuration of cavity dumping and loss modulation test with a CdTe electro-optical cell

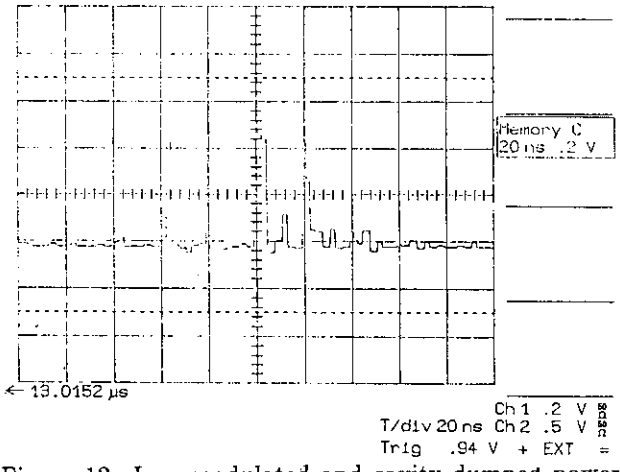

Figure 12 Loss-modulated and cavity dumped power output vs. time

UCSB has also demonstrated cavity dumping using an intracavity silicon Brewster plate which is switched to a mirror using a visible laser to produce charge carriers. That group has also demonstrated injection locking which seems to give stable single mode operation at the injected frequency.

Simulations by both the Dutch group FELIX and at Duke have demonstrated the feasibility of using a Michelson or Fox-Smith resonator to phase lock multiple bunches in a FEL driven by a RF linac. Figure 13 shows the two cavity configurations which allow missing between adjacent microbunches in the optical cavity. Figure 14 shows simulations of the evolution of the spectral power in the laser as the laser turns on. One can select one of the longitudinal modes using a Fabry-Perot interferometer in order to get a very high resolution tunable laser in the infrared. This could be used for spectroscopy in the infrared.

Finally, the push to shorter wavelengths has been aided by the characterization of UV mirror degradation by Deacon Research. In figure 15 we show the losses induced on a mirror by synchrotron radiation from the Brookhaven storage ring. The losses reach a maximum and then disappear. This must be done slowly enough that thermal damage is not sustained on the mirror surface.

The possibility of operating in the VUV has been raised by the demonstration of high reflectivity in a

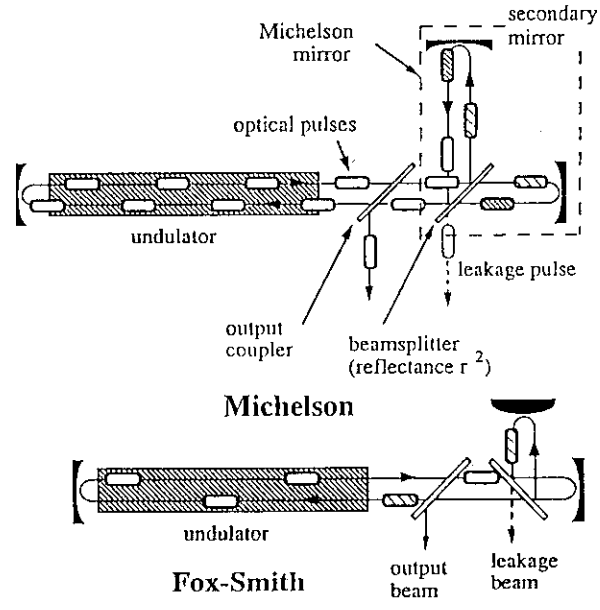

Figure 13 Two cavity configurations which allow missing between adjacent microbunches in the optical cavity.

whispering gallery mode mirror at 85nm by Newnam at Los Alamos. That group demonstrated 89% reflectivity at 85nm using a sequence of 9 mirrors each bending the beam by 20%. The high reflectivity was attained using in vacuo deposited aluminum in a UHV environment.

In the future, optical cavity developments should dominate advancements in the field of free-electron lasers since the gain medium is more or less understood.

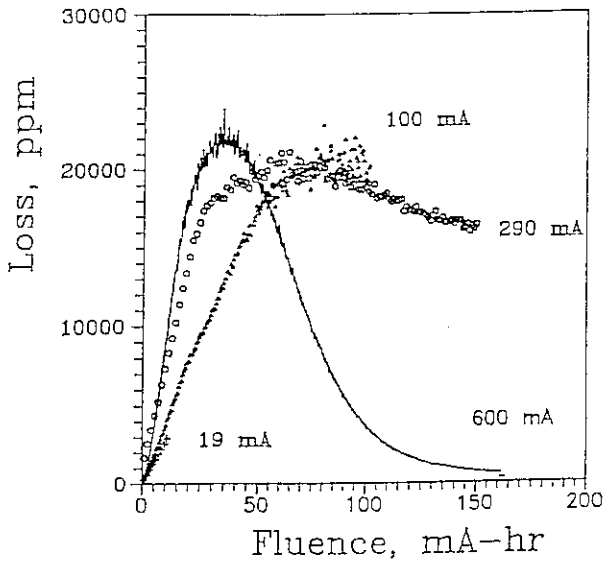

Figure 15 Losses induced on a mirror by synchrotron radiation from the Brookhaven storage ring

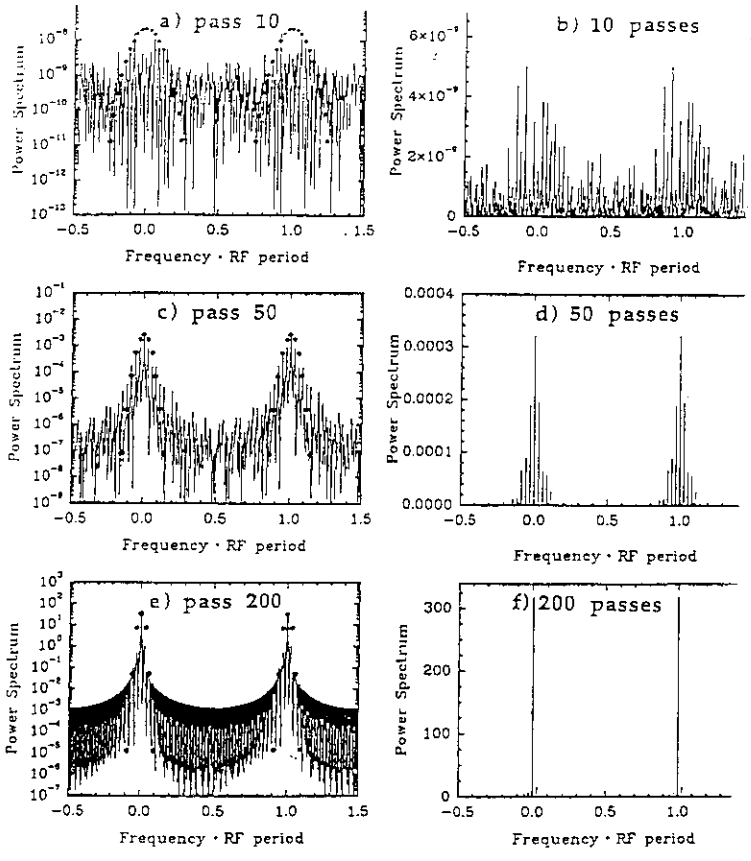

Figure 14 Simulations of the evolution of the spectral power in the laser as the laser turns on

4. PHOTON STORAGE RING:POSSIBLE NEW SCHEME FOR A FREE-ELECTRON LASER

Hironari Yamada

Quantum Equipment R & D Department,
Sumitomo Heavy Industries, Ltd.
2-1-1 Yato-cho, Tanashi-city, Tokyo 188, JAPAN

1. Introduction

The photon storage ring(PhSR) is the name given to a newly proposed instrument, which accumulates synchrotron radiation, functions like an undulator, and thus has the potential to be a new type free-electron laser.[1] In this scheme relativistic electrons move in a circular orbit instead of in an undulating trajectory. Radiation from the circulating electrons is reflected ,back to the same orbit by a cylindrical mirror surrounding the electron orbit, and interacts with the electrons leading to modulation of the electron density. In this paper we only discuss the electron storage ring which has an exactly circular orbit, with the mirror positioned concentric to the electron orbit. The PhSR may be feasible when the electron storage ring having an orbit diameter less than 1 meter is used. Such a machine, which is called AURORA , is now available.[2] The cylindrical mirror curvature is made so that the reflected radiation always coincides with the electron bunch when it contacts the orbit. This apparatus possesses the best features of the undulator[3]. Advantages of using the PhSR for an FEL are the following. 1)The radiation power is fully extracted through a simple exit opening in the mirror surface. 2)Off-tangentially emitted radiations are focused at the electron orbit by the cylindrical mirror regardless of the magnetic field strength. 3)The mode of the generated light wave in the cylindrical mirror cavity has a strong azimuthal electric field component collinear to the electron velocity. This azimuthal electric field has the same phase velocity as that of the electrons.

In the next section we discuss the principle for generating spontaneous coherent radiation in the PhSR. Section 3 is devoted to the mechanism and features of FEL emission. We give some idea on the maximum power and the minimum wavelength obtainable from the PhSR in section 4.

2. Principle for spontaneous coherent generation in the PhSR

The PhSR is composed of a number of bending magnets producing synchrotron radiations from relativistic electrons and mirrors surrounding the electron orbit. One can imagine it to be like an electron storage ring(ESR) placed in the middle of a ring of wall mirrors or a large cylindrical mirror. The schematic configuration of such a PhSR is given in Fig.1, where the electron orbit is an exact circle. The mirror is shown just for convenience as a single solid unit having one photon beam exit channel. The exit channel, which can be several, is just a simple opening in the mirror surface. The importance of this simple opening is that in the case of a conventional FEL the photons between cavity mirrors are extracted through either a half-mirror or a Q-switch, thus limiting the efficiency of photon-beam extraction. In the case of the PhSR 100% of the photons are extracted through this simple opening. The vertical profile of the mirror is designed to focus the photon beam onto the electron orbit. The mirror is placed under high vacuum .co

between the poles of the magnet on the same plane as the electron orbit. The position of the mirror is arranged to ensure that the electron orbit and the mirror curvature are exactly concentric. If the electron orbit and the mirror curvature are concentric, it is apparent geometrically that any synchrotron radiation emitted in a tangential direction from the electron orbit will be reflected back tangentially into the same orbit by the cylindrical mirror. As a consequence all radiation is gathered by the cylindrical mirror and follows the determined paths, finally leading to the exit opening. Because of this fact the instrument was named the photon storage ring. The synchrotron radiations normally wasted onto the chamber wall are all utilized by the help of the cylindrical mirror.

If the mirror radius is set at an arbitrary value, a series of photon bunches will be observed at the exit channel at almost random time intervals. It is, however, possible to combine photons originating from different electron bunches by adjusting either the mirror radius or the electron orbit radius. Specific setting makes it possible that at the moment the reflected photon bunch contacts with the electron orbit, one of the electron bunches will reach the same point. Assuming that the ESR is in operation with two electron bunches, the condition that any reflected photon bunch coincides with another electron bunch is simply calculated. According to the configuration in Fig. 2, photons are emitted at point A by the electron bunch x. These photons recontact the electron orbit at point C after reflection at point B, within time T_p, shown by $T_p = 2\rho \tan(\theta)/c$, where ρ is the radius of the electron orbit, and c the speed of light. The angle θ is defined as AOB, where O is the center of curvature. The electron bunch y takes time T_e to arrive at point C, shown by $T_e = (2\theta + \pi)\rho / v_\theta$ where v_θ is the angular speed of the relativistic electrons. If $T_p = T_e$, the electron and photon bunches meet together with exact timing. The relationship between the electron orbit radius and the mirror radius R is given by the equation: $R = \rho/\cos(\theta)$. For instance taking the electron orbit radius to be 0.5m, we have a solution to the above coincidence condition giving R as approximately 1.485846m.

It is apparent that since the two

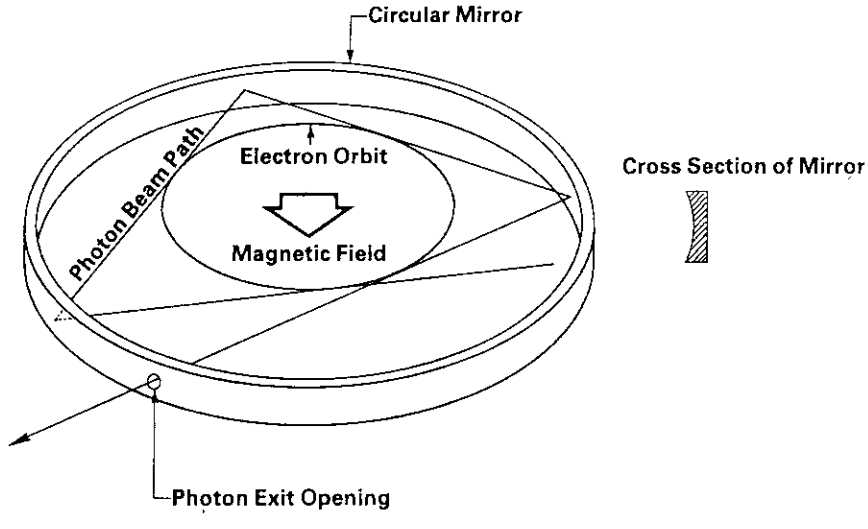

Fig. 1. A schematic view of the proposed photon storage ring.

electron bunches are symmetrically located, the meeting of the photons with one electron bunch is followed by the meeting with the other electron bunch. Also note that the above condition is satisfied at any point on the electron orbit. As a consequence any reflected photon bunch always meet with one of the electron bunches as they contact with the electron orbit. In other word electrons are always associated with the reflected radiation.

The above discussion is based on a condition that photons are bounced only once before intersecting electrons, however photons might be bounced more than once, and also the electron bunch is not necessarily the one immediately following the bunch which first emitted the photons under consideration but could be any later bunch including the original bunch. A general form of the condition for the meeting of electrons and photons can then be written taking into account the number of reflections, q, and the number n, indicating the n'th electron bunch following the last one. Additionally the harmonic number, k, is not necessarily two. Thus the equation becomes:

$$0 = 2q\rho\tan(\theta)/c - (2q\theta + 2n\pi/k)\rho/v_{\theta}. \quad (1)$$

Set the mirror radius according to Eq.(1), then the reflected photon bunches are superimposed and appears in the same time interval as the electron bunches when q=1. It is well known that synchrotron radiation is incoherent light, and the simple superposition generally produces incoherent radiations.

The spontaneous coherent radiation is, however, possibly generated in the PhSR, when the mirror radius is precisely set to an appropriate value, as a result of interference of radiations. This mechanism is better understood from Fig.3. In this figure the circulating electron beam is viewed from the stretched photon path representing the z-axis, which finally leads to the exit channel. In reality, the mirror is assumed to be placed between the arcs of the electron orbits. In the previous paragraph we discussed the capability of adjustment of the timing between photons and electrons to cause them to coincide at the peak of each electron orbit in the figure. This implies that even a phase between one electron and one light

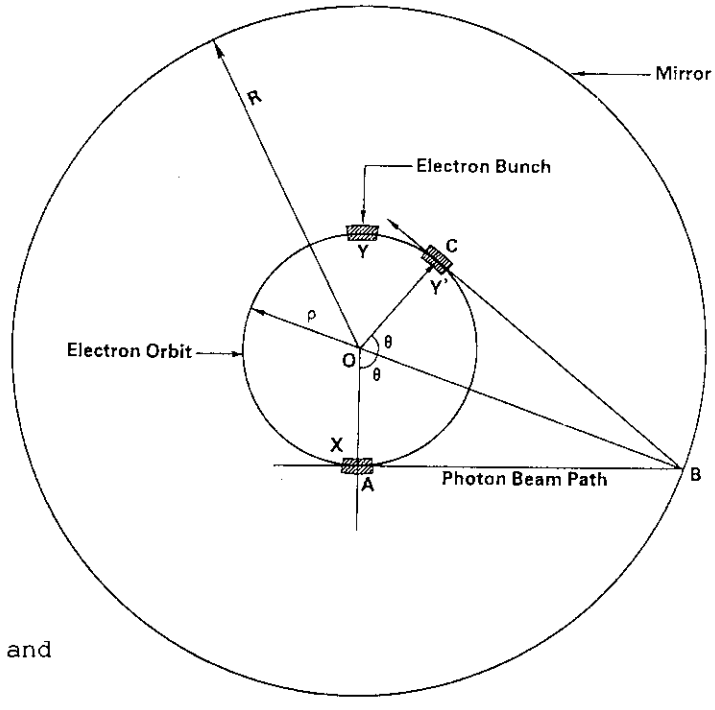

Fig.2 Diagram explaining synchronous relationship between the electron bunch and the light pulse.

pulse can be precisely adjustable. Radiation is emitted from the tops of the orbit at the desired periodicity so as to interact coherently. One can see here the similarity of configuration between the PhSR and the undulator, except that only part of the periods of "wiggle" is present. The wavelength λ of the spontaneous coherent radiation is given by the following equation:

$$m\lambda/c = (2q\theta + 2n\pi/k)\rho/v_{\theta} - q(2\rho\tan(\theta) \pm \mu\lambda)/c, \quad (2)$$

where m, an integer is a higher harmonic number of the wave. It is important to note that μ is necessary to take into account the progress of the phase when the photon is reflected by the mirror. The minimum wavelength λ of the generated coherent radiation depends roughly on the size of the electron bunch. Also we can say that it depends on the extent of the electron density modulation under the laser oscillation.

Equation (2) actually represents three different operation modes which can be selected by the mirror radius. The first mode appears when the mirror radius is set so that the radiations from different electron bunches interferes with each other. In this case the minimum obtainable wavelength of the coherent radiation is longer than the electron bunch size which is a couple of cm in the case of AURORA[1], or the extent of the electron density modulation. On the other hand, when only one electron bunch is made to be involved in the interference, a fundamental wavelength shorter than the bunch size is possible, since the radiations from the same individual electron interfere coherently. This second mode is obtained for n/k=1 in Eq.(2). The third mode is selected when the mirror surface is set close to the electron orbit. The radiations from the same electron always interfere. This specific mode, which is more like the undulator, is given for n = 0 and q = 1 in Eq.(2). For instance set the mirror radius to be 0.501m with an electron orbit radius of 0.5m, then a fundamental wavelength of 84 μm is obtained. A smaller mirror radius generates a shorter fundamental wavelength, although the minimum mirror radius is limited by the electron beam size. When the electron beam path is too close to the mirror surface, the effect of the wake field to the electron beam may become serious. In the section 4 the problem of beam size is again discussed in more detail.

One advantage of the PhSR is the focussing power of the radiation due to the cylindrical mirror. The radiation emitted off-tangentially is again focused at the electron orbit after each reflection. This compares favorably with the undulator in which the radiations emitted off-axially simply diverge. This likely feature is explained in Fig.4. The radiation emitted at point A at an angle α with regard to the tangential line merges again at point A' on the electron orbit, while the radiation emitted in the tangential direction contacts the orbit at point A". Separation of the points A' and A"

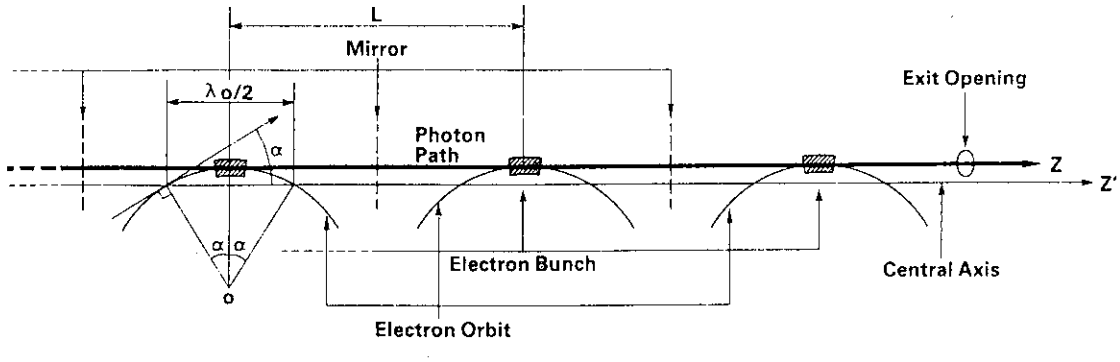

Fig.3 The electron trajectory is viewed from the stretched photon path as z-axis. Equivalence of the PhSR to the undulator is demonstrated.

increases as this emission angle, α increases. However the timing between the light pulse and the electron is almost unchanged by α, since both the light pulse and the electron bunch take an equally greater time to arrive at point A'. Taking into account the emission angle α, Eq.(2) is modified as shown:

$$m\lambda = (2q\theta + 2n\pi/k)\rho/\beta_\theta - q(2\rho\cos(\alpha)\tan(\theta) + \mu\lambda). \quad (3)$$

The radius r shown in Fig.4 is of the circle to which the off-tangentially emitted radiation contacts tangentially, and is related to the emission angle α as given: $r = \rho\cos(\alpha)$. On the other hand, the angle 2θ through which the radiation travels from the point of emission to the point of the next contact(one period of the PhSR), is correlated to α. The shift of θ is, here, expressed as a function of α for small values where $\alpha << \theta$:

$$\theta - \theta_o \simeq \cos(\alpha)\tan(\theta) - \tan(\theta_o) \simeq \alpha^2/(2\tan(\theta_o)), \quad (4)$$

where θ_o is the value of θ at $\alpha = 0$. Substituting Eq.(4) in (3), one can see that Eq.(3) is independent of α, and is identical to Eq.(2). So the wavelength shift is negligibly small for small values of α. In fact α is as small as $1/\gamma$, where γ is the Lorentz factor and is of the order of milliradian. It is concluded that if the electron orbit is an exact circle and the mirror is made ideally, there are, in principle, no factors which deteriorate the interference effect.

3. Mechanism for coherent generation

Amplification of the radiation in the PhSR results from coupling the coherent light wave and the electrons, which leads to modulation of the electron density at a spacing of the resonating wavelength. Only when this modulation is generated, does the sum of the radiations become coherent and gain is expected. The PhSR should function as an FEL, since it follows the same principle as the undulator as discussed in the previous section. However, two major differences must be recognized; first, that the corresponding single period of the PhSR is, in the normal sense, incomplete and second, that the interaction between the wave and electrons occurs continuously along the electron orbit. Also it is important to

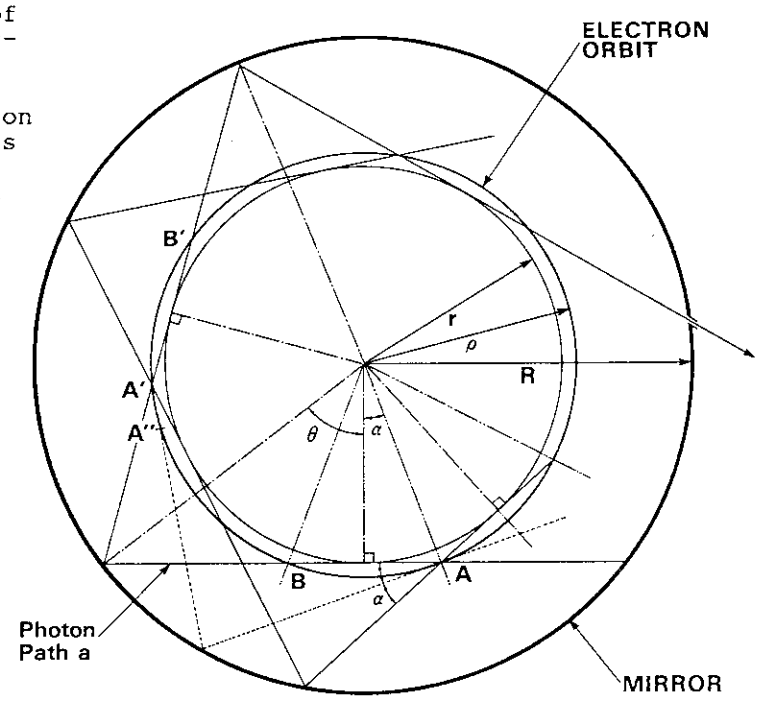

Fig.4 Focussing mechanism of radiation in the photon storage ring. The radiation emitted off-tangentially is always focused at the electron orbit. The laser emission is expected to propagate along the off-tangential line such as path a.

note that the electron energy is refreshed at every revolution. In the following, we will focus our discussions to these particular aspects of the PhSR.

Let's suppose that coherent radiation is generated in the PhSR, this radiation should propagate along an off-tangential line such as path a in Fig.4 to prepare for the deceleration of the electrons. Only when the radiation path acrosses the electron orbit, the electric field component of the radiation appears in a direction of the electron velocity. Furthermore, once the interaction occurs at point A in the mode decelerating electrons, the interaction should occur again at point B in the same mode for a successive coherent generation. To accomplish this scheme, the phase of the coherent light wave must be shifted by 180 degrees as the beam progresses from point A to B. This resonance scheme is essentially the same as that for the undulator-based FEL. Then the resonating wavelengths(λ_R) must satisfy the relationship:

$$(1/2+m')\lambda_R = 2\rho(\alpha/\beta_\theta - \sin(\alpha)), \quad (5)$$

where m', an integer is a higher harmonic number, ρ is the electron orbit radius, α indicates the emission angle of the radiation path from the tangential line as shown in Fig.4, and β_θ is the electron angular velocity relative to the speed of light. The resonance condition for the undulator-based FEL is obtained in the same fashion as described above, although the formula is slightly different from Eq.(5), due to the difference in the shape of the electron beam trajectory which is not exactly a circular path. It must be, however, stressed that in the case of the undulator the resonance wavelength is uniquely determined by this sort of equation, but it is not the case for the PhSR, since the photon path under consideration is selected arbitrarily. If the angle α is appropriately selected any wavelength satisfies the above equation. For this reason the resonance wavelength must be determined either by external or by other internal means. When the wavelength is selected, the coherent radiation must follow the particular radiation path which is subjected by Eq.(5). The modulation develops from the spontaneous coherent radiations stored in the PhSR due to the mechanism discussed in the previous section. So the wavelength is determined by the mirror radius setting relative to the electron orbit radius following Eq.(3), and the gain appears for the radiations propagating the particular path which satisfies Eq.(5). Selection of the wavelength is achieved more effectively by the help of gratings partly replaced with the mirror. The grating is made so that the selected coherent wave follows the radiation path determined by Eqs.(5) and (3). The value m = 0 in Eq.3 may be chosen, because it is no longer necessary to select the wavelength through Eq.(3). The cylindrical mirror may be partly replaced by the gratings so as to minimise resultant radiation power losses. An alternate method to select the wavelength is to inject a powerful laser beam along a selected radiation path, again determined by Eqs.(5) and (3). In this case the PhSR is used as an amplifier.

The mechanism of coherent generation in the PhSR follows the same principle as that of the undulator, but the electric field component is differently generated along the electron orbit. The coherent radiations emitted with either + or − α with regard to the tangential line add coherently at the electron orbit, since both light pulses travel exactly the same distance until they contact the electron orbit again. The interference of these two coherent light pulses generats a strong electric field collinear to the direction of the electron velocity. In fact this azimuthal electric field must be strongest at the electron orbit because of the focussing power. It is also noted that the phase velocity of this azimuthal electric field at the electron orbit is almost same as the angular speed of the electrons. So the electrons experience the deceleration or acceleration force continuously until the electrons and the wave go to totally out of the phase due to their energy loss.

The azimuthal electric field (E_θ) discussed above may be analyzed as a problem of waves in a circular cylindrical cavity with short height. The eigen functions for this problem are given by Bessel's function, and the transverse elctric field component is expressed by the derivative of Bessel's function J(kr) as shown:

$$E_\theta = AJ'(kr)\cos(n\theta)\sin(k_3 z)e^{i\omega t} \quad (6)$$

The frequency of the transverse electric mode (TE mode) is determined by the fact that J'(kr) must be zero at the circular cylindrical mirror surface. There is an infinite discrete set of modes. In the case of the PhSR, the modes are, in practice, selected either by the processes discussed earlier; internal means, or by external means such as a grating, or injection of a laser beam. It is worthwhile to mention that such transverse electric modes have actually been observed in a circular cylindrical ruby laser when particular modes were selected externally[4]. So the dynamical analysis of the electron motion should take this transverse electric mode generated along the beam trajectory into account.

4. Wavelength and output power

In the previous section, we discussed the static nature of the PhSR leading to the coherent generation, and examined the necessary fundamental conditions. In order to calculate the gain of the PhSR-FEL, a dynamical analysis of the electron motion under the dipole magnetic field and the transverse electric field discussed above has to be carried out along the beam trajectory. The size of the electron beam and the accuracy of the mirror surface also have to be taken into account for a realistic simulation. The quantitative analysis of the electron motion and the gain is now under progress.[5] In this section we discuss the required mirror surface accuracy, and the possible minimum obtainable wavelength. The saturation power is also calculated without concerning the details of the beam dynamics.

The accuracy of the mirror curvature is an important factor in a discussion of the monochromaticity and the minimum wavelength. The inaccuracy ΔR of the mirror curvature causes a deviation of the phase $\Delta\Phi$ as given by the following equation,

$$\Delta\Phi = 8\pi\cdot\sin(\theta)\cdot\Delta R\sqrt{N}/\lambda, \quad (7)$$

where N is the number of bounces. Within the present limit of technology the achievable accuracy can be within a few nanometers. Thus the minimum obtainable wavelength is limited to the order of hundreds of nanometers on assumption that the number of the bounces is around 1000. As long as visible light is concerned the mirror might not limit the wave length.

For a more realistic estimate, it is necessary to take into account the size of the electron beam, the amplitude of the betatron oscillation, and the synchrotron oscillation. It is noted that one period of the PhSR, which is 2θ is comparable to or longer than its betatron oscillation period, when the first and second modes of the wavelength selection mechanism in section 3 are chosen. This is compared with the period of the undulator, which is much shorter than its betatron oscillation. If the electron position is displaced in the radial direction by the betatron oscillation from its previous value at the successive meeting, the phase between electrons and photons will be changed. Since the period of the PhSR is comparable with that of the betatron oscillation, the displacement can be substantial. In order to cancel out this effect the betatron number might be chosen to be as close as $(q\theta + n\pi)/(p\pi)$, where p is a positive integer, q is the number of reflections. In this way we can set photons to always meet electrons at the same phase of the betatron oscillation. If the third mode of the wavelength selection mechanism is concerned, we need not worry about this problem, since the period of the PhSR is very short compared to the betatron oscillation.

The synchrotron oscillation is another problem, as it periodically varies the electron energy. The shift in electron energy changes the electron orbit radius, which causes a phase shift between electrons and the coherent radiation. The energy shift, ΔE, of the relativistic electron corresponds to the variation in electron orbit radius, $\Delta\rho$, according to the relationship $\eta\,\Delta E/E = \Delta\rho/\rho$, where η is the momentum compaction factor. Usually the synchrotron oscillation has a much longer period than that of the electron revolution. In the case of AURORA which has 0.5m orbit radius, 650 MeV electron energy, and about 100 keV synchrotron oscillation amplitude, since the synchrotron oscillation period is 100 times longer than the revolution time, the energy shift per revolution is less than

10 keV on average. This value corresponds to a radial displacement of about 7 μm. This amount is considerable, but it should be remembered that the energy of the major portion of the beam remains unchanged by the synchrotron oscillation. The energy loss due to the synchrotron radiation itself is rather considerable, which is 31keV per revolution under the present scheme of AURORA, even though the energy is refreshed at each revolution. The shift in the wavelength $\Delta\lambda$ is calculated according to the following equation:

$$\Delta\lambda = (2q\theta + 2n\pi/k)\,\eta\,\Delta E/E. \qquad (7)$$

Thirty-one keV corresponds to a variation of 0.1mm, which is apparently too large for short wavelengths. An appropriate design for the electron storage ring is quite important for the construction of the PhSR. For instance 300 MeV might be a reasonable electron energy to be chousen. The energy losse due to synchrotron radiation is only 1.4 keV, which results in only 15 μm of the shift in wavelength. It should, however, be remembered that the low energy electron beam must be selected at the expense of lower synchrotron radiation yield per unit orbit length. In summarizing sub-milimeter wavelengths seem not too difficult to generate within the present scheme of AURORA and the mirror fabrication technology. To improve the performance of the PhSR to a wavelength less than 1 μm, we may require a reduction in the electron orbit radius and in the electron beam size. The operation of the electron storage ring at higher harmonics may help the situation, as is known from Eq.(2). The increased rf-cavity number will also improve the matching condition, since it reduces the amplitude of the synchrotron oscillation.

The intensity($dI(\omega)/d\Omega$) of the spontaneous coherent radiation is simply calculated as a superposition of the normal synchrotron radiations coherently as shown by:

$$\frac{dI(\omega)}{d\Omega} = \frac{e^2}{3\pi^2 c}\left(\frac{\omega\rho}{c}\right)^2\left(\frac{1}{\gamma^2} + \Psi^2\right)\cdot$$

$$\left[K^2_{2/3}(\xi) + \frac{\Psi^2}{\gamma^{-2}+\Psi^2}K^2_{1/3}(\xi)\right]\left(\sum_N f^N \delta\left(\frac{\omega}{\omega_o} - m\right)\right)^2 \qquad (8)$$

where the definitions of the synchrotron radiation intensity are taken from Chapter 2.2 of ref.[6]. The above equation is valid for all integer harmonic number m, because the electron beam experiences the deviation only in the one direction as shown in Fig. 3 and the radiation emitted off-tangentially focuse at the electron orbit. The reflection coefficient, f, of the mirror and the number of reflections, N, is also taken into account. If the electron orbit is a perfect circle and the electron beam size is negligibly small, the intensity of the specific wavelengths is enhanced by a factor of $(\Sigma fN)2$ over that of the normal synchrotron radiation. Since the number of bounces N is effectively infinite, this factor becomes $1/(1-f)2$.

The maximum power of the FEL emission obtainable from the PhSR is calculated in a sophisticated manner as shown in the following. The maximum power is limited by the amount of the phase shift due to the total energy loss of the electrons in one revolution(or in one aceleration period if the number of rf-cavities is more than two). When the electrons lose their energy continuously in the PhSR due to the spontaneous.

emission as well as the stimulated emission, the electron position will be shifted to an inside orbit, and then appears to be advanced azimuthally. This phenomena, called a negative mass effect, is totally different from that of the undulator, in which the electron position is shifted relatively backward due to the energy loss. The laser power saturates when the phase shift due to the shift in the orbit radius, $\Delta\rho$ reaches; $\Delta\rho\alpha < \lambda/2\pi$. Then the corresponding total energy loss (ΔE) of one electron in one revolution is given by the following equation:

$$\Delta E = \frac{E}{\eta}\left(\frac{\lambda}{2\pi\rho}\right)^{2/3}, \qquad (9)$$

where η is the momentum compaction factor, E is the electron energy. Note that the energy loss due to stimulated emissions is equal to the amount being subtracted for the total energy of the synchrotron radiation, given by ΔE-E(SR). It is concluded from Eq.(8) that a longer wavelength and a shorter electron orbit radius produces more output power from the PhSR. Give an example for 100 μm wavelength, the maximum obtainable radiation energy from one electron in one revolution is 306 keV when the electron energy is 300 MeV, while the energy removed as synchrotron radiation is only 1.4 keV. Of course it must be remembered that the actual maximum extraction power is limited by the rf power, which is 30 KW in the present scheme of AURORA. Furthermore the total extracted power is largely depend on the electron beam quality. The energy spread due to the electromagnetic interaction itself must be also taken into account. Not all the electrons may experience the maximum energy loss, but it is expected that no matter how samll the gain is, as long as it has a positive value, the laser power should grow until the maximum energy loss of one electron finally reaches the above value. The above value for the one electron energy loss is considerably large.

The laser power obtainable from the PhSR comes from the energy of the electromagnetic field which causes the electron the above amount energy loss. Thus much more radiation power than the electron energy loss in one revolution is accumulated within the cylindrical mirror cavity. The mean electric field, $\langle E_\theta \rangle$, which contributes to the electron energy loss on average is given as:

$$\int -e v_\theta \langle E_\theta \rangle dt = 2\pi\rho e\langle E_\theta \rangle = \Delta E\text{-}E(SR). \qquad (10)$$

The energy density, u, of the radiation at the electron orbit is:

$$u = \frac{\epsilon}{2}\{\langle E_\theta \rangle^2 + \langle E_r \rangle^2\}, \qquad (11)$$

where $\langle E_r \rangle$, the radial component of the electric field, is linked to $\langle E_\theta \rangle$ through a factor F which is usually much larger than unity. Then the average energy, U is calculated as follows:

$$\frac{dU}{dt} = S\cdot\Delta\tau\cdot f_r\cdot c\cdot u$$

$$= S\cdot\Delta\tau\cdot f_r\cdot c\cdot\epsilon\left[\frac{F(\Delta E\text{-}E(SR))}{e2\pi\rho}\right]^2, \qquad (12)$$

where S is the cross sectional area of the laser beam to be observed, and f_r is the revolution frequency. Pulse width of the laser beam, $\Delta\tau$, which is similar to the electron bunch size, is also taken into account. As is shown here, the PhSR comprises a promising new type of free-electron laser which is expected to generate extremely high power.

5. Conclusion

A new type of free-electron laser named "Photon Storage Ring"(PhSR) is proposed. The primary features of the PhSR are obtained from a simple geometrical analysis, which may be summarized as follows. (1)The simple opening in the mirror surface provides complete photon beam extraction, whereas the Fabry-Perot type cavity for the conventional FEL provides partial extraction. So most of the generated synchrotron radiation is utilized. (2)The PhSR is, in principle, equivalent to an undulator having an infinite number of periods. In addition the radiation emitted off-tangentially is focused again at the electron orbit by the surrounding mirror regardless of the magnetic field strength, so that an ideal interference effect is expected. (3)The introduction of the strong magnetic field which increases the radiation rate per length

of the electron orbit, never causes any deterioration of the interference effect, while in the case of the undulator the magnetic field strength must be limited so that the K-value is close to or smaller than unity. (4)The specific wavelength enhanced by the interference is tunable by changing the radius of the electron orbit. (5)A strong electric field collinear to the electron velocity is induced along the beam orbit, and interacts with electrons continuously leading to modulation of the beam density. All the above indicated features favor the new type of free-electron laser based on the PhSR.

The author would like to express sincere thanks to Professors K. Shimoda(Keio Univ.), K. Mima(Osaka Univ.), and T. Sasaki(KEK) for their valuable discussions.

References

[1] H.Yamada etal., Rev.Sci.Instrum. Vol.60(7) (1989) 1786.
[2] H.Yamda; Japanese J.Appl.Phys. (Letter), Vol.28(9) (1989) L1665.
[3] For instance S.Krinsky etal.; "Handbook of Synchrotron Radiation",Vol.1a, Ed. E-E.Koch, North-Holland, 1983, p146-158.
[4] T.Yajima, F.Simizu, and K.Shimoda; Japanese J.Appl.Phys. Vol.2 (1963) 322.
[5] K.Mima, K.Simoda, and H.Yamada to be published.
[6] S.Krinsky etal.; the same book as ref[3], p80.

5. COHERENT SYNCHROTRON RADIATION BY A SHORT ELECTRON BUNCH

T. Nakazato, M. Oyamada, N. Niimura, S. Urasawa R. Kato and Y. Torizuka(a),
Laboratory of Nuclear Science, Tohoku University
Mikamine Taihaku-ku Sendai 982, Japan
022-245-2151

Y. Shibata, K. Ishi, T. Ohsaka, T. Takahashi, H. Mishiro and M. Ikezawa,
Research Institute for Scientific Measurements, Tohoku University
Katahira Aoba-ku Sendai 980, Japan
022-227-6200

Y. Kondo,
Department of Applied Physics, Faculty of Technology, Tohoku University
Aramaki Aoba-ku Sendai 980, Japan
022-222-1800

ABSTRACT

Coherent effects in synchrotron radiation (SR) have been observed for the first time from 180 MeV short electron bunches of 1.7 mm using the Tohoku 300 MeV Linac. The intensity of the coherent SR was about 10^5 times as strong as that of incoherent SR at wavelengths of 0.33 to 2.0 mm. This enhancement factor roughly corresponds to the number of electrons in a bunch. The SR intensity showed a quadratic dependence on the electron beam current. The radiation was mainly polarized in the orbital plane. The possibility of induced rf in a vacuum chamber was excluded experimentally. An electron linear accelerator will be applied to a strong light source from infrared to millimeter wavelengths instead of the storage rings. The bunch length of shorter than 1 mm can be observed by the spectrum measurement of coherent SR.

I INTRODUCTION

It was January, 1989 that the coherent synchrotron radiation (SR) was observed (1) for the first time from the short electron bunch obtained by the Tohoku 300 MeV linac. In this paper we will present further conformation and new experimental results.

Coherent effects of radiation in an accelerator were considered theoretically by L. I. Schiff (2) in 1946 as the power loss limiting the energy achieved by the accelerator. In 1982 the possibility of intense coherent SR in an electron storage ring was proposed by F. C. Michel (3) from viewpoint of the astrophysics of the pulsars. A small bunch of the electrons might emit coherent SR at wavelengths which are comparable to or longer than the longitudinal bunch length. The SR intensity was expected to be intensified by the number of electrons in a bunch, which is about 10^{10} in an ordinary electron storage ring. Therefore we might be able to obtain an intense photon flux with a continuous spectrum in far-infrared to milli/submillimeter wavelengths.

A positive sign of the presence of coherent SR has been observed by J. Yarwood et al. (4) in SRS, Daresbury. However, its existence has not been conclusively established by their experiments nor by those of E. Schweizer et al. (5) in BESSY, Berlin. In a recent experiment G. P. Williams et al. (6) at NSLS, BNL could observe no enhancement. In these experiments the wavelength region observed was much shorter than the bunch length, which is several centimeters in the ordinary storage rings. In this paper we will take "bunch length" to be the longitudinal bunch size.

Table 1 Parameters of the experimental condition.

Accelerator	
Accelerating frequency	2856 MHz
Beam energy	180 MeV
Beam energy spread	0.2 %
Beam current	2 μA max
Pulse width of the burst	0.1 - 2 μsec
Repetition of the burst	300 Hz
Longitudinal bunch length	
without debuncher	1.7 mm
with debuncher	15 mm
SR measurement	
Bending magnetic field	0.247 T
Acceptance of SR	70 mrad
Analyzing range	0.1 - 2 mm
Resolution	1 cm^{-1}

II EXPERIMENTAL METHOD

As the experimental equipment is described in detail in Ref.1, the parameters of the experimental condition is concluded in Table 1.

Followings are those of improvement on the experiment of Ref.1. A long bunch of 15 mm could be obtained by using an energy compressing system (7) or a debuncher. The SR spectrum was monochromatized by gratings and longwave pass filters in the FIS-3 far-infrared spectrometer (Hitachi Co. Ltd.), and detected with a liquid-He-cooled Si bolometer. To avoid absorption by water vapor all the light passage was evacuated. The only material in the light path was a quartz window separating the beam line vacuum and the monochromator vacuum.

The absolute sensitivity of this measuring system was calibrated with a mercury discharge lamp, which was supposed to be a blackbody radiation source of 4000 K (8,9) at these wavelengths.

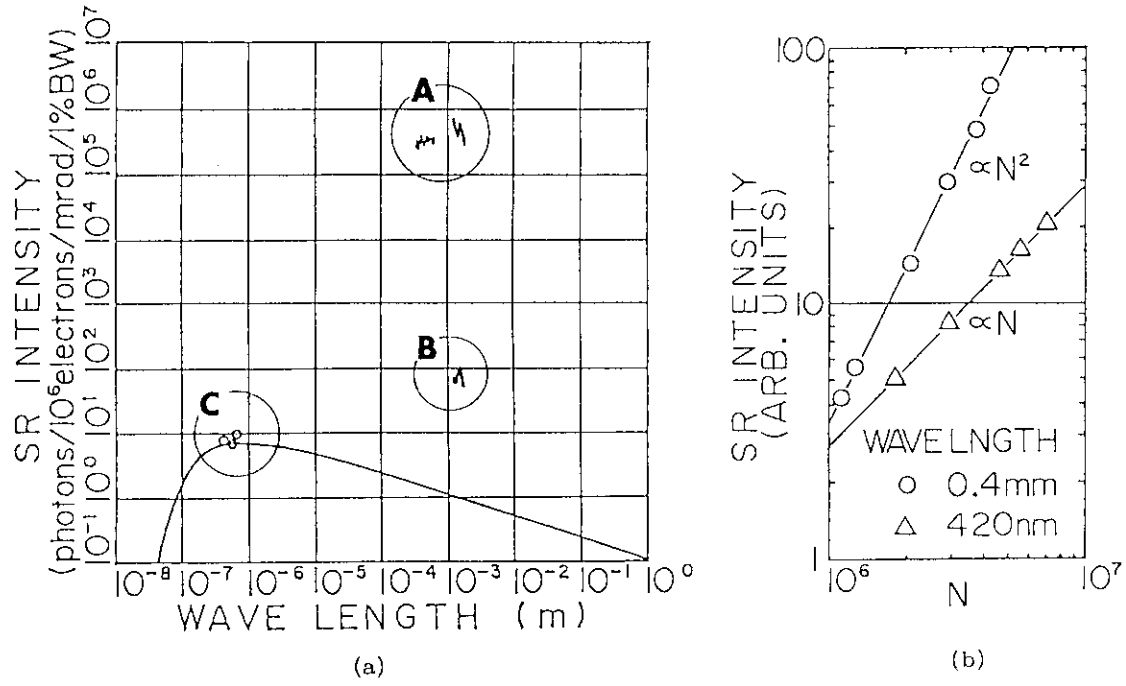

Fig.1. Observed SR spectra (a) and beam current dependence of the SR intensity (b).
(a) Data in circle "A" and "C" are the spectra for the bunch length of 1.7 mm, and in "B" for 15 mm. All the data are measured with the same optical system. A solid curve shows the incoherent SR intensity calculated for this experimental condition. These intensities are normalized for a bunch of 10^6 electrons.
(b) N is the number of electrons in a bunch, which is proportional to the beam current. The values of intensity should not be compared between two wavelengths.

The SR intensity at visible wavelengths was measured with the same optical system and same calibration procedure in order to confirm the correctness of the absolute data. A photomultiplier tube with color glasses and interference filters was used instead of the Si bolometer. A calibrated halogen lamp was used as a standard visible light.

III EXPERIMENTAL RESULTS

As is shown in circle "A" of Fig.1.(a), the SR intensity is drastically enhanced at long wavelengths, comparable to the bunch length. The enhancement factor, defined as the ratio of intensities of observed SR and calculated incoherent SR, is 1.5 to $7.0\text{X}10^5$ for "A". According to the theory (6) of coherent SR, this enhancement factor is a product of N, the number of electrons in a bunch, and the square of the bunch form factor, the Fourier transform of the spatial electron distribution in a bunch. As the SR intensity is normalized for $N = 10^6$, the bunch form factor at these wavelengths is considered to be 0.4 to 0.8 for a 1.7 mm bunch. In contrast with "A", the intensity for the 15 mm bunch shown in "B", and so also the square of the bunch form factor, reduced by a factor of about 10^{-4}.

Data in "C" at visible wavelengths are consistent with the calculated incoherent SR, and this confirms the absolute magnitude of the data in this experiment. However, the data points in this figure are not corrected for the vertical acceptance because of lack of knowledge about the vertical angular distribution of coherent SR, i.e. 100 % vertical acceptance is assumed.

An obvious intensity decrease is not perceptible in "A" at wavelengths shorter than 1.7 mm, the bunch length. This spectrum suggests that the electron bunch from the linac has a complicated form. For, if it had a simple shape like a Gaussian, the intensity of coherent SR would change drastically around the wavelength comparable to the bunch length.

The SR intensity is proportional to N^2 at a wavelength of 0.4 mm, while to N at 420 nm (Fig.1.(b)). In the previous experiments in the same conditions (10) the SR intensity was almost proportional to N at a wavelength of 0.02 mm, though the absolute intensity was not measured. Therefore a big growth of the SR intensity is expected at wavelengths between 0.02 and 0.33 mm.

Fig.2. shows the degree of polarization of the observed SR. The polarization of SR has been measured to be P = 0.73 and 0.92 at wavelengths of 0.4 and 1.5 mm, respectively. The radiation

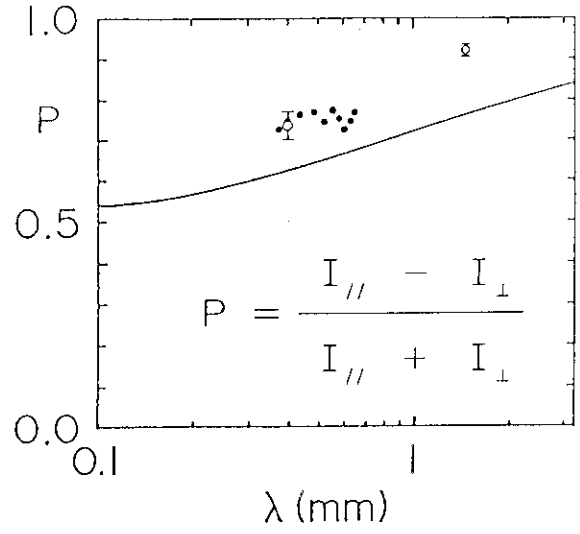

Fig.2. Observed degree of polarization P. P is defined by the expression in the figure, where $I_{//}$ and $I_{\perp}$ are the SR intensities which have an electrical vector parallel and perpendicular to the orbital plane, respectively. The solid curve shows the calculated value for ordinary SR with the same optical aperture.

is mainly polarized in the orbital plane. The diffraction correction must be done to compare these values with observed P.

IV CONCLUSION

The observed SR intensity is proportional to N^2 and enhanced by about N times that of incoherent SR. The intensity of SR depends on the bunch length strongly. As induced rf effects were excluded experimentally (1), we conclude that we observed coherent SR produced by electron bunches at wavelengths of 0.33 to 2.0 mm.

V DISCUSSION

It is demonstrated that the bunched electron beam accelerated by a linac has sufficient feasibility as a strong light source at milli- and submillimeter wavelengths. If we suppose a bending radius of 1 m, a 100 MeV electron linac with a high peak current is suitable for the applications.

A single bunch of $5\text{X}10^{10}$ electrons with a length of 1.5 mm has been already achieved (11). The bunch compressing methods have been considered and a bunch length of the order of 70 um is obtained by a calculation (12). A higher

accelerating frequency will make a shorter bunch. Those efforts for the research and development of the linear colliders will give an important technical basement to application of coherent SR. A complemented application of coherent SR is a bunch form monitor of the linear colliders, for its spectrum is regarded as the square of the bunch form factor.

Experiments for studying the transient phenomena will be enabled by the intense and extremely short, in the order of picosecond, pulse radiation from the electron linac beam. The details of the application in the fields of solid state physics, chemistry and biology etc. are discussed in Ref.5.

ACKNOWLEDGMENT

We wish to acknowledge helpful discussion with the staff of the Tohoku Linac. We would like to thank the members of the linac group and Mr. Tsutaya for their technical support and assistance.

REFERENCES

(a) Present address: Atomic Energy Research Institute, Nihon University, Surugadai Chiyoda-ku Tokyo 101, Japan.
(1) T. Nakazato, M. Oyamada, N. Niimura, S. Urasawa, O. Konno, A. Kagaya, R. Kato, T. Kamiyama, Y. Torizuka, T. Nanba, Y. Kondo, Y. Shibata, K. Ishi, T. Ohsaka and M. Ikezawa, Phys. Rev. Lett. 63, 1245 (1989).
(2) L. I. Schiff, Rev. Sci. Instrum. 17, 6 (1946).
(3) F. C. Michel, Phys. Rev. Lett. 48, 580 (1982).
(4) J. Yarwood, T. Shuttleworth, J. B. Hasted and T. Nanba, Nature 312, 742 (1984).
(5) E. Schweizer, J. Nagel, W. Braun, E. Lippert and A. M. Bradshaw, Nucl. Instr. and Meth. A239, 630 (1985).
(6) G. P. Williams, C. J. Hirschmugl, E. M. Kneedler, P. Z. Takacs and M. Shleifer, Phys. Rev. Lett. 62, 261 (1989).
(7) M. Sugawara T. Ichinohe, S. Urasawa, M. Oyamada, T. Kubota, A. Kurihara, O. Konno, Y. Shibazaki, T. Terasawa, K. Nakahara, S. Nemoto, M. Muto, K. Shoda and Y. Torizuka, Nucl. Instr. and Meth. 153, 343 (1978).
(8) J. Bohdansky, Z. Phys. 149, 383 (1957)
(9) A. J. Lichtenberg and S.Senic, J. Opt. Soc. Am. 56 75 (1966).
(10) T. Nakazato M. Oyamada, N. Niimura, S. Urasawa, O. Konno, T. Kamiyama, Y. Torizuka, M. Ikezawa, T. Nanba and Y. Kondo, Research Report of Laboratory of Nuclear Science, Tohoku University, 21-1, 94 (1988), (Unpublished.)
(11) J. Rees, in the Proc. of 1986 Linear Accelerator Conf., SLAC, Stanford, California, p209 (1986).
(12) S. A. Kheifets, R. D. Ruth and T. H. Fieguth, SLAC-PUB-5034, 1989

6. STORAGE-RING FREE ELECTRON LASER EXPERIMENT AT ETL

K. Yamada, T. Yamazaki, S. Sugiyama, T. Tomimasu, T. Mikado,
M. Chiwaki, R. Suzuki, and H. Ohgaki

Electrotechnical Laboratory,
1-1-4 Umezono, Tsukuba City, Ibaraki 305, Japan
0298-58-5679

1. INTRODUCTION

Free electron lasers (FELs) have a potential to lase with high power and high efficiency in a wide spectral range from microwave to soft X-rays and are now receiving a great attention as a promising tunable radiation source for various applications, such as nuclear physics, solid state physics, nuclear fusion, photochemistry, medical science, and so on. Among several kinds of accelerators, a storage ring is now recognized as the most favorable candidate to achieve short-wavelength FEL oscillation. We are aiming at the FEL oscillation at a visible to UV wavelength region using an electron storage ring and an optical klystron. Now we are making experiments to get FEL oscillation at visible wavelength around 590 nm with electron energy of 240 MeV using the ETL storage ring TERAS. So far, three major elements for FEL: electron beam, optical klystron and optical cavity, have been investigated[1] and FEL-gain measurements are now under way. Oscillation experiment is also being prepared.

In this paper we report the results of the basic researches on the FEL elements as well as the gain measurement. We will briefly show the preliminary results of cavity-length tuning to achieve the laser oscillation.

2. ETL STORAGE RING TERAS

ETL storage ring TERAS[2] is schematically shown in Fig.1. The average diameter of the ring is 10 m and the maximum electron energy is 800 Mev. In FEL experiments the energy is set at around 240 Mev, which enables us to get visible light around 590 nm. In addition to the main RF cavity driven at 171.62 MHz, a Landau cavity, which can feed the frequency-doubled RF power,[3] is also employed to reduce the spatial fluctuation and the energy spread of the electron beam caused by the coupled-bunch instability. Typical characteristics of TERAS is listed in Table 1.

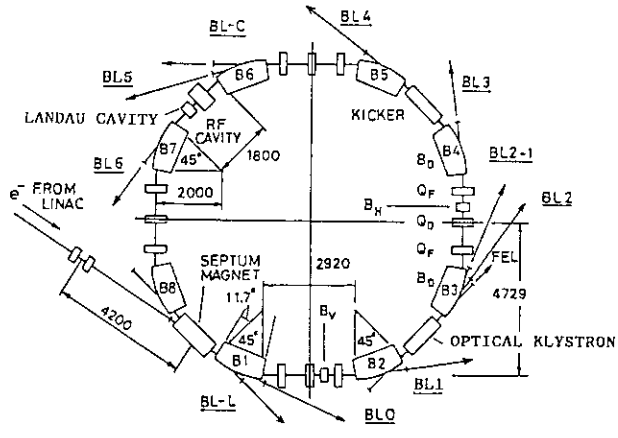

Fig.1 Schematic view of ETL storage ring TERAS.

Table 1 Characteristics of TERAS

Energy	150 - 800 MeV
Circumference	31.45 m
RF frequency	171.62 MHz
Harmonic number	18
Stored current	250 mA
Relative energy spread	$\sim 1\times10^{-3}$

The optical klystron is mounted in a 1.8-m straight section. The optical cavity is composed of low-loss concave mirrors whose radius of curvature is 3 m. The cavity length of about 5.238 m is

finely adjusted so as to synchronize the round-trip light pulse in the laser cavity with the electron bunches by two vacuum mirror manipulators driven by stepping motors and piezoelectric actuators with the accuracy of less than 2 μ m.

The energy spread of the electron beam is one of the most critical factors of the laser gain. The energy spread was estimated by measuring the modulation on the spontaneous-emission spectra from the optical klystron. The modulation rate f (which can be calculated by $f=(I_t-I_b)/(I_t+I_b)$, where I_t and I_b indicate the successive top and bottom intensity of the modulated spectrum) is approximately related to the energy spread (σ_E/E) as follows

$$f \sim \exp[-8\pi^2(N+N_d)^2(\sigma_E/E)^2]. \quad (1)$$

Figure 2 shows the dependence of the energy spread estimated by eq.(1) on the stored current. In the figure, the data in 17-bunch operation are also shown in addition to those in 18-bunch operation now employed. The current dependences of σ_E/E are $I^{0.27}$and $I^{0.17}$ for 17-bunch and 18-bunch operation, respectively. The energy spread is around 1×10^{-3} for the stored current of several tens of milliamperes which is used in FEL experiments.

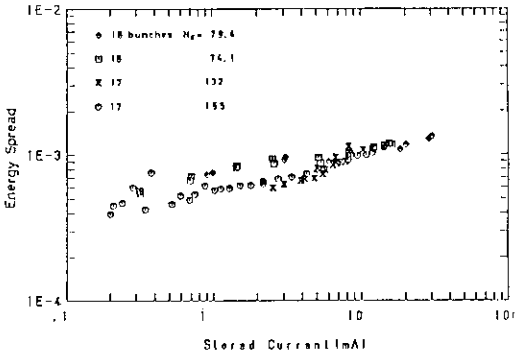

Fig.2 Current dependence of relative energy spread at 217 Mev.

The beam sizes have an influence on the electron density in the bunch and resultantly the laser gain. The bunch length and the lateral beam sizes were measured by observing the synchrotron light or spontaneous emission with a fast photodiode and a CCD camera.[1] The current dependence of the bunch length was measured at the beam energy of 220 MeV and it was found that the bunch length is expressed as, $\sigma_z=206I^{0.2}$ (ps), the dependence of which is similar to that of the energy spread.

The current dependence of the lateral beam sizes were measured at the energy of 320 MeV in 17-bunch operation. The anomalous beam sizes were found to be roughly proportional to $I^{0.5}$.

In usual operation, there are 18 bunches in the ring. However, in the FEL experiments, it is preferable to eliminate the redundant bunches which do not contribute the peak laser gain to avoid the mirror damage by the intense UV component in the undulator radiation. To remove the redundant bunches selectively, a RF-KO (radio-frequency knockout) method was carried out by feeding a frequency-divided ring RF signal mixed with the betatron frequency to a perturbation electrode. Figure 3 shows the typical example of the bunch structure before (above) and after (below) the knockout. It is found that only three bunches, which can synchronize with an identical light pulse in the laser cavity, remain in the ring with the beam current of 12.4 mA(4mA/bunch). The RF-KO method is not necessarily reliable at the moment, since the operation parameters of the ring are quite complicated because of the use of Landau cavity and the ring condition is very sensitive to them. We are now trying to find the optimum parameters for stable 3-bunch operation.

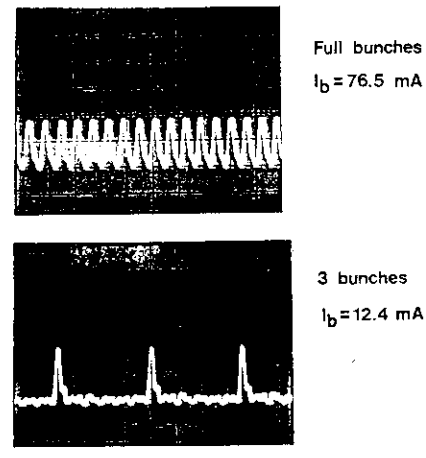

Fig.3 Bunch structure before (above) and after (below) the RF-KO.

3.OPTICAL KLYSTRON

Because of the short straight section of the ring, an optical klystron (OK) was employed to enhance the laser gain. Figure 4 shows the schematic view of the optical klystron[1] used in the present experiment. Two usual undulators and a dispersive section between them were composed of permanent magnet blocks made of NEOMAX-35 (Sumitomo Special Metal Co.), which is a compound of B, Nd, and Fe, and has higher remanent field

than $SmCo_5$. Magnet separations in the two undulators and the dispersive section can be independently adjusted mechanically. So the parameters, K and N_d, can be set independently also. The typical parameters of the OK are listed in Table 2.

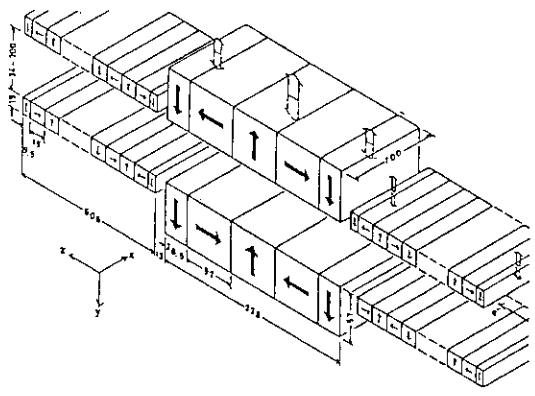

Fig.4 Schematic view of optical klystron

Table 2 Parameters of optical klystron.

Magnet	NEOMAX-35
Total length	1.47 m
Undulator period	76 mm
Number of period in undulator	8 x 2
Magnet spacing in undulator	34 - 200 mm
Typical magnetic field in undulator	0.31 T (40 mm)
K for FEL	2 - 2.3
N_d for FEL	70 - 100

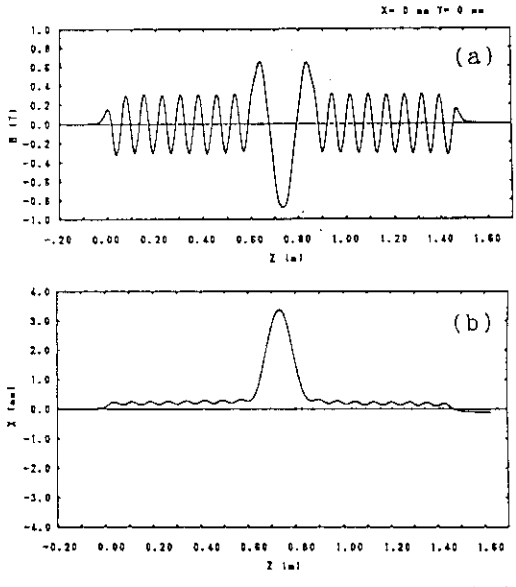

Fig.5 z distribution of B_y (a) and electron trajectory (b).

Figure 5 (a), (b) show the z-direction distribution of the magnetic field in the y direction, measured with a Hall probe, and the trajectory of an electron with energy of 250 MeV in the x-z plane, calculated from the measured magnetic field. The final displacement x is -0.13 mm which is mainly caused by the mechanical errors in the construction of the OK. However, this error does not have any influences on the ring operation.

4.OPTICAL CAVITY

As shown later, the laser gain expected with our device is rather low, typically of the order of 10^{-4}. Therefore extremely low-loss cavity mirrors are necessary to achieve laser oscillation. The round-trip cavity loss was measured in the air by the cavity decay time method.[4] The experimental set up is shown in Fig.6.

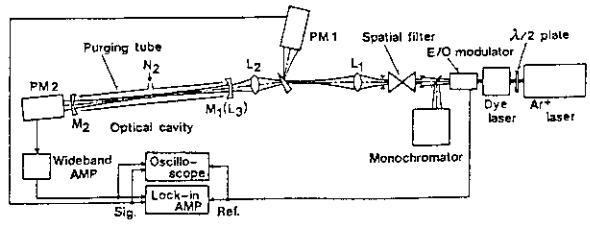

Fig.6 Experimental set up for cavity-loss measurement.

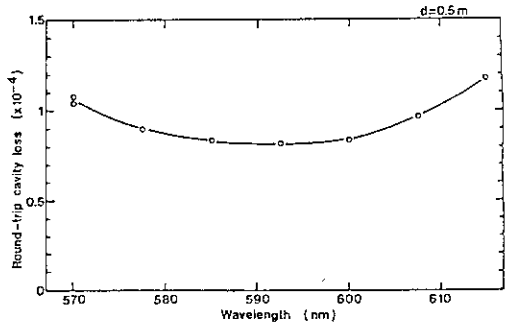

Fig.7 Wavelength dependence of round-trip cavity loss.

The output of an Ar^+-laser pumped dye laser is chopped with an E/O modulator and introduced into the cavity through a spatial filter and mode matching optics to minimize the diffraction loss. Owing to the long lifetime of photons in the cavity, the leading and trailing edges of the chopped laser light are exponentially tailed. By measuring the specific time of the tail τ, the round-trip cavity loss P is calculated to be $P=2d/(c\tau)$ where d is the cavity length and c is the light velocity. Actually, in spite of measuring τ, the effective

phase difference between the input and output waveforms $\delta\phi$ is measured by a two-phase lock-in amplifier. In this case τ is related to $\delta\phi$ by $\tan(\delta\phi) = 2\pi\nu\tau$. Since the cavity loss to be measured is very low, the results of observation are considerably affected by the dust and/or aerosol in the air. In the present experiment they were successfully eliminated by passing a small amount of dried nitrogen in a tube inside the cavity instead of a costly clean room. Figure 7 shows the typical wavelength dependence of the round-trip cavity loss. The loss is observed to be less than 1×10^{-4} at around 590 nm. The observation of the degradation of mirror reflectivity due to the irradiation by the undulator radiation is in progress.

5. THE LASER GAIN

A Madey's theorem describes that the small-signal gain is proportional to the derivative of the spontaneous-emission spectrum,[5] and in case of an OK the gain G_o per pass is expressed as[6),7)]

$$G_o = 1.12\times10^{-13}[\lambda_o(N+N_d)N^2/\gamma^3]K^2 \times [JJ]^2 f\rho_e F_f, \quad (2)$$

where λ_o is the undulator period in meter, γ is the electron energy in the unit of the rest mass energy, [JJ] is the Bessel function factor: $[JJ] = \{J_1(K^2/[4+2K^2]) - J_0(K^2/[4+2K^2])\}$ for the fundamental wavelength, f is the rate of modulation on the spontaneous-emission spectrum, ρ_e is the peak electron density in m^{-3}, F_f is the filling factor caused by the lateral overlap of the electron bunch and light pulse. In our case, the peak gain is estimated to be $G_o = 3\times10^{-4} f F_f$ for the stored current of 1 mA/bunch from eq.(2).

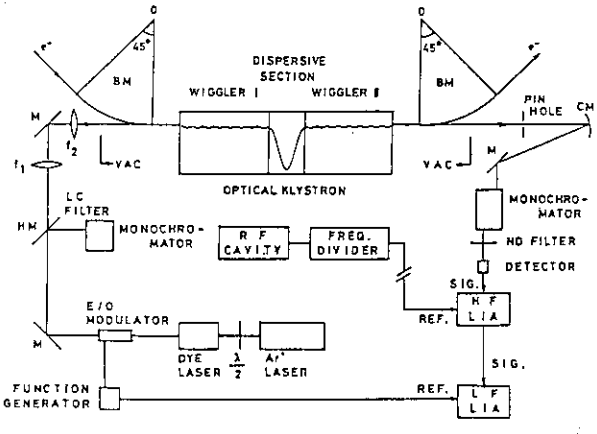

Fig.8 Experimental arrangement for gain measurement.

The laser gain is being measured by using an external dye laser pumped by an Ar^+ laser. This scheme is the same in principle as that used by ACO group.[8)] The experimental arrangement is shown in Fig.8. The storage ring is operated in 3-bunch mode with the electron energy of around 240 MeV. The parameters, K and N_d, of the optical klystron are 2.2 and 73.5, respectively. The CW dye laser beam is modulated by an E/O modulator and interacts with the electron beam in the optical klystron. The output light is detected by a fast photodiode after passing through an iris and a monochromator to reduce the spontaneous-emission component. At this time E/O modulator is used to change the direction of polarization alternately by eliminating the output polarizer, instead of modulating the light amplitude. This enables us to avoid the impedance modulation of the photodiode.[8)] The photodiode signal is amplified by a wideband amplifier and sent to a high-frequency (HF) lock-in amplifier with a response up to 50 MHz where only the signals in synchronism with the electron bunches are selectively picked up. The output of the HF lock-in amplifier contains both the stimulated-emission component and the spontaneous-emission component. Since the stimulated-emission component oscillates with the modulation frequency of the external laser, it can be extracted by a low-frequency (LF) lock-in amplifier locked by an output signal from an E/O-modulator driver. The final signal from the LF lock-in amplifier S_{RF} is proportional to the average FEL gain. The photodiode signal is also fed directly to the LF lock-in amplifier with a mechanical chopper in front of the monochromator. In this case the output signal S_{LF} is proportional to the input laser power. The average gain is estimated from the ratio between S_{RF} and S_{LF}.

This detection system should be absolutely calibrated. With the input laser off and the chopper in front of the monochromator again, spontaneous emission having the same temporal structure as that of the stimulated emission enters the measuring system. By using the signal through both HF and LF lock-in amplifiers, V_{RF}, and that through only LF lock-in amplifier, V_{LF}, the average gain $\bar{G}$ is given by

$$\bar{G} = (S_{RF}\cdot V_{LF})/(V_{RF}\cdot S_{LF}). \quad (3)$$

The peak gain $\hat{G}$ is estimated to be

$$\hat{G} = GT_o/(2m\sigma_z), \quad (4)$$

where T_o is the revolution time of the electron bunch in the ring, σ_z is the bunch length and m is the number of bunches in the ring. Typical peak gain spectra as a function of electron energy

observed at the wavelength of 597.2 nm are shown in Fig.9.

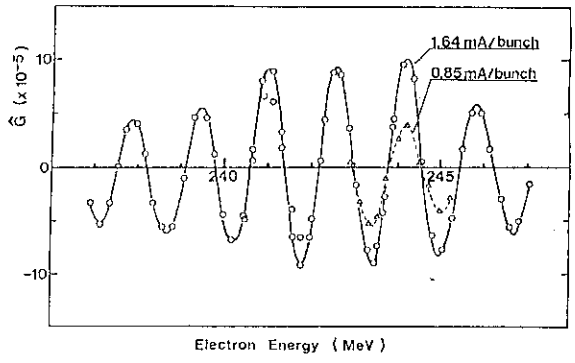

Fig.9 Typical peak gain spectra.

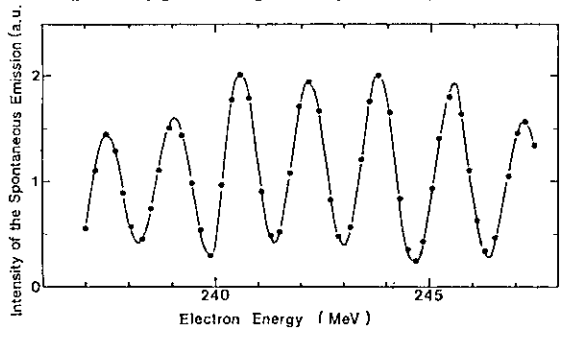

Fig.10 Spontaneous-emission spectrum.

An alternating structure of gain and absorption peculiar to the optical klystron is clearly found. The maximum peak gain is about 1×10^{-4} for the stored current of 1.64 mA/bunch and it decreases down to 0.4×10^{-4} for 0.85 mA/bunch. These values are in good agreement with the predicted one by eq. (2), considering the modulation rate and the filling factor. Figure 10 shows the spontaneous-emission spectrum for very low current at the observation wavelength of 597.2 nm. The Figs. 9 and 10 clearly show that the peak gain is roughly proportional to the derivative of the spontaneous emission spectrum as predicted by the Madey's theorem. Figure 11 shows the dependence of the peak gain on the stored current per bunch in low current region. Although the maximum peak gain observed is about 1×10^{-4}, which is just above the initial round-trip cavity loss, the peak gain tends to increase rapidly with the beam current in this current region. Therefore, by increasing the beam current as well as improving the beam quality, such as beam energy spread, beam sizes, and so on, we can expect to reach the threshold for laser oscillation in spite of the degradation of the cavity-mirror reflectivity due to the irradiation by the spontaneous undulator radiation.

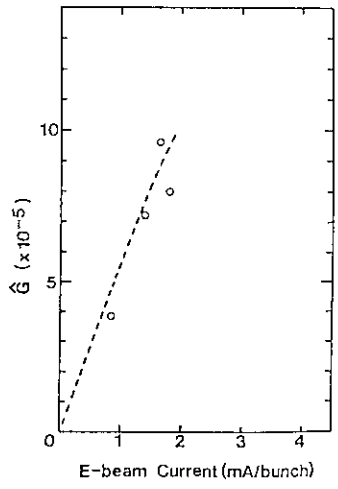

Fig.11 Current dependence of peak gain.

6. CAVITY-LENGTH TUNING

To achieve the laser oscillation, precise synchronism of the round-trip light pulse in the cavity with the

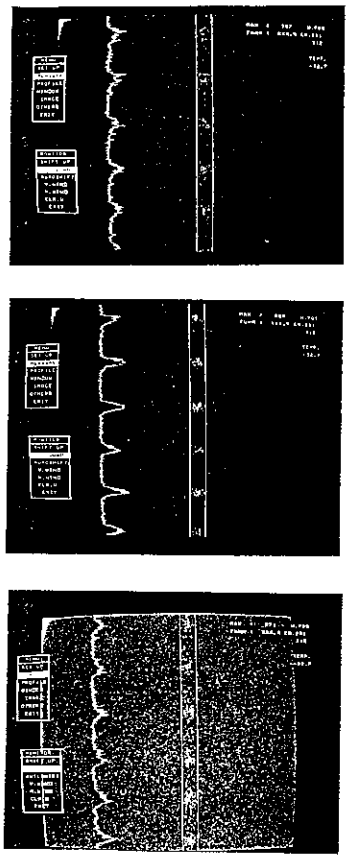

Fig.12 Observation of output light from cavity with cavity length detuned by +0.4 mm (a), almost tuned (b) and detuned by -0.4 mm (c).

electron bunches are critical. An experiment of the cavity-length tuning is now under way. The cavity length can be precisely tuned by observing the shape of light pulses resonating and slightly penetrating the cavity mirror. Since the time interval between bunches in the ring is only 5.8 ns in normal operation, we used a streak camera to observe the pulse waveform. Figure 12 (a), (b), and (c) show the typical results when the optical cavity is detuned by +0.4 mm, almost tuned and detuned by -0.4 mm, respectively. In the case (b), the light pulse in the cavity overlaps with the light pulses from the successive bunches and the light out of the cavity is observed as a pulse train with temporally symmetric shape and relatively high peak intensity, corresponding to the successive electron bunches. On the other hand, when the cavity length is slightly detuned, the pulse shape becomes asymmetric with the trailing edge (a) or the leading edge (c) followed by the round-trip light pulses.

In the present experiment the resolution of this technique is rather bad, ± 0.4 mm, since the reflectivity of the cavity mirrors has been degraded through a fair amount of irradiation by the UV radiation. However, in the recent experiment, it has been found that the resolution can be improved at least by an order of magnitude by using a sufficiently low-loss cavity mirrors.

7. SUMMARY

We have been making basic experiments for FEL oscillation at around 590 nm using the ETL storage ring TERAS and an optical klystron. The peak gain measured was about 1×10^{-4} for the stored current of 1.6 mA/bunch which was in good agreement with the rough estimation, considering the measured energy spread and sizes of the electron beam. Although this value is just above the minimum round-trip cavity loss measured by the cavity-decay time method, a larger gain will be required to reach the threshold for laser oscillation, owing to the rapid degradation of the cavity mirrors irradiated by the UV component in the undulator radiation. However, according to our experimental result, we can expect much larger gain by increasing the stored current. A high-tune ring operation may be also effective to get higher gain through an increase of the electron density. A preliminary experiments to achieve laser oscillation together with the gain measurement at higher beam current are in progress.

The authors would like to thank Mr. S. Sato, and Mr. H. Usami for their collaboration in performing the preliminary experiments. They are also grateful to Dr. Y. Miyahara for his advice on the double RF system. This work has been supported by Special Coordination funds for the Promotion of Science and Technology until 1988, and Peaceful Utilization Technology of Nuclear Energy from 1989, both from the Science and Technology Agency.

REFERENCES

1) T.Yamazaki, et al.,"TELL-TERAS Activity Report 1980~1986", Electrotech. Lab., 1987, p.72; T.Nakamura, et al., ibid., p.72, Mar. 1987; T.Nakamura, et al., Proc. 6th Symp. Acc. Sci. Tech., Tokyo, 1987, p.262; T.Yamazaki et al., Proc. 3rd Joint Symp. of Acc. for Nucl. Sci. and Their Appl., Riken, 1987, p.81; T.Yamazaki et al.,Proc. SPIE 1133, 62(1989); T.Yamazaki et al., Proc. 2nd International Symp. on Advanced Nuclear Energy Research, Mito, 1990, (to be published).
2) T.Tomimasu et al., "TELL-TERAS Activity Report 1980~1986", Electrotech. Lab., 1987, p.21.
3) Y.Miyahara et al., Jpn. J. Appl. Phys., **22**, L733(1983).
4) J.M.Herbelin et al., Appl. Opt. **19**, 144(1980).
5) J.M.J.Madey, Nuovo Cim. **50**, 64(1979).
6) D.A.G.Deacon et al., Appl. Phys. **B34**, 207(1984).
7) M.Billardon, et al.,IEEE J. Quantum Electron. **QE-21**, 805(1985).
8) D.A.G.Deacon et al., Trans. Nucl. Sci. **NS-28**, 3142(1981).

7. FEL Researches on Induction Linac at ILT / ILE Osaka University

K. Imasaki, T. Akiba, K. Mima, S. Miyamoto, N. Ohigashi, Y. Tsunawaki,
S. Kuruma, Y. Kitagawa, C. Yamanaka, and S. Nakai

Institute for Laser Technology
Institute of Laser Engineering, Osaka University
Suita Osaka 565 Japan

I. INTRODUCTION

Institute for Laser Technology and Institute of Laser Engineering have a cooperative program for high power FEL using an induction linac.[1] The final purpose of development of a high power FEL is to use it as an energy driver of inertial confinement fusion. But before this, there are many interesting applications as a laser acceleration, plasma heating and diagnostics and so on.

For the first step, we started to develop GW level FEL system for the application of laser acceleration.

II. FEL SYSTEM

1. Total System

A total system that we planned is shown in Fig. 1. Induction linac is drived by pulsed power source which is synchronized with Lekko XIII CO_2 laser system. Lekko XIII which has output of 1 TW in a ns is used to pump Raman laser of which wavelength is 400 ~ 1000 μm. Induction linac has injector of 6 stages and accelerator of 6 stages. We have completed the induction linac and wiggler I.

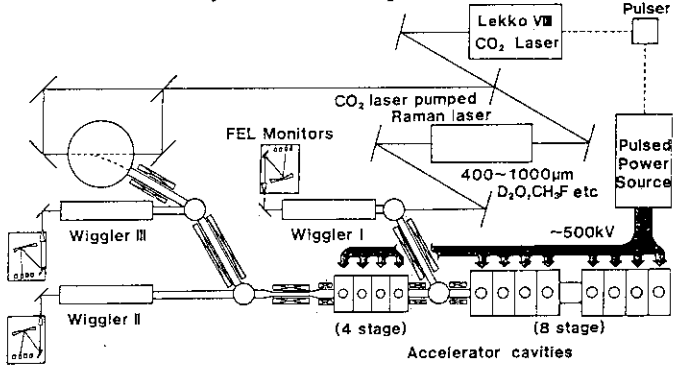

Fig. 1 Total system of induction linac at ILT / ILE

Wiggler II was designed and under construction. Wiggler III is under designing.

Tab.1. FEL Facility at ILT/ILE Osaka Univ.

- Induction Linac
  - 12 stage x (500 ~ 750 kV)
  - 5 kA (at e- gun)
  - 100 ns pulse length
  - $\Delta E \simeq \pm 2$ %
- E-Beam Gun
  - brightness ~ 10^4 A/cm^{2}rad^2
- Beam Transport
  - Solenoid/Hermholtz coil /Trilpet Q-Mag./Steering Mag.
  - Beam aperture at entrance of transport section
  - emmitance selector
- Wiggler
  - Wiggler I : planer permanent magnet
    - $\lambda w = 6$ cm $N = 30$ $K \simeq 0.5 \sim 2$ (Tapered)
  - Wiggler II : Helical pulsed electro-magnet
    - $\lambda w = 3$ cm $N = 30$ $K = 0.5 \sim 1$
  - Wiggler III : pulsed electro magnet
    - $\lambda w = 3$ mm $N = 100$ $k = 0.1$
    - (under designing)

These parameters are shown in Tab.1. Fig. 2 shows the photograph of induction linac.

(1) Beam Generation

An electron beam is generated and accelerated at a diode. The diode is field emission type and the cathode of velvet is used. The current and normalized emittance is 10 KA and 10^4 A / $cm^2 rad^2$, respectively. The 8 stage induction linac can produce a 4 MeV electron beam. The beam is transported from the induction linac to the wiggler by the axial magnetic field generated by six Holmholtz coils. The axial magnetic field profile and a calculated beam envelope between the diode and the entrance of the wiggler are shown in Fig. 3. In the induction linac the electron beam with 1.2 KA current and 0.05 rad.cm emittance is confined to 20 mm radius by the axial magnetic field with the intensity of 400 G. The magnetic field is increased by the final Helmholtz coil to 700 G to

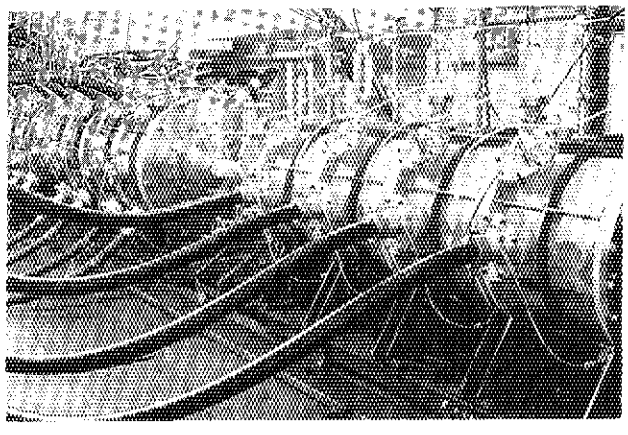

Fig. 2 Photograph of induction linac

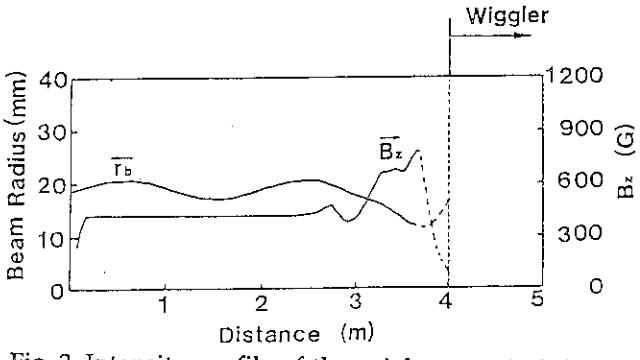

Fig. 3 Intensity profile of the axial magnetic field and calculated envelope of the electron beam

injected the beam into the wiggler. The beam is focused to 15 mm radius at the entrance of the wiggler field. A diagnostic section is located in this coil region. The current is monitored by a Faraday cup.

(2) Interaction Region

A wiggler I which we used for the experiments consists of planer permanent magnets. The period of the wiggler is 60 mm and the number of the period is 30. Each five period composes one block of the wiggler. The wiggler field on axis for each block can be varied from 4.5 kG to 500 G by changing the gap independently. This makes taper the wiggler to achieve high efficiency. The relations among the gap separation and the wiggler field and the K parameter are shown in Fig. 4. In the experiment, the wiggler filed is 2.47 kG.

One of a key issues of the FEL experiments is a transport of the electron beam. Vertical focusing is provided by an wiggler field. For horizontal focusing a simple quadrupole like

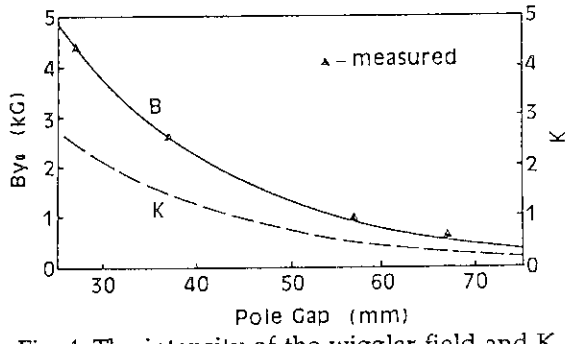

Fig. 4 The intensity of the wiggler field and K parameter versus wiggler gap separation.

magnetic field is applied. The quadrupole is field generated by the coil pair as shown in Fig. 5. These magnets are used to stabilized the electron orbits in the wiggle plane with a gradient of 30 G / cm which slightly reduces the vertical focusing. This field introduces perturbation less than 4 percent to the wiggler field at the edge of the waveguide. No solenoidal focusing is used in the interaction region.

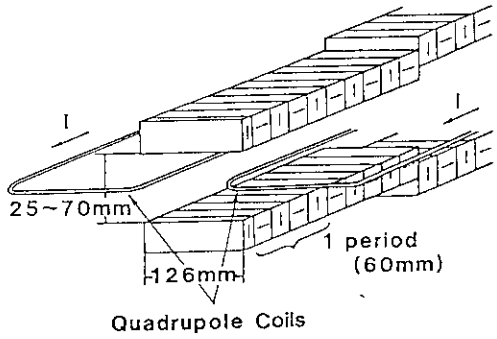

Fig. 5 Newly designed quadruple magnets for horizontal focusing of the electron beam. The gradient of the field is about 30 G/cm.

The copper rectangular waveguide with the cross section of 29 mm × 58 mm (WRJ-4) is employed. Dominant waveguide mode is assigned to be TE_{01} mode. The beam current is monitored by the Faraday cup. Time integrated beam profile is monitored by the Cherenkov light which is generated by the polyimide film. The current along the wiggler is shown in Fig. 6. At

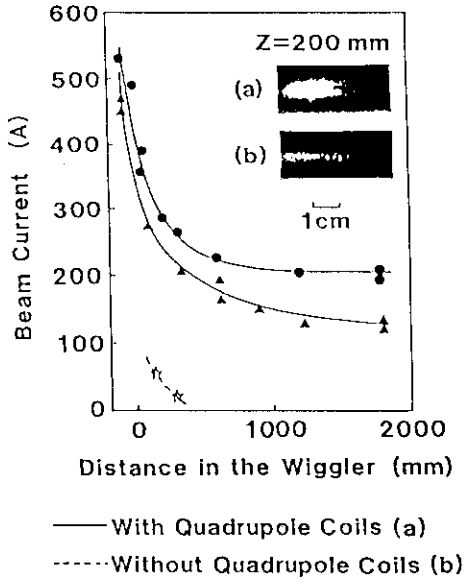

Fig. 6 Transmittance current versus axial distance in the wiggler. Time integrated beam profile at 200 mm downstream from the beginning of the wiggler shows the focusing of the electron beam when the quadruple field was applied.

210 mm downstream from the wiggler entrance, the beam is focused 3 mm in vertical direction and 13 mm in the wiggler plane. The beam 200 A, 3 MeV is transported to the end of the wiggler when the quadrapole field is applied.

Both the beam current data and the beam profile shows mismatching of the beam at the injection of the wiggler. This causes the beam to hit the waveguide wall. A stronger focusing of the beam at the entrance of the wiggler may increases the current transmission.

(3) Microwave Diagnostic

Output radiation is monitored by a crystal detector calibrated at 75 GHz. This detector is located at 2 m downstream from the wiggler end to avoid the beam damage. The waveguide is tapered to the small cross section (22.9 × 10.2 mm) waveguide. About 10 % of the output power can be monitored.

III. EXPERIMENTAL RESULTS AND DISCUSSION

The energy, current and pulse width of the electron beam are 3 MeV, 200 A and 100 ns, respectively. The experimental parameters is in the "High Gain, Strong pump" regime.

The spontaneous emission from the beam passing through the wiggler is observed. Output waveform of FEL is shown in Fig. 7. The full

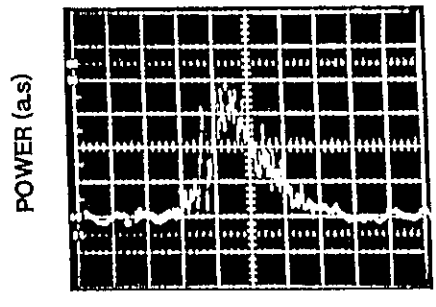

Fig. 7 Output waveform of super-radient mode FEL monitored by a crystal detector

width of half maximum (FWHM) of the output was 100 ns. Output power is about 2 kW. The wavelength of FEL is estimated to be 1.2 mm.

The gain is measured by changing interaction length. The radiation power versus the interaction length is shown in Fig. 8.

One pass gain is 30 dB. The loss of the waveguide is 0.09 dB, which is negligible small compared with FEL gain. The obtained gain is lower than that estimated from the cold beam gain (3) because of the effective energy spread of the electron beam which is induced by the emittance and the misalignment. The experimental gain agrees with the simulation when the effective beam energy spread is set to be 3.7 %.

Future Plan of High Power Experiment

For high power FEL experiments the high power radiation source is required. Optically pumped gas laser which will be used to produce the high power (10 kW - 1 MW) with the wavelength from 100 μm to 2 mm, when we use 100 GW level CO_2 laser Lekko XIII as a pump laser. At least the input laser power is expected 100 kW, then the 30 dB amplification may lead to the 100 MW output. Saturation power level is estimated to be the order of 5 - 10 % of the beam power. This conversion efficiency is expected to be 30 % by the patering of the wiggler (4). Thus 600 MW beam may produce 200 MW far infrared radiation.

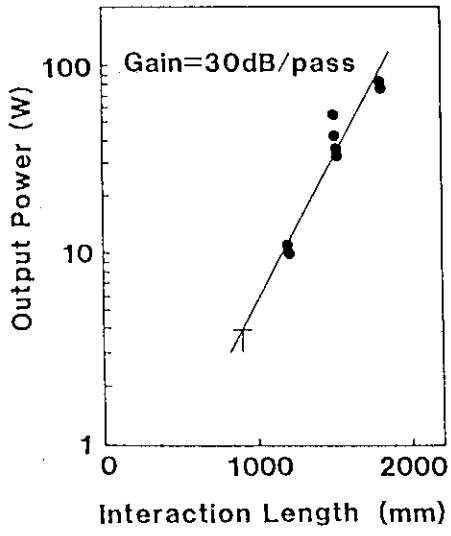

Fig. 8 Small signal gain in the super-radiant mode as a function of wiggler length.

IV. SIMULATION FOR INDUCTION LINAC FEL

For achieving high conversion efficiency of the electron beam energy to the radiation, we simulate the saturation processes of the amplification by a three dimension waveguide mode simulation code (WAGOS).

By the simulation, it is found that the conversion efficiency enhancement by the tapering is very sensitive to the number of the excited waveguide modes.

In the simulation, the FEL parameters are set as shown in Table 2. The radiation wavelength is matched with the CH_3F laser namely, 498 μm, from the resonance condition,

$$\omega^2 = \left(k_z^2 + k_\perp^2\right)c^2 + \omega_p^2 / \gamma_0$$

$$\omega = (k_z + k_w)V_z - \omega_p / \gamma_z\sqrt{\gamma_0}$$

$$V_\perp / c = -K / \gamma_0$$

$$\gamma_0^2 = 1 - V_\perp^2 / c^2 - V_z^2 / c^2$$

Table 2

Wiggler	wavelength	6 cm
	length	1.8 m
	B-field	2.36 kG
Radiation wavelength		498 μm
Beam energy		6 MeV
current		2 kA
radius		3 mm
waveguide radius		10 mm

The wiggler K value is determined as

$$K = \left\{ \gamma_0^2 - \left(\frac{\gamma_0^{\tilde{\omega}}}{1 + \tilde{\omega}\left[1 - (\beta_{nm} / \tilde{r}_c \tilde{\omega})^2\right]^{1/2}} \right)^2 - 1 \right\}^{1/2}$$

where $K = eB_w / k_w mc^2$, $r_c = k_w r_c$, $\omega = \omega / k_w c$, and β_{nm} are the zeros of the Bessel function of the mth order. When the excited mode is TE_{11} mode, the wiggler is determined to be 2.36 kG, which is the initial field strength of the tapered wiggler.

In Fig. 9 we compare the spatial evaluations of the radiation between a single mode excitation case and a multimode excitation case. In those simulations, the injected radiation intensity is Pi = 800 W / mode. Note that this corresponds to AE = 10^{-5}, and the filling factor = 0.25 in Fig. 8. Here the wiggler field decreases form 2.36 to 1.4 kG between $Z / \lambda_w = 20$ and 30. In the multimode case, the TE_{11} mode is not amplified after $z / \lambda_w = 16$. On the other hand, in the single mode case, the amplitude increases after $z / \lambda_w = 20$ up to $eA_s / mc^2 = 2 \times 10^2$ which is two times higher than that for multimode excitation case. The energy extraction efficiencies are 20 % and 5 % for the (1, 1) mode in the case of Fig. 9a and 9b respectively.

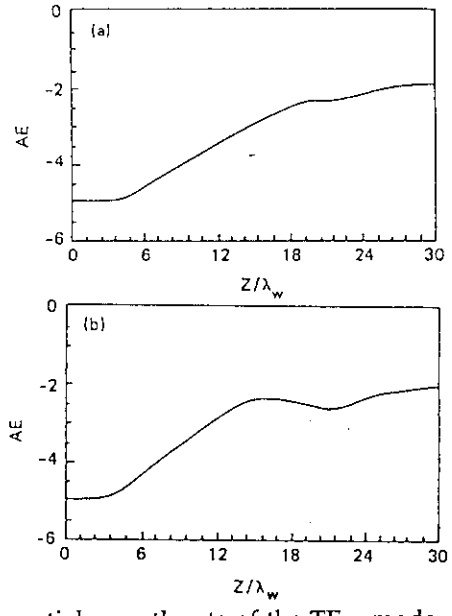

Fig. 9 spatial growth rate of the TE_{11} mode. (a) signal mode excitation, where the TE_{11} and TM_{11} modes have finite amplitudes ; (b) multimode excitation case, where TE_{1n} and TM_{1n} (n = 1, 2,3) are excited.

V. CONCLUSION

Preliminary experiment of the super-radiant mode FEL is performed. A new designed quadrapole magnets can focus the electron beam of 200 A current and 3 MeV energy. FEL output of 1 kW level is observed. One path gain is about 30 db of 100 W level is observed. One pass gain is about 30 dB. 100 MW level output is expected when optically pumped gas laser is injected.

REFERENCES

(1) T. Akiba, M. Fukuda, M. Noma, N. Inoue, K. Tateishi, K. Imasaki, S. Miyamoto, N. Ohigashi, K. Mima, S. Nakai, and C. Yamanaka, Nucl. Instrum. and Methods Phys. A259 115 (1987)

(2) P. Sprangle, R. A. Smith and V. L. Granstein in "Infrared and Millimeter Waves" 1 Chap. 7, 279 (1979)

(3) T. J. Orzechowski, E. T. Sharlemann, B. Anderson, V. K. Neil, W. M. Fawley, D. Prosnitz, S. M. Yarema, D. B. Hopkins, A. C. Paul, A. M. Sessler, and J. S. Wurtele, IEEE J. Quantum Electron. QE-21 831 (1985)

8. STUDIES ON A FREE ELECTRON LASER USING RELATIVISTIC ELECTRON BEAM SOURCES

Y.Kawamura*, B.C.Lee**, M.Kawai***, and K.Toyoda*

* *Riken, The Institute of Physical and Chemical Research, Wako-shi Saitama, 351-01, Japan*

** *Department of Physics, KAIST, Cheongryang, Seoul, South Korea*

*** *Department of Physics, Faculty of Science, Tokai University, Hiratuka-shi, Kanagawa 259-12, Japan*

Abstract

Periodical short pulse trains were observed in the waveguide mode free electron laser oscillations, which could be explained as a self mode-locked oscillations of the free electron laser. The spectra of the spontaneous emission and the induced emission were observed, which were in good agreement with theoretical calculations.

1.Introduction

In order to obtain a free electron laser (FEL) operation[1,2], relativistic electron beam with small energy spread and high current density is essential. Intense relativistic electron beam (IREB) can produce a very high current electron beam, but the energy spread is very large, which is assumed to be due to the formation of the plasma cathode[3].

Two types of cold relativistic electron beam source for the studies of FEL have been developed. One of them is a new type of a cold relativistic electron beam source (CREB)[4], in which the IREB is generated in the first gap of the acceleration tube and additionally accelerated by another eight acceleration gaps. The acceleration energy, current, and pulse duration of the electron beam are about 0.5MeV, 10~30A/cm^2, and > 1μs, respectively. The acceleration voltage was kept constant within ±1% for about 200ns. The other type of the cold relativistic electron beam source is the relativistic photo electron (RPE), which makes use of a UV pulse laser to induce photo-electrons from metal cathode[5]. The forth harmonic of a Q switched YAG laser is irradiated on the metal cathode. The photo-electrons are then accelerated to relativistic energy. The acceleration energy, the current, and the pulse duration are about 0.5MeV, 1~2A, and 8ns, respectively. The transverse energy component was measured to be less than 17eV[6], which implies that the energy spread is extremely small.

Using the RPE, the waveguide mode FEL using a planar wiggler was constructed, and spontaneous emission and FEL gain were measured, which were in good agreement with the theoretical predictions. Using the CREB as an electron beam source of the FEL, laser oscillation was obtained. Periodical short pulse trains were often observed, which could be explained as self mode-locked oscillations of FEL. The pulse width and the pulse train intervals of the periodical short pulse trains were about 4ns and about 24ns, respectively.

2.Experiments and discussions

The experimental set up is shown in Fig.1. RPE is produced by irradiating Zn cathode target with the fourth harmonic (266nm, 30mW, 8ns) of Nd-YAG laser beam with successive acceleration up to about 500keV, of which energy is supplied by a Marx type electrostatic accelerator. Good controllability in the transverse position of the electron beam was obtained by using two pairs of steering magnets in horizontal and vertical direction. The electron beam is injected into the interaction region through an aperture (D=4.5mm).

The interaction region is composed of a linear wiggler, a rectangular waveguide (axb=2.29cmx1.02cm), and an axial guiding

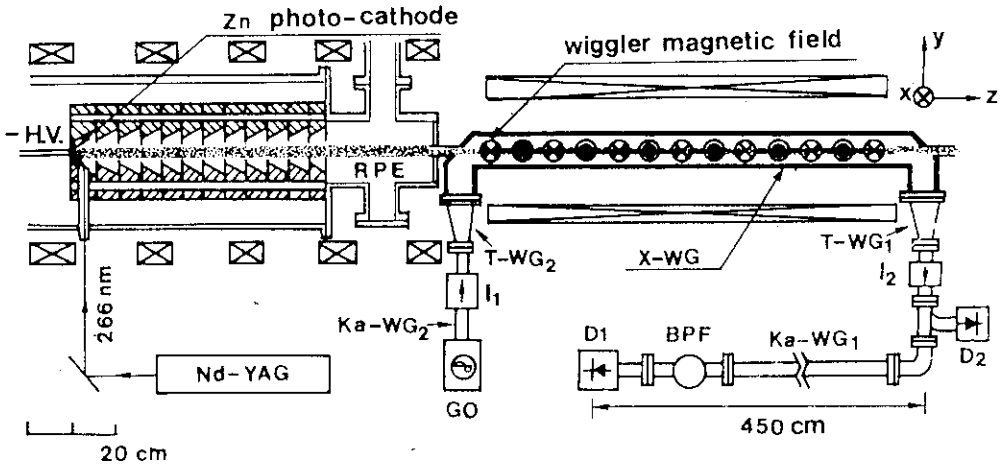

Fig.1 Schematic diagram of experimental apparatus for measurement of various characteristics of FEL.

Table 1. Experimental parameters for the measurement of a small signal gain.

Electron beam		Wiggler		Waveguide	
Energy	: 0.5MeV	Pitch length	: 5cm	Size	: 22.9 x 10.2mm
Current	: 1A	Number of pitch	: 15	Cut off	
Pulse length	: 8ns	K value	: 0.05 ~ 0.5	wavelength	: 18.6mm
Energy spread	: $<10^{-4}$				

magnet (B_0=1kG~10kG). The periodic linearly polarized wiggler magnetic field is produced by passing current through the linear electromagnet windings. The total number of periods is 18 and the first and the last 1.5 periods are adiabatic region. These experimental conditions are summarized in Table 1.

Figure 2 shows the transmission of the electron beam through the interaction region (the ratio of current at the end of wiggler to that at the entrance of the wiggler) as a function of guiding magnetic field strength for various K values of the wiggler. The arrow shows the calculated value of the resonant magnetic field strength. The rapid decrease in transmission near the magneto-resonance results from the current loss to the waveguide wall, as the transverse excursion of the electron beam increases to infinity. Furthermore, the drift velocity of guiding center due to nonuniform distribution of transverse wiggler field increases near the resonance and the electrons are kicked-off from the orbit.

For the purpose of spectrum analysis of the spontaneous emission, the radiation signal from about 1 Amp., 526keV electron beam was introduced into a 70cm - long rectangular waveguide

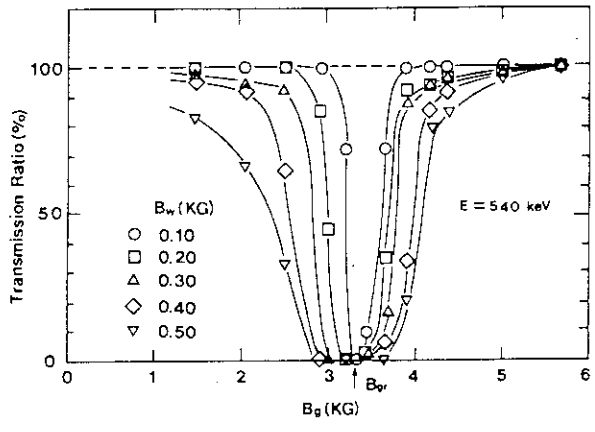

Fig.2 Transmission of electron beam through the interaction region with the wiggler as a function of guiding magnetic field strength. (V_0=0.849c)

(34GHz, 0.711cmx0.356cm) whose cut-off frequency for TE_{10} mode is 21.09GHz. And then the signal was filtered by a cylindrical cavity filter (32~36GHz for optimum operation, Q=800) and was measured by a crystal detector. The field strength of the guiding magnet and the wiggler in the interaction region was 2.1kG and 0.36kG respectively, being sufficiently far from the mag-

neto-resonance region. Output power of about 0.1mW was observed from 32GHz to 36GHz with about 2GHz FWHM, which is in good agreement with the theoretically predicted spectral width of spontaneous emission ($\Delta\upsilon/\upsilon\cong 1/15$) as shown in Fig.3.

The experimental scheme for the gain measurement was shown in Fig.1. Monochromatic microwave (34.4GHz, 20mW in CW) from a Gunn oscillator is injected into the interaction region. The output signal was measured by the same method as described above. For example, under the condition of B_g=2.1kG, B_W=0.36kG, 2.29cmx 1.02cm waveguide and 34.4GHz microwave injection , the resonant electron energy is 526keV.

The waveguide is oversized for 34GHz, and many modes are possible to exist as shown in Fig.4. But the investigation on the matching condition showed that the TE_{10} mode is the only one mode that can stimulate the electron beam to radiate. For the other modes, the velocity of electron satisfying the matching condition exceeds the light velocity in free space, which is impractical.

Experimentally, under the same condition above, absorption or gain coefficient of about 0.3/Amp. was observed as shown in Fig.5, which means that this system works as a free electron laser facility in Compton regime in the tenuous electron beam limit. The theoretically calculated

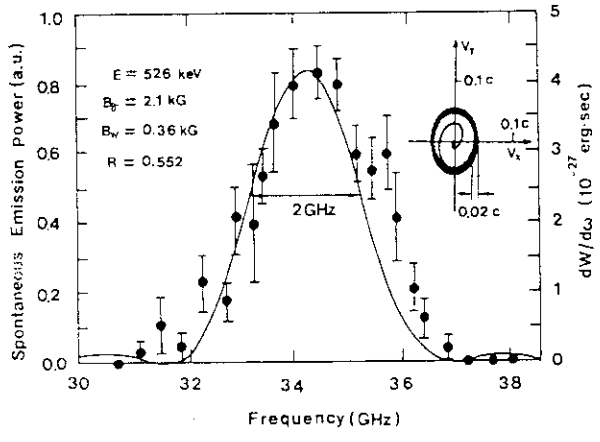

Fig.3 Spectrum of spontaneous emission power measured as a function of frequency (dots) and the energy radiated by an electron per unit frequency calculated theoretically (solid line). The vertical scale of the power measured is adjusted such that the vertical position of the dot for the peak power near 34.4GHz coincide with the peak of the theoretical curve.

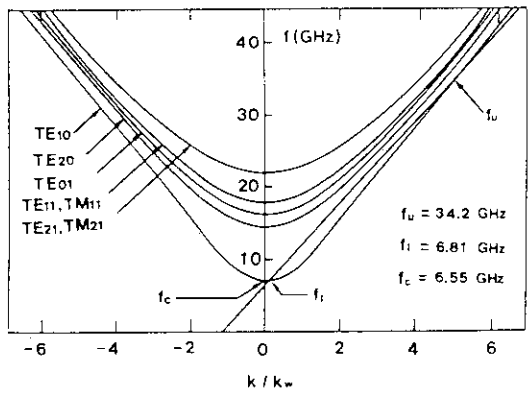

Fig.4 Dispersion carves of various waveguide mode.

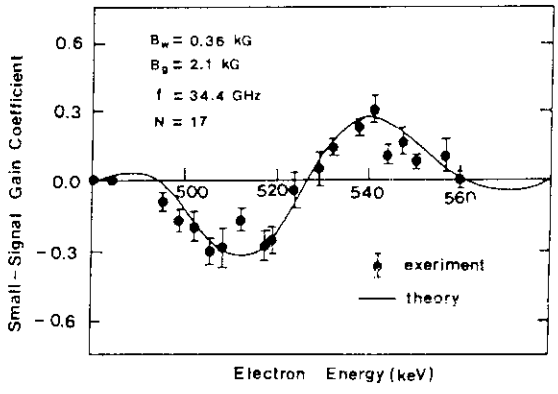

Fig.5 Small-signal gain coefficient (Γ_w, $P_{out}=P_{in}e^{\Gamma w}$ where P_{in} is the input power and P_{out} is the output power) of 20mW, 34.4GHz microwave as a function of the energy of RPE.

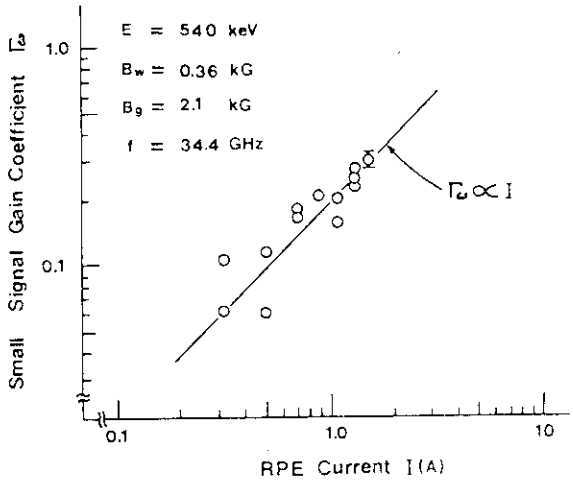

Fig.6 Variation in the small-signal gain coefficient as a function of the current of RPE (dots). The solid line is a linear regression.

value of the gain coefficient is drawn by a solid line, which is in good agreement with the experimental result.

Figure 6 shows the small-signal gain coefficient as a function of the current of RPE. The current of RPE is varied by changing the intensity of the 4-th harmonics of Nd-YAG laser pulse incident on the photo-cathode. The dots represent the measured value of gain coefficient and the solid line is a linear regression. The gain coefficient is proportional to the current in the range of 0.3~1.5A, which means that the FEL apparatus works in the low-gain Compton regime in the teneous-beam limit. The plasma frequency corresponding to 1.5A of 540keV RPE current is 0.12 GHz, and it is much smaller than the frequency of the injected microwave.

Figure 7 shows the variation of small-signal gain coefficient as a function of the wiggler magnetic field. The error bar represents the standard deviation over 5 shots. The parallel speed($\beta_{//}$) of a fixed-energy electron decreases and thus the matching condition changes as the wiggler magnetic field increases. The numerics written beside data points represent the energy of RPE. Note that the gain coefficient is proportional to the square of the wiggler magnetic field in the limit of weak pumping (B_W=0.2~0.6kG). This is also a proof for the operation in the low-gain Compton regime.

Using the CREB as an electron beam source, the FEL oscillation was obtained. The acceleration voltage and the current of the CREB were 517keV and about 10A, respectively. The magnetic field strength of the guiding coil, B_g, and the wiggler, B_W, were 2.6kG and 0.52kG, respectively. Periodical pulse trains were often observed.

Figure 8 shows the oscillation characteristics of this system as a function of the wiggler magnetic field strength B_W and the RPE current. The bars of the data represent the region of the current in which the oscillations occasionally occurs. (Consequently, the solid line represents the experimental conditions which gives the threshold for oscillation)

Figure 9 shows a typical waveform of the periodecal pulse train, whose pulse width and pulse train intervals were about 5ns and 24ns, respectively. This waveform could be considered to be a self mode-locked oscillation[7]. The pulse train interval, 24ns is in good agreement with the

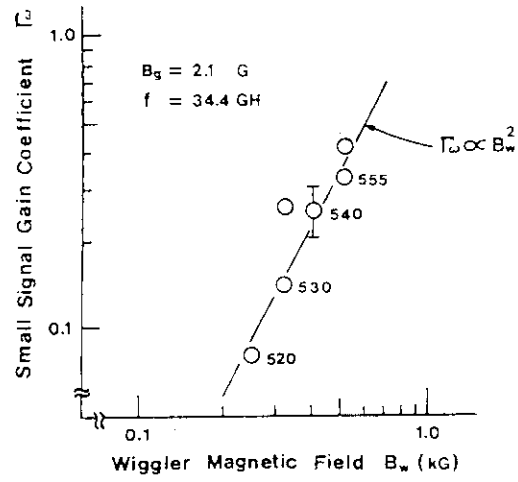

Fig.7 Variation in the small-signal gain coefficient as a function of the wiggler magnetic field.

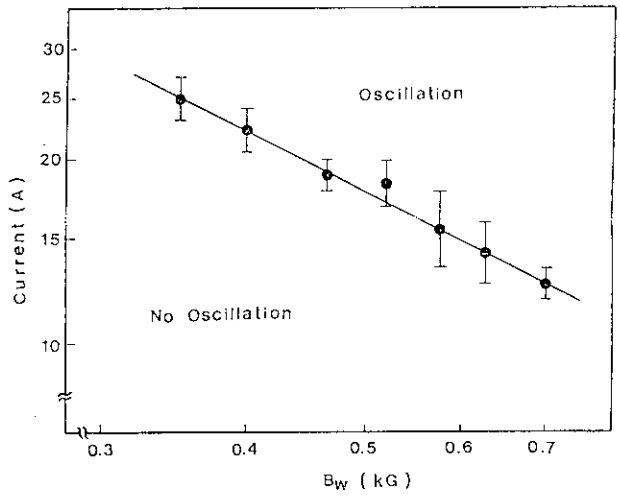

Fig.8 Diagram of the RPE current and the wiggler magnetic field strength B_W, which gives the threshold for oscillation.

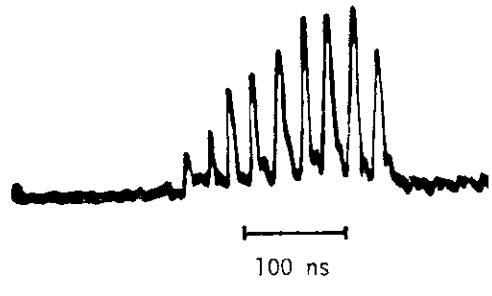

Fig.9 A typical waveform of the periodical short pulse trains.

theoretical calculation under the assumption that the oscillation occurs at the lower branch of the TE_{10} waveguide mode.

3.Conclusions

We constructed a FEL system using linearly polarized wiggler and rectangular waveguide, and investigated the operation characteristics by using tenuous cold relativistic electron beam. The spectra of the spontaneous emission and the induced emission were in good agreement with theoretical calculations. Periodical short pulse trains were observed, which could be explained as self mode-locked oscillation of a free electron laser.

Reference

[1]D.A.G.Deacon, et.al., Phys.Rev.Lett. 38,892 (1977).
[2]S.H.Gold, et.al., Appl.Phys.Lett. 43,922(1983).
[3]M.Kawai, et.al., J.Appl.Phys. 24,1347(1985).
[4]M.Kawai, et.al., J.Appl.Phys. 66,2789(1989).
[5]Y.Kawamura, et.al., Appl.Phys.Lett. 45,307 (1984).
[6]M.Kawai, et.al., Appl.Phys.Lett.45,1287(1984).
[7]Y.Kawamura, K.Toyda and M.Kawai, Appl. Phys.Lett. 51,795(1987).

9. LONG PULSE ROTATING REB FOR CIRCULAR FREE ELECTRON LASER

H. Ohta, T. Mizuno, H. Sekita, Y. Naito, M. Kitora, and H. Saito

Institute of Space and Astronautical Science
3-1-1 Yosinodai, Sagamihara, Japan 229

ABSTRACT

A long pulse (microsecond pulse length), high voltage (500KV), medium current density(50-150A/cm^2) relativistic electron beam is generated from field emission diode with velvet cathode. Diode characteristics including beam divergence angle and gap closure velocity are measured. In the initial experiment, this beam is applied to a circular free electron laser, and the preliminary experimental result is present. In the second phase, diode voltage will increase up to 1.2MV.

1. INTRODUCTION

Most of free electron laser (FEL) experiments in long wavelength region may be classified into two groups from the standpoint of electron beam generation - high voltage/short pulse experiments, and low voltage/long pulse experiments. The former experiments have employed high voltage (>500KV), short pulse (<100ns) power supply, such as induction linear accelerator and pulseline machine (Marx generator combined with pulse forming line). Their field emission type relativistic electron beam (REB) diode with metal or carbon cathode can not be applied for microsecond pulse operation, because of gap closure by expanding cathode plasma. In the latter experiments with low voltage region less than 200KV, a conventional thermionic electron gun can be utilized to obtain long pulse with microsecond pulsewidth. However, it is technically difficult and expensive to apply a long pulse thermionic electron gun in high voltage with MV range. Also, their beam current is not high enough for some FEL applications.

We have been developing high voltage(0.5-1.5MV), medium current density(50-150A/cm^2),long pulse (microsecond pulse length) REB generator with velvet field-emission diode. This long pulse beam is applied to a circular FEL[1,2], where the beam rotates azimuthally under an axial magnetic field and azimuthally periodic wiggler magnetic field in the radial direction.

2. EXPERIMENTAL INSTRUMENT

2-1. POWER SUPPLY

In order to obtain a long pulse REB, a Marx generator with 1.5MV voltage and 20KJ storage energy is directly connected to a REB diode. There is a shunt resister Rs of CuSO4 solution, in parallel to the REB diode, to adjust discharge time constant CRs. If the effective diode resistance Rd is much larger than Rs (Rd>>Rs), most of the discharge current flows in Rs and the voltage waveform is almost independent of the temporal variation of Rs or the diode current fluctuation. The diode voltage remains almost constant in the time scale of t<<CRs. The remaining period t≳CRs of the discharge provides decreasing voltage waveform. In parallel to the diode, we will install a diversion discharge gap, which is triggered by a excimer laser pulse, in order to avoid long exposure of the diode and power supply to the high voltage.

2-2. REB GENERATION

We found that a field emission diode with velvet cathode has slow gap closure characteristics and is suitable for long pulse operation. It is probablly due to relatively low electron temperature of cathode surface plasma, which is generated by occluded, gas-enhanced field emission from velvet surface. The threshold surface electrical field to emit electron beam from velvet cathode is approximately 25kV/cm. The medium beam current density of 50-150A/cm^2 is observed above the threshold. Figure 1 shows the diode voltage and current waveform. The diode voltage remains almost constant for early 0.7μs duration. The effective gap distance D is calculated in use of Child's current formula and is indicated in Fig.2. In early phase of <1μs, D decreses rapidly with expanding velosity 5cm/μs. However, in later phase of >1μs, slow plasma expansion with 0.2-0.5cm/μs is observed. Shefer et.al.[3] proposed a theoretical model of field emission diode with expanding cathode plasma, which predicts the existance of rapid-expanding early phase and slow-expanding later phase. Our experimental data are qualitatively consistent with the model. The temporal variations of beam emittance and divergence angle are measured by means of pepper pot method. The typical beam divergence angle is 40mrad.

3. ROTATING BEAM AND CIRCULAR FEL EXPERIMENT

We have applied this long pulse REB to circular FEL. An annular velvet cathode emits a hollow beam, which is propagated through a cusp magnetic field. The axial velocity is converted to

the azimuthal velocity, and a REB rotates under a uniform axial magnetic field. We obtain a rotating beam with energy 450keV, current 20A, pulse length 1μs, radius 6.0cm, beam thichness 0.5cm, and v_θ/v_o =0.9-0.95, where v_θ , and v_o denote total, and azimuthal velocity, respectively. Figure 3 shows the beam pattern of this rotating REB in a uniform magnetic field. However, the beam radius spatially fluctuates along the uniform magnetic field because of a finite width effect of cusp transient region[4]. We will modify the spatial profile of cusp magnetic field to suppress this coherent off-centering.

A wiggler magnet system is designed and constructed for the circular FEL. The wiggler periodicity N=12, the wiggler field strength B=800G, the inner and outer gap radius is 5.5cm, 7.0cm, respectively. We propagate the rotating REB through the wiggler magnetic field. Fig.4 is the beam pattern at the end of the wiggler. It is observed that the rotating REB motion is modulated by the wiggler field with periodicity N=12.

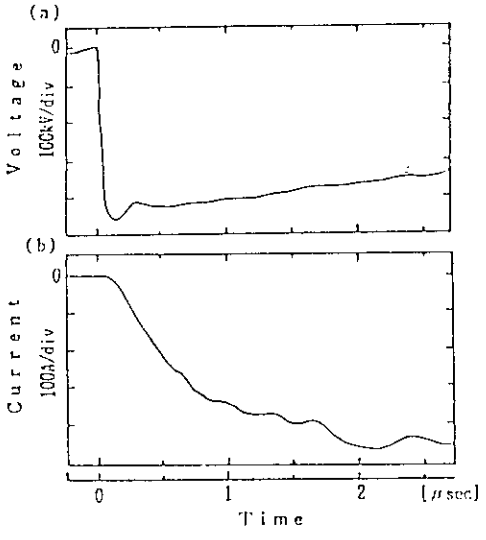

Fig.1. Waveform of long pulse REB diode with velvet field emission cathode. voltage (a),and current(b).

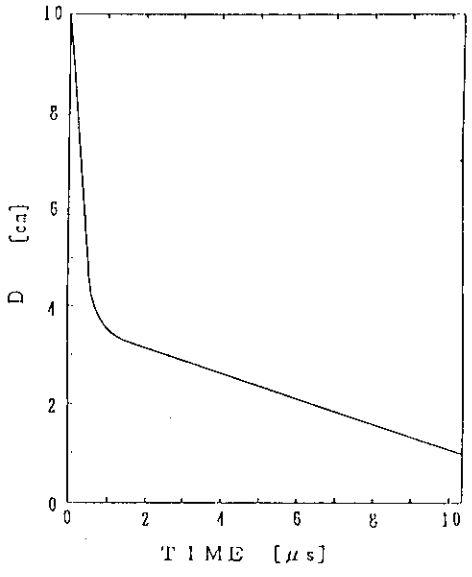

Fig.2. Temporal variation of effective gap distance D calculated from Child's Law. Peak diode voltage = 370KV, cathode-anode distance=10cm.

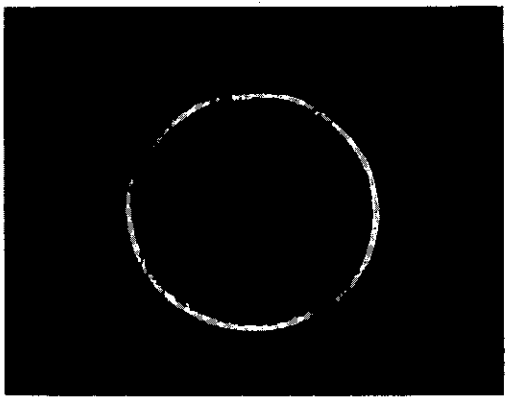

Fig.3. Beam pattern of rotating REB in a uniform axial magnetic field at 30cm down from cusp transition.

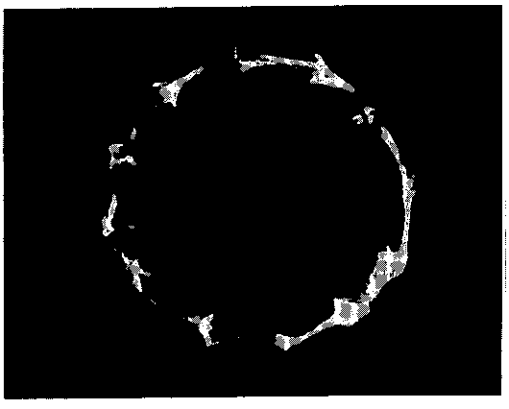

Fig.4. Beam pattern at the end of wiggler magnet of circular FEL (45cm down from cusp transition). Beam motion is modulated by wiggler field with periodicity N=12.

REFERENCE

[1] W.W.Destler, et al. Phys. Fluids 28, 1962(1985)
[2] H.Saito and J.S.Wurtele,Phys.Fluids30,2209(1987)
[3] R.E.Shefer, et al. Phys. Fluids 31, 930(1988)
[4] M.J.Rhee and W.W.Destler, Phys.Fluids17,1574 (1974)

10. FREE ELECTRON LASER EXPERIMENTS IN EUROPE

Y. PETROFF
LURE - Laboratoire mixte CNRS - CEA - MENJS
Centre Universitaire, 91405 ORSAY - FRANCE
64 46 80 01

ABSTRACT

The purpose of this paper is to present a short description of the FEL activities in Europe. We are considering only experiments which have been already funded and are under construction. About 17 FEL projects are going on, most of them in the Compton regime.

1 - INTRODUCTION

Since the first operation of a FEL by J. Madey and his group[1] most of the laser oscillations have been obtained in the U.S.A. with the exception of the Orsay experiment[2] (1983 on ACO and 1989 on Super ACO) and more recently the Novosibirsk one (1988)[3]. However the situation is changing and about 17 projects are under construction in Europe. They are trying to cover a broad band going from the mm region to the ultra violet. It is impossible to describe thoroughly those experiments in a limited space ; they will be presented per country.

The table I presents the projects already funded. The first column gives the location and the name, the second the type of electron machine, the third the energy (MeV) and the last one, the expected energy range of the laser.

FRANCE	Type	Energy (MeV)	λ(μ)
ACO(Orsay)	SR	150-240	0.4-0.7
+ Super ACO (Orsay)	SR	600-800	0.2-0.7
* CLIO (Orsay)	L	30-70	2-20
* ELSA (Bruyères le Chatel)	L	20	3-20
GERMANY			
DELTA (Dortmund)	SR	500-1000	0.1-0.4
* DARMSTADT	SCL	35-50	2.5-5.3
ITALY			
ENEA (Frascati)			
a)	M	20	20-40
b)	RM	50	1-35
c)	CD	5	100-400
LISA (Frascati)	SCL	25	11-18
ELFA (Milano)	SCL	7-10	3000
SEAFEL (Legnaro)	EA	3	2500
NETHERLAND			
*FELIX (Nieuwegein)	L	15-45	5-160
TWENTE			
a)	L	25	0.2-20
b)	RM	25	20
c)	D	1.5	1500
USSR			
+NOVOSIBIRSK	SR	350	0.2-0.6

+ in operation today SR = storage ring M = microtron L = R.F. Linac RM =race track microtron

* expectted in operation within a year SCL = supercon. Linac EA = Electrostatic accelerator D = Diode CD = Cerenkov device

Table I : F.E.L. projects in Europe

2 - DESCRIPTION OF THE EXPERIMENTS

2-1 A.C.O. (Orsay)

The first F.E.L. emitting in the visible was operated in 1983[4] at Orsay on the old storage ring ACO, built in 1964. Despite of the reduced performances of this ring, studies were conducted during several years (until 1987) giving precious informations on the F.E.L. physics (discovery of the Q switch operation, the macrotemporal structure of the laser...). The ACO F.E.L. was moved on Super ACO in 1987.

2-2 Super ACO (Orsay)

It is a 0.8 GeV storage ring devoted to synchrotron radiation experiments. It belongs to the new generation of machines caracterized by a low emittance ($\varepsilon_x = 3.8\ 10^{-8}$ m.rad) and a large number of insertion devices (4 for the moment, 6 possible). It is injected with positrons, to improve the stability and the lifetime of the beam.

For F.E.L. experiments, Super ACO is operated at 600 and 650 MeV, with two stabilized opposite bunches, separated by 120 ns. The permanent magnet optical klystron is made of two undulators of 10 periods of 13 cm each, and 0.5 m long dispersive section in the middle with a maximum deflection parameter K = 5.75

The first laser operation was obtained in the visible at 6000 Å[5]. The laser operates now during several hours from 50 to 2mA per bunch.

- The wavelength tunability is 500 Å, limited by the mirror bandwidth.
- The maximum extracted power has been 290 mW (theoretical prediction 478 mW) for a ring current of 89 mA.
- Usually the laser oscillates on the TEM_{oo} mode but several modes TEM_{on} with n up to 5 can be observed.
- However the more important result has been the first observation of deterministic chaos in a F.E.L. [6]. This has been obtained by modulating the R.F. frequency.
- Experiments are underway to obtain a spectral narrowing by the insertion of a dispersive element inside the optical cavity, the Q switch operation and the oscillation around 2500 Å.

2-3 CLIO (Orsay)

The CLIO collaboration between three laboratories started in 1986 in order to build an infrared F.E.L. at LURE (Orsay)[7]. For that an S band R.F. linear accelerator is under construction. The table II gives the parameters of the electron beam.

The R.F. linac consists of a 100 KV dispenser cathode gun, a 500 MHz prebuncher, a S band standing wave buncher followed by a S band travelling wave accelerating section 4.5 meter long

Energy range :	30-70 MeV
Micropulse length :	10 ps
Micropulse peak current :	110 A
Micropulse charge :	1 n C
Macropulse length :	up to 12 μs
Macropulse peak current :	< 300 mA
Macropulse repetition rate :	12.5, 25, 50 Hz
Average beam power :	up to 7.5 Kw
Normalized emittance :	≤ 150 π mm. mrad
Energy spread :	~ 1 %

Table II - Electron beam parameters

The 3 GHz buncher of 1.5 MW and the accelerating section of 25 MW are fed by a 28 MW peak output Thomson-CSF klystron.

In order to obtain enough gain at low wavelength together with a proper energy extraction at longer wavelength a two component undulator has been built. It is made of two identical undulators of length $L = 0.96\ m = 24\ \lambda_o$ (λ_o is the period = 4 cm). Moreover the second undulator can be tapered.

The laser is expected to be tunable in the range 2-40 μ.

The calculated peak power (per micropulse of 10μs) is 100 kW, the average power varying between 50 and 6 W.

The first oscillation is expected for January 1991.

2-4 ELSA (Bruyères le Chatel)

The purpose of this laser is to obtain high power and high efficiency. To reach this goal the following components are under construction :

- a photo injector using a R.F. gun cavity at 144 MHz to produce electron bunches.
- a 433 MHz 3 cell cavity powered by a 6 MW peak power and 200 μs pulse duration klystron.
- a tapered hybrid undulator using permanent magnets and pulsed coils[8].

The photoinjector is very similar to the one built at Los Alamos[9].

The optical mirror mount is based on concepts developed at Spectra Technology Inc[10].

The simulations show that extraction efficiencies between 0.5 and 4 % could be obtained for λ = 15-25μ. The laser peak power could be as large as 50 Mw and the macropulse average power around 100 kW.

The laser oscillation is expected by the beginning of 1991.

2-5 DELTA (Dortmund)

The Dortmund Electron Test Accelerator (DELTA) is a low emittance ($\varepsilon_x \sim 10^{-8}$ mrad) storage ring under construction at the University of Dortmund [11]. It is based on a FODO lattice structure, similar to the one used by J. Madey for his 1 Gev ring and it is optimized for F.E.L. operation : small horizontal emittance, short bunch length, high beam current, large energy acceptance, strong radiation damping. Two straight sections of 20 m length will be available for insertion devices. The energy available will vary between 500 and 1000 MeV.

The first experiment will be based on an optical klystron, using electromagnet undulator. A gain of 10 % is expected at 4000 Å with E = 500 MeV and I = 30 mA.

In a later stage, by increasing the energy to 1 Gev, oscillation is expected in the UV. Finally a high gain F.E.L. is planned to reach wavelengths of about 250 Å or even below.

2-6 DARMSTADT

The Darmstadt F.E.L.[12] is based on a 130 MeV superconducting electron accelerator S-DALINAC[13]. For the F.E.L. experiment the energy used will vary between 35 and 50 MeV.

The injector of the superconducting accelerator has gone into operation about 3 years ago and acceleration tests with the main linac have been carried out recently. The emittance and energy spread of the electron beam was found to be within the design values.

The pulsed high current electron source has been tested successfully. It delivered beam pulses with a length of less than 2ns, a peak current of more than 30 mA and a normalized emittance of less than 2π mm mrad. These beam pulses will the be chopped to about 0.4 ns and bunched to 5ps by a system consisting of a subharmonic chopper and prebuncher resonator both operating on the 5^{th} subharmonic of the linac frequency at 600 MHz.

The undulator is being built in the wedged pole configuration with a periodic length of 3.2 cm and a peak magnetic field of more than 0.4 T. The number of period is 80, its total magnetic length amounts to 2.56m. The field tolerances with respect to magnetic field variation, first and second field integrals have been chosen to decrease the small signal gain by no more than a factor of two.

The optical cavity has a length of 15m. The results of the F.E.L. simulations are given in table III.

wavelength (μ)	2.57-5.24
gain (%) 1A	9.4 (2.57 μ)
	13 (5.24 μ)
peak out put power (kw)	510 (2.57 μ)
	405 (5.24 μ)

Table III - Results of the F.E.L. simulations

This laser will be the first continuous wave F.E.L and its pulse structure will consist of photon pulses with a duration of 2 ps at a repetition rate of 10 MHz.

First oscillation is expected by the end of 1990.

2-7 ENEA (Frascati) - Microtron F.E.L.

The main characteristics of the experiment are given in table IV. The apparatus is now in operation. Measurements[14] to establish the e-beam characteristics, including the measurement of spontaneous emission spectra, have been carried out. Amplification has been observed and oscillation should be obtained very soon.

MICROTRON		
Parameter	Achieved	Design Goal
Electron beam energy (MeV)	20	20
Electron bunch duration (ps)	20	20
Macropulse duration (μs)	10	12
Current macropulse (mA)	160	200
Peak current (A)	3.2	4
Normalized horizontal emittance (m-rad)	7.5×10^{-4}	7.5×10^{-4}
Normalized vertical emittance (m-rad)	2.5×10^{-4}	2.5×10^{-4}
Energy spread	0.12 %	0.12 %
UNDULATOR		
Pure $SmCo_5$ constant parameters		
Period (cm)		5
Number of periods		45
Gap (cm)		0.9 - 7
k patameter at 1.3 cm gap		2
k parameter at 2.4 cm gap		1
OPTICAL RESONATOR AND FEL CHARACTERISTICS		
Parameter	Achieved	Design Goal
Resonator length (m)	6.37	6.37
Reflectivity of the end mirror (copper)	99 %	99 %
Reflectivity of output coupler (coated Si)	97 %	97 %
Total losses	~ 4 %	~4 %
Laser wavelength (μ)		20-40
Gain per pass at $\lambda = 32$ μ, i = 200 mA		10 %
Average laser power at $\lambda = 32$ μ and at 150 Hz repetition frequency (W)		5
Peak power (micropulse) (MW)		1
Peak power (macropulse) (kW)		40

Table IV - F.E.L. Device Characteristics

2-8 ENEA (Frascati) - Racetrack-microtron

This project in under development. It consists of a 50 MeV racetrack microtron. The goal is to cover the 1-35 μ energy range.

2-9 ENEA (Frascati) - Cerenkov Device

This project started in 1986. It is based on the interaction of a relativistic e-beam with a dielectric slab :

the goal is to produce a laser source in the far infrared[14] (100-400 μ) with a peak power of the order of 100kW. The parameters of the experiment are given in table V

accelerator	microtron
e-beam energy	5 MeV
e-bunch duration	20 ps
macropulse duration	4μs
average current	200 mA
peak current	4 A
vert. emittance	6 π mm. mrad
horiz. emittance	18 π mm. mrad
energy spread	0.5 %
DIELECTRIC SLAB PARAMETERS	
material	polyethylene
thickness	2.5 - 5 μm
length	200 mm
width	25 mm

Table V - Cerenkov device parameters

2-10 LISA (Frascati)

This F.E.L. is based on a superconducting linear accelerator. The main parameters are summarized in table VI[15]

Energy (MeV)	25-49
Bunch length (mm)	2.5
Bunch charge (pC)	40
Peak current (A)	5
Emittance (π mrad)	10^{-5}
Energy spread	2.10^{-3}

Table VI - Parameters of the accelerator

The superconducting cavity frequency is 500 MHz, an harmonic buncher has been inserted to achieve the high peak current required for F.E.L. operation. The microbunch repetition rate is 50 MHz.

The F.E.L parameter are given in table VII

Number of undulator periods :	50
Undulator wavelength (cm) :	4.4
Undulator parameter K :	0.5-1
Radiation wavelength (μ) :	11-18
Optical cavity length (m) :	6
Cavity passive losses (%) :	2

Table VII - F.E.L. parameters

Taking account emittance, energy spread and slip page effect the expected gain on the fundamental is 10 % and 5 % on the third harmonic Commissioning of the machine is foreseen to be performed at the end of 1990 and laser oscillation is expected in 1991.

2-11 ELFA (Milano)

ELFA[16] (Electron laser facility for acceleration) has both a fundamental and a technological goal. The fundamental goal is to test with short bunches the existence of three different high-gain regimes :

- the already observed steady-state regime
- weak superadiance
- strong superadiance

The ELFA accelerator will provide a 400 A-10 MeV electron beam. Its basic components will be a photocathode injector and one superconducting 4 cell LEP module at 352 MHz.

The beam specifications are given in table VIII

- Current (A) :	400
- Bunch length (ps) :	150
- Charge per bunch (nc) :	60
- Energy spread (%) :	1
- Emittance (mrad) :	10^{-3}

Table VIII - Beam parameters

The undulator will be composed joining up two sections : a hybrid wiggler will be the first section and an electromagnetic wiggler the second one. Both wigglers will have canted poles in order to get focusing in vertical and horizontal planes. The electromagnetic wiggler will allow for tapering.

The FEL is expected to emit around λ = 3mm. The optical parameter will depend very strongly on the high gain regime obtained.

The time schedule is not very precise for the moment.

2-12 SEAFEL (Legnaro)

The main goal of this project is to search for CW operation ranging from cm up to mm wavelength.

The accelerator, a Cockroft-Walton type, is being assembled at LNL-Laboratori Nazionali di Legnaro (Padova)[17]. The energy is 0.7 MeV the intensity I = 3A, the energy spread 10^{-4} mrad, and the normalized emittance 10^{-4} mrad.

A multistage collector is added to recover as many electrons as possible (> 99 %).

The undulator has a period of 3 cm and a 1,5 m length. The expected power is 100 kW at λ = 2.5 mm.

2-13 FELIX (Rijnhuizen)

This FEL is under construction at the FOM-Institute.

The accelerator for FELIX[18] consists of a triode gun, a prebuncher, a travelling wave buncher and two travelling wave linac sections. The beam can be bent into two undulators at two locations, after the first (15-25 MeV) and after the second linac (25-45 MeV). By installing different undulators the group will try to cover the wavelength range from 3 to 160 μ.

Tuning will be achieved by varying the undulator gap width to obtain rapid tuning.

The design parameters are summarized in table IX

30-90	--	Lorentz factor
5-80	μ	EM wavelength
65	m	Undulator period
< 4400	G	Peak undulator field on axis
38	--	Number of undulator periods
< 1.9	--	Undulator strengh
247	cm	Undulator length
194	pC	Charge per microbunch
70	A	Peak current
0.2	A	Average current during macropulse
3	ps	Micropulse length
1	GHz	Micropulse repetition frequency
20	μs	Macropulse length
10	Hz	Macropulse repetition frequency
1	mm	Rms electron beam radius
2	mm	Rms microbunch length
0.35	%	Energy spread
50	π mm mrad	Normalized emittance
100	μJ	EM energy per micropulse (3ps)
100	kW	EM power per macropulse (20μs)
1	%	Bandwidth (without etalon)

Table IX - Basic parameters for FELIX, Stage I

One important objective of this project is to obtain narrow band radiation. This should be achieved via phase locking of the micropulses by means of an intracavity etalon, combined with external selection of a single cavity mode. This technique is only effective when there are a large number of circulating pulses in the cavity.

The laser oscillation is expected by beginning of 1991.

2-14 TWENTE

The TWENTE University has three projects :

the first one deals with a linac FEL with a photo-cathode gun delivering a maximum current of approximately 300 to 400 A. The energy will be 25 MeV.

2-15 TWENTE

Study of a racetrack microtron[19] has started. It will take several years before operation.

2-16 TWENTE

The Raman FEL consists of a 1.5 MeV, 1 KA field emission diode and a electomagnetic undulator.

2-17 NOVOSSIBIRSK

The F.E.L. experiment is installed on a bypass of VEPP-3 storage ring. The electron beam characteristics are given in table X.

Energy (MeV) :	350
Energy spread :	9.10^{-4} (for 20mA)
Emittance (mrad) :	4.10^{-8} (for 20mA)
Bunch length (mm) :	100 (for 20mA)
Peak current :	6
Beam size : σ_x (mm) :	0.45 (for 20mA)
σ_y (mm) :	0.2 (for 20mA)
76 MHz RF voltage (KV) :	100

Table X : Electron beam parameters

The magnetic device is an optical klystron, which was first proposed by Vinokourov and Skrinsky[20]. It consists of two electromagnetic undulators separated by a 3 pole dispersive section. Each undulator has 33.5 periods and a length of 3.4 m.

The optical cavity consists of two mirrors with curvature radii of 10 m, at a distance of 18.7m from each other.

The gain is 10 % at 6000Å, 5.5 % at 4000Å and 2.5 % per pass at 2500Å.

Laser oscillation has been obtained in the range 5 800-6900Å, 3750-4600Å and 2400-2700Å.

The measured laser power is 6mW at 6300Å and 2.5mW at 2500Å. The laser micropulse have a duration time of about 200ps. According to that the out put peak power is 25kW and 9kW at 6300Å and 2500Å, respectively in the Q switch mode. Within the optical cavity the peak power is correspondingly 2.5MW and 1MW.

The future plans are the increase of the lasing power, the narrowing of the bandwith and the shortening of the lasing wavelength.

3 - CONCLUSION

It is clear from this review that the field of F.E.L. is quite active now in Europe, after a rather slow start. Next year at least 6 lasers should be in operation.

REFERENCES

(1) D.A.G. Deacon et al - Phys. Rev. Lett. 38, 892, (1977)
(2) M. Billardon et al - Phys. Rev. Lett. 51, 1652, (1983)
(3) I.B. Drobyazko et al - Proceedings of ECO 2 Paris 24-25 April 1989 - SPIE Vol 1133 Free Electron Lasers p. 2. (1989)
(4) P. Elleaume et al - Journal de Physique 45, 989, 1984
(5) M.E. Couprie et al - see Ref. 3 p 11 and to be published.
(6) M. Billardon - Phys. Rev. Lett. (to be published)
(7) J.M. Ortega et al - Proceedings of the Tenth Intern. FEL Conference NIM A285, 97 (1989)
(8) R. Dei-Cas et al - see Ref 7 p. 320
(9) J.S. Fraser and R.L. Sheffield - I.E.E.E. J. Quantum Electronics QE-23 (9) 1489, (1987)
(10) D.M. Shemwell et al - N.I.M. A 259, 56 (1987)
(11) F. Brinker et al - XI Internat. Conf. on Free Electron Lasers - August 1989 - Naples - USA, to be published
(12) V. Aab et al - see Ref 3 p. 82
(13) V. Aab et al - see Ref 7 p. 75
(14) E.P. Garate - N.I.M. A 259, 125 (1987)
(15) M. Castelano et al - see Ref 3 p. 34
(16) R. Bonifacio et al - see Ref 3 p. 70
(17) I. Boscolo et al - Ref 3 p. 102
(18) P.W. Van Amersfoort et al - see Ref 7 p. 67
(19) G.J. Ernst et al - see Ref 7 p. 71
(20) N.A. Vinokourov, A.N. Skrinsky - Preprint of the Institute of Nuclear Physics 77-59 Novosibirsk 1977
(21) I.B. Drobyazko et al - see Ref 3 p. 2

11. SURVEY OF FEL RESEARCH IN ISRAEL

Shlomo Ruschin
Faculty of Engineering, Tel-Aviv University
Ramat-Aviv 69978, Israel
972-3-5450765

I. INTRODUCTION

Research in the field of FELs has been performed in Israel since the end of the 70's. The experimental work first concentrated on basic physics of FEL processes like measurements on Smith-Purcell radiation and the mechanisms of electron trapping and other non-linear processes. These projects took place at Tel-Aviv University where additional basic experiments are planned. At the Hebrew University of Jerusalem an intense relativistic beam was operated based on a Febatron accelerator where diagnostic methods were investigated together with the concept of wigglerless FEL. Using a pulsed intense relativistic beam produced by a 0.7 MV PI accelerator, FEL operation in a lowbitron mode was demonstrated in a joint RAFAEL (Ministry of Defense laboratories) - TAU project. Presently a main effort is taking place on the operation of a full scale FEL based on an electrostatic TANDEM accelerator located at the Weizmann Institute. This FEL will operate in the mm to FIR range and is expected to demonstrate quasi-CW function. This survey includes only experimental FEL related research. Theoretical topics were also studied by various research groups in the country, The reader is generally referred to the proceedings of the Annual International FEL conferences between the years 1980-1989 where Israeli researchers reported extensive research work.

II. ANGULAR RADIATION PATTERN MEASUREMENTS OF SMITH-PURCELL RADIATION[1]

In this work experimental measurements of Smith-Purcell radiation was reported for electrons in the range between 60-100 keV and for a variety or gratings. The main emphasis laid on quantitative data acquisition on radiation intensity and angular emission patterns. This data was compared to theoretical predictions of various existing models in order to check their validity. Due to the close relationship between spontaneous and stimulated emission, data from spontaneous emission measurements can be used to draw conclusions concerning FEL devices based on Smith-Purcell interaction. These conclusions included here feasibility and optical configurations for different types of oscillator and resonator devices.

$$\lambda_n = -\frac{D}{n}(\beta^{-1} - \sin\eta) \qquad (1)$$

where D is the grating period, β the electron's normalized velocity, n a negative integer and η the elevation angle. The insensitivity of the wavelength on the azimuthal angle ς was also checked. An interesting feature of the work was the finding that the measured radiation angular distribution had a maximum intensity at azimuth angles different from zero. From the theoretical point of view, good agreement was exhibited with the theory of Van den Berg.[2] Specific resonator configurations were proposed for efficient FEL radiation sources based on Smith Purcell interaction. This work was carried out by researchers from Tel-Aviv University.

III. VELOCITY DISTRIBUTION AND ENERGY DIAGNOSTICS IN INTENSE GUIDED RELATIVISTIC ELECTRON BEAMS

Within this work, which was carried out at the Center for Plasma Physics, in the Hebrew University of Jerusalem, a method was presented by which the average parallel velocity of an intense guided relativistic beam could be determined.[3]

The experimental system consisted of a Febatron electron gun which provided 80-100 nsec pulses with voltages of up to 500 kV. After filtering the beam through a series of diagraphms, a narrow electron beam was obtained which was inserted into a drift tube. The beam current was measured by means of a disk collector located at the end of the tube, while the radial electrostatic potential V_c, induced due to the space charge of the beam was monitored by means of a co-axial cylindrical capacitor. The average drift velocity could be found with the help of the ratio between the collected current and the coaxial capacitor's voltage. As a result, real time information of the average axial velocity of the e-beam could be gathered including the fraction of the total electron kinetic energy converted into axial motion. The average drift velocity was found to be always considerably less than that calculated by means of the diode voltage. In a subsequent work[4] the method was further developed for providing simultaneous knowledge of the distribution of the axial velocities and γ - the relativistic factor of the beam. Measurement of the parallel velocity distribution was achieved by insertion of a

magnetic hill into the tube. Analysis of the current reflected by the hill as a function of the height of the hill yielded the desired beam characteristics. Again, the axial velocity distribution could be determined at various times during the current pulse.

IV. LONGITUDINAL WIGGLER FREE ELECTRON LASER (LOWBITRON)

In this work, the Lowbitron - a longitudinal wiggler beam interaction device was experimentally demonstrated for the first time.[5] This device, first proposed and analyzed by McMullin, Bekefi and Davidson[6] is based on an hybrid mechanism which combines two classes of electron instabilities, namely, the cyclotron resonance mass instability and the FEL instability. In the interaction scheme, a thin beam of relativistic electrons acquires a large transverse velocity component before entering the interaction region. Within the region, it travels under the influence of a combined axial magnetic field and a longitudinally polarized periodic wiggler magnetic field. The experiment setup consisted of a 740 kV 10 nsec electron beam accelerator. By means of an iris aperture placed on the anode, a 4 mm pencil electron beam carrying about 400 Amp was extracted. The output radiation was coupled via a polyethilene window attached to a horn antenna which terminated the drift tube. The radiation spectral content was then analyzed by a grating spectrometer. The measured frequency spectrum was in the range of 60-140 GHz. In general, this spectrum consisted of two peaks which fitted well the theoretical model calculation based on the intersection of the beam dispersion curve with the waveguide TE_1 dispersion curve. Good quantitative agreement of the measured power with the analysis of McMullin et al. was also demonstrated. This work was carried out within a joint project by the Applied Physics Department at the Ministry of Defense and Tel-Aviv University.

V. EXPERIMENTS IN A TWO COUNTERPROPAGATING LASERS COMPTON-SCATTERING FEL SCHEME

This project, performed at the Faculty of Engineering, Tel-Aviv University, reported[7-9] the observation and investigation of synchronous energy exchange between nonrelativistic electrons and the ponderomotive (beat) force of two counterpropagating intense pulsed CO_2 laser beams, operating at different frequencies in a stimulated Compton-scattering scheme. The interaction occurred in the nonlinear (trapping) regime, the physics of which is the same as that which occurs in laser accelerators and efficiency-enhanced free-electron lasers with long wigglers. The experiment is a first demonstration of the principle of inverse FEL acceleration and electromagnetic pump FEL operation in the nonlinear (trapping) regime. It can also be described as a demonstration of a "traveling beat-wave" Kapitza-Dirac effect in the nonlinear regime. Two different mechanisms of enhanced energy transfer were observed - electron trapping and phase-area displacement.

In order to observe an appreciable interaction effect between the electrons and the traveling beat wave, the electron velocity must be synchronized with the beat-wave phase velocity $v_r = (\omega_s - \omega_w)/(k_s + k_w)$ (for a static wiggler $\omega_w = 0$). The relative velocity between the electron and the wave can be scanned by applying an axial E field. In the nonlinear regime, where deep ponderomotive potential wells (traps) form, two different physical situations may occur: (1) Electrons inserted into the interaction region are within the phase-space area of initially synchronous traps [trapping]. (2) The opposite case of no initial trapping. If the axial E field and other interaction parameters are uniform along the entire interaction length, the initially trapped electrons occupy closed trajectories inside the trap area, and remain trapped despite the accelerating field. In both cases the initially untrapped electrons accelerate or decelerate freely, following open phase-space trajectories. Transitions between trapped and untrapped electron trajectories are possible only if the interaction parameters are changed nonadiabatically in either the axial or time dimension, or if the electron is displaced transversely across the optical beams.

An additional mechanism of radiative energy extraction termed "phase-area displacement"[10-11] (PAD) results in enhanced signal amplification when the entire e beam scanned through the synchronism condition. In PAD, as opposed to electron trapping, signal amplification is accomplished by either reversing the taper in a tapered wiggler, or by reversing the polarity of the dc field. In both PAD schemes, trapping conditions at the entrance to the interaction region are avoided, and all the electrons are scanned through the energy of synchronism at some point along the interaction region, resulting in a net energy extraction from the entire electron beam.

The experimental concept, as depicted in Fig.1 with the baseline parameters listed in Table I, was described in detail by Olshan et al.[6] Two transversely excited atmospheric (TEA) CO_2 lasers produced the 9.3 μm signal wave and the 10.6 μm wiggler wave, both of which were operated in single longitudinal and transverse cavity modes. Their 100-nsec duration pulses were synchronized to arrive simultaneously at the interaction region during the 10 μsec pulse of the electron beam. The ~ 1 keV electron-beam voltage was matched to the synchronism condition at either the entrance to the interaction re for setting trapping conditions [Figs. 1(a) and 1(c)] or within the interaction region for PAD conditions [Figs. 1(b) and 1(d)]. The e-beam energy spread was $E_{th} \simeq 4$ eV, with a grid-controlled current of 10-50 μA.

An axial electric force was exerted along the interaction length by employing the ohmic potential drop along the copper coil when a 1-msec, 500-A current pulse is applied to it. Accelerating or decelarating fields were achieved by changing the direction of the current. The coil current also provided an axial magnetic field which bent the e beam and guided it along the interaction region.

Both retarding-potential and time-of-flight electron-energy-analysis techniques were employed for diagnosing the electron-radiation interaction effects.

The successful demonstration of energy exchange by nonlinear regime Compton scattering in this experiment makes way for further fundamental interaction and FEL related studies in a small-scale laboratory system. Further experiments were carried out with this system which studied important interaction aspects of phase-area displacement and trapping mechanisms; for example, effects of nonadiabatic changes in the interaction parameters and incoherence of the wiggler and signal waves.[8-9]

VI. IR -mm WAVE FEL BASED ON A TANDEM ELECTROSTATIC ACCELERATOR

In this project,[12,13] based on the 6 MeV Tandem electrostatic accelerator located at the Weizmann Institute, Rehovot, research teams are collaborating from Tel-Aviv University, the Weizmann Institute, RAFAEL (Ministry of Defense Laboratories) and the Negev Nuclear Research Center. The goal of the project is to develop a unique quasi-CW highly monochromatic and intense radiation source which will be able to operate in the entire mid-IR-FIR-mm wavelength regime. (15 μ to 3 mm).

In the positive terminal straight geometry Tandem configuration (Fig. 2) the electron beam is transported with simple straight electron optics all the way from the electron gun to the collector, accelerated in the first section (between e-gun and terminal) and decelerated at the second section. At the terminal the fully accelerated electron beam interacts with the magnetic wiggler inside an optical cavity where a significant fraction of its energy is extracted:

$$\frac{\Delta E}{E} \simeq \frac{1}{2N_W} \tag{2}$$

where N_W is the number of periods (typically 10-100). The average e-beam current that can be transported in the accelerator in steady state is determined by the charging current I_{ch} of the H.V.-P.S. (in the case of Van-de Graaff - the charging belts) and the collection efficiency $\eta_{coll} \equiv I_{coll}/I_{emit}$ of the beam transport:

$$I_{av} = \frac{I_{ch}}{1 - \eta_{coll}} \tag{3}$$

Eqs. (1) and (2) determine the average radiative power

$$P_{av} = I_{AV} \Delta E/e \tag{4}$$

Note that the source of the radiative power are the power supplies PS_2, PS_3, which replenish the energy loss of the electrons to the radiation field. With proper design of the collector system (multistage depressed collector) most of the electric power of the power supplies transforms into radiative power, and very high total power efficiency (in excess of 50%) may be expected.

Typical charging current level I_{ch} is hundreds of μAmp (in Van de Graaff) hence $\eta_{coll} > 99.9\%$ is required in order to get $I_{AV} \sim 1$ Amp (needed for sufficient gain). Higher current level $I_0 > 1$ Amp or smaller collection efficiency may be allowed in pulsed operation. Also higher instantaneous current can be obtained in a short pulse (tens of μsec); however in this case if leakage current hits the terminal, it discharges the effective capacitance between the terminal and ground and one experiences an undesirable voltage drop.

With these parameters high power levels can be obtained from the FEL: with $\Delta E \simeq 30$ keV and I = 1 Amp, Eq.4 predicts a power level of P = 30 kWatt.

During the preliminary research phase of the Israeli FEL collaboration an important technical effect characteristic to the straight geometry Tandem FEL configuration was discovered on the modified 6 MeV Tandem accelerator of the WI[13]. This effect of long stable pulse operation is important for the experimental research project proposed, and in fact makes the WI Tandem FEL facility the only one presently fit for studies of single mode, mode competition, coherence and nonlinear regime dynamics in quasi-CW FELs.

The experimentally observed effect was a droop-free stable behavior of the HV-terminal voltage for a long electron beam pulse even when leakage current was high and the transported current exceeded significantly the value given by Eq.3. Within the resolution of the measurement apparatus the stability of the terminal during the electron beam long pulse was at worst $\Delta V_T/V_T = 3\times10^{-4}$. This was measured under conditions of poor collection efficiency of the e-beam: $\eta_{coll} = 50\%$.

Using a capacitance network equivalent circuit to describe the deceleration tube it was possible to provide a reasonable explanation to the long pulse effect based on the capacitance network isolation of the terminal from points in the center of the deceleration column where most of the leakage current is incident. According to the model calculation even with a very high leakage current of $I_{ch} = 0.2$ Amp. (which can certainly be improved) a voltage drop of $\Delta V_T/V_T < 5\times10^{-5}$ at $V_T = 2.5$ MV is expected in a 100 μsec long pulse. Even in a 1 msec pulse a tolerable droop (less than the gain tuning width) of only 5×10^{-4} would be expected.

It should be appreciated that this effect can only happen in the positive terminal configuration (Fig.1) and will not happen in the negative terminal configuration (like the UCSB experiment), where the high current power supply, placed in the terminal, discharges the terminal capacitance right away, whenever the returning collector current is lower than the cathode current. This simple "technical effect" makes the WI Tandem FEL, which is the only present operating straight geometry positive terminal FEL facility, a unique vehicle for demonstrating unequivocal single mode operation and attaining unprecedented spectral purity of a FEL in a quasi-CW operation.

The planned stages of research of the Tandem FEL project are summarized in the following:

(1) The construction of a mm wavelength Quasi CW FEL based on the 6 MeV Tandem accelerator in the WI. The device will be operated at high power and high unprecedented level of coherence when operating at a single longitudinal and transverse mode of the cavity.

(2) Extending the FEL operation regime to the mid-IR ($\lambda \approx 15$ μm), by developing new microwiggler optical klystron technology.

(3) Besides these specific scientific and technical goals the FEL collaboration will address the important scientific applications (in solid state physics, biology, medicine and chemistry) and other applications that the quasi-CW FEL may have as a unique source of coherent IR-mm wavelength radiation.

TABLE I. Experiment parameters.

Signal power	0.25 MW
Wiggler power	0.25 MW
Signal wavelength	9.261 μm
Wiggler wavelength	10.59 μm
Optical-beam waists (w_0)	1.77 mm
Coil current	0.5 KA
Energy spread (FWHM)	3 eV
Interaction length	0.6 m
Electron current	10 μA
Electron velocity	2.0×10^7 m/sec
Axial electric field	65 V/m
Resonance energy	1.153 KeV
Ponderomotive field	369.7 V/m
Trap depth	1.409 eV
Resonant phase ψ_r	0.2 rad

REFERENCES

(1) A. Gover, P. Dvorkis and U. Elisha, J. of the Opt. Soc. of America B, Vol.1, No.5, 723 (1984).

(2) P.M. Van den Berg, J. Opt. Soc. Am., **63**, 1588 (1973).

(3) P. Avivi, Ch. Cohen and L. Friedland, Appl. Phys. Lett., **42**, 948 (1983).

(4) P. Avivi, Ch. Cohen and L. Friedland, Rev. Sci. Instrum., **57**, 346 (1986).

(5) I. Shraga, Y. Goren, Ch. Leibovitch, S. Eckhouse and A. Gover, Appl. Phys. Lett., **49**, 1412 (1986).

(6) R.Z. Olshan, A. Gover, S. Ruschin and H. Kleinman, Phys. Rev. Lett., **58**, 483 (1987).

(7) R.Z. Olshan, A. Gover, S. Ruschin, H. Kleinman and A. Friedman, Phys. Rev., **A38**, 5206 (1988).

(8) Z. Sheena, S. Ruschin, A. Gover and H. Kleinman, Nucl. Inst. Meth. in Phys. Res., **A285**, 239 (1989).

(9) Z. Sheena, S. Ruschin, A. Gover and H. Kleinman, to be published in IEEE J. of Quant. Electron . (1990).

(10) N.M. Kroll, P. Morton and M.N. Rosenbluth, IEEE J. Qunat. Electron, **QE-17**, 1436 (1981).

(11) M.N. Rosenbluth, B.N. Moore and H.V. Wong, IEEE J. Quant. Electron., **QE-21**, 1026 (1985).

(12) I. Ben-Zvi, A. Gover, E. Jerby, J.S. Sokolowski and J. Wachtel, Nucl. Instr. and Meth. in Phys. Res., **A268**, 561 (1981).

(13) A. Gover, E. Jerby, H. Kleinman, I. Ben-Zvi, B.V. Elkomin, P. Fruchtman, J.S. Sokolowski, B. Mandelbaum , A. Rosenberg, J. Shiloh, G. Hazak and O. Shahal, 11th Intern. Conference on FEL, Naples, FL, U.S.A., 1989.

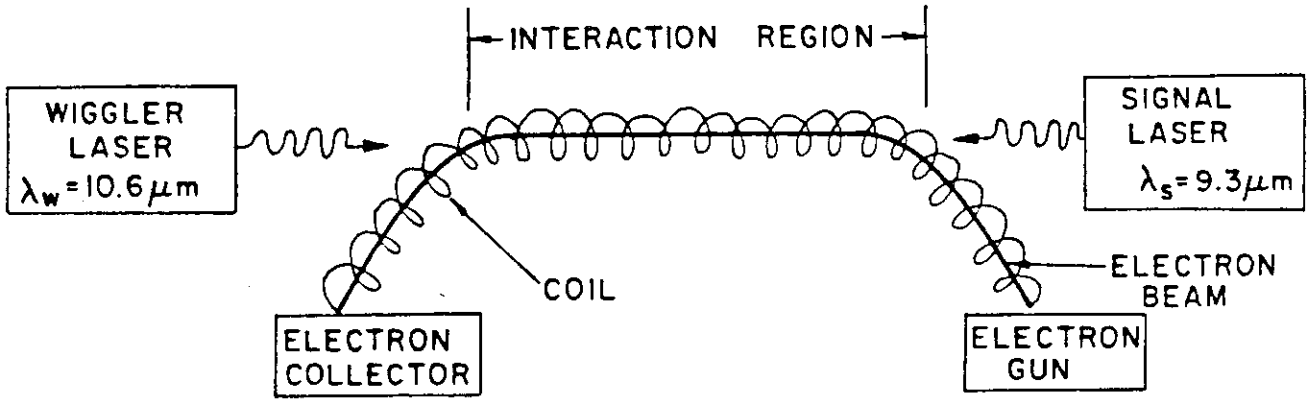

Fig. 1: Schematics of Two-Laser Compton Scattering Interaction

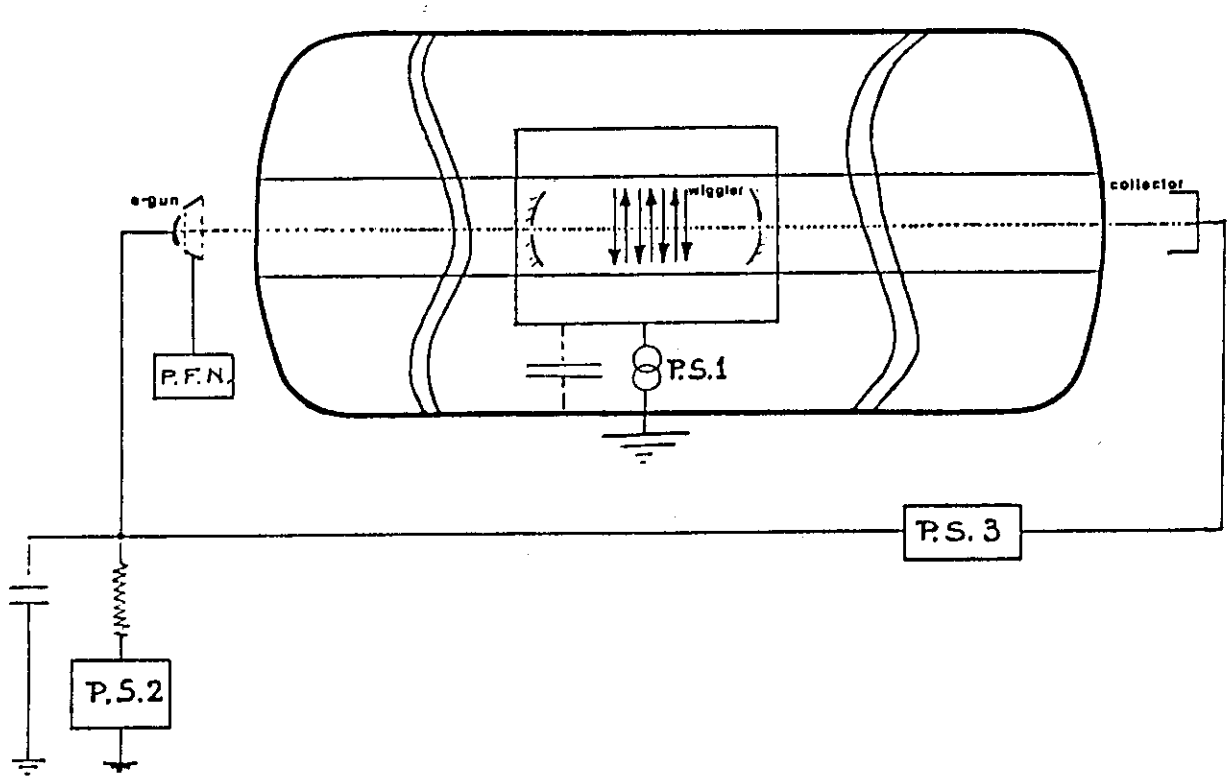

Fig. 2: Schematics of the Tandem accelerator and power supplies including the free electron laser.

12. DESIGN STUDY OF A FAR-INFRARED FREE ELECTRON LASER WITH A 20MeV RF LINEAR ACCELERATOR

S.NAKATA, C.TSUKISHIMA, T.HIFUMI,
S.OKUDA, S.SATO, and Y.YASOJIMA
Advanced Electrotechnology Department
Central Research Laboratory
Mitsubishi Electric Corporation
1-1, Tsukaguchi-Honmachi 8 Chome, Amagasaki, JAPAN 661

April 28, 1990

Abstract

A FEL in the far-infrared region has been designed using a low energy RF linear accelerator. First we estimate a small signal gain from spontaneous emission using the Madey's theorem. In the calculation following effects are included: an actual field distribution (using a measured magnetic field), beam envelope in the phase space through the undulator, energy spread, and electron beam mis-alignment to the undulator axis. We have developed a code which can simulate three dimensional processes of the electron interaction with multi-mode laser fields in the undulator. From this code we could obtain the time dependent bunching process of electrons and amplification of the laser field. During the calculation we assume an electron beam of $20MeV, 100mA$ with a pulse length of $3\mu s$, and an undulator of 28 periods,$6cm$ periodic length and $2.5kG$ peak field. The results from these calculations show that the small-signal gain over 40 % can be obtained, but mis-alignment of the beam severely degrades the gain. The results also show that the output power of several MW can be obtained under the above conditions. Considering the simulation results, a FEL beam line was constructed and the beam size at the undulator was measured. And electrons were focused enough for the FEL experiment.

1 Introduction

A Free Electron Laser(FEL) was first proposed as an optical device by Madey in 1970 [1] and offers a variety of advantages over conventional lasers. For example, it is feasible to operate FELs from the far infrared to the vacuum ultra-violet by changing the electron beam energy. By using the intermediate beam energy (several tens of MeV), FELs could become a high power sourcein the far infrared light source and there are few conventional high power lasers in that region. The gain of FEL is calculated using a theoretical formula [2]. In an actual FEL system, however, there are many effects to reduce the gain. In this paper, we present the calculated results.

2 Three-Dimensional Simulation Codes

In this section we will describe details of our simulation codes to calculate the small signal gain and strong signal gain.

2.1 Small Signal Gain

A theoretical FEL gain(G) for mono-energetic electrons can be calculated by Eq.(1)

$$G = -32\sqrt{2}\pi^2 \frac{(\lambda_L^3 \lambda_w)^{1/2}}{S} \frac{I_p}{I_A} N_w^3 f(x), \qquad (1)$$

where,

λ_w : Undulator wavelength

λ_L : Laser wavelength

I_A : Alfven current of $1.7 \cdot 10^4 A$

N_w : Number of undulator period

I_p : Peak current of a micro bunch

f(x) : Gain function

S : Beam cross section.

The equation (1) indicats that the gain was about 60%. The estimation of actual FEL gain by Eq.(1)is very useful, but is not enough to calculate a real gain including several effects. We developed a simulation method of estimating FEL gain in the actual system.

In the calculation we first calculate the beam orbit in the undulator, obtain spectrum of the spontaneous emission and estimate the gain by Madey's theorem. The equation of a relativistic electron motion in the undulator is as follows,

$$m_0 c d\gamma\beta/dt = -q \cdot (\mathbf{E}_L + \beta c \times (\mathbf{B}_L + \mathbf{B}_w)), \quad (2)$$

where

$\mathbf{B}_w$:Undulator magnetic field

$\mathbf{E}_L$:Laser electric field

$\mathbf{B}_L$:Laser magnetic field

γ :Lorentz factor of the electron.

The longitudinal velocity was obtained from momentum conservation. The magnetic field in the x-direction was negligibly small (B_x=0) because of the transverce pole width of our undulator was wide compared with the electron orbit, as shown in our previous paper [3].

According to the Madey's theorem [4],the stimulated energy loss of the electron through the undulator (related to the FEL's small signal gain) is proportional to the derivative of its spectrum of spontaneous emission. When the initial Lorentz factor of the electron at the entrance of the undulator is set to γ_i and the final one at the exit is set to γ_f, the energy loss in the undulator $< \gamma_f - \gamma_i >$ is obtained as follows,

$$< \gamma_f - \gamma_i >= \frac{1}{2} \frac{E_0(eV)^2}{(2mc^2(eV))^2} \cdot \frac{d}{d\gamma_i} \left| \int_{-L/2}^{L/2} \frac{dz}{\beta_{\parallel}^0(z)} \cdot \beta_{\perp}^0(z) \cdot e^{j(\omega t - kz)} \right|^2 \quad (3)$$

where ω is the frequency of laser field. Thus amplification of the laser power is given as follows:

$$G = \frac{mc^2 | < \gamma_f - \gamma_i > | (I_p/e)}{\frac{1}{2} \varepsilon E_0^2 \cdot c} \quad (4)$$

In this simulation code we include the following effects to estimate the actual FEL gain in our experimental system.

1. Actual beam size through the undulator
2. Actual beam divergence through the undulator
3. Energy distribution
4. Distribution of electrons on the phase space
5. Beam mis-alignment effects
6. Actual magnetic field effects (field inhomogeneity et. al.)

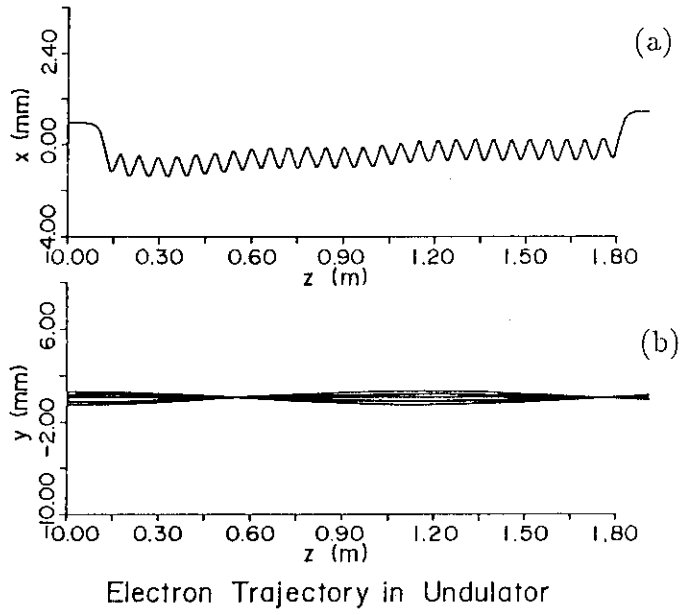

Figure 1: Electron beam trajectories in the actual undulator on the x-z plane (a) and on the y-z plane (b).

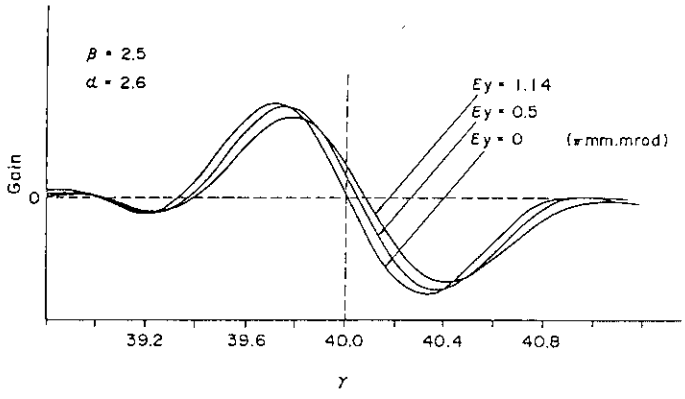

Figure 2: Small signal gain in arbitrary unit for several emittances

Figure2 shows the calculated gain curve for several emittances. The peak of the gain curve shifts to right side in the figure by the effects of emittances, indicating that the laser wavelength become longer and the gain decreases from the ideal one (zero emittances). As a result, the peak gain decreases to 72% of the ideal one.

The effects of the beam mis-alignment on the gain were also estimated. Fig.3(a) is the gain curve with the parameter of the beam vertical mis-alignment, Fig.3(b) is the gain curve, the parameter here is the beam divergence in the vertical mis-alignment and Fig.3(c) is the dependence of the gain at fixed wavelength of 40 μ m on the beam mis-alignment and beam divergence mis-alignment. In Fig.3(a), the peak value of the gain decreases very rapidly according to the beam mis-alignment. On the other hand, the mis-alignment of the beam divergence has slight effects on the peak of the gain but the wavelength of the laser at maximum gain becomes longer. From Fig.3(c), the accuracy of beam positioning is obtained. The beam mis- alignments, especially in vertical, should be less than $0.3mm$ and $1.0mrad$ not to degrade the gain more than 5%.

2.2 Strong Signal Gain

As a linear simulation code is not enough to estimate the laser output power or waveform, we developed a single particle simulation code including non-linear effects, i.e. electron-photon interaction.
The basic equations of the simulation are Hamiltonian (5) and Maxwell equation (6),

[Hamiltonian]

$$H = \gamma mc^2 = [(\mathbf{P} - q\mathbf{A})^2c^2 + m^2c^4]^{1/2} \qquad (5)$$

[Maxwell equation]

$$\nabla^2\mathbf{A} - \frac{1}{c^2}\cdot\frac{\partial^2\mathbf{A}}{\partial t^2} = -\mu_0 q\sum_i \mathbf{v}_i\delta(\mathbf{r}_i) \qquad (6)$$

In the calculation the following conditions were assumed for simplicity.

[linear wiggler potential]

$$\mathbf{A} = \mathbf{e}_x A_w(1+\frac{\mathrm{k}_w^2 y^2}{2})\cdot cos(\mathrm{k}_w z) \qquad (7)$$

$$K = \frac{qA_w}{mc} = \frac{qB_w^{max}\lambda_w}{2\pi mc} \qquad (8)$$

$$\lambda_L = \frac{\lambda_w}{2\gamma^2}(1+\frac{K^2}{2}) \qquad (9)$$

[Hermite-Gauss laser potential]

$$\mathbf{A} = \mathbf{e}_x\sum A_{lm} \qquad (10)$$

$$A_{lm} = \frac{mc}{q}a_{lm}g_{lm}cos(\mathrm{k}_L z - \omega_L t + \theta_{lm}) \qquad (11)$$

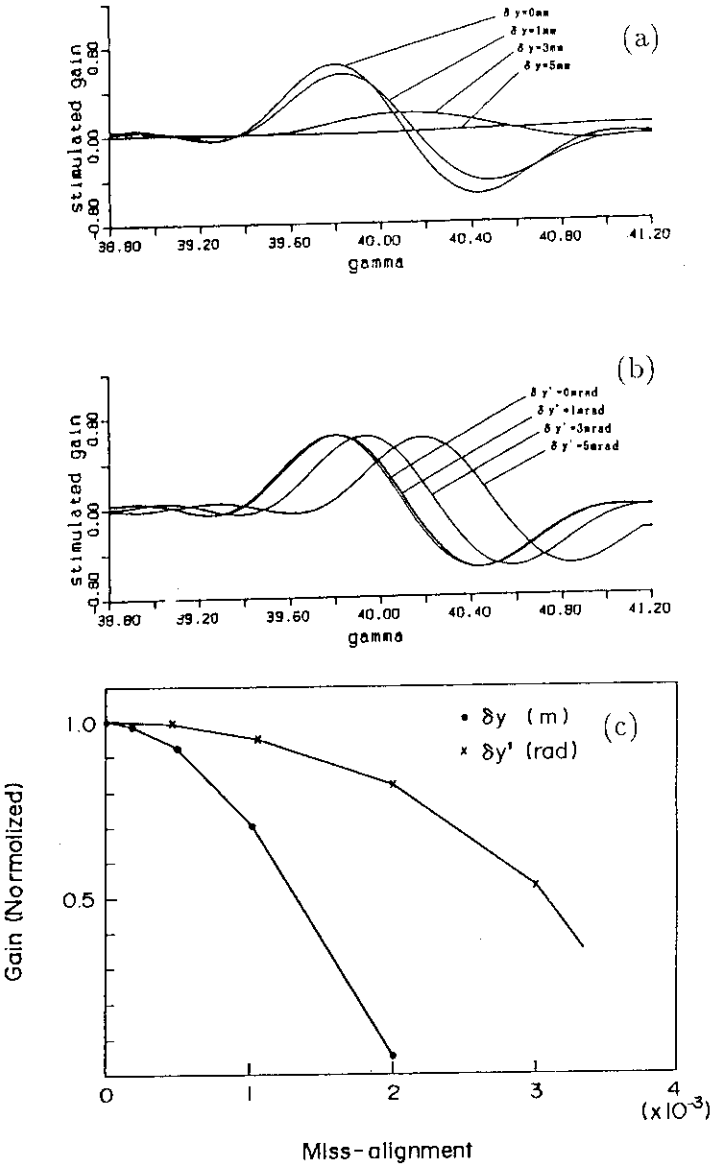

Figure 3: The gain reduction by the beam mis-alignment (a) the dependence of the gain curve on the beam mis-alignment; (b) the dependence on the beam divergence mis-alignment; (c) the gain reduction by the beam mis-alignment, the laser wavelength was fixed at 40 μ m.

$$g_{lm} = \left(\frac{2}{\pi\, l!m!(1+\zeta^2)}\right)^{1/2} H_l\left(\frac{2\rho_x}{(1+\zeta^2)^{1/2}}\right) H_m\left(\frac{2\rho_y}{(1+\zeta^2)^{1/2}}\right) exp(-\frac{\rho_x^2+\rho_y^2}{1+\zeta^2}) \quad (12)$$

$$\theta_{lm} = \frac{\rho_x^2+\rho_y^2}{1+\zeta^2}\zeta + (l+m+1)arctan\,\zeta \quad (13)$$

$$x = w_0\rho_x \quad (14)$$

$$y = w_0\rho_y \quad (15)$$

$$\zeta = (z-z_c)/z_R \quad (16)$$

where

$H_n(x)$: Nth order Hermite polynominals

w_0 : Beam waist

z_R : Rayleigh length

z_c : Z-coordinate of the waist.

The above Hamiltonian equations are normalized for simplicity as follows.

[Normalized equations]

$$\beta_z = 1-\frac{1}{2\gamma^2}(1+\Gamma_{0x}^2+\Gamma_{0y}^2+K^2cos^2(k_w\xi)+K\Gamma_{0x}cos(k_w\xi)) \quad (17)$$

$$\frac{d\phi}{d\xi} = k_w+(1-\frac{1}{\beta_z})k_L \quad (18)$$

$$\frac{d\rho_x}{d\xi} = \frac{z_R}{w_0}\frac{1}{\gamma\beta_z}(\Gamma_{0x}-Kcos(k_w\xi)) \quad (19)$$

$$\frac{d\rho_y}{d\xi} = \frac{z_R}{w_0}\frac{1}{\gamma\beta_z}\Gamma_{0y} \quad (20)$$

$$\frac{d\Gamma_y}{d\xi} = \frac{w_0}{z_R}\frac{1}{\gamma\beta_z}Kk_w^2\rho_y cos(k_w\xi)(\Gamma_{0x}-Kcos(k_w\xi)) \quad (21)$$

$$\frac{d\gamma}{d\xi} = -\frac{1}{\gamma\beta_z}k_L(\Gamma_{0x}-Kcos(k_w\xi))\sum lma_{lm}g_{lm}sin(\phi-k_w\xi+\theta_{lm}) \quad (22)$$

$$\frac{da_{lm}}{d\xi} = \mu_0\frac{z_R^2q^2}{w_0^2m}\frac{N\sigma_b}{nk_L}\sum_i\frac{\beta_x}{\beta_z}a_{lm}g_{lm}sin(\phi-k_w\xi+\theta_{lm}) \quad (23)$$

For normalization the following relations are used.

$x = w_0\rho_x, y = w_0\rho_y,\ z = z_R\xi = \beta_z ct$

$k_w z = k_w\xi,\ k_L z = k_L\xi,\ \gamma_0\beta_{0x} = \Gamma_{0x}$

$\gamma_0\beta_{0y} = \Gamma_{0y}, P_y/mc = \Gamma_y$

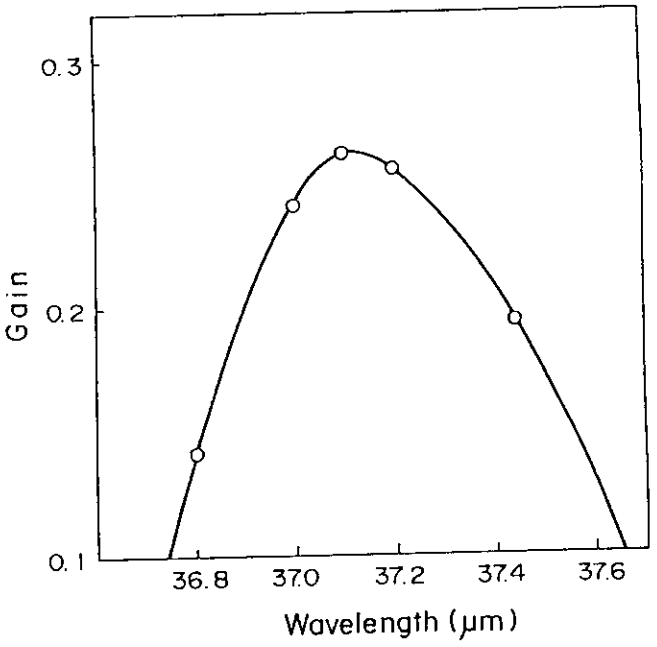

Figure 4: Amplification of $10kW$ laser as a function of laser wavelength

$\beta_z cdt = z_R d\ \xi$

An initial beam distribution of every micro bunch is calculated by using random number. In the simulaton, the total number of particles in one laser wavelength is 4000.

Figure(4) shows the gain as a function of the wavelength. In the calculation, an initial laser power of $10kW$, which was $6.25\cdot10^{-5}$ of electron beam power, was assumed. The maximum amplification is obtained at the laser wavelength of $37.1\mu m$,which is slightly different from the value obtained by small signal gain ($37.4\mu m$).
Simulations were performed at the wavelength of $37.1\mu m$. In the following, the results of simulation will be discussed.

Figure (5) indicates that the electrons are bunched as they pass through the undulator.

Figure(6) is the laser output power. Figure(7) shows the gain dependence on the laser energy. The gain at medium laser powers($100W \leq$ power $\leq$ sevral MW) is about 40%and is very similar to small signal gain. The laser power increases exponentially upto several MW during 75 pass of electron, but the gain slightly decreases as the power increases over several MW. Over several MW of the laser power the gain decrease very drastically. The ratio of the laser power and the electron beam power at that range is about $1/N_w$. As the calculation starts from zero level of laser power, there exists numerical errors during the initial stage where the laser power is less than $100W$.

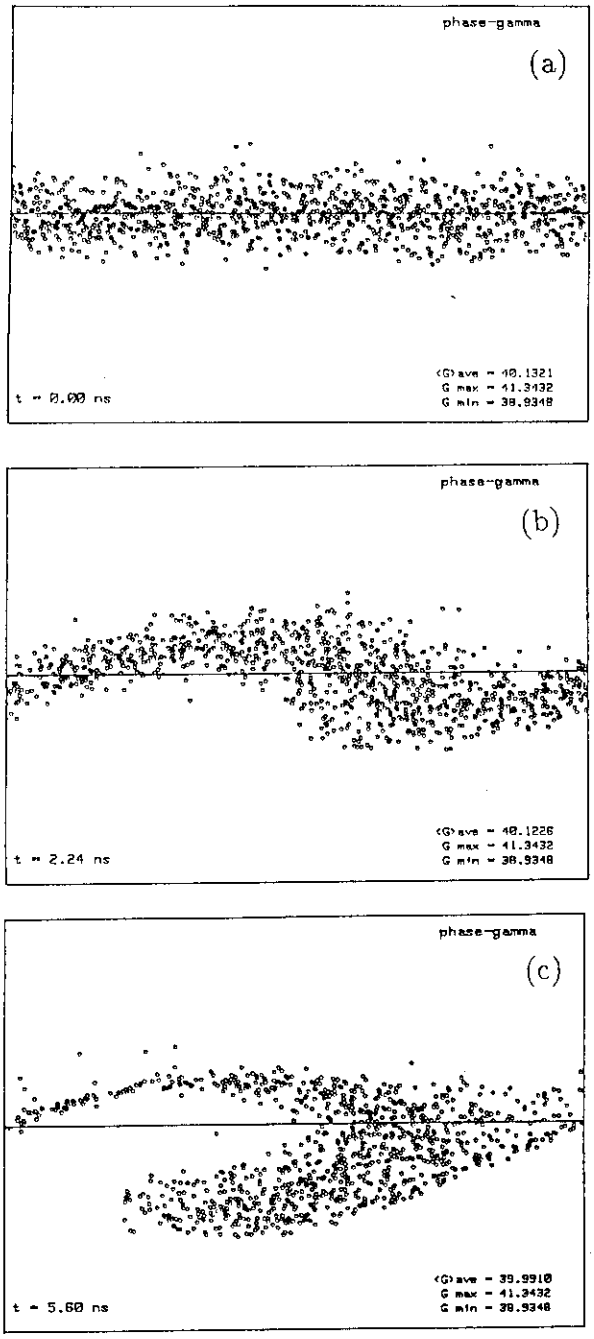

Figure 5: beam evolution and bunching at optical wave length in electron phase space, at undulator entrance(a), center(b) and exit(c)

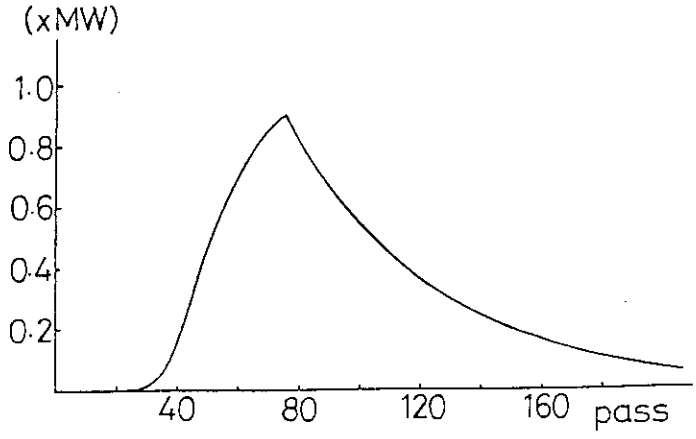

Figure 6: Growth of the laser power from noise

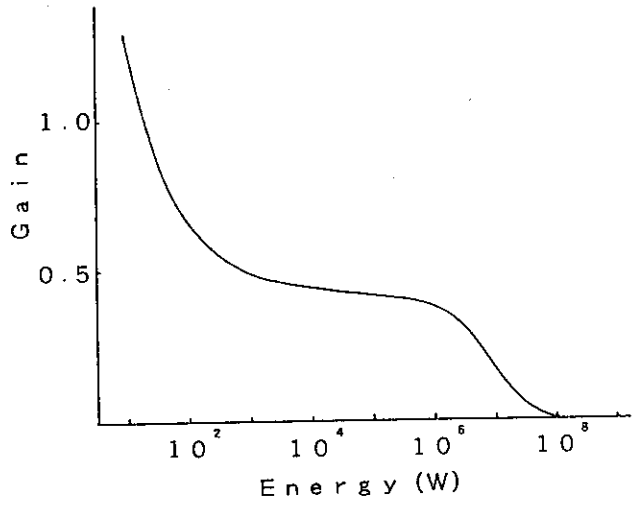

Figure 7: Saturation of the laser gain

Table 1: Main parameter of our Linear accelerator,Undulator and FEL.

Linear accelerator		
	Energy	$20MeV$
	Current	$100mA$
	Pulse width	$3.0\mu s$
	$\varepsilon_{x90}\%$	$1.04 \cdot 10^{-6}\pi$ mrad
	$\varepsilon_{y90}\%$	$1.14 \cdot 10^{-6}\pi$ mrad
	$(dp/p)_{full}$	$\pm 1\%$(full)
Undulator		
	Period	$6cm$
	Length	$168cm$
	Magnet gap	$35mm$
	Magnetic field	$2.5kG$
	K-value	1.4
	Periods	28.
	field error	0.06%
FEL		
	Wave length	$40\mu m$
	Theoretical gain	60%

3 Experiment

The main parameters of our linear accelerator, undulator and FEL are summarized in Table 1.

A RF linear accelerator of $2.8GHz$ was used in our experiment. The beam energy was $20MeV$ and the peak current of the macro-pulse was $100mA$ of $3.0\mu s$. The emittances of the electron beam were measured by a Q-magnet and wire-grid profile monitor. About 90% of the beam were in the emittance of $1.04\times10^{-6}\pi mrad$ in the x-direction and $1.14\times10^{-6}\pi mrad$ in the y-direction(Fig.8). The beam current within $\pm1.0\%$ of energy spread was measured by a beam damper and was about $100mA$.

The experimental layout is shown in Fig.9. The coordinates, shown in Fig.9, are used through this section. The x-,y-,z-axis are the beam wiggling direction , undulator field direction and beam direction, respectively.

The beam line had 3 bending magnets ($BM1, BM2, BM3$), 8 quadrupoles magnets ($QM1$ $QM8$) and several steering magnets as shown in Fig.9. The beam size through the beam line is also shown in Fig.10. The calculated beam sizes were based on the measured emittances.

In the beam line, several kinds of monitors were installed to measure the beam parameters and align the electron beam through the undulator: 3 wire-grid monitors($WG1$ $WG3$) for beam profile monitor,4 screen monitors ($SM1$ $SM4$) for beam position monitor, 3 current transformers ($CT1$ $CT3$) for current monitor. Furthermore one beam-scraper was installed in the high dispersive section to control the beam energy spread at the undulator section.

The twiss parameters at the entrance of the undu-

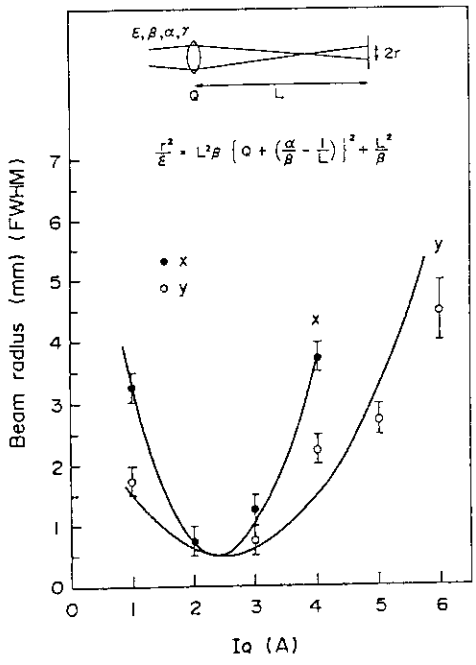

Figure 8: Beam size vs. Q-magnet current

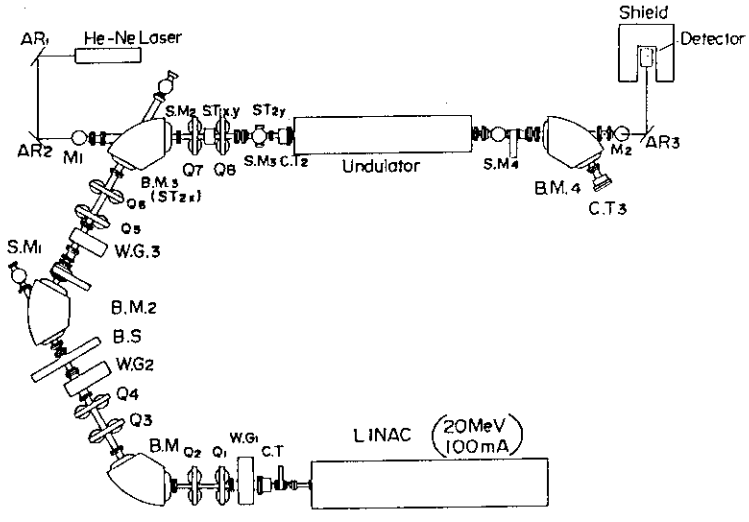

Figure 9: The layout of the beam transport line for the FEL experiment.

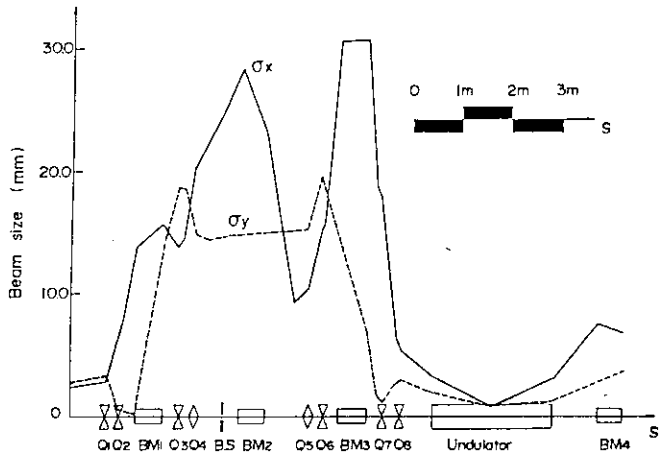

Figure 10: The beam size(90% of the electrons are contained)in the beam transport line

lator were $\beta_x = 0.22, \alpha_x = 8.8, \eta_x = -0.18, \beta_y = 0.012$ and $\alpha_y = 0.25$. The undulator was $1.64m$ long and has linearly polarized magnetic fields. The details of the undulator were described in our previous paper [3]. The magnetic field was $2.5kG$, at the magnet gap of $35mm$ and the K-value was 1.4 at that time. The r.m.s. field error of 0.06% was obtained by adjusting the pole holders. The optical cavity consisted of two Au coated spherical mirrors with a central pin-hole of $1mm$ diameter for output coupling. The electron beam radius at the entrance and the exit of the undulator were measured by screen monitor. Figure(11) shows that the HWHMs in the x-direction and y-direction at the entrance were $1.15mm$ and $1.0mm$,respectively and at the exit were $0.714mm$ and $0.464mm$. These value are almost the same value obtained by the calculation.

4 Conclusion

We developed the two 3-dimensional particle simulatoin codes (linear and nonlinear) for FEL gain calculation. The linear simulation code can calculate the gain dependence on real beam envelope in the phase space, field error, electron beam mis-alignment. On the other hand the nonlinear simulation code can calculate the energy transfer from electron beam to laser beam accurately and can obtain the laser mode in the cavity and time dependent output laser power.
By linear simulation, FEL gain is about 5%/A and is about 70% of the theoretical value. The simulation also indicats that the gain would be reduced severely by beam mis-alignment ,especially in the vertical direction.
By nonlinear simulation, the following results are ob-

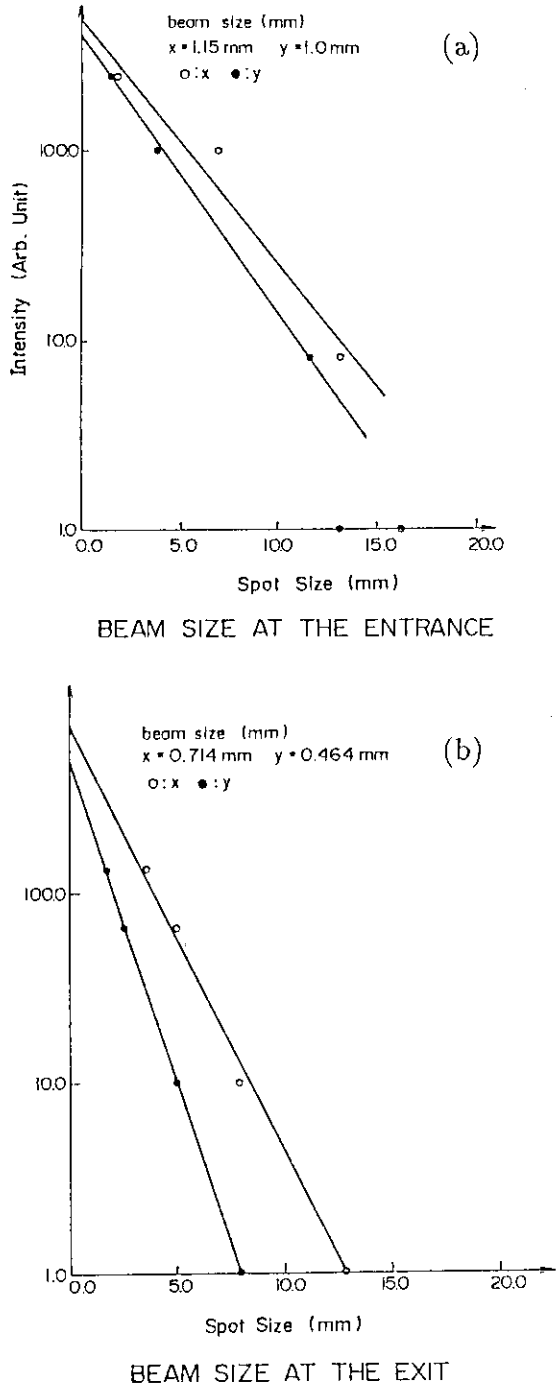

Figure 11: Dstribution of the intensity of the screen monitor at the entrance(a) and the exit(b)

tained. An amplification at 10kW input laser power is maximized at wavelength of 37.1μm and was slightly different from the value estimated by the small signal gain curve. By fixing the wavelength at that value, the growth of the laser power is simulated and the results indicate that the gain is almost the same value obtained from linear simulation and the laser power increases exponentially upto several MW during 75 pass of electron but the gain slightly decreases as the power increases over several MW. By considering the simulation results, an experimental beam line was constructed and the beam size at the undulator are measured by screen monitor. The obtained beam size were almost the same value of the calculated one and would be small enough for the FEL experiment.

Acknowledgment

We thanks Drs. T.Tomimasu,T.Yamazaki and T.Nakamura of Electro Technical Laboratory(E.T.L.) for their invaluable advises , and the other members of our group for their useful discussions.

References

[1] J.M.J.Madey, J.Appl.Phys., 42, 1906,1971

[2] W.B.Colson,Phys. Lett., 29, 187,1976

[3] C.Tsukishima and S.Nakata, in Proc. of The 13th LINEAR ACCERELATOR MEETING IN JAPAN,168 (1988)

[4] J.M.J.Madey, IL NUOVO CIMENTO, 50, 64,1979

13. SIMULATION OF HIGHER HARMONICS GENERATION IN FEL

Shin-ichiro KURUMA, Kunioki MIMA* and Katsuhiro OHI**
Institute for Laser Technology, 2-6, Yamadaoka, Suita, Osaka, Japan
*Institute of Laser Engineering, Osaka University, 2-6, Yamadaoka, Suita, Osaka, Japan
**Faculty of Engineering, Kansai University, 3-3-35, Yamate, Suita, Osaka, Japan

I. Introduction

In order to have large gain of FEL, it is necessary to enlarge the strength of wiggler magnetic field. But if the K parameter that depend on the wiggler magnetic field and period is larger than one, then the magnitude of higher harmonics become larger. So, in the region of short wavelength radiation, the damage of the mirror is larger. But if we can pick up the higher harmonics radiation effectively, then we can get shorter wavelength region with using the low energy electron beam. So it is important to analyze the characteristic of higher harmonics generation to be compact the FEL system. Hence we develop the 1-D multi frequency simulation code that can describe the nonlinear evolution of fundamental and higher harmonics radiations. By this simulation code, it is possible to analyze the coupling of fundamental and higher harmonics radiations. In section II, the model equations are described. In section III, the numerical example and discussion are described. And section IV is devoted to summary.

II. Model Equation.

The electron beam is assumed to propagate along z-direction which is parallel to the plane wiggler axis. Vector potential of the wiggler magnetic field is given as,

$$\underset{\sim}{A}_w(z)=K(z)\cos k_w z\ \underset{\sim}{e}_x, \tag{1}$$

where $\underset{\sim}{A}_w(z)$ is normalized by mc^2/e and $K(z)$ is K-parameter of wiggler magnetic field. And $\underset{\sim}{e}_x$ is the unit vector of x-direction. Vector potential of electromagnetic radiation fields that are normalized by mc^2/e are assumed as follows,

$$\underset{\sim}{A}_s(t,z)=\sum_n a_{sn}(z)\cos\{k_{sn}z-\omega_{sn}t+\theta_{sn}(z)\}\ \underset{\sim}{e}_x, \tag{2}$$

where $a_{sn}(z)$ is the amplitude function of the radiation field and $\theta_{sn}(z)$ is the phase sift function. Microscopic current density is given by the summation over individual particles,

$$\underset{\sim}{j}(t,z)=-(en_bL/N_T)\sum_i \underset{\sim}{v}_i(z,t_{i0})\delta[t-\tau_i(z,t_{i0})] /v_{i0}(z,t_{i0}), \tag{3}$$

where N_T is the total number of beam electrons in the interaction region of length L, n_b is the average electron density, $\underset{\sim}{v}_i(z,t_{i0})$ is the velocity of the i-th electron at the position z, where the i-th particle is assumed to enter the interaction region (i.e. cross the z=0 plane) at time t_{i0}. Substituting the current density of Eq.(3) into Maxwell equation with Eq.(2) and carrying out the Fourier transformation with respect to t, we obtain

$$a_{sn}'(z)=-(\omega_p^2 K\beta_{z0}/2k_{sn})\langle(1/\beta_{zi}\gamma_i)J_{-n/2}(\alpha)\sin\phi_{ni}\rangle, \quad (4)$$

$$\theta_{sn}'(z)=-(\omega_p^2 K\beta_{z0}/2k_{sn}a_{sn})\langle(1/\beta_{zi}\gamma_i)J_{-n/2}(\alpha)\cos\phi_{ni}\rangle, \quad (5)$$

$$\phi_{ni}=(n+1)\psi_i+\phi_n, \quad (6)$$

$$\alpha=(1+k_{sn})K^2/8\gamma_i^2, \quad (7)$$

where ω_p is the plasma frequency of the electron beam normalized by $k_w c$ and β_{z0} is the initial average velocity of the electron normalized by the speed of light. Prime denote a derivative with respect to $z_p=k_w z$ and we neglect the terms of second derivatives of z_p. In Eqs.(4) and (5), $\langle\ldots\rangle$ represents a time average over a period of the fundamental wave, namely $2\pi/\omega_{s0}$. And ψ_i is the ponderomotive phase of i-th electron to the fundamental radiation,

$$\psi_i'(z)=1-k_{s0}(1-\beta_{zi})/\beta_{zi}, \quad (8)$$

$$\beta_{zi}=\{1-(1+K^2/2)/\gamma_i^2\}^{1/2}, \quad (9)$$

And the equation of motion of i-th particle is

$$\gamma_i'(z)=(K/2\beta_{zi}\gamma_i)\Sigma_n k_{sn}a_{sn}(z)J_{-n/2}(\alpha))\sin\phi_{ni}. \quad (10)$$

In Eqs.(4)-(10), subscript i is the particle number and subscript n is the radiation mode number, namely n=0,1,2,3,... represent fundamental, 3rd, 5th, 7th,... harmonics mode respectively. Both the linear and non linear evolutions of a FEL amplifier can be investigated by Eqs.(4)-(7) with Eqs.(8)-(10) for the orbits of an ensemble of electrons having initial phases $-\pi<\psi_{i0}<\pi$.

III. Numerical example and discussion

The parameters are chosen as follows that correspond to the experiment at ILE. The wiggler period λ_w=6cm, wiggler magnetic field strength B_w=3.2kG(K=1.8), electron beam energy E_b=6MeV(γ=12.74), electron beam current I_b=100A, electron beam radius r_b=3mm. In this case, the radiation wavelength of fundamental mode is approximately λ_{s1}=515μm. And we neglect the effect of space charge wave, because the parameter $\omega_p/\gamma_0\sqrt{\gamma_z}$≃0.02 is much smaller than one. In Fig.1, we show the temporal evolutions of the radiation power strength for the fundamental, 3rd,5th,7th and 9th harmonics modes. The initial power of fundamental mode is about 1kW and that of higher harmonics modes are zero. In this figure, the saturation is occur at z=2m and the saturation powers of fundamental(λ_{s1}=515μm), 3rd(λ_{s3}=172μm), 5th(λ_{s5}=103 μm) harmonics are P_{s1}=30MW, P_{s3}=1MW and P_{s5}=0.15MW respectively. In Fig.2, we show the beam current dependence of the saturation powers of fundamental, 3rd and 5th harmonics modes. In this figure, we can see the output powers are proportional to the electron beam current to power 1,17.

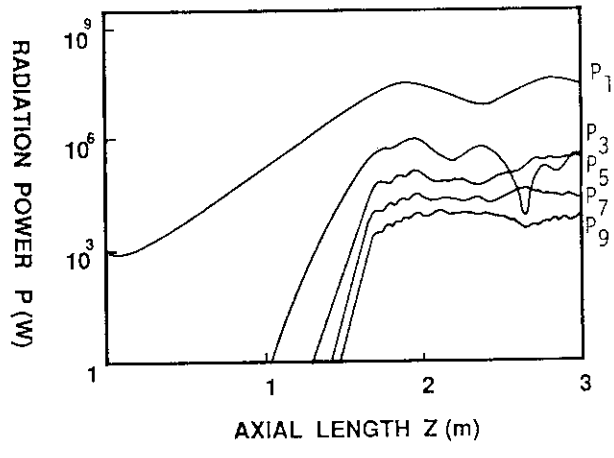

Fig.1 Temporal evolution of the radiation powers

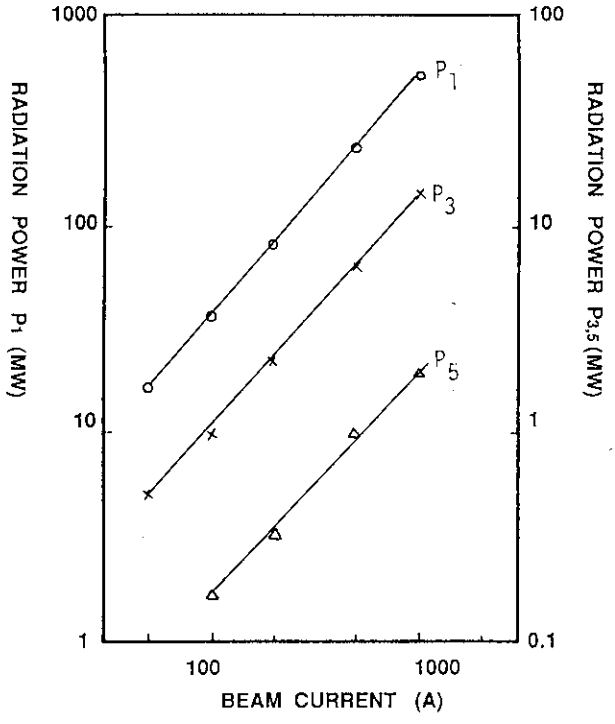

Fig.2 Beam current dependence of the saturation powers

IV.Summary

The one dimensional multi frequency simulation code for analyzing the higher harmonics radiation of FEL is developed. By the simulation using this code, the power ratios of 3rd and 5th harmonics to the fundamental radiation are clarified. And the electron beam dependence of the radiation output powers have also founded.

14. CONSIDERATIONS FOR HIGH-BRIGHTNESS ELECTRON SOURCES

R. A. Jameson

Accelerator Technology Division, MS H811
Los Alamos National Laboratory
Los Alamos, New Mexico, USA 87545

Introduction

Particle accelerators are now used in many areas of physics research and in industrial and medical applications. New uses are being studied to address major societal needs in energy production, materials research, generation of intense beams of radiation at optical and suboptical wavelengths, treatment of various kinds of waste, and so on. Many of these modern applications require a high intensity beam at the desired energy, along with a very good beam quality in terms of the beam confinement, aiming, or focusing. Considerations for ion and electron accelerators are often different, but there are also many commonalities, and in fact, techniques derived for one should perhaps more often be considered for the other as well. We discuss some aspects of high-brightness electron sources here from that point of view.

Brightness

A primary figure of merit for accelerators is the beam brightness, defined as the beam power (or current when the energy is fixed) divided by the phase space appropriate to the problem at hand. Phase space for the beam as a whole is six-dimensional, describing the physical size of the beam and the change in size with time or distance; the area projected on one plane is called emittance.

In free-electron lasers (FELs), the laser wavelength that can be obtained is fundamentally limited by the relationship $\varepsilon_n = \beta\gamma\lambda$ between the normalized electron beam emittance and the laser wavelength. Thus one would like to make the electron beam emittance as small as possible, but on the other hand, a large peak current is also desireable so that more single-pass gain can be obtained with a smaller a_w wiggler parameter. Also, accelerators are expensive, so their makers strive to maximize output and quality at high efficiency. The problems of achieving and preserving high brightness are different for non-relativistic and relativistic beams.

Beam Brightness Limitations In Nonrelativistic Linacs

The achievable beam intensity and quality are nonlinearly related, and raising the intensity tends to spoil the quality, or conversely, trying for better quality may limit the current. (The beam quality or emittance that we are most concerned with here is the effective area occupied by the beam in phase space, defined by computing the centroid and the projected rms emittance ellipses of the particle distribution and passing ellipses of that shape through each particle.) Achieving high-brightness accelerated particle beams involves work on both the numerator and the denominator of the brightness equation -- beam intensity divided by beam quality.

The numerator can be raised by brute force, but the large power requirements and engineering problems that result can be formidable, and better system efficiency becomes a key issue. A given accelerator channel can accelerate only a certain amount of current, depending on the imposed constraints. If more current is desired, the constraints or basic parameters might be changed, or several accelerator channels or modules could be used. The latter approach would multiply the system power requirement directly; therefore, one

* This work was supported under the auspices of the U.S. Department of Energy.

would prefer to find a more efficient way to raise the current, if possible.

Decreasing the denominator of the brightness factor involves building low-emittance (but also intense and, therefore, bright) particle sources and then preserving the source brightness through all the subsequent steps of beam transport and acceleration to the final energy and the beam target. Due to basic beam dynamics, the minimum phase space volume in an accelerator is no smaller than the emittance of the particle source.

Thus, in the final design for an application, many factors constrain the brightness that can be achieved. However, in recent years, a few key requirements and procedures have been elucidated that have major effects on achieving higher brightnesses.

The main problem at nonrelativistic velocities is space-charge effects. The beam particles must be charged to be accelerated, and all have the same sign, so they tend to repel each other. When the beam intensity is increased, the forces in the bunches becomes such that defocusing occurs. In a bunched beam of ellipsoidal shape, defocusing takes place in both transverse direction against the external focusing, and also in the longitudinal direction acting against the phase stability mechanism. Such effects mainly take place at low velocity when the particles are very sensitive to electric fields; the situation improves at higher velocity.

Matching

Simple but very effective design equations for nonrelativistic transported or accelerated beams can be obtained by writing general rms envelope equations for the beam as it is constrained in the accelerator channel. The external channel-focusing forces are offset by the internal space-charge forces in the beam; a beam-current limitation of the channel is reached when the focusing and space-charge forces cancel (in practice, errors and other factors force operation below this limit). The simplest form[1] of the envelope equations for an ellipsoidal bunch in an accelerator approximated by a weakly coupled harmonic oscillator system is

$$\varepsilon_t = \sigma^t a^2/N\beta\lambda \quad \text{and} \quad \varepsilon_l = \sigma^l b^2/N\beta\lambda \qquad (1)$$

in terms of the transverse and longitudinal planes, where ε_t and ε_l are the transverse and longitudinal rms emittance, a is the average transverse rms beam radius, b is the physical rms bunch length, and σ^t and σ^l are the phase advances of the oscillatory motion in phase space over the period $N\beta\lambda$. The σ terms each can be expanded into two terms, one containing the machine parameters and the other containing the beam current and also the beam sizes a and b, explicitly. It is necessary to solve both parts of Eq. (1) simultaneously; the result is a beam that is "matched" to the shape factors of the machine acceptance phase space. We know that the effective emittance of mismatched or mis-steered beams can grow. It is important to note that these equations apply locally; thus they should be applied not only as initial conditions at the entrance point of various sections of a machine, but also with care to ensure they remain true at every point.

Choice of Rf Frequency

The envelope equations can be solved for two quantities---for example, the current and one other. The constraints imposed on various parameters can strongly influence the solution. We found that if maximum current is the goal (disregarding emittance), then lower operating frequencies are favored. But *if high brightness is the goal, the maximum current achievable for a fixed transverse emittance strongly favors higher frequency linacs and strong external focusing.* This result basically arises from the smaller amount of charge per bunch in a higher frequency system with given phase advances per focusing period, and from the smaller beam size if the focusing is strong. While space-charge forces are increased in a small beam, the spatial extent over which the beam thermal energy is distributed is smaller, and the latter effect dominates[2].

Free Energy Balance and Minimization

We continue with the rms model of the coupled harmonic oscillator accelerator system with an ellipsoidal nonrelativistic beam bunch. In space-charge-dominated beam/accelerator systems, effective emittance growth could occur if the average energy in each of the coupled degrees of freedom is unequal[1]. Equating the rms quantities $\langle v_i^2\rangle = \langle v_j^2\rangle$ and $\sigma_i^2\langle x_i^2\rangle/N\beta\lambda = \sigma_j^2\langle x_j^2\rangle/N\beta\lambda$ produces another equation:

$$\varepsilon_l/\varepsilon_t = \sigma^t/\sigma^l = b/a \qquad (2)$$

where the particle velocities v and positions x are averaged over each degree of freedom, for example, transverse and longitudinal.

Systems satisfying the three equations of Eqs. (1) and (2) are both matched and "equipartitioned."

Again, the condition can be applied locally and should be applied at injection and all along the machine, if possible, to ensure minimum emittance growth. We are still only beginning to explore the full ramifications of satisfying simultaneously the matching and equipartitioning constraints on linac design. Unfortunately, it may not easy, within the limitations of other constraints, to prepare an equipartitioned beam for injection or to always maintain the energy balance; thus, the desirability of equipartitioning joins the list of properties among which tradeoffs must be made. The physics of the energy balance requirement on achieving high brightness is very compelling, however, and much more work is needed in this area.

The physical mechanisms for the space-charge-induced rms-emittance growth from free-energy redistribution have been clarified[3] as a charge-density redistribution occurring within about one-quarter of a plasma oscillation period of the system, and as a slower kinetic-energy exchange toward equipartitioning. The basic equation[4] for a bunched beam with linear focusing in three degrees of freedom is

$$(1/\langle x^2\rangle)\,(dE_x^2/dt) + (1/\langle y^2\rangle)\,(dE_y^2/dt) + (1/\langle z^2\rangle)\,(dE_z^2/dt) = (-32/mc^3\beta^3\gamma^3N)\,[d(U_n)/dt] \quad , \tag{3}$$

where E is defined as four times the true rms emittance ε, N is the number of particles in the bunch, and U_n is the *nonlinear* field energy proportional to the difference between the space-charge field energy of the actual beam and that of an equivalent uniform beam with the same rms properties. Thus, the time rate of change of the squared emittance is proportional to the rate of change of the nonlinear field energy. In the matched and space-charge-dominated case, the rms beam sizes stay approximately constant, therefore Eq. (3) can be integrated and a final emittance predicted. For the transverse plane,

$$E_{xf}^2 = E_{xi}^2\left(\frac{2+P_i}{2+P_f}\right) - \frac{16G_x(b/a)}{(2+P_f)}\left(\frac{K_3^2\,L}{\sigma_{ox}}\right)^{2/3}(U_{nf}-U_{ni}) \quad , \tag{4a}$$

and for the longitudinal plane,

$$E_{zf}^2 = E_{zi}^2\left(\frac{2+P_i}{2+P_f}\right)\frac{P_f}{P_i} - \frac{16\,P_f\,G_z(b/a)}{(2+P_f)}\left(\frac{K_3^2\,L}{\sigma_{oz}}\right)^{2/3}(U_{nf}-U_{ni}) \quad , \tag{4b}$$

where i and f signify initial and final emittance, G's are bunch geometry factors, σ_o's are zero-current phase advances, K_3 is a bunched-beam perveance, and P is the partition parameter defined as $P = \langle z'^2\rangle/\langle x'^2\rangle$ and is a nonrelativistic measure of the kinetic-energy asymmetry in the rest frame of the bunch. The terms show the contribution to emittance growth from charge redistribution and from equipartitioning. If the initial charge distribution is nonuniform, the charge redistribution will always occur in about one-quarter plasma period (about one cell in a high-current machine). Movement toward equipartitioning will occur if the intensity is above a threshold---a concise theory for the threshold and the rate of the movement is not available.

Beam Halo Formation

The nonlinear space-charge forces also act to produce a low density halo around the beam. Nonlinear focusing forces (including abrupt changes) can cause filamentation in phase space and contributions to halo formation. A theory for halo formation is not yet available, but it is probable that the behavior of these particles in the outer fringes of the distribution, where they are more likely to be scraped off as beam loss, is based on similar matching and energy balance requirements. Empirical research in progress has produced some indications that channels designed to specifically control quantities like energy balance, phase advance or tune depression, and so on, along the channel may produce brighter beams on both an rms and a total basis.

Beam Brightness Limitations In Relativistic Beams

Beam Breakup (BBU)

Space-charge defocusing is not a contributor to emittance growth at high energies. Here the limitation comes from the phenomena called beam break up. The linac structure can be excited, not only on the fundamental accelerating mode, but, like an ordinary waveguide, on other modes, the most dangerous of which are transverse hybrid modes that can affect the beam. These modes can be excited by particles traveling off the cavity axis, or by cavity asymmetries. Along a single cavity the interaction of the beam with such a transverse mode can lead to an unstable situation when the current is above some threshold; this is called regenerative beam break up (BBU). In a long accelerator, each cell, although below the threshold of oscillation, can nevertheless behave like an amplifier. A long chain of such amplifiers, even if each gain is small, can

eventually deflect the beam out of the channel; this is called cumulative beam break up.

Described alternatively, the electromagnetic fields of leading particles can interact with boundary discontinuities in the system[5], producing scattered radiation that can reach trailing charges and influence their motion. These waves are called wakefields; their integrated effect on particles passing through them can cause effective emittance growth that dilutes brightness, or, if serious enough, can cause beam breakup.

The effects are combatted by eliminating boundary discontinuities wherever possible, changes in the accelerating cell geometry, and by making geometrical changes in successive structures, to prevent the beam from synchronizing with the offending modes.

The development of wakefield theory and simulation has now become very extensive; for the present purpose, it suffices to say that *the BBU effects in rf structures become more serious as the operating frequency is raised*, and this becomes a limitation in high-brightness designs. For high-energy physics colliders, the operating frequency might still be tens of GHz, but with extremely tight tolerances. In an electron linac driver for a high-power, cw free-electron laser, for example, the BBU and heat removal considerations would dictate a frequency choice of around 400 MHz.

Electron Beams

Initial Generation of Electrons

In recent years, the requirements of free-electron lasers has spurred the development of higher brightness electron sources and accelerated electron beams.[6]

Thermionic electron sources have a lower emittance limit determined by the emitter size and the transverse component of electron thermal motion. Typically, at 1160 K the emitted electrons have an average transverse energy of 0.1 eV, and the current density capability is ≤ 10 A/cm^2.

Semiconductor photoemitter sources have an effective temperature of 0.2 eV, about twice that of a typical thermionic emitter, but the photoemitter can deliver a current density of ≥ 600 A/cm^2, so the source can be thirty times or more brighter. Furthermore, the light-activated source allows the spatial (transverse) and temporal (longitudinal) profiles of the emitted electron bunch to be carefully tailored.

As outlined above, we want to achieve uniform distributions because a matched, uniformly distributed and energy balanced beam avoids emittance growth.

Initial Acceleration of Electrons

Having achieved a bright thermionic or photocathode source, the quality must be preserved as the electrons are accelerated to relativistic velocities. DC electron guns can be used; the electrodes are carefully designed to cancel the space-sharge forces by shaping the electrodes to maintain a uniform current density. The current density uniformity must be maintained through the dc gun and subsequent accelerator up to high enough energy that the beam is sufficiently relativistic and the space charge effect becomes negligible -- perhaps around 15 MeV for an intense beam. If this can be done, the final beam emittance can be near the temperature of the beam at the cathode. The dc acceleration does not have the problem of the time varying fields found in rf accelerators, but the dc voltage cannot be very high (few hundred keV) and a transition to an rf linac is often made. To approximate a dc field during the bunch transit, a third harmonic can be added, with amplitude 1/9 that of the fundamental and phased to decelerate the bunch at the peak acceleration of the fundamental.

The low electron mass means that an approximately adiabatic approach such as the radiofrequency-quadrupole (RFQ) would consume an impractical amount of physical space. Thus the opposite approach has been developed for rf linac applications using the photocathode source. The photocathode is mounted at the entrance of an rf cavity, where in two cells, an energy gain of perhaps 2.5 to 3 MeV is applied over the very short distance of two accelerating gaps. The idea here is to bring the electrons to a relativistic energy so abruptly, over such a short distance and time, that emittance growth from space-charge forces is minimized. Other measures are taken to preserve emittance, including linearization of the cavity radial electric fields and separate phasing of the two accelerating cavities. Although this system is not periodic, the physical arguments still have some relevance. Experimental results have confirmed the approach, and optimization work continues. Simulations using the fully electromagnetic code MASK are in agreement with the oberved performance. The action in this type of injector is very complex, and so while the physics of emittance growth in non-relativistic beams indicates what is needed in principle, further work is needed to achieve more linearity and uniformity in practice.

Electron Acceleration to Relativistic Velocities

During further acceleration to energies where space-charge forces become negligible, continued care would be taken to insure matching, linearity of fields, equipartitioning, and distribution uniformity. Energy spread from the electron bunch phase width along the RF wave might need to be compensated, for example with alternating phasing of linac sections. Beam loading compensation would be provided.

At some energy, BBU considerations would become important. The transition between the regime influenced by space-sharge and that influenced by BBU might need special consideration.

Summary

Production of high-brightness electron beams is complicated by the low electron mass and consequent high space-sharge forces while the electrons are nonrelativistic. With a photocathode directly mounted in an rf cavity, rapid preacceleration minimizes emittance growth; the motion is very complex, but the the theory of emittance growth developed for ion beams provides guidance. Matching, equipartitioning, distribution uniformity, and field linearity are important. As the electrons approach relativistic velocities, phase-space mixing ceases and space-charge forces become negligible. Careful matching is still required, and beam breakup effects must be avoided. The same considerations would apply to beams accelerated by induction linacs.

References

1. R. A. Jameson, ``Beam Intensity Limitations in Linear Accelerators,"
IEEE Trans. Nucl. Sci., 28 (3), June 1981, p. 2408, and ``Equipartitioning in Linear Accelerators," Proc. 1981 Linear Accelerator
Conference, Los Alamos National Laboratory report LA-9234-C, February 1982, p.
125.

2. T.P. Wangler, "Linac Physics Design for APT", Accelerator Production of Tritium, ERAB Review, October 25, 1989, Los Alamos National Laboratory.

3. T. P. Wangler, R. S. Mills, K. R. Crandall, "Emittance Growth in
Intense Beams," Proc. 1987 IEEE Particle Accelerator Conference, IEEE Catalog No. 87CH2387-9, p. 1006.

4. I. Hofmann, "Emittance Growth," p. 183, and T. P. Wangler, F. W. Guy and I. Hofmann, "The Influence of Equipartitioning on the Emittance of Intense Charged Particle Beams," Proc. 1986 Linear Accelerator Conference, Stanford Linear Accelerator Center report SLAC-303, p. 340.

5. P. B. Wilson, ``Introduction to Wakefields and Wake Potentials,"
Physics of Particle Accelerators, AIP Conference Proceedings 184, New
York 1989, p. 526.

6. R. L. Sheffield, ``High-Brightness Electron Injectors: A Review," 1989
Particle Accelerator Conference, Chicago, Illinois, March 20-23, 1989, to be
published.

15. Present Status of FEL Research at Los Alamos National Laboratory

Stanley O. Schriber
Accelerator Technology Division
Los Alamos National Laboratory
Los Alamos, New Mexico

Photoinjector is under development at Los Alamos National Laboratory. The photoinjector greatly reduces the size and complexity of an FEL because of the following reasons;

1) very compact
2) few components
3) produces a very bright electron beam. Lower energy brings a short accelerator owing to high gradient accelerator system. The photocathode can make pulses close in time and high brightness beam allows a short wiggler. These makes a wiggler short.

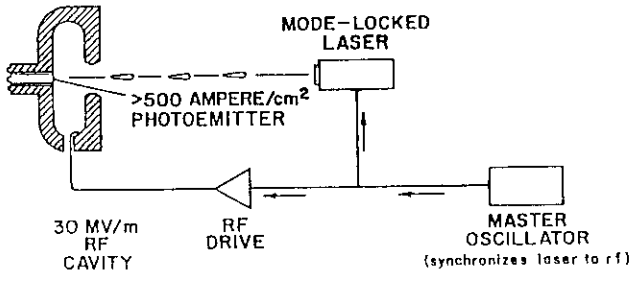

Figure 1 New design of the photoinjector

	Thermionic	LaB_6	Cs_3Sb
kT (eV)	0.1	0.2	0.2
J_{max} (A/cm^2)	10.	200.	600.
Brightness (A/m^2-rad^2)	$1.2X10^{11}$	$1.6X10^{11}$	$4.8X10^{11}$

Brightness can be increased using magnetic compression.

Tabel I Comparison of the maximum beam brightness

New design is shown in Fig.1 ,which minimizes the emittance growth by eliminating bunches and accelerating rapidly. The accelerating gradient of the RF cavity is 30MV/m. The master oscillator synchronizes the mode-lock laser to RF. Current density is more than $500A/cm^2$.

The comparison of the maximum beam brightness is shown in Table 1. The electrons from the thermionic cathode have less transverse energy, which means lower emittance. The photocathodes such as LaB_6 and Cs_3Sb have high current density, which brings high brightness. This is the reason why we are interested in the photoinjector.

The frequency of the RF-Gun test cavity is 1300MHz. The cavity is designed for linear radial electric field. The average accelerating field on axis is over 30MV/m with a maximum surface electric field

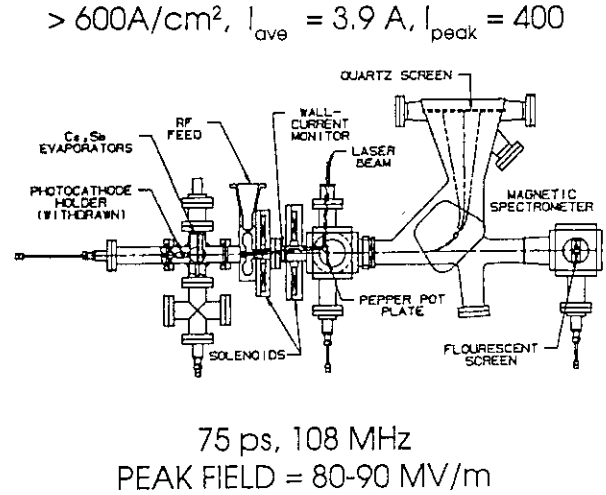

Figure 2 Set-up of the emittance measurements on single cavity experiment

of 60MV/m. The pressure in the cavity is 2×10^{-10} torr. The retractable Cs_3Sb photocathode is used. The set-up of the emittance measurements on single cavity experiment is shown in Fig.2. The current density is over $600A/cm^2$, the average current is 3.9A and the peak current is 400A. As the electrons strike and heat the quartz screen, the outgas from the screen goes back to the cathode and poisons the photocathode, so the small aperture is installed in the middle of the transport line to keep high vacuum near the photocathode.

590A peak current is obtained from less than $1cm^2$ cathode at 3MeV. This means that 16ps electron beam pulse of 13.2nC from cathode expands to 22ps by the end of the first cavity. The temporal response of the cathode is within 3ps of incident light pulse. The maximum charge extracted for a 108MHz train of 75ps pulses is 27nC per micropulse and the average current is 2.9A.

HIBAF(high brightness accelerator FEL) is planed as following;

1) make electron beam brightness measurements at 17MeV
2) make beam transport measurements at 40MeV through complex beamline- bends
3) operate FEL oscillator at 2.8microns with high brightness electron beam.

The accelerator is operated at 17MeV. The initial agreement of spot sizes from experiment and simulation is less than 20%. The experiment of final 17MeV emittance measurement is being prepared. Drive laser is operated and spatial profile is accepted. HIBAF photoinjector based electron source is shown in Fig.3.

The use of the photocathode make it possible to design a compact FEL. Compact FEL and more compact future FEL are proposed in Fig.4 and Fig.5.

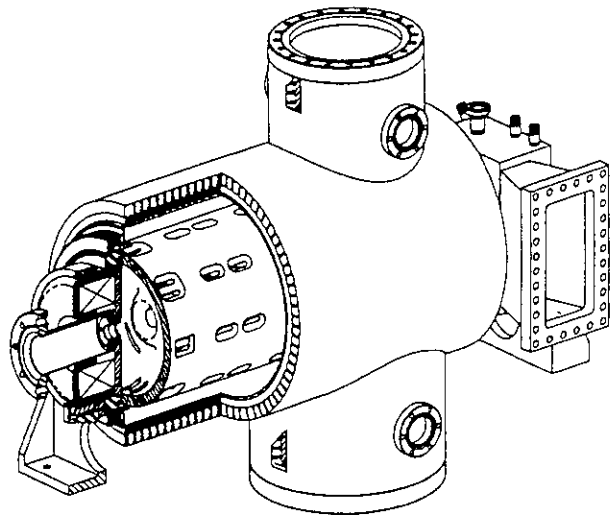

Figure 3 HIBAF photoinjector based electron source

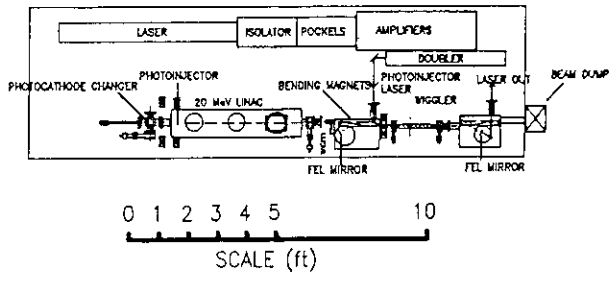

20 MeV, 10 μS MACROPULSE, 20 π·mm·mrad
350 A, PEAK SURFACE FIELD = 60 MV/m

Figure 4 Compact FEL design using photoinjector

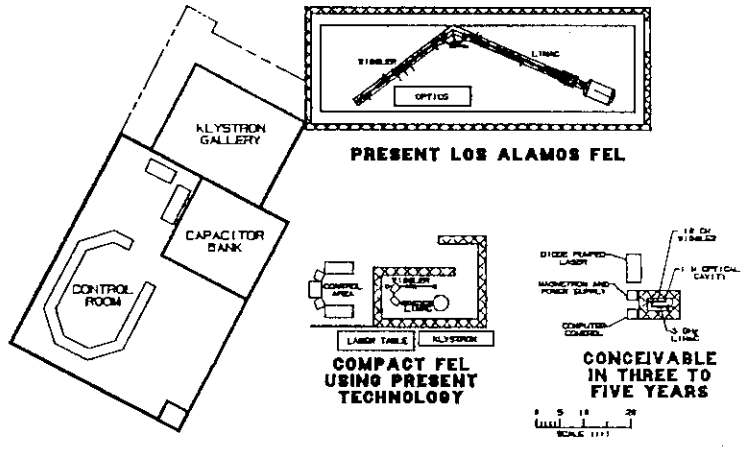

Figure 5 Comparison of the size of future FELs

16. THE RF LINAC FREE-ELECTRON LASER PROJECT AT THE UNIVERSITY OF TOKYO

H.Ohashi, T.Hara, R.Hajima, S.Kondo and M.Akiyama
Department of Nuclear Engineering
University of Tokyo
7-3-1 Hongo, Bunkyo-ku, Tokyo 113 Japan
81-3-812-2111

1. Introduction

A program in infrared FEL research is in progress at the University of Tokyo. The goal of this program is to realize a compact FEL in the infrared region of the spectrum employing an existing 15 MeV rf linear accelerator. The accelerator, which was originally constructed as an irradiation source for radiation effects studies, have been modified to meet projected FEL experiments. After finishing the modifications to the accelerator, we are now characterizing the electron beam properties.

In this paper we present our FEL project laying emphasis on the improvement in the electron beam quality.

2. Accelerator

We have an accelerator system which is composed of two parallel S-band(2856MHz) linacs in Nuclear Engineering Research Laboratory of our university. The system is called a twin-linac system and is used to investigate the primary processes on radiation chemistry. One linac is used as the irradiation source and the other is used to produce an analyzing Cerenkov light. A time interval between the two beams is controlled by rf phase shifters with high temporal resolution.(Fig.1)

These linacs produce the electron beams which have energies of 15/25 MeV, a peak current of 7A and a pulse width of 4.5μsec. These linacs are suitable for FEL studies because of the low energy and the relatively long pulse width. We decided to employ the lower-energy linac for the FEL experiments and measured its electron beam properties, because it is easier to be reconstructed than the higher-energy one. The results showed the energy spread of the electron beam was 2%FWHM and the beam emittance was 100πmm mrad. To provide the electron beam with better quality to meet the requirements for the FEL experiments, we have made modifications to the linac as described below.

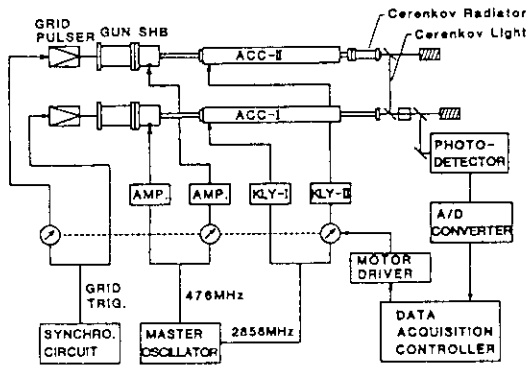

Fig. 1 Schematic of twin-linac system

2-1 Emittance Measurement System (Fig.2)

An emittance measurement system with a screen beam profile monitor has been developed. The beam profile on the ceramics screen is taken in a image processor through a CCD shutter camera. The camera is synchronized with a electron beam triggering signal.

The beam spot size is estimated from the processed data and is assumed to vary quadratically with focusing strength of quadrupole magnets located upstream of the profile monitor. The beam emittance is calculated from the coefficients of the quadratic relation which is obtained from fitting the measured data. The normalized emittance of the electron beam before the modifications was measured to 100πmm mrad. As compared with this, preliminary measurement of the improved linac showed that the emittance is decreased to 17πmm mrad.(Fig.3)

2-2 Double Pre-Bunchers

Double pre-bunchers was newly installed in the injection section of the linac to reduce the energy spread and to increase the peak current of the electron beam. Phase and power of the microwave fed into the two pre-bunchers can be controlled independently.

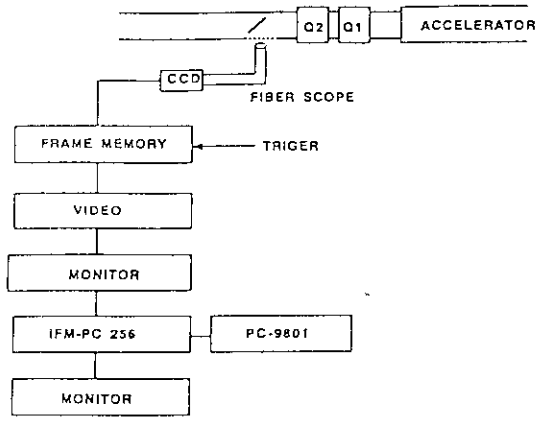

Fig. 2 Emittance measurement system

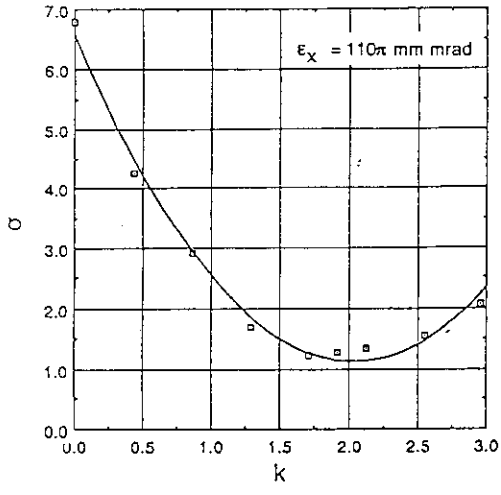

Fig. 3 Example of measured beam spot size vs quadupole field strength

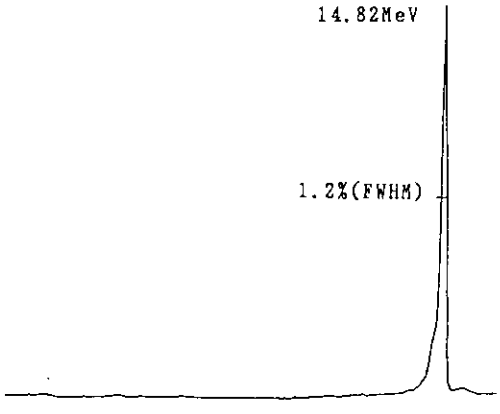

Fig. 4 Measured energy spectrum of the electron beam with the double pre-buncher

A simulation code has been developed to examine operation parameters of the pre-bunchers. The simulations showed that 1% energy spread can be obtained by adjusting the pre-buncher parameters. Experimentally, the energy spread of the linac with the double pre-bunchers is measured to be 1.2%. (Fig.4)

2-3 Low-Emittance Electron Gun

The electron gun which has been used hitherto was designed to produce a single electron pulse of very high charge. Its design was not optimized from a standpoint of the electron beam quality. So we have designed and installed a low-emittance electron gun on the linac. It employs an EIMAC Y-646E(1cm^2 area) dispenser cathode instead of Y-796 which was originally used.

The design has been made using the EGUN code under the conditions that,

(1) current more than 400mA can be extracted at 90kV voltage,

(2) calculated normalized emittance is comparable to the value limited by the electron thermal motion(5πmm mrad), and

(3) electron beam diameter at the outlet of the gun is small enough to avoid aberration effects in the downstream focusing elements.

The newly-designed gun was fabricated and installed on the linac after some preliminary experiments on a test stand. As described previously, the beam emittance was considerably decreased with this electron gun. (Fig.5)

2-4 Beam Stability

To enhance electron beam stability in the pulse, new PFN(Pulse Forming Network) units were installed into an electron gun pulser and a klystron pulser. The rf phase drift in the pulse can be controlled within 4 degrees. The pulse width is extended to over 6μsec and the fine control of the pulse shape becomes possible.

3.FEL Project

With the improved 15MeV linac we are planning to make infrared FEL experiments. A wiggler of 40mm wavelength and 25 periods is under calibration. The FEL parameters have

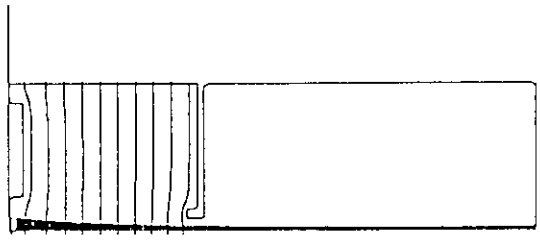

Fig. 5 Electrodes geometry and calculated electron trajectoies of the low-emittance electron gun

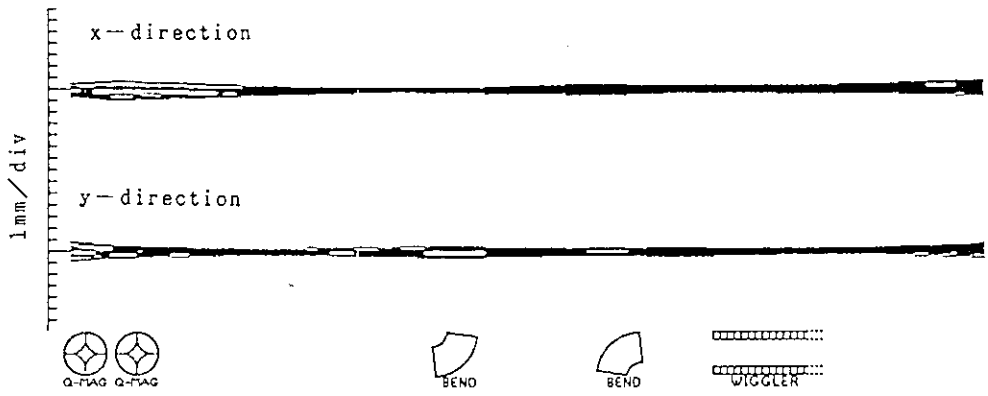

Fig. 6 Beam transport calculation for the achromatic bending line

been calculated using a 3D FEL simulation code under the condition of the beam quality of 1% energy spread and 10πmm mrad emittance value. The peak current was conservatively assumed to be 7A. If a 1/6 subharmonic prebuncher operate successfully, the peak current of about 40A can be obtained. The gain per pass is predicted to be 21 to 99% at the optical wavelength of 26 to 39μm, which is sufficient for saturation of the optical wave in the pulse. (Table 1)

A beam line for the FEL experiments was constructed with four bending magnets. The line was designed to be achromatic so that the electron beam is non-dispersive in the FEL section. It is important to keep the electron beam diameter small in this section. Simulations using PARMELA predicted that the beam can be transported with the beam diameter of less than 2mm in this beam line. (Fig.6)

4. Summary

We have described the improvements and measurements of the electron beam quality of our linac for the FEL experiments. The linac is now under adjustment to further increase the electron beam brightness. The FEL experiments are expected after installation of the optical system.

Table 1 Parameters of the FEL project

Electron Beam	
Energy	15 MeV
Peak Current	7 A
Beam Diameter	2 mm
Pulse Width	4.5 μs
Pulse Repetition	50 pps
Energy Spread	1 %fwhm
Emittance	10 π mmmrad
FEL	
Wiggler Period	40 mm
Number of Periods	25
Wiggler Gap	20 - 30 mm
Cavity Length	3.15 m
Output Coupling	4 %
Optical Wavelength	26 - 39 μm
Gain per Pass	21 - 99 %
Peak Power	2.4 - 4.5 MW
Average Power	16 - 29 W

17. JAERI FEL Program based on Superconducting Linac

Yuuki Kawarasaki
Department of Physics, JAERI
Tokai, Ibaraki 319-11

Abstract:

JAERI FEL Program based on a superconducting linac is briefly overviewed, including a status report.

The R&D planning for a long-term schedule is first discussed, focusing on the choices on the type of FEL's regime and accelerator there used. The R&D schedule is tentatively divided into three phases:

Phase-I; Basic R&D for an infrared FEL oscillator.

Phase-II; For a visible wavelength oscillation, the increase of the beam energy by means of beam-recirculation.

Phase-III; High-power output through an energy-recovery method.

A superconducting linac of lower radio-frequency(~500 MHz) is found to be a most suited one to our purpose.

Specifications of the linac in the Phase-I are:

Injector gun — thermoionic gridded Pierce(2~4 mm), applied voltage; 250 kV, pulsing format; 2~4 ns width every 80 ns (127 MHz) separation during 1 ms (macropulse), repetition; 10 Hz(macropulse).

Sub-harmonic buncher — $\lambda/4$ coaxial resonator (normal conducting), frequency; 87 MHz(1/6 of main r.f.), gap voltage; 30~60 kV.

Harmonic buncher — re-entrant cavity (normal conducting),frequency; 508 MHz, gap voltage; 10~40 kV.

Pre-accelerator — two superconducting single cavity, independently phasing and feeding.

Main accelerator cavity — superconducting 2 (unit) × 5 (cell cavity), effective length; 2 × 1.5 m.

1. Introduction

The final objective of the JAERI's (Japan Atomic Energy Research Institute) free-electron laser (FEL) program shall lie on the industrial applications in the nuclear energy field for definitely peaceful use: 1) Enrichment of fuel element, uranium- 235 from natural uranium, possibly 2) Waste management (OMEGA- Project: Options Making Extra Gains of Actinides and fission products) support through group partitioning of radioactive wastes, and 3) Others, e.g., decommissioning of nuclear reactor power plants. Thus high-power FELs shall be inevitably needed, whose wavelengths must range over infrared through ultraviolet.

However, the direct pursuing of this final feature of the FEL system seems undoubtly too adventurous, or even unrealistic, because the FEL technology looks like requiring far advanced accelerator's and related ones. Thus the whole schedule of the R&D dare preferably be divided into some adequate developmental phases. Accordingly, the first phase is naturally devoted to the most basic R&Ds on a concise FEL system, but aiming at an infrared or far-infrared lasing even at low power level. The separation of uranium isotopes in a so-called molecular method requires a light source of 16 μm which coincides with the wavelength region just aimed at in this R&D phase. This FEL scheme, however, must have the feature to be easily extensible to the final one during the later phases. On the other hand, low- power FELs of longer wavelengths can further be expected to be useful tools for basic science researches; physics of condensed matters, biomedical and biochemical researches, because nowadays no conventional lasers so far are easily available in the wavelength region longer than 10 μm.

2. Considerations on the FEL Scheme and the Schedule

There are two FEL's regimes, conventionally so classified: Compton and Raman regime. First, we must have decided which regime shall be adopted, because in general the type of accelerators depends on this choice. World-famous ones are: RF- linacs at Stanford University, at Los Alamos National Laboratory and at Boeing Aerospace Company, and storage rings at Orsay, France and at Novosibirsk, U.S.S.R. and Van de Graaff type at Santa Barbara, University of California; all in Compton regime, while induction linacs, ETA and ATA, at Lawrence Livermore National Laboratory; in Raman regime.

We have since been continuing the operation of a 120 MeV normal conducting RF(S-band(2856 MHz)) linac, similar to the Stanford normal conducting linacs, SLAC or Mark III, for neutron nuclear data measurements and other research purposes, e.g., positron generation. This linac is now used as the injector of a small(300 MeV) storage ring, JSR. Thus we could decide without hesitation the adoption of a so-called Compton regime FEL scheme and the use of an RF-linac rather than a storage ring, because at the beginning time of this program, the JSR was not yet installed.

However, there remained another decision on whether this RF- linac could suitedly be used for our purpose or a new dedicated one should be constructed. The required beam quality did seem far from that of the FEL's specification even after some modifications for the improvement of the beam characteristics of this linac. Furthermore, in a normal conducting RF linac, CW operation for high power output is seemingly difficult, even if the beam quality would be guaranteed, from the view point of cost- effectiveness. This view may invoke many debates. However, the following considerations may be enough to make us decisively convinced that a superconducting linac scheme must be adopted.

Three normal conducting linacs have been newly built or greatly modified for the FEL projects and then succeeded in oscillations: the first one is the 20 MeV standing wave mode L- band(1300MHz) linac at LANL[1] in oscillation at an infrared wavelength, the second the Boeing Aerospace Company's(BAC's) 120 MeV traveling wave mode L-band (1300 MHz) linac[2] at a visible wavelength, and the last the modified Stanford Mark III (traveling, S-band(2856MHz)) linac[3] at an infrared wavelength.

The former two linacs operate in longer macropulse duration(>100 μs), being provided by specially prepared components; klystrons and their pulse power supplies. The last linac is the old Mark III, where the conventional injector gun and pre-buncher are replaced by a so-called RF-gun and a momentum filter, by which high quality beam can eventually be injected into one unit of the Mark III waveguide.

The first FEL oscillation at Stanford[4] has reasonably been succeeded, using HEPL's superconducting linac(SCL) which can accelerate high quality beams in long macropulses. Thus a SCL is attractive if greater accelerating field gradient(>5MV/m) in a cavity is achievable. In recent years, the remarkable progresses of this matter(~10 MV/m) have been reported from TRISTAN's at KEK[5] , Japan, and from CEBAF's, USA[6] . Furthermore, here at JAERI, the project of a heavy ion boosting RF-linac[7] for the Tandem Van de Graaff accelerator (20 MV) is now in progress, using many of a niobium quarter-wave resonator for quadruple increase of the ion-beam energies. Here the Tandem accelerator is serving the beams for the researches of nuclear physics, nuclear chemistry, materials science, including solid- state physics and so forth. The project is the upgrading of the performance, being proposed some ten years ago. The various techniques of cryogenics and high Q cavities developed here will explicitly be helpful and consequently influential.

In the RF-linac driven FEL operation, an energy-recovery configuration, or recuperation scheme, is desirable and forthcoming for high-power oscillation, because an FEL efficiency (laser power vs. beam power) is still a few to several percents and the remaining beam power is dumped out unless it is reused. The tests of this configuration have been successfully performed both at LANL[8] and at HEPL.[9] The LANL's uses two structures: one as an accelerator and another as a decelerator, while the HEPL's SCL uses a technique of beam recirculation. The recirculation is also applicable as an energy doubler, tripler and so more. Furthermore, solid-state RF amplifiers can hopefully be used, because the cavity losses in SCL are negligible. The net FEL power consumption may stay under almost several tens KW in average. The present state-of-the-art of solid-state amplifiers in the frequency range of UHF for TV broadcasting service can enough fulfill the requirement. The serious consideration on choice of RF-amplifiers, especially klystrons or triodes or tetrodes, is usually needed in designing normal conducting linacs both of electron and of heavy-ions. The lifetimes of solid-state amplifiers can be expected much longer than types of vacuum tubes, which seems reducing the total cost and guarranteeing the long-term stability.

And then new finding of high Tc superconductor may somehow influence this choice, because the program period will span over some ten years. Possible uses of such high Tc RF- or magnetic devices, as RF-couplers or magnetic shieldings, will expectedly take place in near future.

On the contrary, in a case of normal conducting CW linac scheme, a main part of the RF-power may go to the wall lose of the accelerating waveguides, and a main part of the cost may also be in their RF-power supplies and peripheral utilities such as cooling system rather than accelerating waveguides or cavities themselves.

The final FEL system must incorporate with the beam recirculation both for energy multiplexing and for energy recovery. The whole program period is accordingly divided tentatively into three phases. The Phase-I is basically devoted to the fundamental R&D of the simplest FEL feature, but aiming at an infrared, say, typically 10.6 μm lasing. This duration may depend on a few factors: number of staff personnels, availability of the budgetary funds and so on. It will range over 5 to 7 years. The present time (fiscal year 1989) is the second year of the phase-I. In Phase-II, the addition of one or more SCL modules with recirculation as an energy doubler or trippler($\sim$100 MeV) will be attempted to work on lasings at visible or ultraviolet wavelengths, and the increase of an output power by means of an energy recovery will then be followed in Phase-III. As will later be discussed, the injector system will be improved in the following phases by replacement of, e.g., a mode-locked laser irradiated photocathode gun.

3. Specification of the Linac in Phase-I

The choice of SCL's frequency is important: e.g., HEPL's at 1300 MHz, CEBAF's at 1500 MHz, TRISTAN's at 508 MHz, and CERN's at 350 MHz. Use of lower frequency is fit to higher beam quality and current intensity without extra cooling below liquid He boiling point, 4.2 K, at 1 atm. The choice of the frequency may actually have a close relationship with that of the RF-power supply, even though there is some difference; high-energy accelerators must feed enough power to the beams, while FELs' can reuse it. Thus, at present, the similar cavity structure as TRISTAN's seems satisfactorily applicable for a main part of the linac. TRISTAN's one cryostat module contains two 5-cell units, i.e., being capable to accelerate beams of 15 MeV(5 MeV/m) to 30 MeV(10 MeV/m), which almost satisfies the requirement for an infrared FEL oscillation. Thus a main accelerating part of the linac is tentatively figured.

The injector design is another key point, because its performance governs strongly the output beam quality. Higher FEL gain requires simultaneously both higher brightness and higher energy resolution of the beam. Novel trials are now proposed for this achievement.[10-12] Higher injection-gun voltage can well prevent the deterioration of beam characteristics from emittance growth. Conventional linacs equip a some 100 KV pulsed beam injector, while novel ones attempt use of a few hundred(200 to 500) KV potential. These values will be attainable both in a D.C. manner and in a pulse mode. The latter is a kind of RF-gun.

There is another FEL's uniqueness of the temporal format of beam pulses, which is far different from that of conventional ones. A simple format may be trains (macropulse) of the micropulses of bunched beam, where the temporal separation of each micropulse must be correctly synchronized with the round trip time of the light traveling back and forward within an optical cavity resonator, i.e., between two mirrors. Typical values of micropulse separation may be a few tens to a hundred and several tens nanoseconds, depending on the length of the optical cavity, which far differs from the period of accelerating RF- frequency; e.g., 0.33 ns at 3 GHz or 2 ns at 500 MHz. A mode- locked laser driven photocathode gun[13] can actually produce micropulse-formatted beams of sufficiently high current density. However, its adoption here seems yet premature in phase-I, even though the feature looks like the best. The R&D of a photocathode system will take a few or several years in our case. A thermoionic cathode gun must accordingly be used and followed by bunchers to obtain the sufficient brightness of the emitted beam. Furthermore, a micropulse formatter(e.g., a beam chopper) is necessary in their vicinity. A gridded gun is expected to work well with an even elaborated grid-pulsing circuit. In this configuration, a subharmonic buncher(SHB) will act as a brightness multiplier, and a longitudinal pulse-length compressor, because the pulse length from the grid-controlled one is an order of nanoseconds, while that acceptable to be accelerated is an order of a few to a few tens picoseconds. Even though a SHB intrinsically makes the energy resolution of the injected pulse beam worse and needs some distance of several meters as drift space, this seems a tolerable choice for the first step. After the SHB, one buncher must positively be inserted for compensation of the energy spread. Both a subharmonic buncher whose frequency is one fourth to eighth of the fundamental, and a buncher may be fabricated in a form of normal conducting cavity. Their RF- power can also be delivered from solid-state amplifiers whose output ranges less than several KWs.

The injection of a few hundreds KeV electron beams to a main unit of accelerating cavities still seems inadequate; in terms of β (=v/c), e.g., 80 KeV electrons' is 0.5, 250 KeV's 0.75, and 2 MeV 0.98, respectively. This leads to necessity of pre- acceleration. Two single superconducting cavities for pre-

acceleration (2∼4 MeV) seem more neat than a normal conducting one. The geometrical beta of the cavities can be set as unity if the RF phasing and amplitude can independently be controlled. Also less than several KWs of RF-power suffices to each cavity from respective solid-state amplifier.

The above considerations allow us to depict the conceptual FEL scheme shown in Fig.1, including the extending option for the R&D in later phases.

SCLs show a definite superiority in its operation performance of longer macropulse or even CW operation and of high beam quality, while they require inevitably a cryogenic equipment to cool down the cavities at liquid He temperature. A completed SCL system must usually include a liquid He refrigerator from which He coolant is distributed through its pipelines, which forces people to do another work and to prepare extra money. Contrarily, cavity tests can usually done without a refrigerator, but in direct use of liquid He preserved in a vessel. Test experiments of the SCL as the basic R&D in phase-I can thus be carried out just like a cavity test. The amount of liquid He consumption depends mainly on the duty ratio of RF-feeding. If the duty ratio is chosen much less than unity, CW, say, 1 percent, then a small closed-loop refrigerator which is nowadays used in a medical instrument, MRI(magnetic Resonance Imaging), where superconducting magnets are operating can be applicable without any distribution lines but being mounted on a vessel top of the cavity cryostat. This proposal[14] seems much attractive and worthy to be introduced, if another problem of mechanical vibration isolation will be solved.

A small value of the duty ratio of the SCL operation will give a good effect to other design factors. Problems of the electric power supply capacity and the radiation shielding are much reduced in difficulty. The simplest FEL scheme in phase-I will use that of so-called single pass. Beam-power gained in the main accelerating cavities must thus be dumped into some adequate absorber, a beam stop. Pulse operation will lead to accumulation of accelerator technology different from that of genuine CW's. The duty of one percent can arbitrarily but reasonably be combined by 1 ms of macropulse length with the repetition of 10 pulse per second of it. The macropulse length of 1 ms is however almost quasi-CW in an electronic sense and quite long enough to the growth time of FEL, a few to several tens microseconds.

Table 1 lists the specification of the SCL in the phase-I, tentatively in quantitative values.

Fig. 2 shows a bird-eye's view of the FEL system of the Phase- I, which will be temporally installed in an old target-room of the shut-down van de Graaff accelerator.

4. Present Status

The most front part of the injector system can independently be designed, fabricated, assembled, and then tested. They are an injector gun, a subharmonic buncher and a buncher with their peripherals. Fig. 3 shows a mechanical sketch of this injector. This part is now under fabrication.

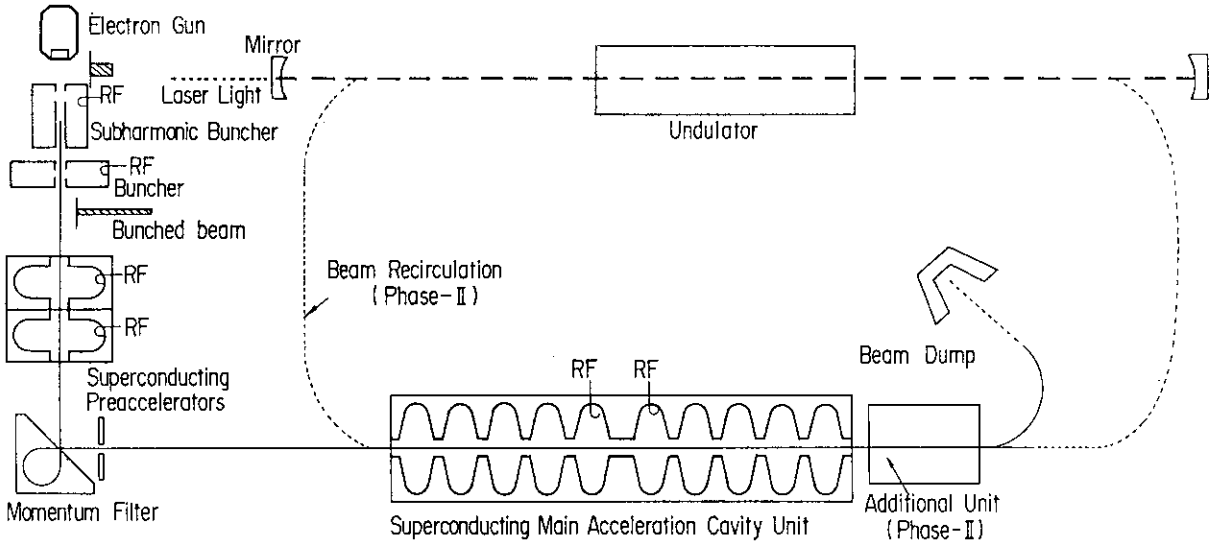

Figure 1 JAERI FEL, conceptual scheme

Table 1. Specification of the SCL in the Phase-I.

Main part of the linac	
Type	superconducting 2(unit) × 5(cavity)
Frequency	508 MHz
Effective length	2 × 1.5 m
Gun(injector-I)	
Type	thermoionic gridded Pierce (2-4 mmϕ)
Applied voltage	250 kV
Pulsing format	2-4 ns width every 80 ns(127 MHz) separation during 1 ms (macropulse)
Repetition	10 Hz (macropulse)
Subharmonic buncher(injector-II)	
Type	$\lambda/4$ coaxial resonator (normal conducting)
Frequency	87 MHz (1/6 of fundamental)
Gap voltage	30-60 kV
Buncher	
Type	re-entrant cavity (normal conducting)
Frequency	508 MHz
Gap voltage	10-40 kV
Preaccelerator(injector-III)	
Type	two superconducting single cavities
Geometrical beta	unity for both

The injector gun consists of: 1) a pressure vessel for high- tension insulation, 2) a Cockcroft-Walton type high-voltage power supply inside the vessel, 3) an electron gun unit, 4) a grid- pulsing circuit, and 5) their peripherals and control. Fig. 4 is a cut-away view of the injector gun. Fig. 5 is that of the gun itself. Here the cathode(Y-646B, Eimac Co.) is mounted on a flat end-flange and the anode is positioned on the top of a cone- shaped support inside the space of a ceramic insulator cylinder. This configuration is not usual but facilitates us to easily design the grid-pulser and maintain it, because an ample space for it is guaranteed.

During the mechanical designs on the components, some beam behavior simulations at the injector gun and along the beam path from the gun through the SHB, the buncher and the pre-accelerating cavities, have been performed: the shape of the electrodes, anode and Wehnelt, has been designed as shown in Fig.6 with the resulted beam profile.

The procurement of superconducting cavities has some actual importance from viewpoints of availability of our man-power for cavity-processing and of cost-performance. There should remain a crucial choice on whether those of KEK type, 508 MHz or those of DESY type, 500 MHz should be adopted. LISA[15] of the INFN group at Frascati, Italy, adopts the latter.

The author thanks the member of the FEL group and people outside the group who have commented on and supported this program, because this paper has a nature of the content that combines their ideas and summarizes their papers, reports, and documents. Some figures are kindly offered from some of the member.

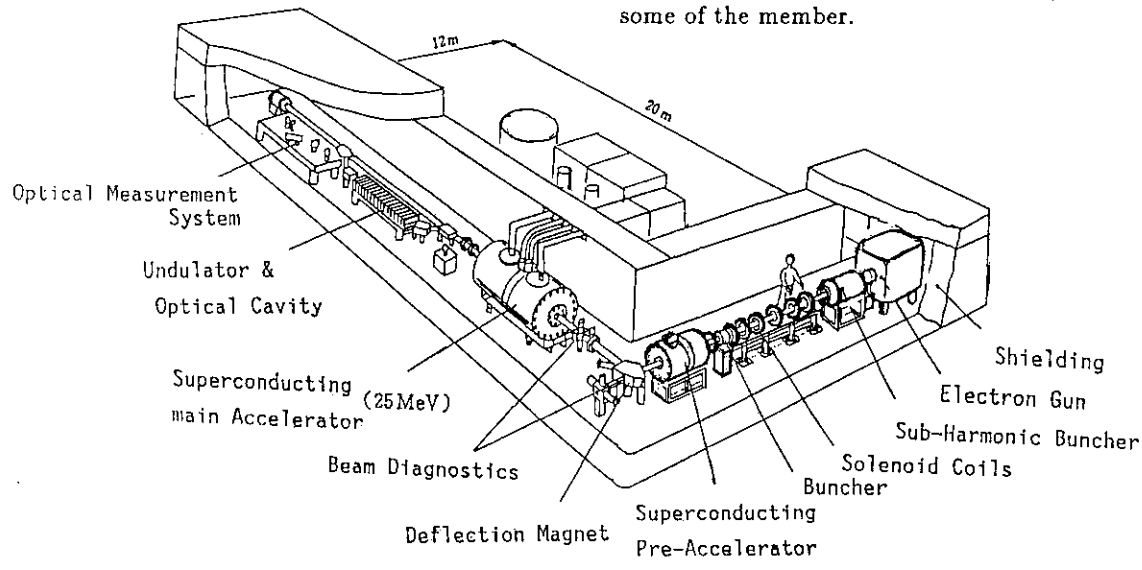

Figure 2 Bird-eye's view of JAERI FEL, in phase-I

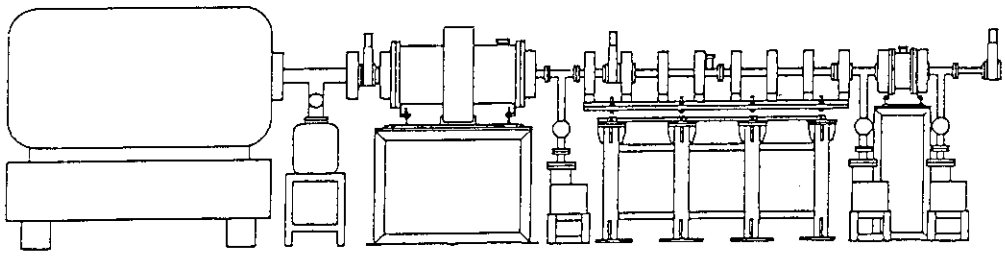

Figure 3 Injector of the JAERI FEL system. The electron gun, the subharmonic buncher, beam transport system with focus coils, and the buncher.

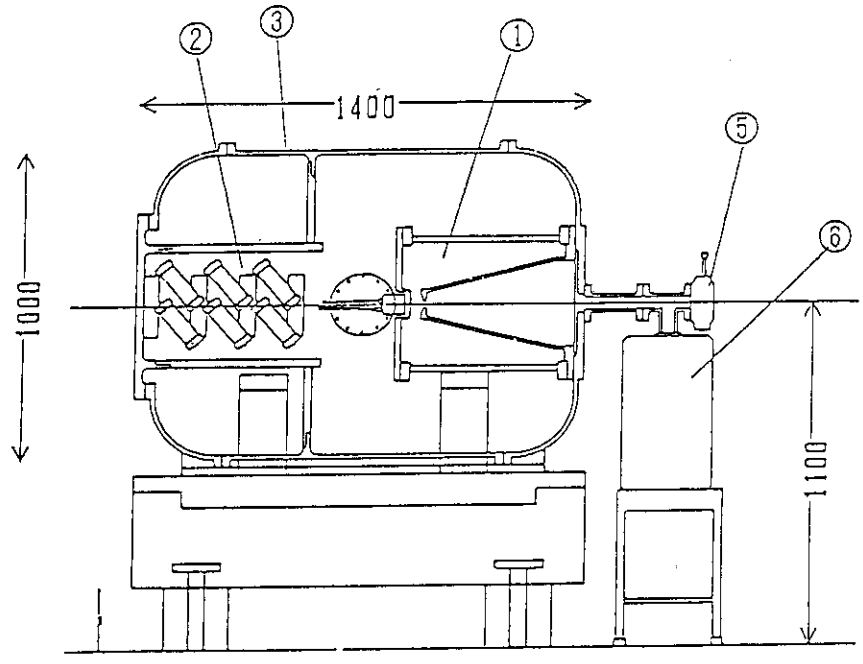

Figure 4 Side view of Gun tank (1)Electron Gun, (2)Cockcroft-Wolton, (3)Vessel, (5)Gate valve, (6)Ion Pump

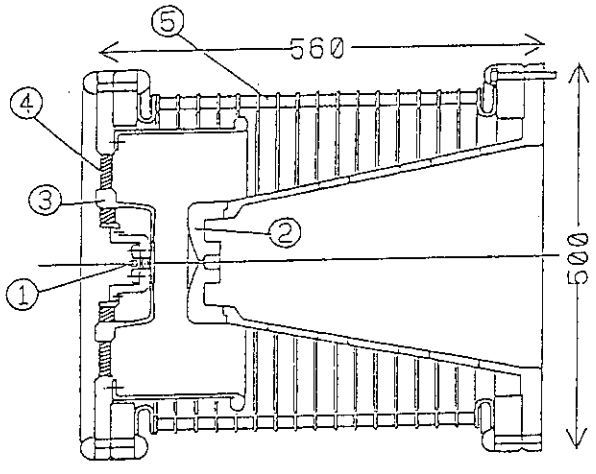

Figure 5 Cross sectional view of electron gun assembly. The anode is mounted on the top of cone shape support which has vacuum openings. Cathode, Grid and Wehnelt are mounted on a flat flange. (1)Cathode Assembly, (2)Anode, (3)Wehnelt, (4)Ceramic Insulator, (5)Ceramic Insulating Cylinder.

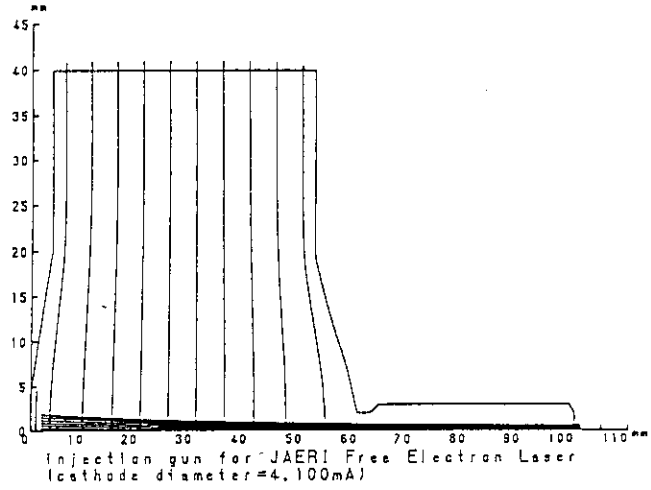

Figure 6 Shape of the problem region boundary and the equipotential lines for the cathode with a 4 mm diameter, a 100 mA peak current and a 300 kV anode voltage. The horizontal axis shows the axial length in mm and the vertical axis shows the radial length in mm. The filled area near the axis shows the beam trajectories from the virtual cathode.

References

1. J.M.Watson, *Nucl. Instr. and Meth., A250 (1986)*, pp. 1-3.
2. J.L.Adamski, W.J.Gallagher, R.C.Kennedy, B.Robinson, D.R.Shottstall, E,L.Tyson, A.M.Vetter and A.D.Yeremian, *IEEE Nucl. Science, NS-32 (1985)*, pp. 3397-3399.
3. S.V.Benson, J.M.J.Madey, J.Schultz, M.Marc, W.Wadensweiler, G.A.Westenskow and M.Velghe, *Nucl. Instr. and Meth., A250 (1986)*, pp. 39-43.
4. D.A.G.Deacon, L.R.Elias, J.M.J.Madey, G.J.Ramian, H.A.Schwettman and T.I.Smith, *Phys. Rev. Letters, 38 (1977)*, pp. 892-894.
5. T.Furuya, K.Asano, Y.Kojima, S.Mitsunobu, H.Nakai, T.Nakazato, S.Noguchi, K.Saito and T.Tajima, *Proc. of 3rd Workshop on RF superconducting*, p. 95, Argonne.
6. H.A.Grunder, J.J.Bisognano, W.I.Diamond, B.K.Hartline, C.W.Leemann, J.Mougey, R.M.Sundelin and R.C.York, *CEBAF-PR-87-017.*
7. S.Takeuchi, T.Ishii, H.Ikezono, M.Ohkubo and N.Shikazono, *JAERI-M, 87-115* , pp. 16-18.
8. C.A.Brau, T.J.Boyd, R.K.Cooper, and D.A.Swenson, *Proc. of International Conference on Lasers, (1979).*
9. T.I.Smith, H.A.Schwettman, R.Rohatgi, Y.Lapierre, and J.Edighoffer, *Nucl. Instr. and Meth., (1987).*
10. T.I.Smith, *Proc. 1986 Linac Conf.*, p. 421, SLAC, (1986).
11. G.A.Loew, R.H.Miller and C.K.Sinclair, *Proc. 1986 Linac Conf.*, SLAC, (1986).
12. J.S.Fraser, *Proc. 1986 Linac Conf.*, p. 411, SLAC, (1986).
13. J.S.Fraser, R.L.Sheffield, E.R.Gray, P.M.Giles, R.W.Springe, and V.A.Loebs, *Proc. 1987 Part. Accel. Conf.* , Washinton, DC..
14. E.Minehara, *private communication* .
15. A.Aragona et al. , *Proc. of EPAC, 1988.*

18. DOUBLE-SIDED MICROTRON FOR FEL AT NIHON UNIVERSITY*

Y. Torizuka, K. Hayakawa, T. Tanaka, T. Iijima, and K. Sato
Atomic Energy Research Institute, Nihon University
7-24-1 Narashinodai, Funabashi, 274 Japan
0474-66-1111

M. Yokota
Department of Physics, College of Science and Technology, Nihon University
1-8-14 Kanda-Surugadai, Chiyoda-ku, Tokyo, 101 Japan
03-293-3251

I. INTRODUCTION

High current, low emittance and small energy spreading width electron beams are needed to oscillate the free electron laser (FEL). To realize these beam qualities a continuous wave (cw) double-sided microtron (DSM) has been designed and constructed since 1984 at Nihon University. The basic configuration are shown in Fig. 1 and design parameters are in Table 1. The 4.55 MeV electron beams at the injection linac are injected into the DSM through the beam transport system, where both longitudinal and transverse emittance is adjusted to match the beam ellipse at the injection point of the DSM. The injected beam is recirculated five turns and reaches the final energy of about 35 MeV.

Table 1 DSM design parameters.

Injection energy	4.55 MeV
Extraction energy	34.5 MeV
Average beam current	300 μA
Field of sector magnets	0.1867 T
Synchronous phase	25 °
Energy gain per turn	6 MeV
Number of recirculation	5 turns
Accelerating tubes	4.283 m × 2
Operating rf frequency	2449.77 MHz
Rf power dissipation	100 kW
Accelerating gradient	0.773 MeV/m

The beam accelerating experiment was performed using pulsed beams of 100 μsec width and repetition rate of 50 pps. The injected beams were recirculated successfully and reached the energy of the designed value in May 1989.

In the following sections, details of individual systems, results of beam accelerating test and application of this machine to FEL are reported.

II. THE INJECTOR LINAC

All the rf systems have been designed so that they operate at 2450 MHz. There are four 50 kW cw klystrons (KL1 ～ KL4 in Fig. 1) made by Thomson CSF, two of them are used in the injector linac. Each klystron is isolated from the accelerating system by using a circulator.

The injector linac consists of 100 keV gun terminal (GUN), rf chopper (CP), prebuncher, buncher (B-ACC) and preaccelerator (P-ACC). The output power of the klystron (KL1) is divided among chopper, prebuncher and buncher via series of directional couplers. The chopper system, which is the same one as in the NIST-Los Alamos race-track microtron(1), consists of two chopper cavities, a sector shaped slit at the mid point of two cavities and two magnetic lenses placed in symmetry near the slit. A circular beam profile is obtained at the slit by adjusting the input rf phase and power, where the beam in relative phase width of 300° is removed and 60° is used.

The electron beam is accelerated 2 MeV in the buncher, and further accelerated 2 MeV in the preaccelerator. Total energy of 4.55 MeV is required in the injector.

The buncher is a 2 m long graded-β (=v/c) accelerating tube of the DAW structure. Combination of values of β and number of cavities was determined by a computer simulation using the field distribution obtained by SUPERFISH(2), which is shown in Table 2. The

* This study has been performed through Special Coordination Funds of the Science and Technology Agency of the Japanese Government.

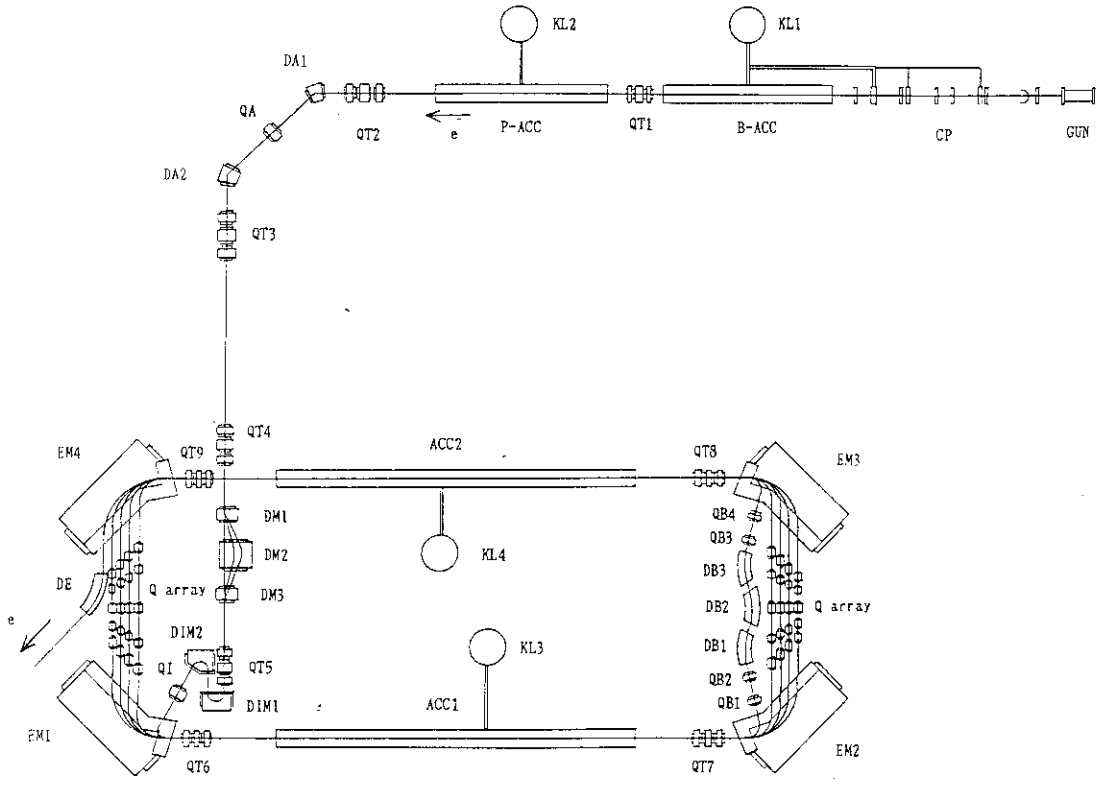

Fig. 1 Layout of the 35 MeV cw double-sided microtron and the 5 MeV injector. KL:klystron, ML: magnetic lens, CP:chopper, PB:prebuncher, B-ACC:buncher, P-ACC:preaccelerator, DA and QA: analyser magnets, DM:longitudinal matching magnet, DI and QI:injection magnets, EM:sector magnet, ACC:4 m accelerating tube, DB and QB:phase matching magnets, DE:extraction magnet, QT:Q-triplet.

preaccelerator is a 2 m long constant β tube of the DAW structure. Each tube has been constructed separated into half parts for convenience of construction, and joined together near the center of the tube with vacuum flanges. There are six movable frequency tuners opposite to washer support stems for fine tuning of the resonance frequency.

Table 2 Combination of cavities in the injector accelerating tubes.

	β	number of cavities
Buncher	0.700	3
	0.850	5
	0.925	10
	0.974	17
Preaccelerator	0.994	32

Ⅲ. INJECTION BEAM TRANSPORT LINE

The beam from the injector is deflected 90° in the achromatic bending system (DA1,QA,DA2), where energy spread is defined by a slit near the Q-singlet QA. The beam with energy spread of 2 % is transported to the DSM.

In order to keep stable acceleration in the DSM, both longitudinal and transverse emittance ellipses have to be matched at the injection point as follows.

The longitudinal emittance ellipse is adjusted to an optimum shape by means of the longitudinal matching magnets(DM1, DM2 and DM3) on the injection beam transport line so that the energy and phase spread is kept minimum during acceleration in the DSM. Adjustment is made by the use of the difference of the orbit length according to the difference of the electron energy and magnetic field in the magnets.

The transverse emittance is adjusted by means of quadrupole triplets(QT1 ～ QT5) on the injection transport line so that the beam size in the DSM is minimized.

The injection point is the dispersive side

of the first sector magnet EM1, where 4.55 MeV electron beam is deflected 120° with an orbit radius of 8.077 cm. Energy dispersion is matched by means of two injection dipole magnets DIM1,DIM2 and Q-singlet QI, then achromatic beam is injected on the axis of the first accelerating tube ACC1.

IV. ACCELERATING TUBES IN THE DSM

Two accelerating sections placed in parallel at a distance of 3 m from each other, which consist of 4.28 m long accelerating tubes with β = 1 DAW structure cavities. Each tube is fed with 50 kW rf power from one klystron. Coupling coefficient was chosen to be about 2.1 of over coupling in order to reduce the fluctuation of the rf field in the tubes caused by beam loading effects, which is a possible maximum value when accelerating field necessary for operation is taken into account. The tube has been constructed separated in four parts and joined together with vacuum flanges. The resonance frequency is tunable more than 2 MHz with a total of 12 movable tuners in each tube.

Since the temperature of cooling water supplied to the tubes is kept constant with accuracy of ± 0.1°, the resonance frequency decreases as increase of the input rf power, which amounts about 250 kHz at cw 50 kW, corresponding to increase of the tube temperature by 6°. The resonance frequency of the tubes has not been tuned during the operation so far, but the rf frequency has been adjusted so that VSWR could be minimized, which is a simple way of tuning when all the tubes are tuned in identical frequency and cooled using the same kind of cooling system. However, a remote tunig system using movable tuner is under construction so that the change of the resonance frequency in each tube caused by the change of the input rf power will be compensated automatically.

V. MAGNET SYSTEM

The beam recirculation system between two accelerating tubes was designed with the aid of computer programs, TRANSPORT(3), TRIM(4) and original program BEAM.

A. Sector magnets

The sector magnets were constructed on the basis of results of field measurements on a model magnet which has the same dimensions as practical ones.

In order to obtain a uniform magnetic field in a wide range, a Purcel gap of 2.5 mm width is introduced between the pole piece and the return yoke. Also shims are installed at the pole edge and the periphery of the Purcel gaps. As seen in Fig. 1, the electron beam is injected to the first accelerating tube after deflected by 120° at the sector magnet, then the beam from the first accelerating tube is deflected by 107° at the next sector magnet. Therefore, the beam at low energy can experience the uniform field in the sector magnet owing to the particular shape of the field boundary.

Each sector magnet is equipped with auxiliary coils, field clamp coils and auxiliary field clamp coils besides the main coils so that all the sector magnets are excited in series at an identical field strength and that vertical defocus and horizontal orbit displacement in the fringing field are controlled precisely.

Field uniformity of the flat region in all the sector magnets were measured by means of a Hall probe in the symmetry plane of the pole gaps, which was estimated to be within ±0.07 %. Additional correcting coils on the pole surfaces will be assembled in order to suppress within ± 0.01 %.

B. Phase matching system

The first recirculating system is distinguished from others in the short straight sections. Since pole pieces of the sector magnets EM2 and EM3 are modulated at non-dispersive sides so that the lowest energy orbit passes well flat regions, the first turn beam is deflected 107°. In this system, the beam from ACC1 is deflected 107°, -37°, 40°, -37° and 107°, then injected on the axis of ACC2. A large phase slip of beam bunch caused by the difference of the velocity between the bunch and the rf phase is compensated in this system by the adjustment of the total orbit length. Horisontal and vertical beam envelopes in first order calculation are shown in Fig. 2 together with the dispersion curve. The behavior of the longitudinal emittance ellipse in this system is the same as in the other short straight sections.

C. Short straight section

Five Q-magnets in each short straight section are necessary for achromatic 180° bending system without beam divergence. The beam envelopes are designed to be symmetric about the third Q-magnet, having waists at the center of the accelerating tubes with no acceleration. Horizontal and vertical envelopes in the first section are shown in Fig. 3. The maximum field gradient of Q-magnets with aperture diameter 28 mm, outer diameter 104 mm and pole width 20 mm is 1100 G/cm, which is possibly an upper limit of field gradient realized without cooling.

Whole envelopes from entrance to the first accelerating tube through exit of the final tube

beam diameter and displacement.

The injection linac particularly the bunching system does not work well because of the low electric field distribution in the low β region as mentioned above. It suggests that the DAW structure may not be adequate in the low region. Accordingly low β cavities with on axis coupled structure is preparing instead of the present one. Also needed is modification of the gun grid structure which causes seriously the divergence of the beam character.

During the operation of the DSM frequently needed was the adjustment of parameters because of the fluctuation of the accelerating energy gain. The rf system to stabilize the fluctuation of the rf phase is progressing. There is also a plan to construct a new building for the space of experiment and for the radiation shielding.

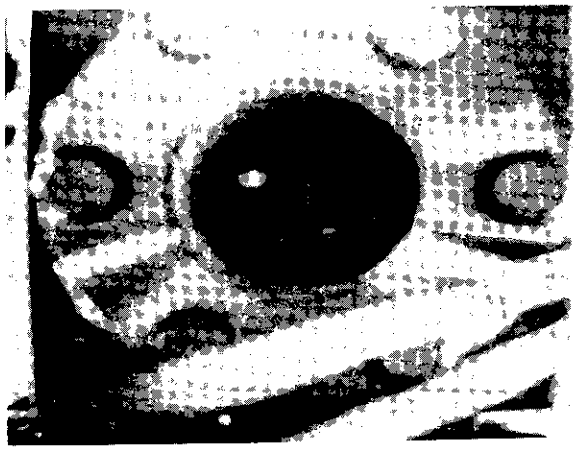

Fig. 6 Observed beam profile at the entrance of the extraction magnet.

VII. APPLICATION TO FEL

As one of applications of the DSM, it is possible to build a FEL which operates in the infrared light region. The general beam character in Table 1 must be modified to match the requirement from the FEL as shown following.

energy variable	10 ~ 35 MeV
micropulse length	3 psec
peak bunch current	5 A
repetition rate	24.5 MHz
(distance between micropulses	12 m)

The wiggler in this case would be a permanent magnet linear wiggler with period 2 cm and normalized vector potential a_W = 0.7 rms. The number of the period could be considered with either 50 or 100 depend on the oscillating condition. Electron beam energies from 10 - 35 MeV yield FEL radiation from 40 μm to 3 μm. The third harmonic FEL operation could permit the expectation of the range to 1 μm. The output power of the FEL for the typical case would be as follows.

intercavity peak optical power	50 MW
peak output power	1 MW
average power	75 W

The light may be used for the study of material science and for the medical application and other many fields.

REFERENCES

(1) M.A.Wilson, R.I.Cutler, D.L.Mohr and S.Penner, IEEE Trans. Nucl. Sci. NS-32, No.5, 3089(1985).
(2) K.Halbach, R.F.Holsinger, W.E.Jule and A.Swenson, Proc. of the 1976 Proton Linear Accelerator Conf., Chalk River, Canada, 122.
(3) K.L.Brown, D.C.Carey, Ch. Iselin and F.Rothacker, SLAC-91(1974).
(4) J.S.Colonias, UCRL-18439(1968).

19. Basic studies of Free Electron Laser and Development of Compact Ring for FEL at Research Laboratory for Nuclear Reactors, Tokyo Institute of Tecnology.

Toshiyuki HATTORI

Research Laboratory for Nuclear Reactors, Tokyo Institute of Tecnology.
O-okayama, Meguro-ku, Tokyo 152, Japan

I. Basic Studies of Free Electron Laser[1] with Undulator

The basic experiment of free electron laser is being planned using 35 MeV L-band linac facillity at Institute of Scientific and Industrial Research, Osaka Unicersity. A Halbach-Type pure Nd-Fe-B planar undulator for FEL is constructed as shown in Fig.1.

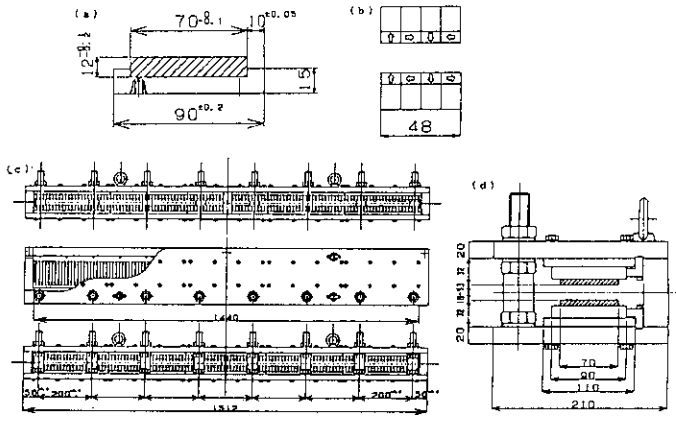

Fig.1 Drawing of undulator

Number and length of period are 30 and λ = 48mm, respectively. For variable gap of the undulator, it has FEL's wavelength of 7μm ～ 21μm at peak on-axis field 0.75kG (undulator's gap of 50 mm)～ 6.05kG(18 mm). The design parameters of the undulator are summarized in Table 1.

Table 1 Design parameters of undulator

Magnet Material			NEOMAX-35H
Magnet dimension		[mm]	12X12X70
Undulator period	λ_u	[mm]	48
Num. of period	N		30
Undulator length		[mm]	1440
Variable gap	L_g	[mm]	18 - 50
Magnetic field range	B_0	[kG]	4.70-0.75
K parameters			2.11-0.34
Wavelength	λ	[μm]	
30 MeV			22.4-7.36
150 MeV			0.90-0.29

Seting parameters

L_g	[mm]	30.0
B_0	[kG]	2.27
K		1.02
E	[MeV]	30
λ	[μm]	10.6

Its magnetic field is measured as shown in Fig.2.

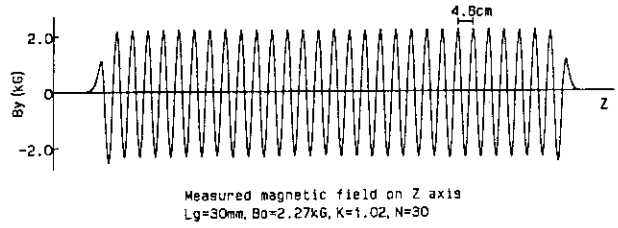

Measured magnetic field on Z axis
Lg=30mm, Bo=2.27kG, K=1.02, N=30

Fig.2 Measured magnetic field on axis

The particle trajectory is calculated in measured undulator field as shown in Fig.3.

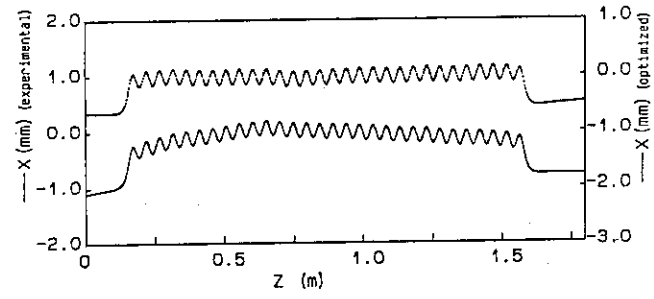

Calculated electron trajectory (X-Z)
E=30MeV, Lg=30mm, Bo=2.27kG, K=1.02, N=30

Fig.3 Calculated electron trajectory

The FEL's gain with computer simulations is reduced to 5 %, which is 12% of ideal one, by the 3-dimensional effect of field inhomogeniety as shown in Fig.4 and 5.

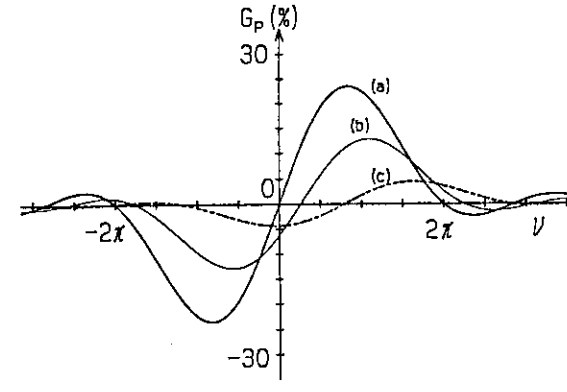

Small-signal gain as a function of frequency mismatch
E=30MeV, I=10A, λ_1=10.6μm (a) ε=0 (b) π (c) 3πmm-mrad

Fig.4 Small-signal gain curve

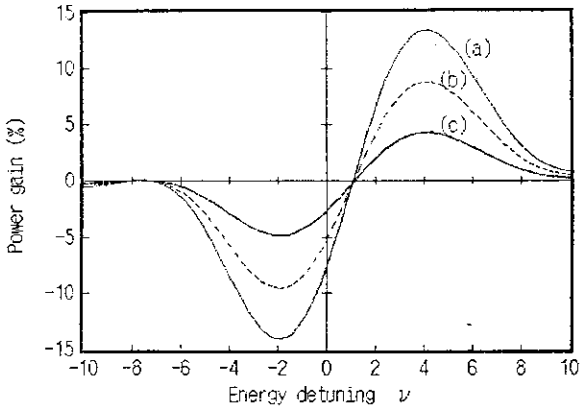

Small-signal gain curve (3-D calculated)
(a) I=30A (b) 20 (c) 10 (E=28MeV; ε=π mm-mrad)

Fig.5 Small-signal gain curve
(3-dimensional calculation)

II. Design of Compact Strage and Acceleration Ring (CSA-Ring) for FEL [2)]

Recently the third generation large SR-Ring for insertion light devices have been designed and under construction in the maine countries. So we designed the CSA-Ring (Compact Strage and Acceleration Ring) for only free electron laser (FEL) as the fourth generation SR-Ring. Then we will be able tom ake its parameters variable and enhance its performance.

The FEL-CSA Ring should be compact and its straight section where a FEL's undulator can be installed is long enough to generate the FEL as shown in Fig.6.

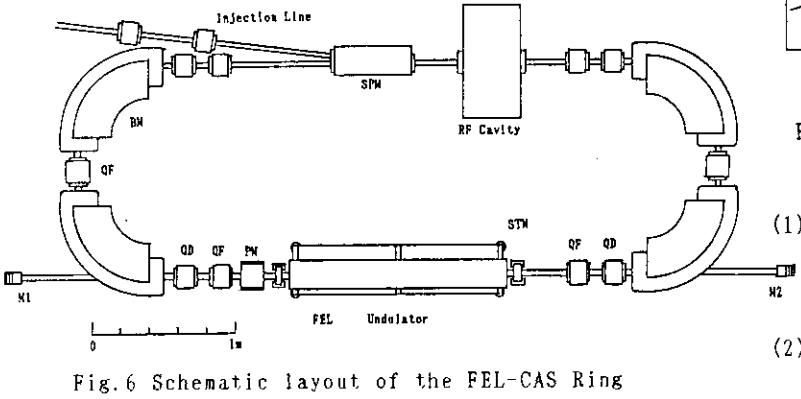

Fig.6 Schematic layout of the FEL-CAS Ring

The choice of the magnetic lattice is also important to achieve the beam storage of low emittance, small energy spread, high current, and dispersion free at the undulator section. The design parameters of FEL-CSA ring are summarized in Table2.

Table2 Design parameters of FEL-CSA Ring

BEAM ENERGY(MAX ENERGY)		150 (300) MeV
CIRCUMFERENCE		11 m
AVERAGE RADIUS	R	1.75 m
BENDING MAGNET	No.	4
	RADIUS OF CURVATURE	0.5 m
	FIELD STRENGTH	10.0 (17.0) kG
QUADRPOLE MAGNET	No.	10
	LENGTH	0.12, 0.15 m
	FIELD GRADIENT	0.99, -1.03, 0.97 kG/cm
LONG STRAIGHT SECTION	No.	2
	LENGTH	2.34 m
BETATRON NUMBER	ν_x	2.26
	ν_y	1.11
RF FREQUENCY		109.1 MHz
RF VOLTAGE		≧20 kV
HARMONIC NUMBER		4
MOMENTUM COMPACTION FACTOR		0.11
RADIATION LOSS		9.0×10^{-2} keV
PRESSUR		1.0×10^{-9} Torr
RADIATION DUMPING TIME	τ_x	43.2 ms
	τ_y	26.6
	τ_E	11.2
NATURAL EMITTANCE	ε_x	1.44×10^{-6} mrad
	ε_y	1.44×10^{-9}
BEAM CURRENT		≧200 mA
BEAM LIFE TIME		≧45 min

We have tried to design a compact storage and acceleration ring with computer program SYNCH. The circumference of the ring is 12(15) m and the electron beam energy is up to about 300 MeV. The long drift space is 3(4) m long, where the beam momentum dispersion is suppressed to be 0. Obtained beta and dispersion functions are shown in FIg.7.

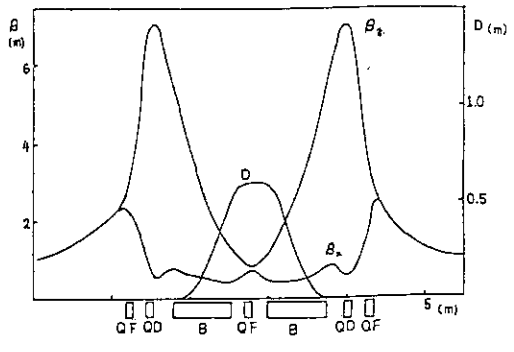

Fig.7 Twiss parameters of half ring

References

(1) A.Okamoto, T.Hattori, Y.Takahashi, M.Yoshizawa, K.Yoshida, F.Fujomoto, Y.Kojima and Y.Honda; Proc. Meeting on Linear Accelerator, 14(1989)174.
(2) T.Hattori, Y.Takahashi, H.Muto, A.Okamoto, Y.Ishii, M.Okamura and T.Hirata; Proc. Meeting on Linear Accelerator, 14(1989)212.

20. The ledatron and the related electron beam devices

Koji Mizuno and Jongsuck Bae
Research Institute of Electrical Communication
Tohoku University, Sendai, 980 Japan

Abstract The ledatron is an electron beam device with a Fabry-Perot resonator and a metallic grating for generating tunable millimeter and submillimeter waves. The fundamental mechanism of the ledatron may be considered as the stimulated Smith-Purcell radiation. The inverse effect was proposed as a candidate for a laser-driven linac. Recent studies on these are reported.

In 1953 Smith and Purcell demonstrated that light is emitted when a high voltage electron beam moves parallel and close to a metallic diffraction grating (Fig. 1) (1). The radiation has been explained physically in terms of the oscillations that must be executed by the charge induced on the grating surface by an electron in the beam. The relationship between the light wavelength, electron velocity, and grating constant is a synchronous, or velocity-matching condition between the electron and the wave. Therefore an inverse and also a stimulated effect should occur in this configuration when a coherent light is incident onto the electron beam. The figure shows a family of this effect.

Fig. 2 explains the stimulated effect, and this is the operational mechanism of the ledatron (2). The Smith-Purcell radiation is reflected by a reflector and is used to bunch the electron beam, leading to a stimulated radiation. The ledatron has been used as a tunable millimeter wave source in the study of solid state spectroscopy (3).

Fig. 3 shows the inverse Smith-Purcell effect (4). The laser light is incident on a grating and is used to change the electron velocity. By the recent progress of high power lasers, interest in the development of laser-driven linacs which could have accelerating gradient such as the order of GeV/m has been stimulated. We have demonstrated experimentally this effect in the submillimeter wave region (5).

Recently a paper was published, on which paper the same configuration as that for the Smith-Purcell radiation could have the possibility of a compact x-ray laser (6). One of the points of this paper is that the effective interaction region over the grating may be much larger than that for the normal Smith-Purcell effect when the electrons impacted the grating. In order to study this point we have measured (7) the strength of the interaction between the electrons and the field in front of the grating by using the inverse Smith-Purcell effect at submillimeter wave region (496 μm). In order to simplify the problem, for the moment we have performed experiments under the condition of the electrons not to impact the grating. Fig. 4 shows the interaction strength (energy spread of the electrons) as a function of the electron position (distance between the grating surface and the electrons). The dotted lines are theoretical tendencies for the 1st and the 2nd space harmonics of the evanescent wave on the grating and show exponential decay of the field with the distance from the grating. The agreement between the experimental data and the theoretical result indicates that the interaction region is as large as that theories for the normal Smith-Purcell effect have predicted, at least when the electrons do not impact the grating. We are now performing experiments in the case for the electrons to impact the grating and at the shorter wavelength such as visible region.

(1) S.J. Smith and E.M. Purcell, Phys. Rev., 92(1953)1069.
(2) K. Mizuno and S. Ono, in Infrared and Millimeter Waves Vol.1 (ed.K. Button)(Academic, New York, 1979).
(3) S. Suto, M. Ikezawa and K. Mizuno, Int'l J. IR & MM Waves, 6(1985)1139.
(4) K. Mizuno, S. Ono and O. Shimoe, Nature, 253(1975)184.
(5) K. Mizuno, J. Pae, T. Nozokido and K. Furuya, Nature, 328(1987)45.

(6) D.B. Chang and J.C. McDaniel, Phys. Rev. Lett., 63(1989)1066.
(7) J. Bae, et al., to be published.

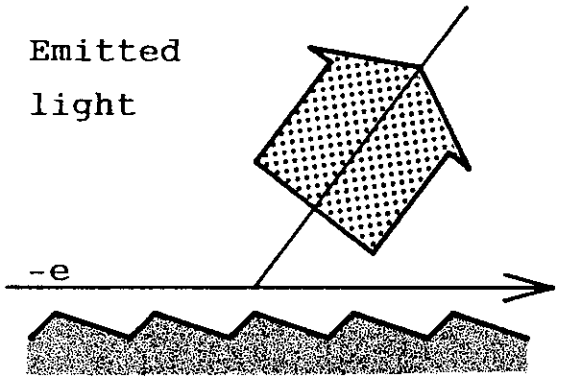

Fig.1 light is emitted when a high voltage electron beam moves parallel and close to a metallic diffraction grating

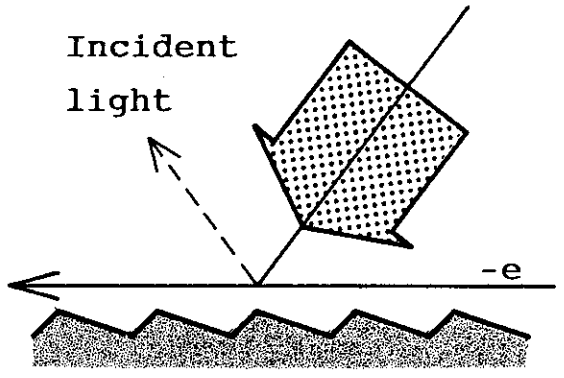

Fig.3 Inverse Smith-Purcell effect

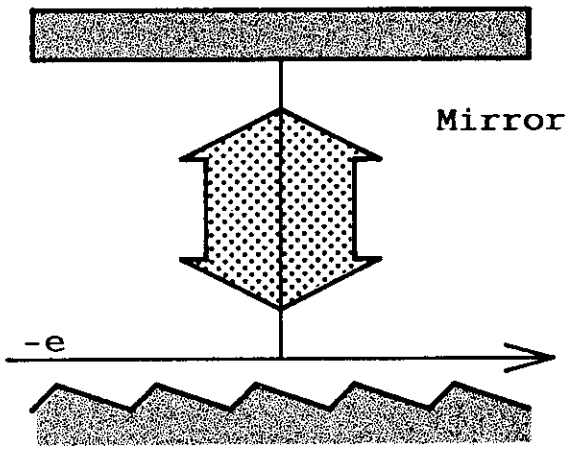

Fig.2 Stimulated effect and operational mechanism of the ledatron

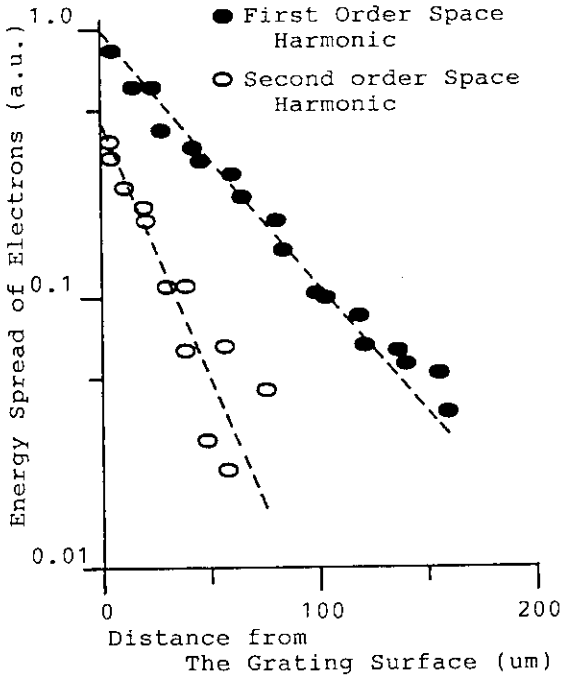

Fig.4 Interaction strength as a function of the electron position

21. A LINEAR COLLIDER IN THE TBA/FEL REGIME

S.Hiramatsu, K.Ebihara, Y.Kimura, J.Kishiro,T.Ozaki, K.Takayama, T.Monaka and H.Kurino*
National Laboratory for High Energy Physics, 1-1 Oho, Tsukuba, Ibaraki-ken, 305, Japan
**Tôhoku University, Sendai, Miyagi-ken, 980, Japan*

ABSTRACT

A 500GeV×2 linear collider in a two-beam accelerator scheme employing multi-stage FELs in the microwave regime has been designed taking into account the longitudinal stability of the driving beam. Some strong limitations on stabilities of the rf power and the rf phase in the multi-stage FEL imposed by a final focus system are also investigated.

INTRODUCTION

A high power rf source is one of the most important key issues for a future high energy linear collider in the TeV region. To obtain a high accelerating gradient, development of a X- or K-band GW-class microwave source is required. As the generation of 1GW microwave at 35GHz by a free-electron laser (FEL) was demonstrated at Lawrence Livermore National Laboratory (LLNL)[1] in 1985, the microwave FEL driven by an induction linac is one of the most promising devices for the GW rf source. In 1982, A.M.Sessler proposed a two beam accelerator concept employing the multi-stage FEL[2] for the high gradient linac with an accelerating gradient of a few hundred MeV/m. In the first version of the TBA concept employing the multi-stage FEL which consists of energy recovery induction units and steady state FELs in a periodic configuration, there were some difficulties in the rf extraction, the rf power transfer between each FEL section passing through the induction gaps of the energy recovery unit, and the accumulation of the rf phase error along the multi-stage FEL structure. To overcome these difficulties, a second version of the TBA concept employing klystron-type FELs (KFEL) was proposed in 1988[3]. In this scheme, the rf power in each FEL stage is not transferred to the next stage and is completely extracted at the end of each FEL stage, and the input rf signal for each FEL is supplied by an individual rf source, for example a klystron of 100kW-1MW driven by a well controlled rf clock.

In the second version TBA concept, although the difficulties in rf manipulation have almost disappeared, a somewhat complicated problem of the rf phase error accumulation still remains to be solved. Extensive theoretical work has been done on this problem at LBL[4] and KEK[5], and the two most important characteristics, the longitudinal stability of the driving beam and the rf phase stability, have been manifested by the macroparticle model. This enables us to design a 500GeV×2 linear collider with the TBA/FEL scheme. However, it is expected that a fractional beam loss in the bunching process may cause rf phase fluctuations exceeding the rf phase tolerance in a linac. Furthermore, investigation of this problem needs more theoretical work and probably a test stand which consists of several stages of KFELs and energy recovery induction units.

Another key issue for the TBA/KFEL is long distance propagation of a multi-kilo-ampere electron beam for driving the FEL. In order to save on construction costs and operation costs, a multi-stage KFEL configuration requires

more than one hundred FEL stages and this means a propagation of the driving beam over a few hundred meters. For the high current beam propagation, a strong resistive wall instability and a beam break-up instability (BBU) especially due to the periodic impedance structure by the energy recovery induction units are expected[6]. One of the promising methods to suppress these instabilities is to introduce a nonlinear focusing force by laser assisted ion channel focusing. The ATA induction linac at LLNL demonstrated the 95m distance propagation of a 7kA electron beam in the ion focusing regime (IFR)[7]. Although the IFR has some complicated problems associated with a hose instability and emittance growth of the driving beam, the experimental investigation on the IFR is going on at the KEK FEL test stand.

R and D work for the linear collider in the TBA/FEL scheme started at KEK and a single-stage X-band FEL which is driven by an induction accelerator energized by magnetic pulse compressors has been constructed for investigation of the FEL performance related to the future linear collider[8]. A preliminary experiment on the IFR feasibility has been demonstrated at this test stand using an 800keV electron beam from the induction accelerator, where about an 1.3kA electron beam was guided through the 2m long ion channel without any external magnetic field[9]. A rf amplification experiment is now in progress.

A SINGLE-STAGE X-BAND FEL TEST STAND AT KEK

A single-stage FEL test stand for 9.4GHz microwave amplification has been constructed at KEK (Fig.1). An 800keV electron beam is generated using a field emission cathode on which a high voltage pulse with 90nsec duration is imposed by four 200kV induction units energized by two magnetic pulse compressors. A 2m long beam transport line for the IFR experiment and a 2m long wiggler are connected to the beam generator. A linearly polarized wiggler which consists of 48 air-core solenoids has 12 periods of 16cm period-length and each period is energized individually for tapering the wiggler field. Table 1 shows the design parameters of the test stand.

Table 1
Design parameters for a X-band 300MW single-stage FEL.

Wiggler Length	L_w	1.92m
Injection Energy	γ_r^i	3
Ejection Energy	γ_r^f	2
Wiggler Peak Field	B_w	1.23-0.59kG (tapered)
Radiation Frequency	f_s	9.4GHz
Input rf Power	P_{rf}^{in}	50kW
Output rf Power	P_{rf}^{out}	300MW
Waveguide Size	a×b	5.5×11cm^2
Energy Spread	$\Delta\gamma/\gamma_r^i$	10-15%
Normalized Emittance	ε_n	0.1-1cm·rad
Beam Current	I_B	1kA

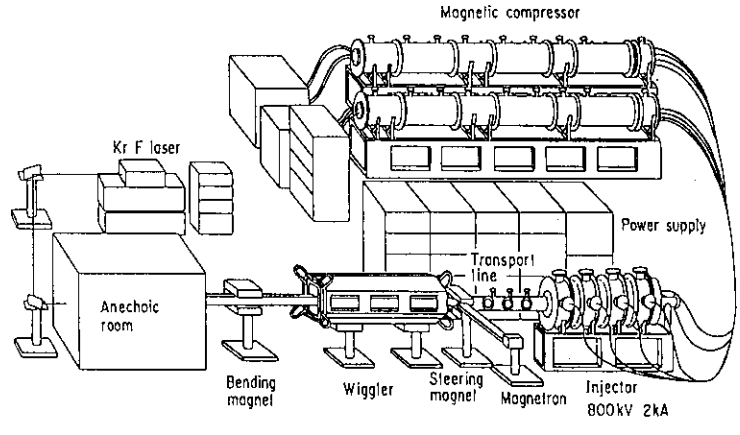

Fig.1 The single-stage X-band FEL test stand at KEK.

A 300MW rf output is expected with an input power of 50kW from the magnetron by the 1kA driving beam with a normalized emittance of less than 1cm·rad and an energy spread of $\Delta\gamma/\gamma \leq 15\%$. Figure 2 shows the evolution of the rf power in the tapered wiggler expected from the simulation code which includes betatron oscillations and longitudinal space charge effect in the driving beam.

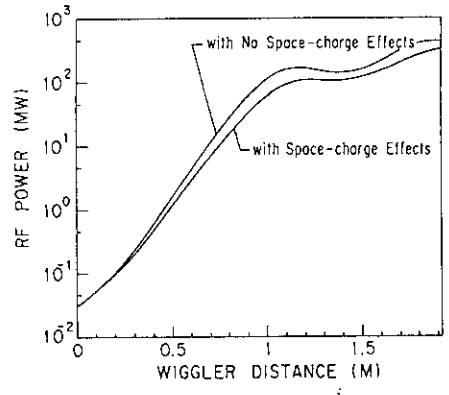

Fig.2 Evolution of the rf power in the FEL wiggler.

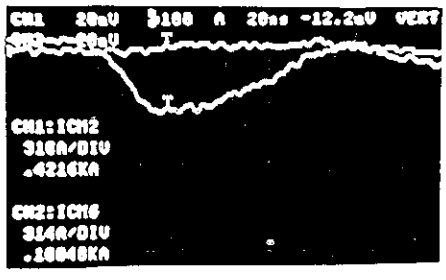

(a) laser/off

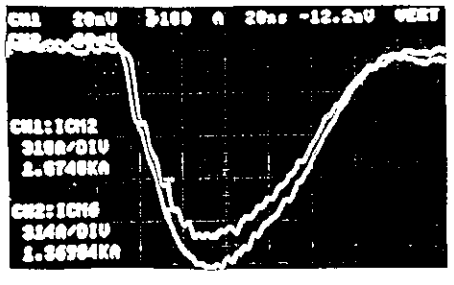

(b) laser/on

Fig.3 Beam transport by laser assisted ion channel focusing. (a) No beam current was observed at 2.2m distance from the cathode. (b) About 1.3kA beam was transported to the same point in the IFR without any external magnetic focusing field.

For the beam current of 840A, a normalized emittance of 0.41cm·rad was obtained by using a 50mm diameter velvet cloth as a field emission cathode. A preliminary IFR experiment has demonstrated the transportation of a 1.3kA electron beam through a 2m long ion channel without any external magnetic field as shown in Fig.3, where a 2kA electron beam was injected into the plasma channel made by irradiation of the diethylaniline gas filled in the transport line at the pressure of $\sim 3\times10^{-4}$ torr by a 100mJ KrF excimer laser. The space charge of the beam head repels out the plasma electrons from the channel and the following part of the beam is guided by the remaining ion channel. At present the experiment on rf amplification is still in progress.

LINEAR COLLIDER IN THE TBA/FEL SCHEME

A FEL driven by a multi-kilo ampere electron beam from the induction linac can generate rf power of order GW capable of producing an accelerating gradient of several hundred MeV/m in a linac. The rf breakdown limit in a linac is expected to increase with increasing rf frequency ($E_0^{limit} \propto f_{rf}^{7/8}$ for f_{rf} <30GHz) and to be higher than 1GV/m at 30GHz[10], so that we assume the accelerating field of 300MV/m at 17GHz in a collider design. To reduce the local accelerating field within 500MV/m in a linac, the attenuation parameter τ should be less than 0.9, and the restriction on the filling time T_f due to the induction linac requires a rf frequency of less than 18GHz. The choice of the rf frequency of 17GHz seems to be adequate for these requirements. Because the filling time T_f is strongly limited by the short pulse duration of the FEL driving beam (~100nsec), T_f is assumed to be 90 nsec in this design.

According to the expression developed by Z.D.Farkas[11], the rf power required in a linac for the accelerating gradient of E_0 is given by

$$\frac{P_0}{L} = \frac{E_0^2}{41.3\eta_s} \frac{L^{1/3}}{(c\tau)^{4/3}} \left(\frac{a}{\lambda}\right)^{3.836} (\beta_g T_\lambda)^{-4/3}, \qquad (1)$$

where a and λ are the cavity aperture and the wavelength, respectively, $\beta_g = v_g/c$ is the group velocity in the unit of

light velocity, L is the accelerating structure length, $\eta_s=(1-e^{-\tau})^2/\tau^2$ is the section efficiency and T_λ is the transit time factor. This equation shows that the peak power in a unit length of the accelerating structure for a given attenuation parameter τ is minimized at $a/\lambda=0.0939$ and $v_g/c=0.809\%$ as follows.

$$(\frac{P_0}{L})_{min}=0.703\times\frac{\sqrt[3]{T_f(ns)}}{\eta_s\tau}[E_0(GV/m)]^2 \quad (GW/m), \tag{2}$$

A small group velocity requires a short accelerating structure because of a small filling time. Furthermore, a small a/λ is not desirable to avoid the transverse-wake effect. The most significant parameter is a/λ which should range from 0.094 to 0.163 in order to minimize the peak power requirement. According to this range, we take $a/\lambda=0.134$ which gives the group velocity of $v_g/c=2.8\%$ and provides a section length of 75cm for $T_f=90$nsec and $\tau=0.84$. This design fits a practical FEL period length, 3m. The output power larger than 2.6GW should be generated in each FEL stage and divided into four to produce an accelerating field of 300MV/m in the 75cm accelerating structure. Because the energy acceptance of the final focus system imposes strong limitations on the energy spread in the linac beam, a high accelerating gradient is desirable to decrease the energy spread caused by beam loading.

In a single bunch operation, the energy spread in a linac caused by a beam loading in the accelerating mode can be expressed by

$$\frac{\Delta E}{E}\cong 0.3\times\frac{en_0rv_g\tau}{E_0}, \tag{3}$$

where n_0 is the number of electrons in a microbunch, r is the shunt impedance, and E_0 is the average accelerating gradient. Therefore the condition on the energy tolerance imposed by the final focus acceptance, $(\Delta E/E)<(\Delta E/E)_f$, gives the limitation on the number of electrons in a microbunch as given by

$$n_0<\frac{(\Delta E/E)_f E_0}{0.3\times erv_g\tau}, \tag{4}$$

Since the luminosity is proportional to n_0^2 in the case of the same intensities in two colliding beams, a high accelerating gradient is desirable for the high luminosity. For example, the luminosity L is limited by this inevitable energy spread as

$$L<1.1\times10^{34}\,H_xH_y\eta_L \quad (cm^{-2}sec^{-1}), \tag{5}$$

for the beam size of $\sigma_x\sigma_y=160\text{nm}\times3\text{nm}$ at the collision point, $(\Delta E/E)_f=0.3\%$, $E_0=300$MV/m, $r=120$MΩ/m, $v_g/c=2.8\%$, $\tau=0.84$ and a repetition of $f_r=1$kHz, where $H_xH_y\eta_L$ is an enhancement factor[10] of order 2-3 due to the beam-beam interaction including the effifiency factor η_L. In practice the energy spread caused by beam loading will be several times larger than that of Eq.(3) by a higher order longitudinal wake potential, however, this type of energy spread is expected to be minimized by adjusting the accelerating rf phase[10]. This means that the luminosity of $10^{34}cm^{-2}sec^{-1}$ can be expected even in a single bunch operation at the high accelerating gradient.

Figure 4 illustrates the conceptual design of the 500GeV×2 linear collider in the TBA/FEL scheme employing the multi-stage KFEL, which is driven by an induction linac of $E_0\cong14$MeV with about 100nsec pulse width. Since the multi-stage FEL performance is made efficient by driving a bunched beam, a buncher FEL which consists of a non-tapered wiggler is placed upstream of the regular FEL sections. This wiggler provides rf power enhancement and longitudinal stability of the driving beam. The wiggler field in each normal FEL section is regularly tapered according to the macroparticle analysis to ensure the longitudinal stability of the driving beam. A decrease of thebeam energy, $\Delta E=1$MeV, which goes into the rf power in each FEL, has to be recompensated by employing an reacceleration unit made from four induction units. A period of the FEL stage has a length of 3m, in which 1.3m is occupied by the wiggler magnet and the remnant is reserved for both the energy compensation induction units and the instrument for rf/beam monitors. An electron beam of about 4kA from the induction linac is injected to the first stage of the multi-stage FEL. Although a part of the injected beam will be lost gradually by the bunching process in the first 15-20 FEL stages, the remaining 2.6kA beam will be propagated stably to the end of the multi-stage FEL and a

17GHz microwave of about 2.6GW will be generated at each FEL stage.

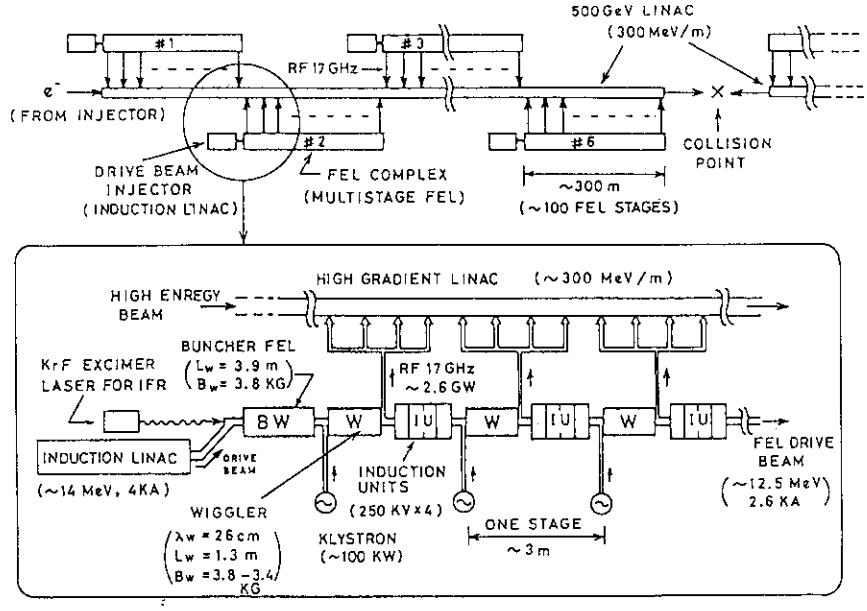

Fig.4 Conceptual illustration of the 500GeV×2 linear collider in the TBA/FEL scheme.

STABILITY OF THE MULTI-STAGE KFEL

The capability of the multi-stage FEL as a rf source for a linac is strongly dependent on stable rf generation in each FEL stage. The fluctuations in the rf power and phase cause the difficulties in the desired collider performance, especially in the energy acceptance $(\Delta E/E)_f$ of the final focus system. One of the typical design examples of the high luminosity final focus system shows that the energy spread of the linac beam is desired to be less than 0.3% for a 300m×2 final focus length[12]. This small acceptance imposes a very strong stability condition on the rf phase fluctuation. For example, a small phase fluctuation $\Delta\phi_s$ less than 4.4° is desired for each multi-stage FEL.

To manifest essential features of the longitudinal stability and to investigate the output rf phase's sensitivity against injection errors of the driving beam, we have developed extensive computor simulations and the macroparticle analysis[5]. A set of equations describing the FEL in one dimension is given by[13]

$$\frac{d\gamma}{dz} = -\frac{e_s b_w}{k_w \gamma_0}\sin\psi , \tag{6}$$

$$\frac{d\psi}{dz} = k_w - \delta k_s - \frac{\omega_s}{2c\gamma^2}\{1+(\frac{b_w}{k_w})^2\} + \frac{d\phi_s}{dz} , \tag{7}$$

$$\frac{de_s}{dz} = \frac{eZ_0}{2mc^2}(\frac{b_w}{k_w})J\langle\frac{\sin\psi}{\gamma}\rangle , \tag{8}$$

$$\frac{d\phi_s}{dz} = \frac{eZ_0}{2mc^2}(\frac{b_w}{k_w})\frac{J}{e_s}\langle\frac{\cos\psi}{\gamma}\rangle , \tag{9}$$

where $\psi=(k_w-k_s)z-\omega_s t-\phi_s$ is a pondermotive phase, e_s and ϕ_s are the normalized signal amplitude and the phase, respectively, b_w is the normalized wiggler field, $\lambda_w=2\pi/k_w$ is the wavelength of the wiggler, and J is the current density of the driving beam. Supposing a tightly bunched beam in the FEL, we adopt the approximation that the beam bunch in the pondermotive potential is described by a macroparticle at the bunch center. In this

approximation, the average quantities represented by the parentheses < > are replaced by the quantities of the macroparticle at the bunch center, and these equations are combined in the universal gain equation[5] as follows for the wiggler which is tapered in the manner of $b_W/\gamma k_W$=constant depending on the driving beam current.

$$y''(s) = -\sqrt{e^{-2y(s)} - \{y'(s)\}^2} + e^{-2y(s)} - 2\{y'(s)\}^2, \quad (10)$$

where y(s) is a logarithm of the normalized signal field e_s

$$y(s) = \ln\{(a|b|/\kappa)e_s\}, \quad (11)$$

and a,b are given by

$$a = \frac{2mc^2}{eZ_0 J}\left\{\frac{k_W\gamma}{b_W(0)}\right\}^2, \quad b = k_W - \delta k_s - \frac{\omega_s}{2c}\left\{\frac{b_W(0)}{k_W\gamma}\right\}^2. \quad (12)$$

Here s=|b|z is the normalized wiggler distance and $\kappa=\sin\Delta\psi/\Delta\psi$ where $\Delta\psi$ is bunch spread in the pondermotive phase. The validity of this macroparticle approach in the multi-stage FEL is also confirmed by multi-particle simulations. The macroparticle approach gives the spatial evolution of beam energy, pondermotive phase, and output rf phase in recursion form from period to period. Assuming a current error $\Delta J=J-J_0$ and an error of the injection energy $\delta_0=\gamma-\gamma_0$, the recursion formula for a small deviation δ_n from the design value γ_0 at the n-th FEL stage is rewritten in a linearized form

$$\delta_n = (1-\mu)^n\left[\delta_0 + \left(\frac{\Delta\gamma}{\gamma_0}\right)\left(\frac{\Delta J}{J_0}\right)\right] - \left(\frac{\Delta\gamma}{\gamma_0}\right)\left(\frac{\Delta J}{J_0}\right), \quad (13)$$

$$\mu = \frac{2\Delta\gamma}{\gamma_0}\left[\frac{\gamma_s^2+\gamma_0^2}{\gamma_s^2-\gamma_0^2} - \frac{\omega_s}{c^2}\left\{\frac{b_W(0)}{\gamma_0 k_W}\right\}^2 y'(|b(\gamma_0)|L_W)\right], \quad (14)$$

and the rf phase advance in the n-th stage is given by

$$(\Delta\phi_s)_n = \int_0^{|b(\gamma_a)|L_w} e^{-y(s)}\sqrt{1-y'(s)e^{2y(s)}}\,ds, \quad (15)$$

where L_W is the wiggler length, $\Delta\gamma$ is the energy gain in the energy recovery unit, $\gamma_s=[(\omega_s/2c)\{b_W(0)/k_W)^2/(k_W-\delta k_W)]^{1/2}$ is the resonance energy of the wiggler in the usual sense, and γ_a is the energy of the macroparticle which is determined by the universal gain equation.

A small energy deviation is known to reach an equilibrium state, $-(\Delta\gamma/\mu)(\Delta J/J_0)$, when the stability condition of $0<\mu<2$ is satisfied. This yields a shot-to-shot fluctuation in the output power of $\Delta J/\mu J_0$. This means the current fluctuation of the driving beam must satisfy the condition of $\Delta J/J_0 \le 2\mu(\Delta E/E)_f N^{1/2} \cong \pm 0.6N^{1/2}$ %, where N is the number of the multi-stage FELs (N=6 in this design). Figure 5 demonstrates how the energy deviation is damped for $\Delta J/J_0=0$ and Fig.6 shows the stable region represented by a wiggler field and an energy gain in the energy recovery unit. If the multi-stage FEL is designed to be $\mu\approx 1$, this energy oscillation damps within a few FEL stages. The output rf power is also stabilized in a similar way.

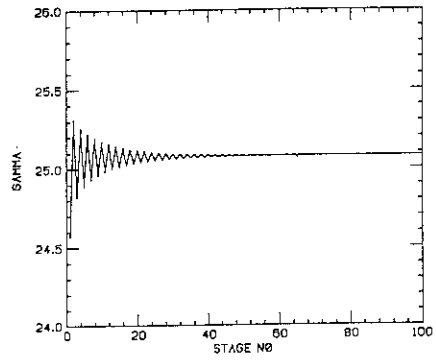

Fig.5 Energy deviation damping in the multi-stage KFEL.

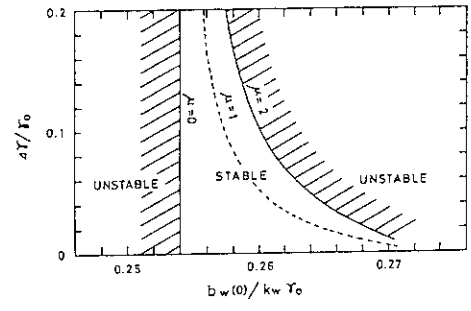

Fig.6 Stable region of the multi-stage KFEL for I_B=2kA.

The bunch stability in the multi-stage FEL has been also investigated in a microparticle approach based on the macroparticle analysis, where the motion of a test particle around the macroparticle is described by a kind of Hill's equation,

$$\xi''(s) + G[\, e^{-y(s)}\sqrt{1-\{y'(s)e^{y(s)}\}^2}\,\varepsilon(s) - H]\,\xi(s) = 0, \quad (16)$$

where ξ is the deviation of pondermotive phase of the test particle from that of the macroparticle, $\xi=\psi-\psi_a$, $\varepsilon(s)$ is a step function which takes a value of unity in the wiggler and zero in the drift region, and G and H are determined by wiggler parameters, design energy γ_0 and longitudinal space charge force,

$$G = 4\kappa\,(\frac{eZ_0J}{mc^2})\,\frac{\gamma_0\gamma_s^6}{(\omega_s/c)^2\{b_W(0)/k_W\}^2(\gamma_s^2-\gamma_0^2)^3}, \quad (17)$$

$$H = \frac{4\pi}{\kappa}\,(\frac{mc^2}{eZ_0J_0})\,(1-\frac{\gamma_0^2}{\gamma_s^2})\,\frac{\omega_s/c}{k_W+k_s+\omega_s/c}\,(1-\frac{\Delta\psi}{2\pi}). \quad (18)$$

The stable region of the solution of this equation is shown in Fig.7 on a two-dimensional parameter plane of G, which is proportional to the driving beam current I_B, and the drift length d between wigglers.

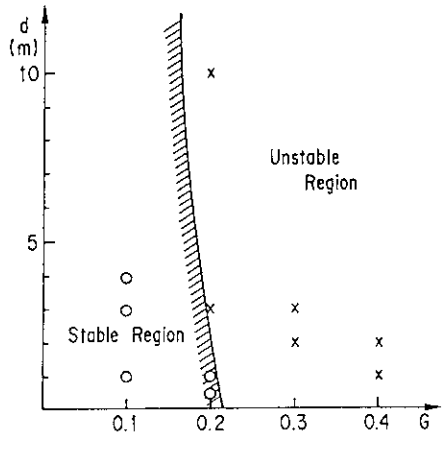

Fig.7 Stable region for beam bunching in the multi-stage KFEL.

The stability criteria shown in this figure are also confirmed by multi-particle simulations. At the points indicated by circles, a stable synchrotron oscillation over 100 FEL stages is confirmed and cross marks indicate remarkable blow-up of the bunch core and beam loss. These results represent that a beam bunch subject in a multi-stage KFEL is essentially stable for a moderate magnitude of rf amplification. In the proposed TBA/KFEL, G is designed to be around 0.1 to manifest bunch stability.

However, the transient process between the buncher FEL and the normal FELs has been demonstrated only by a multi-particle simulation, and which shows that a fractional part of the driving beam is lost gradually along the multi-stage FEL due to phase-space mis-matching caused from the long tail generated in the buncher FEL and the beam current reaches to its equilibrium value after the first 15-20 FEL stages (Fig.8). These losses have to be constant in order to get a constant phasing of the rf signal. Eventually the conversion efficiency from the beam power to the rf power will reach more than 84% for a 100 stage KFEL.

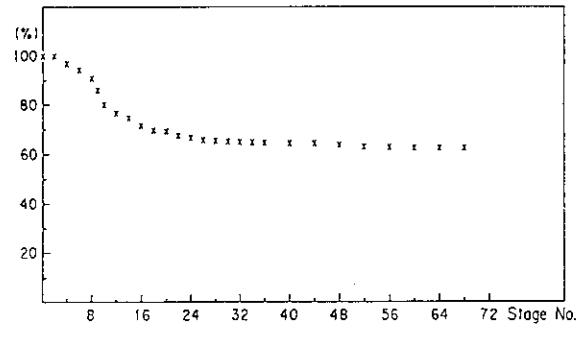

Fig.8 Trapping efficiency of the driving beam in the multi-stage KFEL.

Although the fluctuations in the pondermotive phase and rf phase tend to decrease associated with stabilizing of the energy, the phase shift in the rf phase ϕ_S is inevitable due to a combination of the phase advance in the wiggler and the initial conditions. After the beam current reaches to its equilibrium state, the rf phase deviation can be described by Eq.(15) in the macroparticle model, and is expected to be insensitive to the current error ΔJ, for example, $\Delta\phi_S$ is less than 1° for $\Delta J/J_0$=10%. However, the major cause of the

phase fluctuation is due to beam loss in the bunching process. A typical computor simulation shown in Fig.9 predicts a rf phase fluctuation of about 10° for a 0.3% deviation of the beam current from the injector. This phase fluctuation seems to be a little bit too large for the energy tolerance of the final focus acceptance. More detailed theoretical and experimental investigations are desired on this problem.

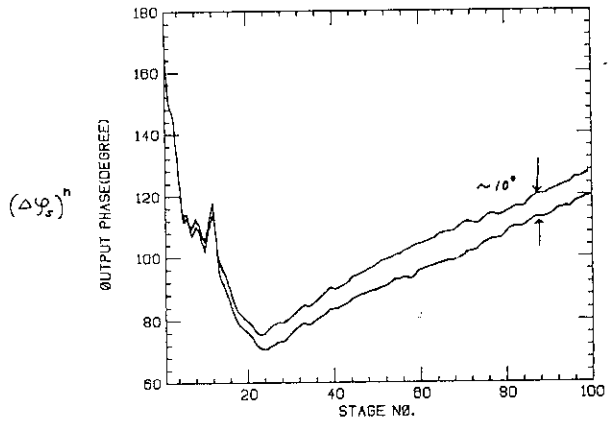

Fig.9 Evolution of rf phase in the multi-stage KFEL. A current error of $\Delta J/J_0$=0.3% in the injection beam causes about 10° phase deviation.

Another key issue for the TBA/FEL is to manifest transverse stability of the high current driving beam. In a multi-stage FEL, a phase mix damping by an energy spread $\Delta\gamma/\gamma$ for the resistive wall instability and beam break-up instability (BBU) can not be expected since the betatron oscillation period λ_β is in the same order of the synchrotron oscillation period ν_s[6]. The growth length, ie., e-folding distane of the instability is expected to be longer than 1km for the resistive wall instability but is expected to be less than 100m for the BBU,

$$L_{BBU}=\frac{4\pi L_g\gamma}{\lambda_\beta\omega_\lambda Z_\perp}\left(\frac{I_0}{I_B}\right)\approx 90\text{m}\,, \qquad (19)$$

where I_0=17kA is the Alfven current, and the beam current of I_B=2kA, the transverse coupling impedance of $Z_\perp$=4×20Ω of the induction gap in the energy recovery unit , a mode frequency of $\omega_\lambda=2\pi\times$800MHz, λ_β=2m, and a period length of L_g=3m are assumed. One of the possible ways to suppress the BBU growth is to introduce a spread in the betatron wavenumber k_β caused by nonlinearity as seen in beam transport in the IFR[7]. The BBU growth in this example can be suppressed by a phase mix damping with $\Delta k_\beta/k_\beta \cong \pi/k_\beta L_{BBU}$ =1.1%. Although the hose instability may cause some problems because the beam energy is almost constant along the multi-stage FEL, it is expected that a strong nonlinearity in the IFR will damp even the hose instability within a few betatron wavelengths. Furthermore a preliminary estimation in the IFR shows that a normalized beam emittance of less than 0.5cm·rad is necessary to prevent beam head erosion and to keep a reasonable equilibrium beam size.

SUMMARY

A 500GeV×2 linear collider in the TBA/FEL scheme has been designed. The linac size will be reduced to about 1.7km by employing six FEL complexes as the rf sources. The high power of 2.6GW at 17GHz is not difficult to generate with FEL which is driven by an induction linac of 14MeV. A combination of the induction linac and the energy recovery units are energized with the magnetic pulse compressors at a repetition rate of more than 1kHz and promises a luminosity of $\geq 1\times 10^{33}\text{cm}^{-2}\text{sec}^{-1}$ in a single bunch operation. The intrinsic feature of the longitudinal stability in the multi-stage KFEL has been proved, and rf phase sensitivity and rf power fluctuation against the driving beam current have been investigated by analytic methods based on the macroparticle approsch and multi-particle simulations. The rf phase fluctuation due to fractional loss of the driving beam in the first 15-20 FEL stages in the multi-stage KFEL may cause a little bit too large fluctuation of the linac beam energy for the final focus acceptance. Optimization of the total system including the final focus system on the tolerance of the rf phase fluctuation will be required. As for the long distance propagation of the high current driving beam, nonlinear focusing in the IFR is desirable to suppress the strong BBU. Detail investigations about the hose instability and the emittance growth associated with the IFR are desired to establish the TBA/FEL concept.

REFERENCES

1. T.J.Orzechowski et al., Phys. Rev. Lett. 57 (1986) 2127.
2. A.M.Sessler, AIP Conf. Proc., No.91 (1982) 154.
3. A.M.Sessler et al., Proc. 10th Int. Conf. on Appl. Acc. in Res. and Ind., Nucl. Instrum. and Methods, B40/41 (1989) 1064.
4. A.M.Sessler et al., Proc. XIV Int. Conf. on High Energy Accelerators, Tsukuba, 1989, to be published.
5. K.Takayama, Phys. Rev. Letters 63 (1989) 516.
   K.Takayama and S.Hiramatsu, Proc. 11th Int. FEL Conf., to be published.
   K.Takayama and S.Hiramatsu, Phys. Rev. A, to be published; KEK Preprint 89-153,1989.
6. K.Takayama, Phys. Rev. A39 (1989) 184.
   D.H.Whittum and G.A.Travisk, private communication.
7. G.J.Caporaso et al., Phys. Rev. Letters 57 (1986) 1591.
8. S.Hiramatsu et al., Proc. 10th Int. FEL Conf., Nucl. Instrum. and Methods in Phys. Res., A285 (1989) 83.
   J.Kishiro et al., Proc. XIV Int. Conf. on High Energy Accelerators, Tsukuba, 1989, to be published; KEK Preprint 89-111,1989.
9. H.Kurino et al., Proc. XIV Int. Conf. on High Energy Accelerators, Tsukuba, 1989, to be published; KEK Preprint 89-109, 1989.
10. P.B.Wilson, SLAC-PUB-3674, 1985.
    R.B.Palmer, SLAC-PUB-4295, 1987.
11. Z.D.Farkas, SLAC-PUB-4722, 1988.
12. K.Oide, SLAC-PUB-4806, 1989.
13. D.Prosnitz et al., Phys. Rev. A24 (1981) 1436.

22. FREE-ELECTRON LASERS

C. A. Brau
Vanderbilt University. Nashville, TN 37235, USA

Abstract: Free-electron lasers represent an altogether new and exciting class of coherent optical sources. Making use of a simple and elegant gain medium - an electron beam in a magnetic field - they have already demonstrated broad wavelength tunability and excellent optical-beam quality. For the future they offer the possibility of generating the greatest focused power ever achieved by a laser. But even before this is achieved, the unique advantages of free-electron lasers, especially their tunability, will make them useful for a variety of important applications in science, medicine, and industry.

1. Basic Principles

1.1. Fundamental theory

The configuration of the electron beam and wiggler magnets in a free-electron laser is shown in Fig. 1[1]. The magnets are arranged with their poles alternating so that the magnetic field reverses every few centimeters. The overall length of the wiggler is typically a few meters, which corresponds to about 100 periods. The electron beam is injected into the end of the wiggler, and travels down its length.

As the electrons proceed down the wiggler they are deflected alternately left and right by the magnetic field and follow a wiggly path. The motions are simple forced oscillations; no subtle

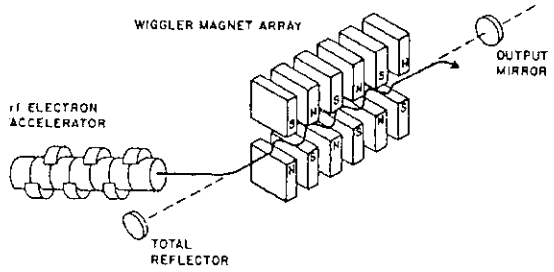

Fig. 1. The radiation from free-electron lasers is created by electrons which are forced to execute a wiggly motion as they pass through as series of magnets which form an alternating magnetic field called the wiggler.

resonant effects are involved. If we place ourselves in a frame of reference moving down the wiggler at the mean velocity of the electrons, we observe that the electrons oscillate back and forth in a straight line perpendicular to the wiggler axis[2]. The situation is similar to that of an electric current running up and down the antenna on a police car, and like the police antenna the electrons radiate energy at the frequency with which they are oscillating.

Observed in the moving frame, the radiation from the electrons goes in all directions, like the

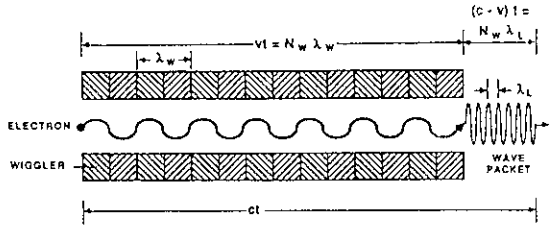

Fig. 2. As an electron moves down the length of the wiggler it emits a wave packet whose length is (c-v)t, where c is the velocity of light, v is the electron velocity, and t is the time for the electron to move the length of the wiggler. If the wiggler contains N_W periods, then the wave packet contains N_W periods as well.

radiation from the antenna. However, in the stationary frame of the laboratory the electrons are moving at nearly the speed of light, and radiation directed toward the sides cannot move very far from the wiggler axis before the electron and its

radiation field have moved down the wiggler. As a result, the radiation appears to be moving almost entirely in the forward direction, parallel to the electron beam. This phenomenon is well known in high-energy particle physics, where Bremsstrahlung (the radiation from the electrons in the wiggler corresponds to magnetic Bremsstrahlung) is observed to be confined within a small cone around the direction of motion of the electron. To an observer standing in the laboratory, then, looking at the radiation produced by a source moving toward him, the frequency is Doppler shifted to a higher frequency, which corresponds to a shorter wavelength.

To calculate this wavelength, we examine the radiation from a single electron travelling down the wiggler with a velocity $v = \beta c$, where c is the velocity of light. As shown in Fig. 2, the electron executes N_W wiggles as it passes through the wiggler. If the wiggles are small, the electron passes through the wiggler in the time

$$t = L_W/v, \qquad (1)$$

where

$$L_W = N_W\lambda_W \qquad (2)$$

is the length of the wiggler, and λ_W the length of one period of the wiggler (the distance over which the magnetic field undergoes one complete alternation and returns to its original value). By the time the electron has reached the end of the wiggler, the front of the wave packet, which was emitted by the electron at the beginning of the wiggler, has moved a distance ct. But the back of the wave packet is just at the end of the wiggler, so the total length of the wave packet is (c-v)t. Since the wave packet, like the wiggler, contains N_W oscillations, the laser wavelength λ_L is given by the expression

$$\lambda_L = \frac{(c-v)t}{N_W} = \frac{\lambda_W(1-\beta)}{\beta}. \qquad (3)$$

We may simplify this expression by recognizing that for relativistic electrons the velocity is nearly that of light, $\beta \approx 1$, so that

$$\frac{1-\beta}{\beta} \approx \frac{(1-\beta)(1+\beta)}{2} = \frac{1-\beta^2}{2}. \qquad (4)$$

To evaluate this we may use the Einstein formula for the energy of a relativistic electron,

$$\gamma = \frac{1}{(1-\beta^2)^{1/2}}, \qquad (5)$$

where γ is just the energy of the electron expressed in units of its rest energy. The rest energy of an electron is $mc^2/e = 0.511$ MeV, where m is the electron rest mass and e the electronic charge. The wavelength is then given by the formula

$$\lambda_L = \frac{\lambda_W}{2\gamma^2}. \qquad (6)$$

In these calculations we have ignored the effect of the wiggle motions on the velocity of the electron through the wiggler. For moderate to strong magnetic fields, the wiggles can significantly increase the path length of the electron trajectory through the wiggler. This slows the average velocity of the electrons through the wiggler and increases the wavelength of the light. When this effect is properly accounted for, we obtain the formula

$$\lambda_L = \frac{\lambda_W}{2\gamma^2}\left[1+\left(\frac{eB_W\lambda_W}{2\pi mc}\right)^2\right], \qquad (7)$$

where B_W is the rms average magnetic induction. This formula is quite accurate for all cases of interest. It implies that in a frame of reference moving with the mean motion of the electrons the frequency of oscillation of the electrons is the same as that of the optical field. Consequently, Eq. (7) is referred to as the resonance condition for free-electron lasers.

Typically, the magnetic field is made as large as possible to maximize the wiggle motion and the electron radiation, subject to the constraint that the wavelength not become too long. This means that the magnetic field term in Eq. (7), $eB_W\lambda_W/2\pi mc$, is generally of the order of unity. Using available permanent magnet material, the average magnetic field strength is typically of the order of 0.5 T for a wiggler period of the order of 2 cm. For an electron energy of 100 MeV, corresponding to $\lambda = 200$, the laser wavelength is $\lambda_L \approx 0.5$ μm, in the green portion of the visible

spectrum. Thus, for convenient values of the wiggler period and the electron energy, we obtain a very useful wavelength.

Since the wave packet emitted by each electron contains only a finite number, N_W, of oscillations, the frequency is imperfectly defined. The spectrum of the radiation corresponds to the Fourier transform of the wave packet radiated by the electron. Thelinewidth of the radiation is therefore of the order of $1/N_W$. Practical wigglers which have been built so far typically contain of the order of 100 periods, so that the radiation has a linewidth of about 1 percent. When this radiation is used to amplify an incident optical beam, forming a laser, the radiation becomes coherent and the linewidth becomes much narrower, comparable to the linewidth of conventional lasers. The radiation also becomes much more powerful.

We can understand how a free-electron laser develops coherence by examining the behavior of a single electron in the wiggler when a coherent optical beam is present. If the optical beam is propagating parallel to the electron, then the electric field is transverse to the motion of the electron. In a coordinate system moving with the mean motion of the electron, as before, we see the electron oscillating transverse to the axis of the wiggler. Therefore,the motions are parallel or antiparallel to the electric field of the optical beam. Near resonance, given by Eq. (7), the optical field has the same frequency as the the electron, in the moving coordinate system. Thus, if the electron and the electric field are in phase, the electric field always points in the same direction as the electron motion and the electron loses energy (since electrons are negatively charged). If, on the other hand, we consider an electron which is half a wavelength ahead of or behind the first electron, it is out of phase with the electric field and gains energy. After a short time, the more-energetic electrons catch up to the less-energetic ones, and the electron beam which initially consisted of randomly distributed electrons soon consists of bunches of electrons spaced at the optical wavelength. The waves radiated by the initially random electrons then add in phase with one another, and the amplitude of the sum is proportional to the number of electrons. The intensity of the radiation, which is proportional to the square of the field amplitude, is then proportional to the square of the number of electrons. Since the number of electrons is very large, typically of the order of 10^8 in the length of the wave packet from a single electron, the coherent emission is much more powerful than the incoherent emission.

The source of the optical beam incident on the free-electron laser discussed above can be either external, from a separate laser, or regenerated from the output of the free-electron laser itself. If the source is external then the free-electron laser is referred to as an amplifier, and the source is called the master oscillator. Clearly, the wavelength of the output beam is the same as that of the master oscillator, and the electron energy and magnetic field must be adjusted to satisfy Eq. (7). If the master oscillator is a conventional laser, then the wavelength is restricted to the specific values achievable with that laser.

Alternatively, the input optical beam may be obtained by taking part of the output beam from previous electrons and returning it to the input end of the free-electron laser. This is illustrated in Fig. 1, where a partially reflecting mirror is used to split the beam coming out of the wiggler into the output beam and the return, or feedback beam, which is reflected back through the wiggler. In this configuration the free-electron laser is referred to as an oscillator. In this case the wavelength can have any value, and corresponds, in general, to the wavelength for which the laser gain, or amplification, is a maximum. This wavelength is given by Eq. (7)[3].

1.2. *Comparison with conventional lasers*

Compared with conventional lasers, free-electron lasers offer a number of important advantages. The first and most obvious is the degree to which free-electron lasers can be tuned. Wavelength tuning can be accomplished initially by the design of the wiggler and the electron accelerator, and various devices have already been operated at wavelengths from the far-infrared to the near-ultraviolet portions of the optical spectrum, as shown in Fig. 3. In addition, it is possible to tune a given device over a large range by varying the electron energy. Most accelerators can be operated over a range of electron energy

exceeding a factor of two, which corresponds to more than a factor of four variation of the optical wavelength. The wavelength ranges achieved in the experiments at Stanford University, Los Alamos National Laboratory, and University of California, Santa Barbara, shown in Fig. 3,

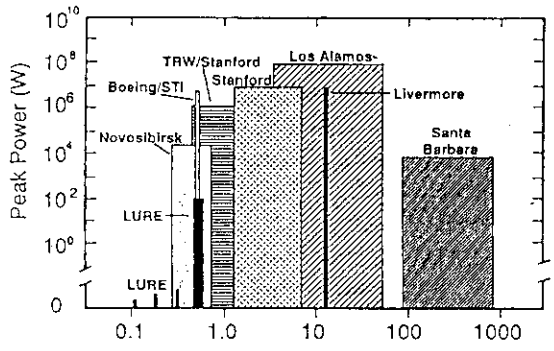

Fig. 3. Free-electron lasers have been operated at a variety of wavelengths from the visible to the millimeter region of the spectrum. Several devices have been tuned over broad wavelength ranges.

represent the broadest tuning range ever achieved by any laser of any type[4,5,6].

An equally important advantage of free-electron lasers is the high power to which their output can be scaled. There are two reasons for this scalability. In the first place, free-electron lasers are able to reject enormous amounts of waste heat. In all lasers, most of the input energy is converted into waste heat. This must be removed by cooling the laser medium or, in the case of gas lasers, which are currently the most powerful lasers, by flowing the hot laser gas out of the laser at very high speed. In the free-electron laser, the waste heat is in the electron beam, which is moving at nearly the speed of light, about a million times faster than a high-speed flowing gas. The electron beam exits the laser in a few billionths of a second, carrying the waste heat with it. Moreover, recent experiments at Los Alamos have shown that the spent electron beam from the laser can be decelerated to recover as much as 70 percent of the leftover energy, thereby increasing the overall efficiency[7]. The second reason why free-electron lasers can be scaled to high power is the availability of high-power accelerators. Although research must be continued to develop electron beams with the very high quality which is required for free-electron lasers, high-power beams already exist. For example, the large electron accelerator at the Stanford Linear Accelerator Center (SLAC) has a 200-kW electron beam operating around the clock, and the large proton accelerator at the Los Alamos Meson Physics Facility (LAMPF) has an 800-kW proton beam which likewise operates 24 hours per day.

These advantages don't come without disadvantages, however. The single, most important disadvantage of free-electron lasers is their high cost. Electron accelerators are expensive, costing more than a million dollars even for a small one, so free-electron lasers don't lend themselves to small devices. On the other hand, in very large sizes the unit cost of laser power becomes quite competitive, and it may be possible, some day, to build free-electron lasers of 100 kW and larger at unit costs of less than $500 per Watt. In the mean time, applications will be limited to those specialized circumstances which can bear the high cost. Fortunately, as discussed below, there are some very important applications which can do this.

2. Laser Experiments

2.1 Technology vs. wavelength

The broad wavelength range spanned by the various free-electron lasers shown in Fig. 3 corresponds not only to a broad range of electron energy but to a variety of accelerator technologies as well. Since almost all wigglers have a period of the order of a few centimeters long, the wavelength of a free-electron laser is largely determined by the electron energy. As a result, since any given type of accelerator is most useful over a certain energy range, it is possible to correlate each type of accelerator with a wavelength range over which it is most useful. This correlation is shown in Fig. 4, where the spectral regions of interest to a number of applications are also indicated. Of course, the relation between energy and wavelength is approximate, since the wiggler period and

magnetic field are somewhat variable, and the spectral regions of interest for the various applications are fuzzy and in some cases overlap. Most importantly, the operating regions for the various types of accelerator technology should not be regarded as well-defined. In particular, the boundaries keep on expanding as the technology improves.

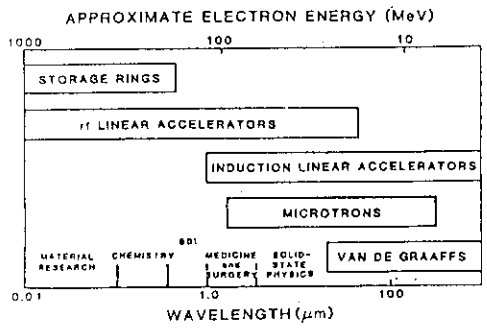

Fig. 4. Various types of accelerator technology are useful for different electron-energy ranges and, accordingly, different laser wavelength regions.

It must also be borne in mind that the electron energy is not the only factor determining the useful wavelength range for each type of accelerator. Both induction linacs and rf linacs can be operated at electron energies sufficient to achieve much shorter wavelengths than indicated in Fig. 7. However, as the wavelength becomes shorter, it is necessary to focus the electron beam more carefully inside the laser beam, and this requires a better electron-beam quality. Specifically, the laws of diffraction show that the product of the radius of a coherent optical beam and the angle with which it diverges is just the optical wavelength, which is preserved through any optical system. Similarly, the product of the radius and divergence of an electron beam represents a measure of the electron-beam quality called the emittance. This quantity is preserved through a good electron transport system. As a rule of thumb applicable to most free-electron lasers, if the emittance is very much larger than the wavelength, then the electron beam cannot be focused inside the laser beam. The emittance is determined largely by the electron source, called the electron gun or injector, and the injector is different for each accelerator technology. Thus, the short-wavelength limit of each technology is set by the injector technology. An exception to this rule is provided by electrostatic accelerators. These devices have excellent emittance, which would make them suitable for operation at very short wavelengths. However, they become prohibitively expensive at voltages above 20 MV, and therefore are not suited for operation at wavelengths outside the infrared. The advantages and limitations of the various accelerator technologies are discussed in the following sections.

2.2. Electrostatic accelerators

Because of their simplicity and reliability, electrostatic accelerators are ideal for the far-infrared spectrum. The first such device is now operating at the University of California at Santa Barbara, where it is already in use not only for free-electron laser research, but also for research in solid-state physics and biophysics[8]. Graduate students routinely operate the free-electron laser in support of the various experiments. A schematic diagram of the device is shown in Fig. 5. The operating range of the accelerator is approximately 2.5 to 6 MeV, which corresponds to wavelengths in the range from 120 to 800 μm. The laser operates with an extremely narrow linewidth, estimated to be better than one part in 10^5[9]. Since electrostatic accelerators are limited to very low charging current, typically less than a milliampere, the electron beam leaving the wiggler is transported back to the high-voltage terminal to keep it charged up. Nearly 90 percent of the charge in the electron beam can be recovered in this fashion, allowing the accelerator to run for 10 to 30 μs before the loss of current discharges the terminal and the accelerating voltage drops appreciably.

To overcome the wavelength limitations imposed by the low voltage of electrostatic accelerators, an interesting set of experiments is about to begin at Santa Barbara in which a high-power microwave beam will be used to act as a very short wavelength wiggler[10]. Such a wiggler field is quite weak, and the gain is expected to be small. But if the experiment is

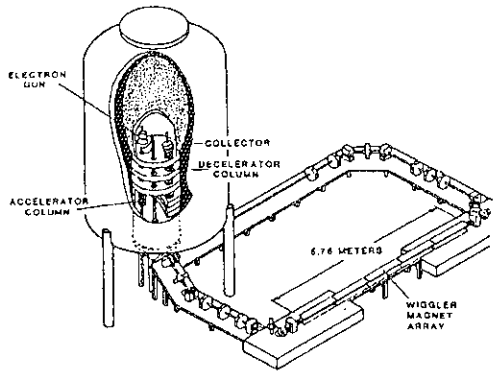

Fig. 5. The electrostatic accelerator at Santa Barbara produces electrons with energy up to 6 MeV with extremely good electron beam quality. These are transported through the wiggler and then back up into the high-voltage terminal on the left.

successful, it will point the way to very much shorter wavelengths, in the visible and ultraviolet, and perhaps even X-ray regions[11].

2.3 Induction linacs

Induction linacs are another type of accelerator which has been used for free-electron laser experiments. The outstanding feature of induction linacs is the very large current which they can accelerate. Typically, these devices can accelerate as much as 10 kA in pulses lasting about 50 ns. However, the large current is usually difficult to collimate inside the laser beam, making these devices most useful at long wavelengths. The ETA at Lawrence Livermore National Laboratory is shown in Fig. 6, and its wiggler is pictured in Fig. 7. This device operates at 3.5 MeV, which corresponds to a wavelength of about 9 mm, in the microwave part of the spectrum[12]. Because of the large current, the gain, or amplification, is very large, and very high peak power and efficiency have been achieved. The laser uses a wiggler specially designed to preserve the electron resonance even when the electrons lose energy as they amplify the optical field. As much as 40 percent of the electron energy has been converted into microwave radiation, which corresponds to a peak output power of 1 GW[13].

Because the electron-beam pulse from induction linacs is so short, these devices do not have time to feed the optical signal back into the wiggler and operate as an oscillator. Thus, induction-linac free-electron lasers operate as amplifiers for conventional lasers. At the present time, a more powerful, 50-MeV accelerator is being used at Lawrence Livermore National Laboratory to extend the performance achieved in the microwave region to the mid-infrared spectrum, using a CO2 laser as the master oscillator.

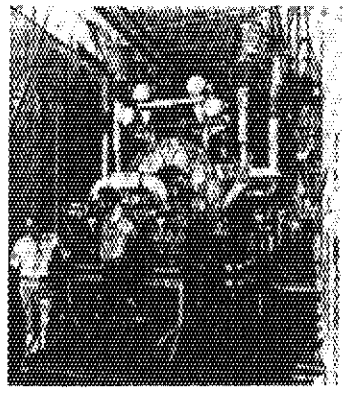

Fig. 6. ETA, shown in this photograph, is a powerful induction linac used for free-electron laser experiments at Lawrence Livermore National Laboratory. It produces an intense electron beam with energies up to 3.5 MeV, and is used in microwave free-electron laser experiments.

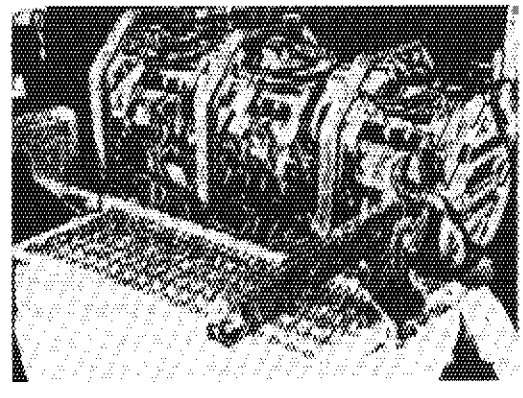

Fig. 7. This photograph shows a section of the pulsed electromagnetic wiggler used in the experiments at Lawrence Livermore National Laboratory.

2.4. rf linacs and microtrons

Since the original free-electron laser experiment of Madey and his co-workers at Stanford, several free-electron lasers have been operated with rf (radio-frequency) accelerators. Most rf accelerators are characterized by high energy and low current, but improvements in injector technology have increased the current and electron-beam quality for free-electron laser applications[14]. The rf linac used in the experiments at Los Alamos National Laboratory, pictured in Fig. 8, is typical of this type of accelerator. The accelerator has an active length of 3 m, and accelerates electrons to 21 MeV with a peak current of more than 100 A. The 5-m long wiggler developed by TRW for free-electron laser experiments at Stanford is shown in Fig. 9. The shortest wavelengths achieved with an rf-linac free-electron laser were obtained recently by a collaboration between teams from Boeing and Spectra Technology[15]. Using a 114-MeV electron beam from a newly built rf accelerator, the groups achieved laser oscillation at 500 nm, in the green part of the visible spectrum. Free-electron lasers of this type also produce extremely good optical-beam quality. In experiments at Los Alamos the collimation of the laser beam was observed to be

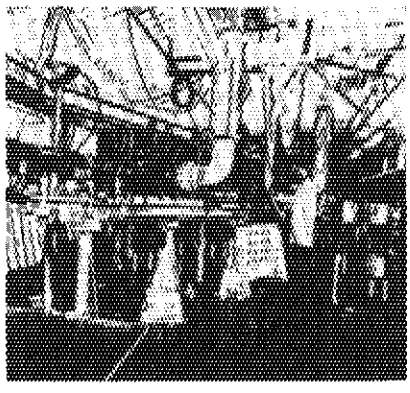

Fig. 8. The rf linac used in the Los Alamos free-electron laser experiments is of conventional design and typifies accelerators of this type used in free-electron laser experiments at several laboratories.

within 4 percent of the physical limit of diffraction, in spite of deliberate misalignment of the optical system and the electron beam[16].

Microtrons are similar to rf linacs except that instead of running the electron beam through many accelerator sections to achieve high energy, microtrons pass the beam through the same accelerator section many times. In principle, this can greatly reduce the cost and size of the accelerator: a 20-MeV accelerator can fit into a few square meters of space. Unfortunately, microtrons

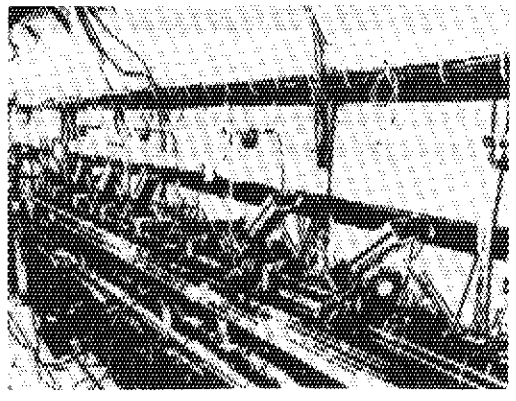

Fig. 9. The wiggler used in the Stanford/TRW experiments uses a permanent magnet structure which is 5-m long overall.

are generally characterized by low current and poor electron-beam quality, and experiments to use them have not yet been successful[17,18,19]. Improvements in these compact devices may make much smaller and cheaper free-electron lasers possible in the future.

In the next few years it should be possible to extend the operation of free-electron lasers using rf accelerators to much shorter wavelengths. The key to this development will be improved electron injectors. New concepts are being developed in which the cathode is placed inside a high-power accelerator cavity, rather than in a dc electric field[20,21]. This should produce much higher current and improved emittance, making it possible to extend free-electron laser operation to the vacuum-ultraviolet and even soft X-ray regions[22].

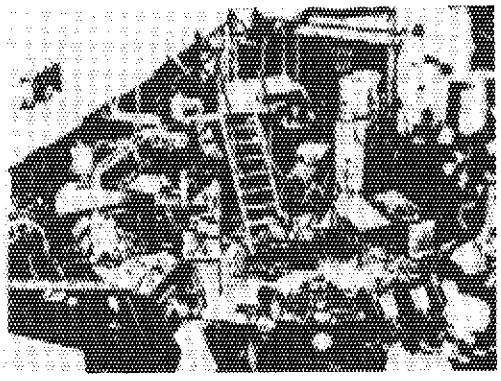

Fig. 10. The free-electron laser at LURE operates on the electron beam circulating in the electron storage ring ACO. The wiggler is shown in the near section of the ring.

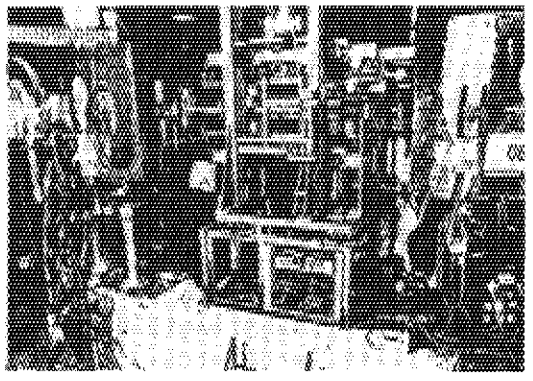

Fig. 11. The wiggler used at LURE, shown in this photograph, consists of magnets above and below the beam line which can be moved away from the beam line while the electrons are being stored in the ring.

2.5. *Storage rings*

Storage rings offer the most elegant approach to free-electron laser technology. In operation, storage rings circulate a "stored beam" of electrons around a ring which is typically several meters in diameter. In modern storage rings the electron beam may be stored for many hours. As the electrons circulate around the ring, they lose a small amount of energy to radiation, which is called synchrotron radiation. This energy must be replaced at each turn by a small accelerator placed in one section of the ring. In addition to being useful for a variety of physics experiments, this radiation has the effect of damping and cooling the electrons stored in the ring to a very low temperature. In this way, the electrons achieve a very small energy spread and become very well collimated. Because they work best at high electron energy, over 100 MeV, and have such good electron-beam quality, storage rings are well suited to free-electron laser operation at very short wavelengths.

The first such laser was operated at the Laboratoire pour l'Utilisation du Rayonment Electromagnetique (LURE), in Orsay, France. A photograph of the storage ring is shown in Fig. 10, and the wiggler is shown in Fig. 11. Operating at an electronenergy of 195 to 233 MeV, the laser produced radiation tunable over the range from 486 to 463 nm, in the blue portion of the spectrum[23]. Because of the low current stored in the ring, which is called ACO, the gain is quite small. Successful operation was made possible by the use of low-loss mirrors for the optical resonator and by the development of a very clever wiggler, called an "optical klystron." Although the laser beam was of rather low average power, about 60 mW, it continued for several hours at a time, which corresponded to the storage time of the electron beam in the ring.

At the present time, several new experiments are being undertaken to extend storage-ring free-electron lasers to the ultraviolet portion of the spectrum. Lasing in the near-ultraviolet has been obtained recently in experiments in Novosibirsk[24], and the first vacuum-ultraviolet radiation was obtained in the form of coherent harmonics of a wiggler operating at a fundamental wavelength of 530 nm[25].

Because of the "figure-eight" motion of the electrons in the wiggler field, alluded to earlier, spontaneous harmonic radiation occurs naturally. To increase the harmonic power and make it coherent, the electrons were bunched at the fundamental wavelength by saturating the laser at that wavelength with a doubled Nd:YAG laser. Due to the nonlinearity of the electron dynamics, bunching occurred at the harmonics as well. The radiation at 177 nm was enhanced a factor of about 350 above the spontaneous emission, while that at 106 nm was enhanced about threefold.

Because the synchrotron radiation, upon which storage rings depend for electron cooling, exceeds the laser radiation, storage rings are not very efficient, and are not suitable for very high power. Nevertheless, they continue to be interesting for operation at short wavelengths.

2.6. Technology directions

In the future, free-electron lasers will be extended to much higher power and shorter wavelengths. Higher power will depend in part on the development of higher-current accelerators, but even more important will be the development of optics capable of operating at high power without damage. Damage to optical coatings has already been observed in free-electron laser experiments at several laboratories, owing to the fact that the optical beam is narrowly confined in the optical resonator and becomes quite intense. However, new optical resonator configurations using grazing-incidence mirrors are being developed, and with improved coatings and higher laser gain it should be possible in the future to achieve power levels exceeding those of any other lasers.

Shorter-wavelength lasers, operating deep in the ultraviolet and beyond, will depend not only on the development of improved injectors, as discussed above, but also on the development of better mirrors. In parts of the extreme ultraviolet and soft X-ray regions (roughly 10 to 100 nm), mirrors have been developed with reflectance exceeding 50 percent, but in other spectral regions no mirrors exist. For those regions where mirrors exist, this reflectance is good enough to support lasing if the gain is more than a factor of four per pass. This appears to be achievable, but better mirrors will help. Alternatively, it may be possible to build very-high-gain wigglers which can amplify the spontaneous emission produced at the beginning of the wiggler and produce a coherent optical beam without any mirrors at all[26,27].

3. Applications

3.1 Research

As has been the case with many new, technological advances born in research laboratories, the first applications of free-electron lasers will be to research itself, in a variety of fields. Compared with alternative light sources, free-electron lasers offer several advantages for research applications. Foremost among these are their tunability and their high peak power and intensity. Among lasers, free-electron lasers are uniquely able to tune throughout previously inaccessible regions of the spectrum, especially in the far infrared, beyond about 20 μm, and (someday) in the far ultraviolet, below about 200 nm. Although conventional lasers already exist in the far-infrared and far-ultraviolet spectral regions, none are continuously tunable and only a few have very high peak power. Besides lasers, other sources of light are also available in these spectral regions. Some, like synchrotrons in the far ultraviolet and thermal sources in the infrared, offer continuously tunable radiation, but none offer the coherence and high intensity (focused power) of free-electron lasers (or other lasers, for that matter).

In the field of biology, for example, tunable lasers may be used to unravel the nonlinear spectroscopy of the genetic material DNA in the far-infrared spectral region[28], and begin to understand the process of "melting," by means of which the DNA unravels and begins the reproductive process. With sufficient laser intensity it may someday be possible to effect conformational changes in the DNA or accomplish other operations. Working at the opposite end of the spectrum, in or near the X-ray region, it may someday become possible with free-electron lasers to create the ultimate image: a hologram of a large, biological macromolecule.

Free-electron lasers offer exciting opportunities in chemistry research, too. No other tunable sources exist for precision spectroscopy - such as Doppler-free spectroscopy - and nonlinear spectroscopy in the far-infrared and far-ultraviolet regions. Moreover, the the extremely short pulses from certain types of free-electron lasers will make it possible to examine the dynamics of chemical reactions on time scales as short as picoseconds. Such fast times are particularly important in the chemistry of liquids. In the emerging field of surface chemistry, tunable free-electron lasers in the far-infrared spectrum will be able to analyze chemical processes occurring on time scales

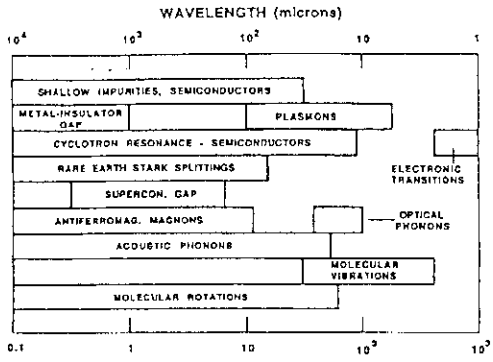

Fig. 12. A variety of solid-state physics phenomena are observable in the infrared part of the spectrum.

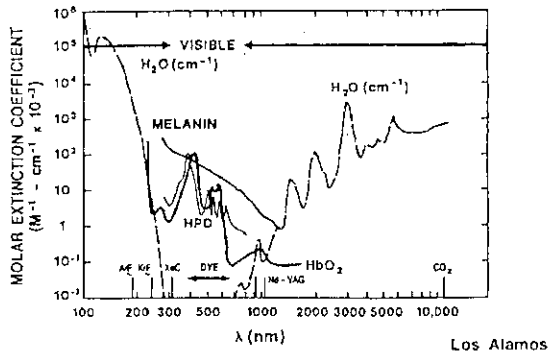

Fig. 13. The absorption of radiation by mammalian tissue is dominated by the absorption properties of water.

shorter than a microsecond.

Solid-state physics is another research area rich in applications for free-electron lasers. Fig. 12 illustrates the variety of phenomena which occur in the far-infrared region of the spectrum[29]. The first free-electron laser built specifically for research in this spectral region is now in active use at Santa Barbara for research in solid-state physics and other applications[30]. The first experiments at Santa Barbara used only the tunability of the free-electron laser for linear spectroscopy. Future experiments will include nonlinear spectroscopy such as excitation of coherent phonons and transient spectroscopy of electron-phonon and electron-electron coupling in semiconductors on a nanosecond time scale.

3.2. *Medicine*

Medicine also offers a large number of opportunities for free-electron lasers. The interaction of laser radiation with mammalian tissue produces a wide variety of effects[31], which can be used for a broad spectrum of medical and surgical applications[32]. The nature of the tissue effect depends on both the wavelength and the pulse length of the laser radiation. Fig. 13 shows how the absorption of the laser beam depends on the wavelength of the laser: because of the properties of water, which is the principle constituent of most tissue, both infrared and ultraviolet light are absorbed in a very short distance, while light in the visible and near-infrared portions of the spectrum is absorbed more weakly[33]. At a wavelength of 3 μm the light is absorbed in less than 10 μm, and the effects of the radiation are extremely localized near the surface. On the other hand, at a wavelength of 1 μm the penetration of light is limited principally by scattering, rather than absorption, and the effects of the radiation spread out over a larger volume. Pulse length is also important in determining the nature of the tissue interaction, as shown in Fig. 14, since thermal conduction can diffuse the heat away from the laser spot. For example, for pulses longer than a second the heat can diffuse more than a millimeter, whereas the heat from microsecond pulses is localized to dimensions of the order of a micrometer. Diffuse heating of tissue is observed to produce burning, cauterization, coagulation, and, in special cases, chemical reactions. On the other hand, intense local heating of very small volumes leads to instantaneous vaporization of the tissue or even to plasma formation and shock wave effects.

These various types of tissue interaction can be used to effect a variety of surgical procedures[35]. For example, continuous or long-pulse Nd:YAG lasers operating at 1 μm have been used to coagulate blood and to actually "weld" arteries together long enough for healing to occur[36]. Continuous-beamargon lasers operating at a wavelength of 0.5 μm are conveniently transmitted through optical fibers but strongly absorbed by thrombus and arterial plaque. These

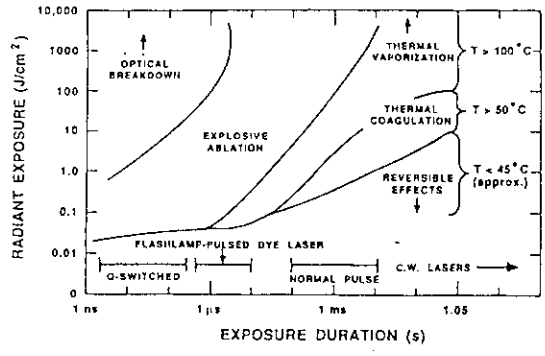

Fig. 14. The nature of the interaction of laser light with mammalian tissue depends on both the laser energy and the pulse length[34].

properties have made them useful for removing plaque which is obstructing blood flow through arteries[37]. Pulsed CO2 lasers, which deposit their energy in very small, well-defined volumes, are used to remove tumors in the central nervous system by vaporizing them[38]. Very intense pulses from Nd:YAG lasers have been shown to fracture kidney stones by means of the shock produced at the surface of the stone, so that the fragments can be passed from the body. Helium-neon lasers, operating at a visible wavelength which is transmitted through the eye, have long been used to reattach retinas by a thermal process. Recently, however, excimer lasers operating in the ultraviolet part of the spectrum, to which the eye is opaque, have been used to reshape the cornea in a process which is believed to be chemical in nature[39].

Given the diversity of tissue effects and procedures which are possible, the advantages of a free-electron laser become clear. Not only are free-electron lasers able to provide wavelengths and pulse lengths unavailable from any other laser - or even combination of lasers - but they can be adapted to the requirements flexibly and in real time. The flexibility makes it possible to get combinations of laser parameters which not only achieve the desired result but which adapt to the limitations of the surgical environment, such as the need to propagate the radiation through an optical fiber to the site of the operation. The real-time adaptability can be used to vary the laser parameters while the surgical procedure is in progress, even using feedback from the operation to control the laser by means of an expert system. For example, the fluorescence from the laser-produced vapor and plasma might be used to control a laser operating on plaque near the arterial wall. If the arterial wall is punctured, the laser wavelength and pulse length can be adjusted to cauterize the wound and seal the perforation.

Photodynamic therapy presents a new and different approach to cancer treatment[40]. It is observed that certain dyes, such as hematoporphyrin derivative (HpD).are more persistently absorbed by tumors than by normal tissue. After about 48 hours after the dye is administered, the tumors are selectively stained. When irradiated by a laser wavelength near 630 nm, the dye releases chemically active singlet oxygen which kills the cells stained by the dye, that is, the tumor cells. This procedure works best, of course, on tumors located in the skin and other accessible parts of the body, such as the trachea. In the future, it may be possible to find more effective dyes, such as dyes which can be activated by nonlinear, two-photon processes at longer wavelengths. This would make the dyes insensitive to low-intensity light, such as sunlight, which is troublesome for patients treated with HpD.

3.3. Industrial processing

Many opportunities for free-electron lasers exist in the industrial sector as well. One of the most promising is microfabrication of semiconductor circuits. In the conventional process, the circuit is imaged from a mask onto the surface of a silicon chip covered with a thin layer of SiO_2 and a layer of photoresist. When the photoresist is exposed to light it is either hardened or softened by the photochemical effect of the light and can be selectively removed by a chemical bath. Subsequently, the SiO_2 can be etched from the exposed areas, where the photoresist has been removed, to form the image of the microcircuit on the silicon chip. At the present time, shorter wavelengths are being exploited to extend this technology to circuit features with dimensions smaller than one micrometer, and synchrotron radiation sources are being built for this purpose.

In the future, however, these processes are likely to be replaced by new technologies which are just now emerging. For example, it is possible to use a scanning laser to print the pattern on the photoresist by direct writing, the way a laser prints the image in a computer laser printer. With sufficient laser intensity, the resist can be removed directly by the laser without the need for chemically developing the image[41]. In fact, with sufficiently high laser intensity, the SiO_2 layer can be removed directly by the laser. It is even possible to use an ultraviolet laser to initiate chemical reactions in a gas or liquid over the surface of the silicon chip to deposit the microcircuit on the chip[42]. By tuning the laser wavelength and/or varying the composition of

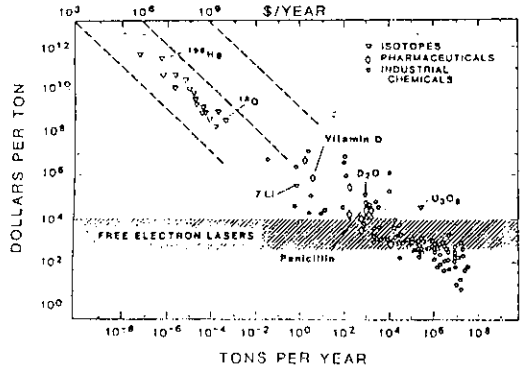

Fig. 15. A large number of specialty chemicals are sufficiently expensive to justify laser processing with a free-electron laser. However, large-scale chemical processing is economical only when the quantum yield (product molecules per laser photon) is large enough to bring down the laser costs.

the gas or liquid, it should be possible to construct various features of the microcircuit. The potential advantages of free-electron lasers in terms of high intensity and tunability at very short wavelengths for applications of this type are manifest.

In addition to microfabrication of semiconductor integrated circuits, lasers may be used for the microfabrication of microminiature thermionic vacuum-tube circuits. Almost as small as semiconductor integrated circuits, the thermionic circuits operate in environments too harsh for semiconductors. In addition to electrical circuits, a variety of miniature mechanical devices, such as gas chromatographs, can be microfabricated from silicon.

The power and wavelength tunability of free-electron lasers makes them intrinsically well suited to large-scale chemical processing. The issue is generally one of the cost of a laser photochemical process compared with the conventional process[43]. This is illustrated in Fig. 15, where the cost of commercially available chemicals is compared with the cost of laser photons[44]. To calculate the cost per ton of laser photons, the following assumptions have been used:

(1) The free-electron laser device has a capital cost of \$40/W to \$400/W, amortized over 5 years (1.6×10^8 s), which corresponds to \$2.5 x 10^{-7}/J to \$2.5 x 10^{-6}/J for photons. Electricity and operating costs are ignored.

(2) Each molecule of product requires one 4-eV (300-nm) photon for its formation, and has an atomic weight of 100, which corresponds to 6.02×10^{27} molecules per metric ton.

It is clear from Fig. 15 that a wide variety of specialty chemicals and isotopes are, at least in principle, economically accessible to photochemical production with free-electron lasers. However, to address the interesting chemicals in the lower right-hand corner of the chart, the process must be highly leveraged. That is, each (expensive) photon must produce a large number of product molecules. In other words, the quantum yield (product molecules per photon) must be large, generally greater than 1000. This is especially true when it is recognized that for large-scale chemical processes the cost of the raw materials typically represents 60 percent to 80 percent of the cost of the final product. Thus, the laser cost must be held to a small fraction of the value of the final product unless laser processing increases the yield and reduces the cost of raw materials, which has been observed.

Two important processes have been identified in which such a large quantum yield is possible. In the first process, a laser is used to purify chemical compounds by removing a few impurity molecules from a large number of desired molecules. A good example is the purification of silane (SiH_4)[45]. High-purity silane is the

starting material for the production of certain types of semiconductors and optical materials. Experiments with an excimer laser at 190 nm have demonstrated that this method produces extremely pure product material with high quantum yield.

A second class of photochemical processes having high quantum yield is that of laser-initiated chain reactions. In this case, a single photon is used to initiate a chain reaction which may yield thousands of molecules of product before the chain is broken. A good example of such a process is offered by the synthesis of vinyl chloride[46]. Vinyl chloride is the starting material for the production of polyvinyl chloride (PVC). In experiments with ultraviolet lasers the quantum yield has been observed to be as high as 20,000.

---

1. In synchrotron-radiation sources, the magnetic field arrangement shown in Fig. 1.1 is usually referred to as an "undulator." "Wigglers" are similar, but have only a few, large, periods and much stronger magnetic fields. However, in free-electron lasers the term wiggler is more commonly used.

2. Actually, if we look closely we observe the electrons to osicillate back and forth transverse to the wiggler axis with a slight longitudinal motion as well. This causes the electrons to follow a "figure eight" motion, but this is of no consequence for the present discussion. The effects of the figure-eight motion are discussed in Chapter 2, where it is shown that the figure eight motions give rise to odd harmonics of the radiation.

3. Actually, to achieve positive gain the laser must operate at a wavelength slightly larger than resonance.

4. S. V. Benson, *et al.*, "A Review of the Stanford Mark III Infrared FEL Program," Proceedings of the eleventh International Conference on Free-Electron Lasers, Naples, FL, August 28 to September 1, 1989.

5. B. E. Newnam, *et al.*, IEEE J. Quant. Electron. **QE-21**, 867 (1985).

6. L. R. Elias, IEEE J. Quant. Electron. **QE-23**, 1470 (1987).

7. D. W. Feldman, *et al.*, IEEE J. Quant. Electron. **QE-23**, 1476 (1987).

8. L. R. Elias and G.J. Ramian, "Status Report of the UCSB FEL Experimental Program," in *Free-Electron Generators of Coherent Radiation*, edited by C. A. Brau, *et al.*, SPIE **453** (SPIE, Bellingham, WA, 1984)

9. L. R. Elias, *et al.*, Phys. Rev. Lett. **57**, 424 (1986).

10. L. R. Elias, *et al.*, Phys. Rev. Lett. **42**, 977 (1979).

11. J. Gea-Bancolche, *et al.*, J. Quant. Electron. **QE-23**, 1558 (1987).

12. T. J. Orzechowshi, *et al.*, Phys. Rev. Letters **54**, 889 (1985).

13. T. J. Orzechowski, *et al.*, Phys. Rev. Lett., **57**, 2172 (1986).

14. The quality, or focusability, of electron beams is described by the quantity called the emittance. This is discussed in Chapter 4.

15. J. Adamski, *et al*, "Visible-Wavelength Oscillator," Proceedings of the Ninth International Free-Electron Laser Conference, Williamsburg, VA, September 14-18, 1987.

16. B. E. Newnam, *et al.*, IEEE J. Quant. Electron. **Qe-21**, 867 (1985).

17. A. Ts. Amatuni, *et al.*, "Generation of Coherent Induced Undulator Radiation," Yerevan Physics Institute Report EhN-727 (42)-84)1984).

18. E. D. Shaw, *et al.*, Nucl. Inst. Meth. **A250**, 44 (1987).

19. F. Giocci, *et al.*, "Status of the ENEA-FEL in the Medium Infrared," Proceedings of the Ninth International Free-Electron Laser Conference, Williamsburg, VA, September 24-28, 1987.

20. S. V. Benson, *et al.*, Nucl. Inst. Meth. **A250**, 39 (1986).

21. J. S. Fraser and R. L. Sheffield, IEEE J. Quant. Electron. **QE-23**, 1489 (1987).

22. B. E. Newnam, "Extension of Free-Electron Lasers into the Extremem Ultraviolet," in *free-Electron Lasers*, Critical Reviews of Optical Science and Technology, edited by B. E. Newnam, SPIE **738** (SPIE, Bellingham, WA, 1984).

23. M. Billardon, *et al.*, Europhys. Lett. **3**, 689 (1987).

24. V. N. Litvinenko, Synch. Rand. News **1** (5), 18 (1988).

25. R. Prazeres, *et al.*, Nucl. Inst. Meth. **A272**, 68 (1988).

26. J. Murphy and C. Pellegrini, J. Opt. Soc. Am. **1B**, 530 (1984).

27. M. Cornacchia, *et al.*, Nucl. Inst. Meth. **A250**, 57 (1986).

28. A. Wittin, *et al.*, Phys. Rev. **A34**, 493 (1986).

29. "The Free-Electron Laser," C. K. N.Patel, *et al.*, report of the Free-Electron Laser Subcommittee of the Solid-State Physics Committee of the National Academy of Science (National Academy Press, Washington, DC, 1982).

30. W. M. Yen, *et al.*, J. Physique **43**, Colloq. C7, 413 (1982).

31. D. H. Sliney, Clin. Chest Med. **6**, 203 (1985).

32. J. A. Parrish and T. F. Deutsch, J. Quant. Electron. **AE-20**, 1386 (1984).

33. R. Straight, private communication.

34. Adapted from D. H. Sliney, Clin. Chest Med. **6**, 203 (1985).

35. J. A. Dixon, "Lasers in Surgery," Current Problems in Surgery **XXI**, No. 9 (Yearbook Medical Publishers, Chicago, 1984).

36. K. K. Jain, IEEE J. Quant. Electron. **QE-20**, 1401 (1984).

37. D. S. J. Choy, IEEE J. Quant. Electron. **QE-20**, 1420 (1984).

38. K. K. Jain, IEEE J. Quant. Electron. **QE-20**, 1401 (1984).

39. E. J. Dehm, *et al.*, Arch. Opthamology **104**, 1364 (1986).

40. J. A. Dixon, "Lasers in Surgery," Current Problems in Surgery **XXI**, No. 9 (Yearbook Medical Publishers, Chicago, 1984).

41. R. Srinivasan, Science **234**, 559 (1986).

42. D. J. Erlich, Nucl. Inst. Meth. **A239**, 397 (1985).

43. R. B. Hall, Laser Focus **18**, 57 (1982).

44. "Laser Induced Chemistry," Jason Report JSR 78-11 (1979).

45. A. Harford, *et al.*, J. Appl. Phys. **51**, 4471 (1980).

46. J. Wolfrum, *et al.*, W. German Patent #293,853 (1981).

23. Operation and Biomedical Application of the Stanford Mark III Free Electron Laser in the 0.5∼8μm Region

R.C.Straight
Utah Laser Institute, Veterans Administration and Univ. of Utah

The Stanford Mark III Free Electron Laser has been used as a research tool by Utah Laser Institute and other investigators since September 1986. The Mark III FEL uses an RF linac to produce a 26-44 MeV electron beam. This allows operation of the laser in the spectral range 2 to 8μm.

The fundamental wavelength range has laser pulse energies from 1 to 120mJ with a peak power as high as 3MW. The macropulse is variable from 0.5 to 3μsec at 15Hz and the micropulse from 0.5 to 2psec.

The second and fourth harmonic wavelength have been generated using non-linear crystals. The second harmonic has been generated from 0.99mm to 1.12mm using lithium niobate and 1.58mm to 1.64μm and 1.80μm to 2.1μm using silver gallium selenide. The forth harmonic has been generated from 495nm to 620nm. A crystal system has been developed to double and quadruple the FEL light.

Experimental results on transmission of FEL light through sapphire and zirconium fluoride fibers will also be presented. The fibers were tested in the spectral range 2-4μm. The theoretical limit for transmission in zirconium fluoride was achieved.

Investigation in progress:
Laser interaction with hard and soft tissue
Gallstone fragmentation
Bone cutting (Fig.1)
Second and fourth harmonic generation
Photodynamic therapy
FEL beam propagation in optical fibers
Analytical spectroscopy of plasma and plumes from FEL
Interaction with biological targets
Nonlinear effects on semiconductor materials
Nonlinear photochemistry

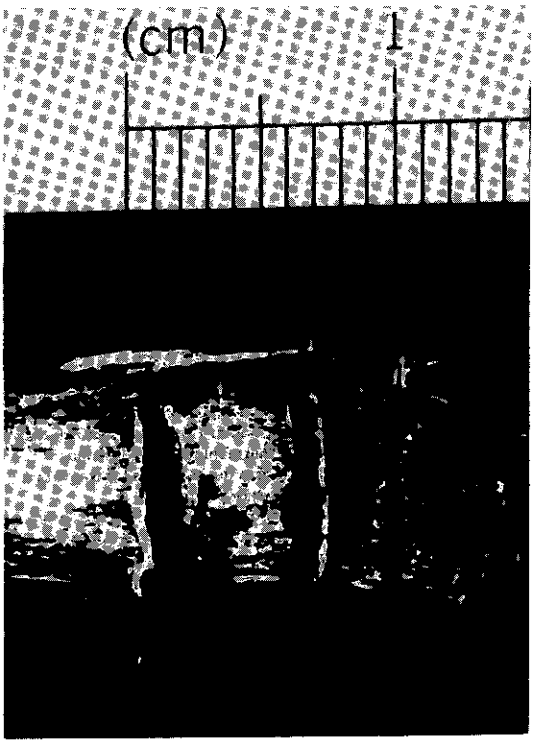

Fig. 1 The comparison of the bone cutting between FEL and CO_2 laser

Appendix 1

Ode to the Tokyo Symposium

An electron both free and quite fast,
Made a laser whose power was vast,
Whose color could vary,
From black to canary,
And whose price will make us wealthy at last.

But the promises proved quite elusive,
And users became quite abusive.
But don't drown in your sorrow,
We'll do better tomorrow,
And make users turn frankly effusive.

So let's toast to the future before us,
Shout FEL praises in chorus.
Pour each other some wine,
Sit together and dine,
And work together, for them there are more of us.

by Charles A. Brau

Appendix 2

Tokyo International Symposium '90 on Free Electron Lasers

Tokyo Toranomon-Pastoral(8F Keyaki)

Program

January 29 (Mon.)

10:00 Welcome Address
Y.Fujiie, Chairman of Promotion Committee on Nuclear Cross-over Research

T.Asaoka, Executive Director, JAERI

K.Ogata, Director-General, Atomic Energy Bureau, Science and Technology Agency

Session A **10:15 ∼ 11:15**
Chairman H.Kuroda Chairman of Specialist Committee on Laser Technology of Nuclear Cross-over Research

A-1 10:15 Birth of FEL and her Future
J.M.J.Madey, Duke Univ.

Coffee Break 11:15 ∼ 11:30

Session B **11:30 ∼ 12:30**
Chairman R.A.Jameson Los Alamos National Laboratory

B-1 11:30 Present Status FEL Research in Japan
K.Mima, Institute of Laser Engineering, Osaka Univ.

B-2 12:00 Recent Developments in FEL Physics in the USA
S.Benson, Duke Univ.

Lunch 12:30 ~ 13:30

Session C 13:30 ~ 15:28
Chairman K.Mima Institute of Laser Engineering, Osaka Univ.

C-1 13:30 Insertion Device Development in Japan
H.Kitamura, KEK

C-2 14:00 The Photon Storage Ring
H.Yamada, Sumitomo Heavy Industries, Ltd.

C-3 14:22 Coherent Synchrotron Radiation by a Short Electron Bunch
T.Nakazato, Laboratory of Nuclear Science, Tohoku Univ.

C-4 14:44 Energy Recovered Linac for New Light Sources
I.Sato, KEK

C-5 15:06 Storage-Ring Free Electron Laser Experiment at ETL
K.Yamada, Electrotechnical Laboratory

Coffee Break 15:28 ~ 15:45

Session D 15:45 ~ 17:35
Chairman C.A.Brau Vanderbilt Univ.

D-1 15:45 Studies about High Power FEL Using Induction Linac
K.Imasaki, Institute for Laser Technology

D-2 16:07 Experimental Studies on Various Characteristics of a Wave Guide Mode Free Electron Laser
Y.Kawamura, RIKEN

D-3 16:29 Present Status of a MicroWave FEL Experiment at KEK
T.Ozaki, KEK

D-4 16:51 Parasitic Wave Excitation in Raman Regime FEL
Y.Kishimoto, JAERI

D-5 17:13 Long Pulse Experiment on Circular Free Electron Laser
H.Saito, Institute of Space and Astronautical Science

Reception 17:45 ~ 19:30 (Keyaki)

January 30 (Tue.)

Session E 9:00 ~ 10:30
Chairman T.Tomimasu Electrotechnical Laboratory

E-1 9:00 FEL Experiments in Europe
Y.Petroff, LURE, Univ. Paris-Sud

E-2 10:00 Present Status of FEL Researches in Israel
S.Ruschin, Tel Aviv Univ.

Coffee Break 10:30 ~ 10:45

Session F 10:45 ~ 12:19
Chairman J.M.J.Madey Duke Univ.

F-1 10:45 Design Study of a Far-infrared Free-Electron-Laser with 20MeV RF Linear Accelerator
S.Nakata, Center Research Laboratory, Mitsubishi Electric Co.

F-2 11:07 Simulation of Higher Harmonics Generation in FEL
S.Kuruma, Institute for Laser Technology

F-3 11:29 Considerations for High-Brightness Electron Sources
R.A.Jameson, Los Alamos National Laboratory

F-4 11:54 Present Status of FEL Research at Los Alamos National Laboratory
S.O.Schriber, Los Alamos National Laboratory

Lunch 12:19 ~ 13:10

Session G 13:10 ~ 14:38
Chairman Y.Petroff LURE, Univ. Paris-Sud

G-1 13:10 The RF Linac Free-Electron Laser Project
at the University of Tokyo
H.Ohashi, Univ. of Tokyo

G-2 13:32 JAERI FEL Program based on Superconducting Linac
Y.Kawarasaki, JAERI

G-3 13:54 Double-Sided Microtron for FEL at Nihon University
K.Hayakawa, Atomic Energy Research Institute, Nihon Univ.

G-4 14:16 Basic Studies of Free Electron Laser and Development
of Compact Ring for FEL at Research Laboratory
for Nuclear Reactors, Tokyo Institute of Technology
T.Hattori, Research Laboratory for Nuclear Reactors,

Coffee Break 14:38 ~ 14:55

Session H 14:55 ~ 16:46
Chairman Y.Kawarasaki JAERI

H-1 14:55 The Ledatron and the Related Electron Beam Devices
K.Mizuno, Research Institute of Electrical Communication,
Tohoku Univ.

H-2 15:17 A Linear Collider in the TBA/FEL Regime
S.Hiramatsu, KEK

H-3 15:39 The Future of FEL Applications
C.A.Brau, Vanderbilt Univ.

H-4 16:24 Operation and Biomedical Applications of the Stanford Mark III
Free Electron Laser in the 0.5-8μJm Region
R.C.Straight, Utah Laser Institute,
Veterans Administration and Univ. of Utah

16:46 Closing Address
H.Kuroda, Chairman of Specialist Committee
on Laser Technology

Appendix 3

Participant List

Abe,Fujio	Science and Technology Agency(STA)
Abe,Takashi	Institute of Space and Astronautical Science
Aizawa,Kiyoshi	Kawasaki Heavy Industries,Ltd.
Amemiya,Yoshiyuki	National Laboratory for High Energy Physics(KEK)
Ando,Masami	National Laboratory for High Energy Physics(KEK)
Aoki,Akio	NKK Corporation
Aoki,Tadashi	Science and Technology Agency(STA)
Asami,Akira	National Laboratory for High Energy Physics(KEK)
Asano,Yoshihiro	Japan Atomic Energy Research Institute(JAERI)
Asaoka,Takumi	Japan Atomic Energy Research Institute(JAERI)
Baba,Hitoshi	Nihon Koshuha Co.,Ltd.
Benson,Stephen	Duke Univ.
Boku,Tetsuhiko	National Laboratory for High Energy Physics(KEK)
Brau,Charles A.	Vanderbirt Univ.
Chyo,Ki	Univ. of Electro-Communications
Ebisawa,Katsuyuki	Toshiba Co.
Enomoto,Atsushi	National Laboratory for High Energy Physics(KEK)
Fujiie,Yoichi	Tokyo Institute of Technology
Fuketa,Toyojiro	Japan Atomic Energy Research Institute(JAERI)
Furukawa,Kohei	Sumitomo Electric Industries,Ltd.
Goino,Yoichi	Nissin Electric Co.,Ltd.
Hajima,Ryoichi	Univ. of Tokyo
Hara,Tohru	Univ. of Tokyo
Hatsuta,Yoshio	Nippon Electric Co.,Ltd.
Hattori,Toshiyuki	Tokyo Institute of Technology
Hayakawa,Ken	Nihon Univ.
Hiramatsu,Shigenori	National Laboratory for High Energy Physics(KEK)
Honma,Atsushi	Hamamatsu Photonics K.K.
Hori,Yoichiro	National Laboratory for High Energy Physics(KEK)
Hosada,Yoshikado	Sumitomo Electric Industries,Ltd.
Hoshi,Hiroshi	Nihon Koshuha Co.,Ltd.
Husimi,Kodi	
Ichikawa,Hayao	Toshiba Co.
Ikuzawa,Katsumi	NKK Corporation
Imasaki,Kazuo	Institute for Laser Technology
Ishida,Hideto	Mitsubishi Heavy Industries Ltd.
Ishida,Tsutomu	Japan Atomic Energy Research Institute(JAERI)
Ishii,Mitsuhiko	Japan Atomic Energy Research Institute(JAERI)
Ishitsuke,Katsumoto	Toshiba Co.
Iwashita,Yoshihisa	Kyoto Univ.

Jameson,Robert A.	Los Alamos National Laboratory
Kabayashi,Hitoshi	National Laboratory for High Energy Physics(KEK)
Kabayashi,Masanori	National Laboratory for High Energy Physics(KEK)
Kamitsubo,Hiromichi	The Institute of Physical and Chemical Research(RIKEN)
Kamiya,Syoji	Kawasaki Heavy Industries,Ltd.
Kamiya,Yukihide	National Laboratory for High Energy Physics(KEK)
Kato,Atsushi	Kishikawa Special Valve Co.,Ltd.
Kato,Makoto	JEOL Ltd.
Kato,Mitsuo	Mitsubishi Heavy Industries Ltd.
Katsura,Tomotaro	National Laboratory for High Energy Physics(KEK)
Kawada,Yutaka	Kobe Steel,Ltd.
Kawaguchi,Yoshihiro	Tokyo Electric Power Co.,Ltd.
Kawai,Chiaki	NKK Corporation
Kawai,Masayoshi	Toshiba Co.
Kawai,Masayuki	Tokai Univ.
Kawai,Yasushi	Institute of Space and Astronautical Science
Kawamura,Yoshiyuki	The Institute of Physical and Chemical Research(RIKEN)
Kawano,Yasumasa	Ishikawajima-Harima Heavy Industries Co.,Ltd.
Kawarasaki,Yuuki	Japan Atomic Energy Research Institute(JAERI)
Kawasaki,Atsushi	Saitama Univ.
Kikuchi,Yasuyuki	Japan Atomic Energy Research Institute(JAERI)
Kishimoto,Yasuaki	Japan Atomic Energy Research Institute(JAERI)
Kishiro,Junichi	National Laboratory for High Energy Physics(KEK)
Kitamura,Hideo	National Laboratory for High Energy Physics(KEK)
Kobayashi,Akira	Kobe Steel,Ltd.
Kohmoto,Naomi	Power Reactor and Nuclear Fuel Development Corporation(PNC)
Kohmoto,Tetsuzo	Tsukuba Research Consortium
Koide,Tsuneharu	National Laboratory for High Energy Physics(KEK)
Koike,Takashi	Hamamatsu Photonics K.K.
Koizumi,Naonori	Ishikawajima-Harima Heavy Industries Co.,Ltd.
Kosarev,Evgenij	National Laboratory for High Energy Physics(KEK)
Kunitani,Minoru	Science and Technology Agency(STA)
Kuribayashi,Shizuma	Mitsubishi Heavy Industries Ltd.
Kuriyama,Yoshihiko	Hitachi Metals,Ltd.
Kuroda,Hiroto	Univ. of Tokyo
Kuruma,Sinichiro	Osaka Univ.
Madey,John M.J.	Duke Univ.
Maekawa,Akiji	Hitachi Engineering Co.,Ltd.
Maezawa,Hideki	National Laboratory for High Energy Physics(KEK)
Matsubara,Takeo	Osaka Science & Technology Center
Matsubayashi,Nobuyuki	National Chemical Laboratory for Industry
Matsumoto,Hirobumi	Nihon Koshuha Co.,Ltd.
Matsumoto,Satoshi	Kawasaki Heavy Industries,Ltd.
Matsunaga,Kenichi	Mitsubishi Heavy Industries Ltd.

Matsushita,Tadashi	National Laboratory for High Energy Physics(KEK)
Mima,Kunioki	Osaka Univ.
Minehara,Eisuke	Japan Atomic Energy Research Institute(JAERI)
Mishima,Yoshizumi	Univ. of Tokyo
Mitsuhashi,Toshiyuki	National Laboratory for High Energy Physics(KEK)
Miyahara,Yoshikazu	Univ. of Tokyo
Miyauchi,Yasuyuki	Ishikawajima-Harima Heavy Industries Co.,Ltd.
Mizuno,Kohji	Tohoku Univ.
Mochizuki,Tetsuro	NKK Corporation
Mori,Sigeru	Japan Atomic Energy Research Institute(JAERI)
Moribe,Yukio	Nippon Electric Co.,Ltd.
Mukohyama,Takehiko	Japan Atomic Energy Research Institute(JAERI)
Nade,Toshiyuki	Osaka Vaccum,Ltd.
Nagato,Kotaro	Kawasaki Heavy Industries,Ltd.
Nagatsuka,Kenji	Nihon Koshuha Co.,Ltd.
Nakahara,Kazuo	National Laboratory for High Energy Physics(KEK)
Nakajima,Yutaka	Japan Atomic Energy Research Institute(JAERI)
Nakamura,Norio	National Laboratory for High Energy Physics(KEK)
Nakamura,Tsuyoshi	Electrotechnical Laboratory(ETL)
Nakata,Syuhei	Mitsubishi Electric Co.
Nakayama,Kouichi	Japan Atomic Energy Research Institute(JAERI)
Nakayama,Takayuki	NKK Corporation
Nakazato,Toshiharu	Tohoku Univ.
Nishi,Masatsugu	Hitachi Ltd.
Nishijima,Akio	National Chemical Laboratory for Industry
Nishikawa,Tetsuji	
Nishimura,Hidetomo	Hitachi Ltd.
Odera,Masatoshi	Sumitomo Heavy Industries,Ltd.
Ogasawara,Munehiro	Toshiba Co.
Ogata,Kenjiro	Science and Technology Agency(STA)
Ohashi,Hirotada	Univ. of Tokyo
Ohigashi,Nobuhisa	Kansai Univ.
Ohkubo,Makio	Japan Atomic Energy Research Institute(JAERI)
Ohkuma,Haruo	Univ. of Tokyo
Ohkuma,Juzo	Osaka Univ.
Ohkushi,Kouzo	Fuji Electric Co.,Ltd.
Ohmori,Chihiro	Univ. of Tokyo
Ohno,Shinichi	Japan Atomic Energy Research Institute(JAERI)
Ohsawa,Satoshi	National Laboratory for High Energy Physics(KEK)
Okazaki,Yukio	Toshiba Co.
Okuda,Shuichi	Osaka Univ.
Ono,Takahide	Yokohama National Univ.
Ouchi,Kazumi	Power Reactor and Nuclear Fuel Development Corporation(PNC)
Ozaki,Toshiyuki	National Laboratory for High Energy Physics(KEK)
Ozawa,Kunio	Hitachi Ltd.

Petroff,Yves	Laboratoire pour l'Utilisation de Rayonnement Electromagnetique
Ruschin,Shlomo	Tel Aviv Univ.
Saidoh,Masahiro	Japan Atomic Energy Research Institute(JAERI)
Saito,Hirobumi	Institute of Space and Astronautical Science
Sakae,Hisaharu	Ishikawajima-Harima Heavy Industries Co.,Ltd.
Sakamoto,Toshiyuki	Science and Technology Agency(STA)
Sakanaka,Syogo	National Laboratory for High Energy Physics(KEK)
Sasabe,Jun	Japan Atomic Energy Research Institute(JAERI)
Sasaki,Ken	Nuclear Energy Data Center(NEDAC)
Sato,Isamu	National Laboratory for High Energy Physics(KEK)
Sato,Kazuo	Nihon Univ.
Sato,Sinji	Mitsubishi Electric Co.
Sawamura,Masaru	Japan Atomic Energy Research Institute(JAERI)
Schriber,Stanley O.	Los Alamos National Laboratory
Sekita,Hitoshi	Institute of Space and Astronautical Science
Shibamura,Yohkichi	NKK Corporation
Shikazono,Naomoto	Japan Atomic Energy Research Institute(JAERI)
Shima,Masahito	Mitsubishi Heavy Industries Ltd.
Shimoyama,Tadashi	National Chemical Laboratory for Industry
Shin,Tatsu	Univ. of Electro-Communications
Shinohara,Kibatsu	Nihon Koshuha Co.,Ltd.
Shioya,Tatsuro	National Laboratory for High Energy Physics(KEK)
Sinnou,Hiroyuki	National Chemical Laboratory for Industry
Straight,Richard C.	Univ. of Utah
Sudo,Yoichi	Japan Atomic Energy Research Institute(JAERI)
Sugiyama,Kazuhiko	Kawasaki Heavy Industries,Ltd.
Sumita,Jiro	Kyusyu Univ.
Suzuki,Toshimitsu	Mitsubishi Electric Co.
Suzuki,Yasuo	Japan Atomic Energy Research Institute(JAERI)
Tahara,Kazunori	Hitachi Metals,Ltd.
Takabe,Masayuki	Japan Atomic Energy Research Institute(JAERI)
Takekoshi,Hidekuni	Kyoto Univ.
Takuma,Hiroshi	Univ. of Electro-Communications
Tanabe,Eiji	Advanced Electronics Technology Inc.
Tanaka,Kazuo	Osaka Univ.
Terabayashi,Noritsuka	Mitsubishi Heavy Industries Ltd.
Teranishi,Eizo	Horiba Ltd.
Tohyama,Shinichi	Power Reactor and Nuclear Fuel Development Corporation(PNC)
Tomimasu,Takio	Electrotechnical Laboratory(ETL)
Toyoda,Koichi	The Institute of Physical and Chemical Research(RIKEN)
Tsunawaki,Keisyo	Osaka Sangyo Univ.
Ueda,Kenichi	Univ. of Electro-Communications

Ueda,Tohru	Univ. of Tokyo
Ukikusa,Hiroshi	Ishikawajima-Harima Heavy Industries Co.,Ltd.
Urano,Takao	National Laboratory for High Energy Physics(KEK)
Usami,Teruo	Mitsubishi Electric Co.
Watanabe,Sinichi	Univ. of Tokyo
Watanabe,Tamaki	Univ. of Tokyo
Watanabe,Yasushi	Science and Technology Agency(STA)
Yabe,Akira	National Chemical Laboratory for Industry
Yamada,Hironari	Sumitomo Heavy Industries,Ltd.
Yamada,Hiroshi	Japan Atomic Energy Research Institute(JAERI)
Yamada,Kawakatsu	Electrotechnical Laboratory(ETL)
Yamakawa,Tatsuya	National Laboratory for High Energy Physics(KEK)
Yamamoto,Hisashi	Hitachi Ltd.
Yamamoto,Shigeru	National Laboratory for High Energy Physics(KEK)
Yamanaka,Chiyoe	Institute for Laser Technology
Yamanaka,Toshiyuki	Mitsubishi Heavy Industries Ltd.
Yamazaki,Hatsuo	Hokkaido Univ.
Yamazaki,Motoshi	Science and Technology Agency(STA)
Yamazaki,Tetsuo	Electrotechnical Laboratory(ETL)
Yasajima,Yoshiyuki	Mitsubishi Electric Co.
Yokota,Mitsuhiro	National Laboratory for High Energy Physics(KEK)
Yokota,Motohide	Science and Technology Agency(STA)
Yokoyama,Minoru	Kawasaki Heavy Industries,Ltd.
Yoshikazu,Masao	Kawasaki Heavy Industries,Ltd.